Crystallography, stable isotope and trace element analysis of *Mytilus edulis* shells in the context of ontogeny

Paul C. Dalbeck

B.Sc. (Hons) University of Glasgow

Thesis presented for Degree of Doctor of Philosophy

Geographical and Earth Sciences, University of Glasgow

Abstract

Living systems exert exquisite control over biomineral production determining mineral type, polymorph, morphology and ultrastructure and ultimately producing biomineral structures that perform a range of functions. In addition to this biological control, the environment also influences aspects of biomineralisation. In marine invertebrates, biominerals record seawater chemistry and temperature at deposition. Past chemistry and temperature information is interpreted via proxies such as oxygen isotope and Mg/Ca ratios in calcium carbonate biominerals and used to help predict future climatic trends. Proxies must be robust and accurate yet the presence of biological or biologically-induced kinetic effects, many of which are a consequence of ontogeny, can make it difficult to isolate the environmental signal. In many cases, proxies are applied without detailed knowledge or assessment of shell microstructures and how this is altered as the animal ages. Interpretation of detailed crystallographic, chemical and isotopic changes in the context of ontogeny is therefore essential.

This study considers crystallography, trace element chemistry and stable isotopic composition of six ontogenetic stages of farmed *Mytilus edulis* collected from a single location at the same time. The shell of *Mytilus edulis* is comprised of two calcium carbonate polymorphs: an outer layer of prismatic calcite and an inner layer of nacreous aragonite, both with very different morphologies.

The crystallographic ultrastructure is analysed through Electron Backscatter Diffraction (EBSD) and Scanning Electron Microscopy (SEM). No significant changes in crystallography are evident between ontogenetic stages. Crystallographic orientation of calcite is more strictly constrained towards the polymorph interface and from anterior to posterior in all stages of ontogeny. Further evidence of ‘mineral bridging’ is observed in nacre.

The minor element distribution varies between the polymorphs, through the shell thickness and between ontogenetic stages. Younger specimens have higher Mg, S and Sr concentrations while older specimens have increasing Na concentrations. Mg and S are present in the calcite layer but are virtually absent in aragonite. While Na and Sr occur in both polymorphs, higher concentrations occur in aragonite. Changes in Na and Sr concentrations in the aragonite layer can be linked to

prismatic bands of myostracal aragonite in the nacre. A decrease in Na concentration through the calcite layer toward the polymorph interface is observed in all specimens. Increases in Mg and S concentration in the calcite layer near the interface are often observed. Greater trace element concentrations are also observed in the umbo region of the shell.

Stable oxygen isotope signatures show small amounts of variation between regions of the shell and between ontogenetic stages. Decreasing $\delta^{18}O$ values are observed in older animals and in the posterior edge of the shell. Large variations of $\delta^{18}O$ are also observed through the shell thickness which cannot be accounted for by environmental changes. The majority of $\delta^{18}O$ data falls within the expected range for equilibrium of calcite and aragonite with ambient seawater. No significant change is observed in $\delta^{13}C$ values between ontogenetic stages or through the shell. Values of $\delta^{13}C$ and $\delta^{18}O$ co-vary in aragonite but not calcite.

Refinement in crystallography occurs in conjunction with changes in trace element chemistry and stable oxygen isotope composition moving towards the shell posterior. This indicates a change as the animal grows, resulting in differences in chemical information retained in different parts of the shell. The differences in trace element chemistry between polymorphs and isotopic and chemistry changes across the shell thickness indicate changes that can be attributed to ultrastructure as crystal habit, polymorph and orientation change occur across the shell thickness.

These results suggest that greater understanding of factors involved in biomineralising systems is required before undertaking work involving application of climate proxies.

Table of Contents

List of Figures

List of Tables

Acknowledgements

This work could not have been achieved without valuable input from a variety of sources. I am grateful to the Engineering and Physical Sciences Research Council (EPSRC) for a Doctoral Training Award which has funded this three year study. I am also grateful to the Natural Environment Research Council (NERC) for providing a grant for work on the NERC Ion Probe Facility at the University of Edinburgh (IIMP 284/1006 to M Cusack).

Many thanks to Prof. Maggie Cusack, as without her advice, encouragement, patience and general good humour this would have been a far tougher task. I am also thankful to Dr. Martin Lee whose assistance in understanding EBSD and 'out-the-seashell-box' viewpoints have contributed greatly to this work. Thanks to Prof Tony Fallick who has also provided guidance in isotope analysis. A special mention to Dr. Jennifer England who was always on hand to put forward thoughts, suggestions and bounce ideas off, as well as Dr Alberto Perez-Huerta who has done the same. This team's list of collaborative publications is testament to our support of each other.

Considerable mentions go to many of the technical staff who have always been on hand to assist with queries and the inevitable equipment malfunctions: Peter Chung (University of Glasgow), Robert McDonald (University of Glasgow) and Paul Edwards (University of Strathclyde) for assistance with the SEM and Electron Microprobe analyses. Terry Donnelly at SUERC, whose tireless dedication to the mass spectrometer is an example to us all. John Gilleece for help with sample preparation and the occasional football chat. Thanks to John Craven and Simone Kasemann (University of Edinburgh) for advice and assistance with Ion Probe analysis and the long evening stints with only a Boddingtons for comfort.

I am also grateful to Dr. Stuart Wright and Rene deKloe of EDAX who have also helped greatly in understanding EBSD. I'd also like to thank Russell Rajendra of the Mineralogical Society for assisting in conference support which has allowed me to present much of this work, which has also led to valuable feedback and advice. I am grateful to John and Nicky Holmyard from Cadderlie Mussels for supplying the mussels and for assistance on age determination and additional background. Thanks to Professor Wolfgang Schmahl and Dr. Gordon Curry for reviewing my

thesis and advice on the corrections. Thanks to Dr Andy Freer for his incredibly clean sense of humour and introduction to the wonderful world of protein chemistry.

Thanks go to the guys of the postgraduate office; my proximity to the coffee machine was often a blessing and 'Friday Beers' have been something to look forward to during tough weeks. Dan and Jamie's continual encouragement at circuits has often helped me blast away hours of frustration and Kate's assistance on formatting has helped massively and reduced much tearing of hair.

Finally, I'd like to thank those who are most important to me and have provided loving support not just in my thesis but through my life which has led to this stage. Mum, Dad, Laura, Stephen and, of course, Anneka. I cannot thank you enough.

Declaration

The material presented in this thesis is the result of three years independent research carried out at Department of Geographical & Earth Sciences and the Scottish Universities Environmental Research Centre. The research was supervised by Prof. Maggie Cusack, Dr. Martin Lee and Prof. Tony Fallick. This thesis repesents my own research and any published or unpublished work by other authors has been given full acknowledgement in the text.

Paul C. Dalbeck

1

Introduction

1.1 Biomineralisation

Living systems produce a wide variety of minerals that have evolved over 545 million years (Knoll, 2003). The biomineral structures perform equally varied purposes (Weiner *et al.*, 2000). The production of these inorganic solids, found in all kingdoms of the Linnaean classification system, has generated significant interest for biologists, earth scientists, materials and medical scientists and is encompassed in the field of biomineralisation.

The functions of biomineralised structures are diverse (Lowenstam, 1981; Lowenstam & Weiner, 1989; Mann, 2001). Protection and support are provided through exoskeletal and endoskeletal construction, cutting and grinding is achieved through the production of teeth and the gravity and magnetic receptors that orientate organisms are just some of the uses. The storage of elements in mineralised structures means biominerals can perform the function of stable ion reservoirs that can be redissolved for reuse in the biological system.

Ca-bearing minerals are most abundant (Lowenstam, 1981). Minerals such as $CaCO_3$ and silica contribute much of the skeletal material of marine invertebrates. Calcium phosphate, $Ca_3(PO_4)_2$ creates the endoskeletal bone for vertebrates as well as associated amorphous precursor phases (Prenant, 1927; Lowenstam, 1972; Simkiss, 1993; Weiner *et al.*, 2003). Other minerals such as iron oxides and metal sulphides are also produced as functional materials in a vast range of organisms.

Biominerals can be produced simply through direct precipitation as a by-product induced by biological activity e.g. many bacteria, where little control is exerted by the living system on the mineral production (Lowenstam & Weiner, 1989; Mann, 2001). However, to create specialized structures, complete control is required in the system. Mann (2001) described several control processes in biomineralisation. The chemistry of the system controls the reaction kinetics of mineralisation. Spatial control provides physical boundaries in which crystals can grow. Structural control through organic matrix mediation provides a framework as well as directing and orientating nucleation. Morphological control is exerted through organic boundaries that change progressively

with time. Morphological control affects the mineral shape being produced and then constructional control is applied to produce higher order structures from assembling smaller sub-units. Thus, biologically controlled mineralisation reveals the crucial interplay between the organic components, the chemistry of the system and the mineral that is generated. Consequently, composite materials of mineralised tissue with an organic framework are formed.

1.1.1 Organic material

For an organic framework to exist within biomineral structures, hydrophobic macromolecules are required to prevent the structure degrading in aqueous environments. This insoluble component can provide the necessary spatial control, as well as mechanical support arranged around the mineralised component which affects the overall final structure (Weiner & Traub, 1984). This structural support is termed the intercrystalline matrix, and normally comprises long chain polysaccharides with insoluble proteins. Examples of intercrystalline components are the proteins collagen in bone (Traub *et al.*, 1989; Weiner & Traub, 1989; 1992; 1992) and amelogenins in teeth (Veiss, 1989) . This material can also be found occluded within the mineral as the intracrystalline matrix, encapsulated during growth of the crystalline material (Addadi *et al.*, 1994; Wilt, 2002; Dauphin *et al.*, 2003b; Rousseau *et al.*, 2005).

However, the hydrophobic surface of the insoluble matrix is not favourable for securing and organising ions and hydrated precursors are necessary for mineral formation (Mann, 2001). A soluble organic component is provided (Weiner, 1979) through acidic macromolecules closely associated with the insoluble fraction. These acidic macromolecules commonly possess binding sites for metal ions such as Ca which are essential for construction of the majority of biominerals (Weiner & Hood, 1975).

The soluble, hydrophilic component is thought to be closely involved in determining the nucleation of the crystals (Weiner *et al.*, 1983; Weiner & Traub, 1984; Addadi *et al.*, 2006), as well as the overall crystal polymorph and habit (Watabe & Wilbur, 1960; Belcher *et al.*, 1996; Falini *et al.*, 1996; Feng *et al.*, 2000c; Thompson *et al.*, 2000; Hou & Feng, 2003; 2006). DeYoreo and Dove (2004) demonstrated the importance of the organic matrix on crystal morphology and how it affects the kinetics of crystal growth. Calcium carbonate crystals grow through spiral structured hillocks with the steps and kinks on these hillocks being fundamental to crystal growth as these are the sites of attachment for growth (Gratz *et al.*, 1993; Mann, 2001). By interfering with these sites, the shapes of hillocks and therefore resultant crystals can be modified. Through step pinning, impurities attach to steps to prevent them physically from growing. Some impurities may bind to some growth steps preferentially over others which produce imbalanced morphologies of the resultant crystal (De Yoreo & Dove, 2004). Kink blocking also does this and stops kinks from

propagating, modifying the crystal shape. Incorporation of impurities onto advancing steps and kink sites can increase the internal energy of the solid crystal, increasing its instability. Volkmer *et al*. (2004) performed experiments on growing calcite crystals *in vitro* using synthesized acidic peptides similar to those found in living systems. Peptides containing a high proportion of aspartame showed an effect on the different crystal faces of the growing calcite. The (012) face was inhibited and the prismatic {110} faces were expressed, with an effect resembling the production of calcite sponge spicules. This modification of the crystal growth was attributed to the lattice structure of the $CaCO_3$, with Ca and CO_3 ions emerging perpendicular from the lattice of the {110} faces providing more optimum orientation for interaction with the ion-binding Asp- or Glu- side chains of the proteins. Orme *et al.* (2001) discussed this with respect to the changes in the energy landscape of the growing crystals by the proteins. Again, the Asp- content is the main factor in the modifications. Asp-rich growth modifiers lowered the rate of attachment and detachment to steps and faces of the growing crystal. Site-specific amino acids would bind to change step-edge free energies, and crystal symmetry was reduced. Wheeler *et al*. (1981) investigated this in the oyster shell and found the organic material suppressed calcium carbonate nucleation and decreased the rate of shell growth indicating the role in regulating biomineralisation.

The enzyme carbonic anhydrase (CA) is present in many carbonate secreting systems (Freeman & Wilbur, 1948; Wilbur & Anderson, 1950; Wilbur & Jodrey, 1955; Gay & Mueller, 1973, , 1974; Wilbur & Saleuddin, 1983) and catalyses the, normally slow, hydration/dehydration reaction of aqueous CO_2 and production of HCO_3^- ions (Krebs & Roughton, 1948). This catalysis is considered to be advantageous in biomineralising systems that require large amounts of carbonate ions for mineral production.

1.1.2 Inorganic influence

The inorganic chemistry of the system also exerts specific controls over the biomineral production. Teng *et al*. (1999) showed the sensitivity of growing calcite to small changes in solution chemistry that would ultimately affect the kinetics of a biomineralising system. Investigations on the effect of minor cations, such as Sr^{2+} and Mg^{2+}, have confirmed this. The presence of Mg^{2+} ions in a calcium carbonate secreting system has been determined as a crucial component in growth modification. Mg has previously been described as an inhibitor of calcite growth (Deleuze & Brantley, 1997; Davis *et al.*, 2000). Mg^{2+} incorporation into the growing crystal lattice, substituting for Ca^{2+}, increases solubility by increasing the free energy within the $CaCO_3$ crystal lattice and ultimately straining the crystal. This role of Mg^{2+}as a growth modifier has been investigated in a number of $CaCO_3$ studies which found Mg to affect crystal morphology e.g. Rautaray *et al.* (2005) as well as

stabilizing amorphous calcium carbonate (ACC), which is thought to be a significant precursor for biomineral formation (Loste *et al.*, 2003).

Mg presence has also affected the resultant polymorph produced. The metastable aragonite formed instead of calcite when Mg concentrations in solution are increased (Kitano, 1962; Fernandez-Diaz *et al.*, 1996; Kitamura, 2001). *In vitro* studies of the influence of Mg on calcite growth also revealed significant effects on promotion and inhibition of $CaCO_3$ growth (Hincke & St. Maurice, 2000). This *in vitro* study demonstrated that 5mM of Mg^{2+} ions inhibited the rate of $CaCO_3$ precipitation, yet lower Mg concentrations ~0.8 & 4mM promoted nucleation and growth of calcite respectively. Mg has also been used in conjunction with organic components to produce similar modification effects (Sugawara & Kato, 2000; Meldrum & Hyde, 2001; Han & Aizenberg, 2003; Jiao *et al.*, 2006) and this has been investigated in the molluscan system *in vitro* (Wilbur & Bernhardt, 1984). However, the control of Mg incorporation in $CaCO_3$ has been continually debated (Katz, 1973; Berner, 1975; Burton & Walter, 1987). Studies have demonstrated a temperature correlation in Mg/Ca ratios in non-biogenic (Mucci, 1987) and biogenic calcite (Lowenstam, 1961; Rosenthal *et al.*, 1997; Lea *et al.*, 1999). Further studies emphasise solution chemistry (Lorens & Bender, 1980; Mucci & Morse, 1983) with growth rate being another debated factor (Major & Wilber, 1991). Wasylenki *et al* (2005a) discuss Mg in calcite growth, without the complications of organic material in the system, and attributed surface processes on crystal faces such as transport and diffusion rates as the determining factor of Mg incorporation rather than temperature, which is affected by the processes employed in a living system.

Incorporation of Sr^{2+} holds further interest as Sr^{2+} affects kinetics of calcite growth (de Leeuw, 2002; de Leeuw *et al.*, 2002) through both promotion and inhibition depending on Sr^{2+} concentration (Wasylenki *et al.*, 2005b). Sr has also been assessed as an indicator of temperature of carbonate formation (Beck *et al.*, 1992) The presence of other ions such as Mg (Mucci & Morse, 1983), growth rate of the crystal (Kinsman & Holland, 1969; Lorens, 1981), crystal morphology (Given & Wilkinson, 1985) and crystal polymorph (Cohen & McConnaughey, 2003) are also thought to affect Sr incorporation into the $CaCO_3$ lattice. The effect of temperature in biogenic carbonate has also been considered a factor (Smith *et al.*, 1979; Rosenheim *et al.*, 2004).

The reason for the presence of monovalent ions in a $CaCO_3$ is still debated. Rajam and Mann (1990) showed that Li^+ could stabilise the {001} face of growing calcite by incorporation through interstitial sites in the lattice. Interstitial sites can be produced through lattice defects, produced in conjunction with other ions in the system which has also been shown to affect Na^+ incorporation (Ishikawa & Ichikuni, 1984; Busenberg & Plummer, 1985). The crystal polymorph produced has a significant effect on the mode of incorporation of monovalent alkali metals as well as the selectivity of the element which is incorporated (Okumura & Kitano, 1986).

1.1.3 Biomineralisation in *Mytilus edulis*

The importance and interactions of the organic and inorganic components have been described in various biomineralising strategies. Particular interest has been placed on the molluscan system, which forms the basis of this study.

The molluscan system is a $CaCO_3$ producer, which can assume a number of different microstructures (Taylor *et al.*, 1969; Wilbur & Saleuddin, 1983; Chateigner *et al.*, 2000) as well as producing different polymorphs. A tough organic sheath known as the periostracum covers the entire shell as a protective outer coating. The periostracum is a quinone-tanned protein, that also acts as a substrate for the initial crystal nucleation of the shell (Simkiss & Wilbur, 1989) (Figure 1.1).

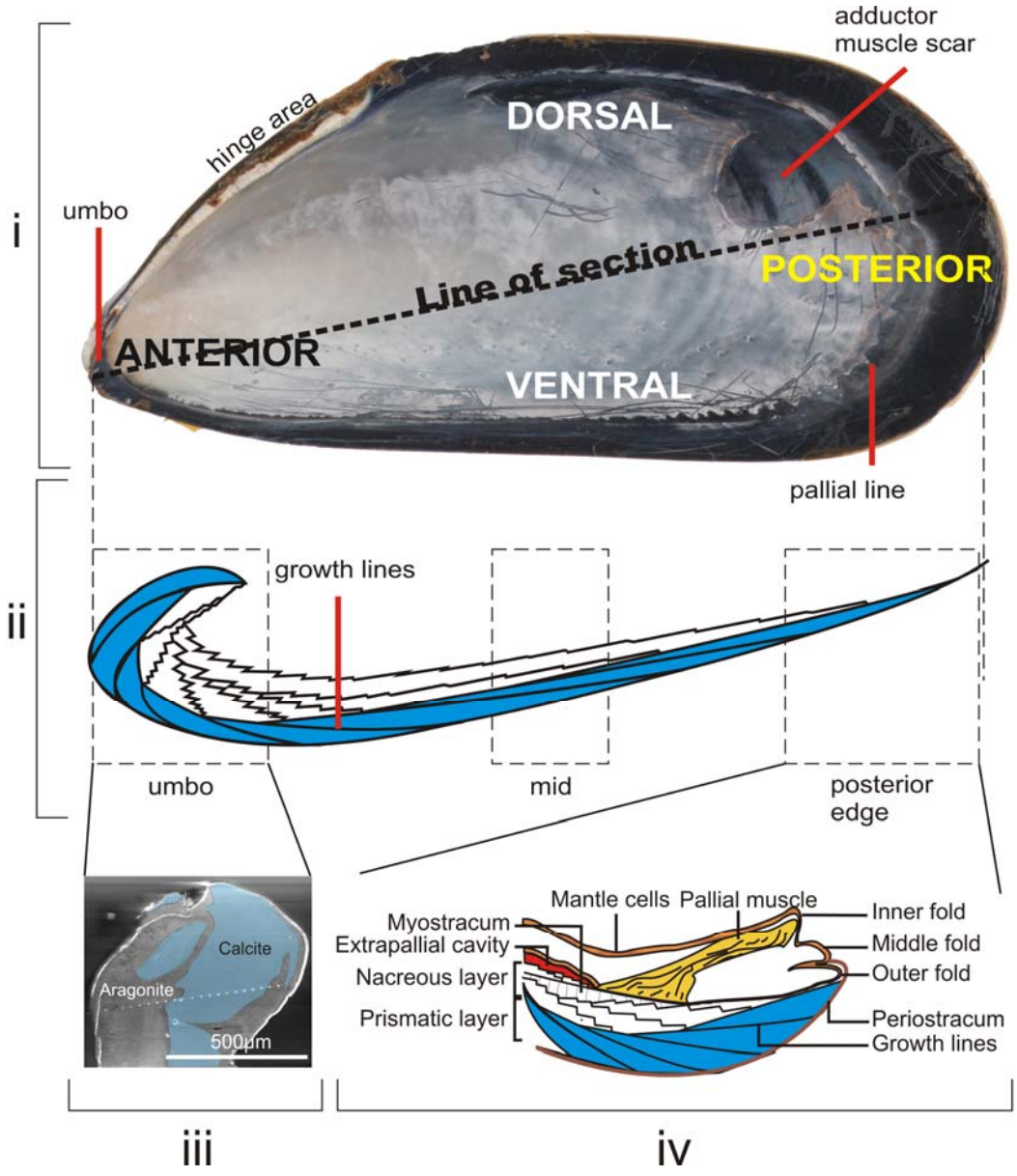

Figure 1.1 *Mytilus edulis* overview. i – Plan view of inner surface of a right valve with main features and line of section indicated. ii – Diagram of representative cross-section with calcite in blue and aragonite in white. Three main areas of interest outlined. iii – Scanning electron microscope image of a cross-section of the umbo of a specimen of *Mytilus edulis* with the shell exterior to the left. The distribution of calcite and aragonite demonstrates the complex nature of the umbo region. iv – the growing front of the mussel, with the soft tissue (mantle) folds involved in producing the prismatic layer and the extrapallial fluid (red) responsible for producing the nacreous layer. Prisms of calcite are produced initially and then aragonite is deposited in a terraced fashion. The internal muscles attach to the prismatic aragonite of the myostracum.

The shell is produced by the epithelial cells of the mantle, in the soft living tissue of the animal. The mantle is a folded sheet of cells and the secretion of different parts of the shell is dictated by different epithelial cells within mantle regions (Beedham, 1958). Sudo *et al* (1997) reaffirmed this using molecular cloning of insoluble proteins found within the different layers of the mollusc, and then used this to locate them *in situ* within the mantle. The mantle forms a region between the inner

shell and itself creating a cavity where $CaCO_3$ and organic constituents of the shell can be produced in a solution, termed extrapallial fluid (Crenshaw, 1972; Misogianes & Chasteen, 1979; Wilbur & Saleuddin, 1983; Simkiss & Wilbur, 1989) (Figure 1.1iv). This arrangement distinguishes the Bivalvia from that of other shell producing phyla such as the Brachiopoda and the Arthropoda. A special type of carbonic anhydrase is found in the mussel mantle (Miyamoto *et al.*, 1996) secreted as an integral component of the organic matrix, located at the site of mineralisation.

1.1.3.1 Mollusc nacre

The $CaCO_3$ produced in the mollusc shell is frequently found in the metastable form of aragonite. The aragonite layer, termed nacre or 'mother of pearl', for its distinctive morphology and arrangement, with a mineral 'brick' and organic 'mortar' configuration (Schmidt, 1923; Addadi & Weiner, 1997), has attracted a significant amount of interest in understanding biomineralisation processes.

Early studies by Erben and Watabe (1974) discussed the production of molluscan nacre, suggesting that an initial mineralised layer, often a prismatic layer, is covered by an organic framework on which the nacre is deposited. The nacre is laid down in layers with individual nuclei in each separate layer growing laterally until they fuse with their neighbouring crystals to create a complete layer. Within the Mollusca, the Bivalvia and Gastropoda produce their nacreous layer in different ways. Bivalves disperse the growth of nacre over a larger surface area resulting in a step-wise growth pattern with growing layers of nacre being covered by new organic layers on which the subsequent layer can form (Wise, 1970b). In gastropods, the nacre grows in conical stacks with laterally growing base tablets at the base of each stack covered by an organic sheet before new nacre tablets form on top. This sequence repeats with all the tablets in each layer fusing to make a complete mineralised layer (Wise, 1970a) (Figure 1.2).

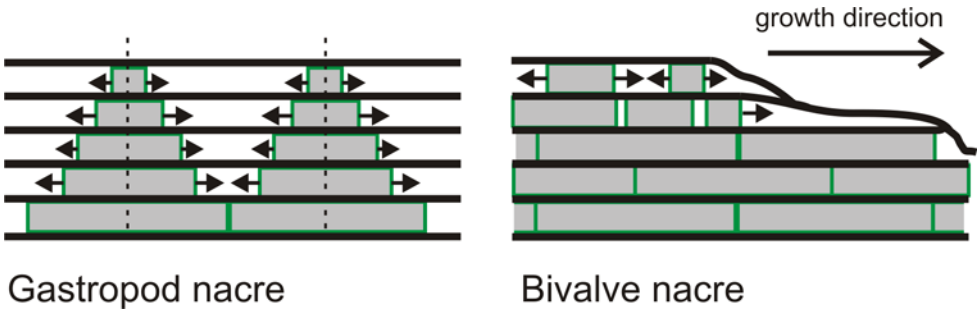

Figure 1.2 Different nacre growth mechanisms between gastropods and bivalves. Individual aragonite nacre tablets (grey) are surrounded by an organic envelope (green). Sheets of organic material (black) are laid down between successive laminae. Based on Mann (2001)

Weiner and Traub (1984) described the role of the soluble and insoluble matrix within mollusc shells and the layered model of the macromolecular sheets in the production of the nacreous layers has been discussed in further investigations (Mann, 2001). The representation of the central core of ß-chitin (Weiner & Traub, 1980) sandwiched between silk-fibroin proteins with an outer layering of the soluble macromolecules has been proposed as the method of determining the growth of the a- and b- axes of aragonite nacre in relation to the direction of the ß-chitin and the silk proteins respectively. The ß-sheet conformation is important in that reactive side chains are located to one side of the chain (Worms & Weiner, 1986). The framework is said to provide well-spaced nucleation points and the soluble macromolecules on the surface are said to have a Ca-binding effect, through the spacing of their amino acid residues which are Asp and Glu-rich. This provides good atomic spacing for the production of aragonite (Weiner & Hood, 1975). From this, arrangement, the mineral is produced epitaxially on the organic substrate. Weiner and Traub (1981) also provided evidence for physical limiting of the vertical growth of nacreous tablets by the 5 layer sheet-assemblage. The negatively charged groups on the soluble outer coating proteins reacting with the Ca in the upper crystal surface preventing any further addition of material.

This model has come under scrutiny, with evidence emerging that structured silk is absent from the matrix (Levi-Kalisman *et al.*, 2001) and that the production of a precursor material in amorphous calcium carbonate (ACC) occurs in mollusc larvae (Weiss *et al.*, 2002) and around the nacre tablets (Nassif *et al.*, 2005). ACC has recently been considered as a significant component of nacre formation (Gehrke *et al.*, 2005; Amos *et al.*, 2007) and described in other biominerals (Beniash *et al.*, 1997; Meibom *et al.*, 2004). ACC is also thought to facilitate mineralisation through lowering the activation energy required for crystal development (Nancollas, 1982).

Addadi *et al*. (2006) proposed a modified model for nacre formation with the silk present as a hydrogel phase which dehydrates as the mineral forms. The silk hydrogel fills chitin-bound compartments where the mineralisation occurs. Cartwright and Checa (2006) proposed that chitin forms a liquid-crystal phase from colloids of chitin in the extrapallial fluid. The mineral phase is first produced as ACC in specialised cells separated from the mineralisation area (Neff, 1972; Mount *et al.*, 2004) which is stabilised through macromolecules to prevent crystallisation (Aizenberg *et al.*, 1996). Evidence for the presence of ACC is in the presence of small nano-granules which have been described in biominerals (Erez, 2003; Cuif & Dauphin, 2004). The ACC granules are protected by individual organic coatings during biomineralisation (Raz *et al.*, 2003). Regions of high organic concentration in biominerals may also represent redundant coatings of these granules (Cuif *et al.*, 2003). The ACC is thought to be transported to the area of mineralisation and nucleated at a specific central point (Checa & Rodriguez-Navarro, 2005) of each matrix compartment. Nudelman *et al*. (2006) determined this central point to possess a carboxylate-

rich protein core surrounded by a ring of sulphate-rich protein that facilitates aragonite nucleation. Mineralizing growth of the nacre tablet proceeds, consuming the ACC and soluble proteins within each tablet compartment, restricted vertically by the overlying matrix and laterally by competitive growth of neighbouring tablets. The continual production of material is still debated, as the above model requires re-construction of the matrix, silk and carboxylate/sulphate protein arrangement for each subsequent layer of nacre deposition. Other investigations have shown that nacre tablets only form in the Bivalvia once a fully mineralised layer is completed below (Checa & Rodriguez-Navarro, 2005). Adjacent tablets in subsequent laminae and also neighbouring tablets of nacre within each layer, show continuity of the crystallographic axes orientation (Hou & Feng, 2003; DiMasi & Sarikaya, 2004; Checa *et al.*, 2006; Dalbeck *et al.*, 2006). This situation suggests mineral-mineral epitaxy through physical mineral bridging (Manne *et al.*, 1994; Schaffer *et al.*, 1997) rather than the proposed organic-mineral epitaxy mechanism above. Models proposed by Hou and Feng (2003) and Cartwright and Checa (2006) incorporate the mineral bridges to the nacre model with pores in the organic matrix allowing mineral growth to penetrate adjacent layers. However, the mineral bridge theory has been debated as no physical evidence of the bridges themselves has been made.

1.1.3.2 Calcite prisms

Calcite in biominerals presents fewer questions than the nacreous layer, as the material produced is the expected stable form of $CaCO_3$ which would be precipitated abiotically. However, this structure is still subject to extensive enquiry.

As discussed above, the outer organic periostracum of the mollusc shell provides a nucleation point for mineralisation to occur. This has been incorporated into models of prismatic calcite growth with regularly spaced spherulitic clusters of calcite forming a nucleation point on the periostracum (Grigoriev, 1965; Taylor *et al.*, 1969). From these nucleation points, calcite crystals then grow in different directions, consuming surrounding organic material (Nakahara *et al.*, 1980) before abutting against neighbouring crystals. Checa *et al* (2005) described these initial points as being cavities within emulsion-like organic material, ordered into a polygonal structure through interfacial tension. The competitive growth between the calcite prisms then dictates the growth with organic matrix forming a thin continuous boundary between individual crystallites. This technique of nucleation and competitive growth of prismatic calcite has also been described in the avian eggshell (Silyn-Roberts & Sharp, 1986; Dalbeck & Cusack, 2006). Barnes (1970) described the growth of spherulitic bundles of aragonite in coral. Crystals inclined favourably to the optimum direction of growth would grow fastest and quickly consume diverging crystallites.

1.1.3.3 Polymorph selection

Early tests by Wilbur and Watabe, (1960) showed that shell matrix from either the calcite or the aragonite parts of the mollusc shell would produce their respective polymorphs from a solution of $CaCO_3$ *in vitro*.

The selectivity of crystal polymorph, or the 'calcite-aragonite' problem (Mann, 2001), is still unresolved. Mann (1988) investigated this with respect to molecular recognition in biomineralisation. Mann's (1988) study indicates the importance of the structural correspondence of proteins, and the electrostatic properties of specific protein side chains through which nucleation is facilitated when the side chains possess a certain charge. In terms of the selectivity of the polymorphism, Mann attributed it to possible stereochemical requirements. The difference between the $CaCO_3$ lattice in these two polymorphs is the stereochemistry of the Ca^{2+} and CO_3^{2-} ions. The most stable (001) face of aragonite displays either all Ca^{2+} or all CO_3^{2-} ions, in the stable (104) face of calcite Ca^{2+} and CO_3^{2-} ions are displayed. To produce a certain polymorph, a matrix surface must be present to provide the optimum orientation geometry for nucleation of a crystal face. The spacing of the Ca-binding amino acids which show similar spacing to that of aragonite (Weiner & Hood, 1975) provide this, emphasising the organic template models discussed above and the importance of the soluble protein fraction.

There is debate as to whether there is a need for the deposition of an organic foundation layer in molluscs in the switch of polymorph from calcite to aragonite. Thompson *et al*. (2000) and Belcher *et al*. (1996) demonstrated that aragonite can be produced without the need for an initial protein template. Lattice spacing in $CaCO_3$ was affected by the addition of soluble proteins and this would facilitate the direct growth of aragonite on top of an existing calcite lattice (Thompson *et al.*, 2000). Crystallographic agreement between crystal faces of calcite and aragonite in the mollusc shell show this to be a possibility (DiMasi & Sarikaya, 2004; Dalbeck *et al.*, 2006). Belcher *et al*. (1996) showed that the polymorph switch between calcite and aragonite could be produced, *in vitro*, by changing the soluble proteins in the system. When a mixture of aragonite proteins were used the crystals produced were the tiles of aragonite similar to that in shell nacre.

However, studies such as Levi et al. (1998) following on from work done by Falini et al. (1996) as well as the models described above (Addadi *et al.*, 2006; Cartwright & Checa, 2006) show the insoluble fractions to be of significant importance at least for controlling the nucleation of crystallisation.

1.2 Use of biominerals as environmental proxies

The process of biomineralisation involves a living system selectively incorporating elements from the surrounding environment and using these to produce a specialised structure through exquisite biological control, and subsequently elements can be discarded from the system as waste products (Lowenstam & Weiner, 1989; Simkiss & Wilbur, 1989; Mann, 2001).

Biological carbonates comprise the largest proportion of the biosphere's carbon reservoir, and therefore the production of carbonate biominerals has a large impact on ocean chemistry, biogeochemistry and the carbon cycle. Further to this, organisms such as coral and molluscs frequently deposit the metastable form of $CaCO_3$, aragonite, rather than or in addition to the expected stable calcite polymorph. The differences in trace element chemistry between the two can also affect ocean chemistry with elements such as Sr being 10 times more accepted into the aragonite structure than calcite (Cohen & McConnaughey, 2003).

Due to the interaction with the environment and the uptake of elements from the ambient surroundings, the concept of environmental conditions being recorded in the resultant mineral is made. This forms the basis for the use of biominerals as palaeoenvironmental proxies which can determine past surface seawater temperatures (SST) and salinities as well as productivity of the water from phytoplankton blooming.

1.2.1 Trace elements

In carbonate-secreting biological systems, Ca, C and O are the major elements which comprise the main minerals produced, generally calcite, aragonite or vaterite. Elements incorporated into the system at significantly lower quantities, typically ~0.1wt%, are described as trace elements. As these elements are not present in significant abundance they rarely form mineral phases and are normally considered as impurities in the system. However, their proportions in the mineral structure can be used to determine a history of growth conditions. A significant amount of interest has been placed on the palaeotemperature potential of Mg/Ca ratios in biogenic carbonate. This has encompassed a vast range of biomineralising organisms such as brachiopods (Lowenstam, 1961; Mii & Grossman, 1994), forams (Nurnberg, 1995; Nurnberg *et al.*, 1996; Elderfield & Ganssen, 2000; Lea *et al.*, 2000; von Langen *et al.*, 2005; Sagawa *et al.*, 2006; Marchitto *et al.*, 2007) and the molluscan shell (Klein *et al.*, 1996a) which have described a correlation between SST and Mg/Ca ratios.

The application of Mg/Ca ratios as an indicator of SST is still debated with biological controls showing an effect on Mg incorporation (Lorens & Bender, 1977; Vander Putten *et al.*, 2000; Freitas *et al.*, 2005; Freitas *et al.*, 2006) in the molluscan shell. Mg/Ca ratios of biogenic carbonate have

also shown variation in constant temperature environments like the avian eggshell (Cusack *et al.*, 2003; Dalbeck & Cusack, 2006).

Sr/Ca ratios have also been used in a similar fashion to the Mg/Ca ratios and often both the Sr/Ca and Mg/Ca ratios are used in conjunction due to the relationship between Sr and Mg in the calcite lattice (Mucci & Morse, 1983). Early work by Dodd (1965; Dodd & Crisp, 1982) have shown the application of Sr/Ca as an environmental indicator in mollusc shells and has also been shown in other biominerals (Stoll *et al.*, 2002; Sosdian *et al.*, 2006; Goodkin *et al.*, 2007). However, similar biological effects influence the Sr/Ca ratio (Rosenberg & Hughes, 1991; Klein *et al.*, 1996b) and precipitation rate also a significant factor (Lorens, 1981; Carpenter & Lohmann, 1992; Stecher *et al.*, 1996). Sosdian *et al*., (2006) applied different Sr/Ca correlation relationships which were dependent on the stage of life of the gastropod. Cohen et al. (2002) also discussed the ontogenetic effect of algal symbionts proportions affecting the Sr/Ca ratios of coral as well as photosynthetic activity associated with these (Cohen *et al.*, 2001).

1.2.2 Stable isotopes

The reconstruction of past climate conditions has also been made possible through pioneering work of Urey, (1947; 1948b; 1948a; Urey *et al.*, 1948) using stable $^{18}O/^{16}O$ and $^{13}C/^{12}C$ isotope ratios in biogenic carbonates as a proxy for seawater temperature, salinity and productivity. This relies on the isotopic composition of the water being represented in the $CaCO_3$ mineral produced. A number of early modifications were made to this original method (McCrea, 1950; Epstein *et al.*, 1951; 1953) producing the classic carbonate palaeotemperature scale.

Lowenstam (1961) applied this to the calcite-secreting brachiopods, prompting further application e.g. Grossman *et al*. (1991; 1993) and significant investigation into other biominerals such as corals and molluscs (Margolis *et al.*, 1975; Anderson & Steinmetz, 1983; Dudley *et al.*, 1986; Klein *et al.*, 1996a; Rahimpour-Bonab *et al.*, 1997; Fischer *et al.*, 1999).

The application of the palaeotemperature equation is complicated by biological activity of the system, so-called 'vital effects' which can result in isotopic disequilibrium. McCrea (1950) and Urey (1951) indicated that reaction kinetics and species-specificity caused deviation from the expected isotopic signature. McConnaughey's work on corals (McConnaughey, 1989a; 1989b; McConnaughey *et al.*, 1997; 2003) has highlighted significant kinetic and biological respiration effects that can affect the isotopic signature. Kinetic effects can arise when variation in growth rate of the organism; whether through seasonal, maturation or even damage repair, faster growing crystals may preferentially uptake different isotopes.

The mollusc shell is produced via the extrapallial fluid (EPF) discussed above (Section 1.1.3). The composition of EPF has generated interest for determining the metabolic and also the kinetic effects over the isotopic signature (Klein *et al.*, 1996b; Owen *et al.*, 2002). Inorganic carbon used to construct the shell from the EPF is found as CO_2 or HCO_3^-, the carbon and oxygen isotopes involved in these molecules are of interest as the carbon in particular may be derived from respiration within the animal. McConnaughey *et al* (1997) also showed that CO_2 circulated through marine invertebrate biominerals accounts for 90% of the C and O incorporated into the mineralised skeleton compared to CO_2 produced for respiration and photosynthesis.

The species–specificity has led to extensive studies to determine which phyla faithfully record isotopic ratios in equilibrium with the ambient conditions (Wefer & Berger, 1991) with species from the Mollusca (Klein *et al.*, 1996a), Foraminifera (Spero & Lea, 2002) and Brachiopoda (Lowenstam, 1961) producing such results. However, variation is also produced within these phyla (Carpenter & Lohmann, 1995) and the phyla Echinodermata show distinct divergence from equilibrium values (Weber & Raup, 1966). Even within a 'reliable' system such as the molluscs, Epstein and Lowenstam (1953) demonstrated that rapid shell repair produced a distinct kinetic effect.

Auclair *et al.* (2003) used the brachiopod *Terebratalia transversa*, to show that equilibrium and disequilibrium occurred between different parts through the shell thickness, with the outermost secondary layer and the primary layer being deposited out of equilibrium. The differences were attributed to kinetics of the system controlling the isotopic signature as the calcite becomes more slowly secreted towards the inner part of the shell. The innermost secondary layer fibres of *T. transversa* are in isotopic equilibrium with seawater (Parkinson *et al.*, 2005). Auclair *et al.* (2003) further considered metabolic effects on the system and whether the same effects would be active in neighbouring molluscs. It was concluded that the carbon ratio was susceptible to metabolic effects but the oxygen ratio was not as influenced by growth rate of the mollusc compared to the brachiopod. The stable carbon isotopic signature is affected in this brachiopod species reinforcing the theory of a metabolic effect (Parkinson & Cusack, 2007). The difference in susceptibility to metabolic effects between the two phyla highlighted the difference between the morphology and mineralising processes of the animals. The molluscs have the shell mineralising fluid medium isolated from the ambient seawater in the extrapallial cavity (Section 1.1.3). If the residence time of carbonate ions within the extrapallial fluid was long enough with large fluxes of water through the animal it was expected that this was long enough for a buffering effect with the surrounding fluid to produce a near equilibrium oxygen isotopic ratio. Auclair *et al*. (2003) suggested that because the brachiopods produce their shell from calcitic fibres enveloped in an organic sheath, this

prevented such a buffering effect which produces a more pronounced shift from equilibrium in the brachiopods.

Lécuyer *et al.* (2004) reaffirmed this with molluscs showing a good correlation with ambient water temperatures. Comparisons of early deposited material against mature, slow-growing parts of the shell displayed low variability in the oxygen isotopic ratio indicating fractionation is not affected by metabolic or kinetic effects. The carbon isotopic signatures still showed a shift from equilibrium.

The presence of carbonic anhydrase is also considered to be important in reducing kinetic effects in biominerals (Weiner & Dove, 2003). As discussed above, this enzyme is integral to matrix proteins in some biominerals and may explain the species-specificity of stable isotope fractionation.

The concept of isotopic equilibrium deposition of material is complicated further with the presence of amorphous mineral phases such as amorphous calcium carbonate (ACC). If ACC is involved in the biomineralising process, the mechanisms surrounding the hydration and dehydration of these precursor materials become important with respect to isotopic equilibrium and remain to be fully understood (Aizenberg *et al.*, 2003).

1.3 Ontogeny and vital effects

Application of equilibrium equations to dynamic living systems is complicated by biological factors, of which some have been briefly discussed above. Ontogenetic effects encompass changes daily and seasonal changes throughout maturity through the life span of a biogenic system.

Some changes in the life stages of an organism, such as larvae to juvenile have represented a change in biomineralising strategy (Lowenstam, 1981). In the avian skeleton, Whitehead and Wilson (1992) described the onset of osteoporosis and the formation of medullary bone at sexual maturity of the animal and the resorption of bone Ca to produce eggshells. Bone mass decreased through the egg laying period and through ontogeny. Bone crystals in the mammalian skeleton also mature through the life of the animal and even after death (Legeros *et al.*, 1987). Spero and Lea (1993) hypothesised a change in mineralisation at the end of the life cycle of a species of Foraminifera that accounted for offsets in expected stable isotopic equilibrium values.

Change in the biological activity of the animal is inevitable through ontogeny. Early work by Zeuthen (1953) revealed the change in oxygen consumption as the animal grows. This is related to the change in metabolism which has been discussed for the mollusc shell (Sukhotin & Portner, 2001) and this has been shown to affect the isotopic composition of the animal (Goodwin *et al.*, 2003). Different metabolic rates also influence the organic distribution in mollusc shells

(Rosenberg *et al.*, 1989; Rosenberg & Hughes, 1991). Thus, if the organic component is closely involved with mineralisation, then the change in metabolism through ontogeny may have an effect on the structure produced and the resultant chemistry. Buening and Carlson (1992) showed changes in Mg content of brachiopod shells related to changes in growth rates and stages of maturity through ontogeny. Hintz *et al*. (2006) also reported the development of age-specific Mg/Ca ratios in forams. Chambers of forams were routinely sampled during ontogeny and enrichment periods of Mg were identified during growth. This observation led to the recommendation of using forams of similar size for palaeotemperature reconstruction. A similar recommendation was made by Spero and Lea (1996) following work on stable isotopic composition of Foraminifera. This study reported significant offsets from expected stable isotopic equilibrium values for carbonate related to variation in metabolic CO_2 through ontogeny and also recommended that studies should use similar sized specimens in palaeoclimate reconstruction. Purton *et al*. (1999; Purton-Hildebrand *et al.*, 2001) showed in molluscs that Sr concentration increased with age. This increase of Sr was related primarily to changes in metabolism through ontogeny as well as variation in growth rate and temperature. This emphasised previous observations in the mollusc shell where Sr was shown to be affected by metabolic rate (Klein *et al.*, 1996b).

Carbonic anhydrase (CA) has been discussed above as an integral component of shell production, with the presence of this enzyme thought to negate kinetic effects in stable isotope ratios. Medakovic (2000) showed that CA varied through different stages of shell development, specifically during larval stages with variation found within the mantle of adult shells often related to sexual maturity.

Further complications which can mask vital effects or environmental effects is the actual crystal structure produced. The mineral phase produced can also have an effect on the chemistry of the shell. As highlighted above, with respect to the coralline skeleton, the metastable form of $CaCO_3$, aragonite, accepts more Sr into the structure than calcite. If amorphous phases are present (Nassif *et al.*, 2005) then this may have an additional effect on the chemistry or isotopic signature.

Distortions in size and morphology of the crystals produced can also influence chemistry incorporation. In biogenic systems, the crystal lattice can be affected by the close association of organic material (Pokroy *et al.*, 2004; Pokroy *et al.*, 2006a; Pokroy *et al.*, 2006b; Pokroy *et al.*, 2006c; Pokroy *et al.*, 2007), the resultant crystal defects can change the dynamics of minor element incorporation. Lorens and Bender (1980) considered that variation of crystal surface area may permit Na incorporation into mollusc calcite.

1.4 Aims of this study

The application of environmental proxies to biominerals is often undertaken with little consideration to the factors discussed above which can complicate the resultant chemistry and isotopic signature of the biomineral produced. It is necessary to consider effects of ontogeny of a living system, the crystal morphology and polymorph produced, and the relationship this has on the ensuing skeletal chemistry. The aims of this study are to investigate these issues and establish any relationships between them in the context of ontogeny, and therefore the implications this has for other biominerals and the application of biogenic minerals as environmental proxies.

Mytilus edulis was selected for this study due to its bimineralic shell, comprising calcite and aragonite allowing investigation of both polymorphs. The two polymorphs display distinctive habits, with prismatic calcite and nacreous aragonite as described above, enabling investigation of crystal size and shape effects on the shell. An ontogenic range of specimens from 10 months old to 36 months old were selected and grouped into six age ranges to investigate variation through ontogeny. Ideally, the entire ontogenetic range would be considered but larval stages were not available restricting ontogenetic range to 10-36 months. The major advantage was that these farmed mussels all experienced the same environmental conditions and growth rate. Thus age could be determined from their overall size.

The details of the rearing, preparation and age classification are detailed in Chapter 2. The crystallographic data, trace element data and stable isotopic data for each stage of ontogeny are detailed in Chapter 3, 4 & 5 respectively.

1.5 Mytilus edulis

Blue Mussel – *Mytilus edulis* (Linnaeus, 1758)

Phylum – Mollusca

Class - Pelecypoda

Order – Mytiloida

Family – Mytilidae

Genus – Mytilus

Species - edulis

Mytilus edulis, the common mussel, also termed blue mussel, is ubiquitous in coastal waters around the British Isles and on the coasts of the Atlantic Ocean and South American coasts. Naturally occurring and farmed, these mussels are harvested for commercial use as well as research.

The mussel shell is a composite of biogenically produced calcium carbonate and proteins. The calcium carbonate assumes the form of two polymorphs: calcite and aragonite, which form the outer and inner layer respectively. A tough outer organic layer, the periostracum (Figure 1.3), provides protection and a nucleation surface for shell formation. Organic material is also found within individual crystals as well as providing a framework for the mineralised component.

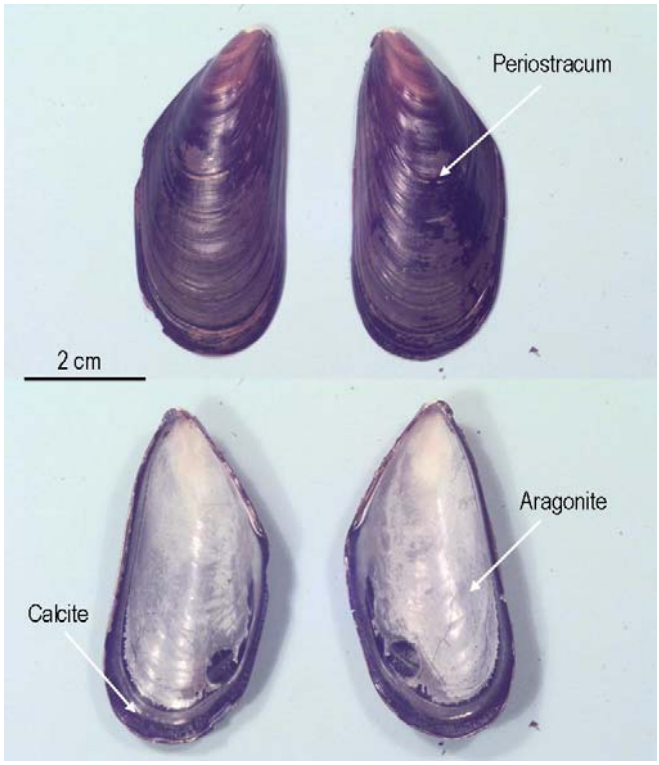

Figure 1.3 Photograph of *Mytilus edulis* specimen showing the outer (upper image) and inner (lower image) views of the valves. The arrows indicate the the periostracum and the two $CaCO_3$ polymorphs.

2

Materials & Methods

2.1 Specimen Collection & Preparation

2.1.1 Specimen collection

In this study, specimens of *Mytilus edulis* were sourced from a commercial mussel farm in Loch Etive (56°27'12.20 N, 5°17'26.63W) (Figure 2.1), a brackish water sea loch, where fresh waters derived from the Scottish highlands meet the salt waters of the open Atlantic.

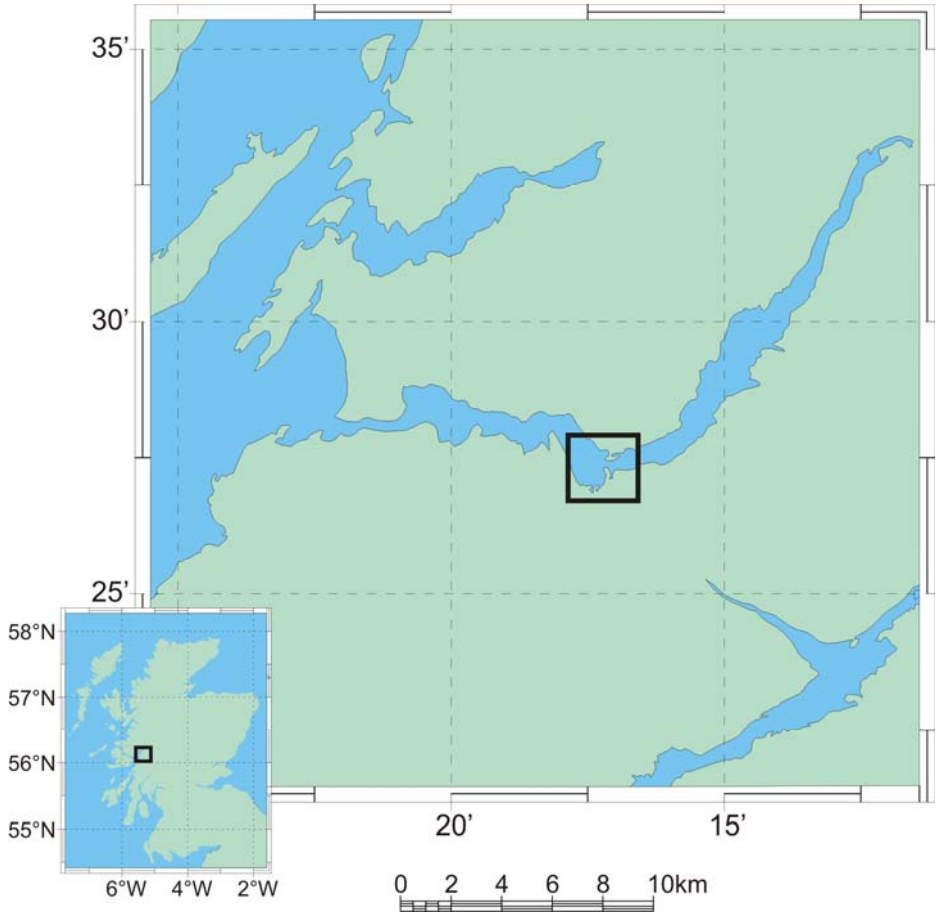

Figure 2.1 Sample collection site located on the shores of Loch Etive. Inset shows the location of the loch in Western Scotland.

The mussels were grown on lengths of rope constantly submerged in the loch waters with the rope lowered deeper into the water as each year, new larvae are added to the upper levels of the rope.

Mussel culturing on submerged ropes reduces tidal effects such as exposing the animal to the open air, creating a hiatus in growth and also reduces the effect of competitive growth typical of naturally occurring populations in inter-tidal zones. This also results in the shells of the farmed mussels in this study are thinner than that of naturally occurring mussels since thicker, robust shells are required in harsher environments such as inter-tidal areas.

On 15/03/05, 5kg of mussels from one rope, spanning <1cm-6cm in length, were collected and delivered to Glasgow University the same day for immediate sample preparation.

2.1.2 Specimen preparation

By measuring along the main anterior-posterior line, a range of 6 different length categories were selected (Figure 2.2): Group A (<1cm), Group B (1-2.5cm), Group C (2.6-3.5cm), Group D (3.6-4.3cm), Group E (4.4-5cm), Group F (5.1-6cm). These represent the age ranges 10-12 months, 12-14 months, 22-24 months, 24-26 months, 34-36 months and 36+ months respectively (J. Holmyard pers comm). This will provide sufficient range to observe changes through ontogeny. Ten specimens were selected for each group.

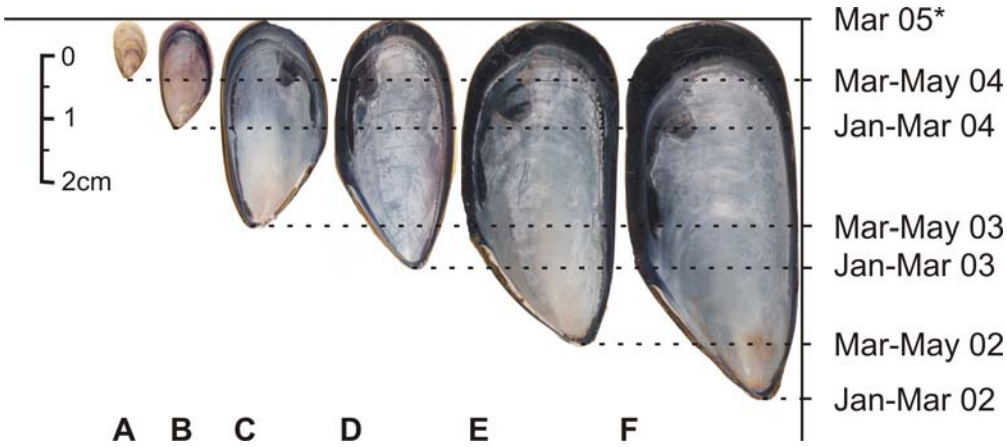

Figure 2.2 Mussel ontogenetic stages A-F. Dashed lines indicate the umbo region (first formed part of shell) and the respective dates for the beginning of growth for each ontogenetic stage. The collection date is marked with (*) and represents the most recent deposit of shell material at the posterior edge, which is the same for all stages. Note that all mussels were introduced to the sample site in May of each year, and that spat production occurred elsewhere.

Each mussel was cut at the main posterior adductor muscle by carefully inserting a scalpel in the opening between the two valves. A hypodermic needle and syringe was then used to collect extrapallial fluid from between the mantle (soft parts) and the inner shell surface taking care not to rupture the mantle and release blood into the system. Extrapallial fluid and soft tissue from individual mussels was separated and stored at -20°C. This processing was carried out on day of collection to ensure that all material was fresh.

The shells were then cleaned using dental tools and small brushes to ensure complete removal of all detrital material such as byssal threads, barnacles and larval mussels. The mussel shells were then transferred to an ultrasonic bath and cleaned using deionised water. These were then air dried and labelled. From each size range, ten mussels were prepared via this method; three mussels from each group of ten were used for analysis and the others held in reserve with some samples fractured and prepared for scanning electron imaging purposes (section 2.5). Each shell was cut using a rock saw along the anterior to the posterior line of section. One half of each shell was prepared for Electron Back Scattered Diffraction (EBSD) (section 2.3.2), Electron Probe Micro Analysis (EPMA) and Secondary Ion Mass Spectrometry (SIMS) analyses, the other half used for mass spectrometer isotopic analysis. Detailed accounts of the preparation for these techniques are described in section 2.2.2, 2.3.1, 2.4.3 & 2.4.2 respectively.

Prior to the work on the ontogenetic suite of samples, trials on sample preparation and analysis were performed on specimens obtained from a local fishmonger.

2.2 Electron Back Scattered Diffraction (EBSD) Analysis

2.2.1 EBSD background

Electron Back Scattered Diffraction (EBSD) has recently emerged as a significant tool in the field of materials science (Wright & Adams, 1991, , 1992; Adams *et al.*, 1993; Wright *et al.*, 1994; Schwartz, 2000). Following early work by Nishikawa & Kikuchi (1928b; 1928a) on diffraction patterns of electrons from crystalline sample surfaces, the development of an automated, *in situ* analysis technique, allowing determination of crystallographic information from materials, has been gradually developed through the last century (Alam *et al.*, 1954; Venables & Harland, 1973; Dingley, 1981; Dingley & Razavizadeh, 1981; Dingley, 1984; Schwarzer, 1997b, 1997a). However, EBSD application in biominerals has only recently been undertaken (Schmahl *et al.*, 2004; Griesshaber *et al.*, 2005; Schmahl *et al.*, 2005; Dalbeck & Cusack, 2006; Dalbeck *et al.*, 2006; England *et al.*, 2007; Griesshaber *et al.*, 2007; Schmahl *et al.*, 2007; Cusack *et al.*, (in press)). EBSD analysis is conducted in a scanning electron microscope (SEM) under vacuum with a specialised camera integrated with a phosphor screen detector. A stationary beam of high-energy electrons is directed at a polished, crystalline sample, tilted relative to the beam normal. The electrons then interact with the first few atomic lattice planes at the sample surface and, dependent on the Bragg function, are then diffracted from the analysed material. These diffracted electrons interact with the phosphor screen to produce distinct bands, termed ‘Kikuchi bands’, which consequently, create an electron backscattered pattern (EBSP) unique to that crystal lattice in a particular orientationn (Figure 2.3). This pattern is collected for each data point and can be used to

construct maps of orientation, texture and phase for a selected sample surface area (Schwarzer, 1997b, 1997a).

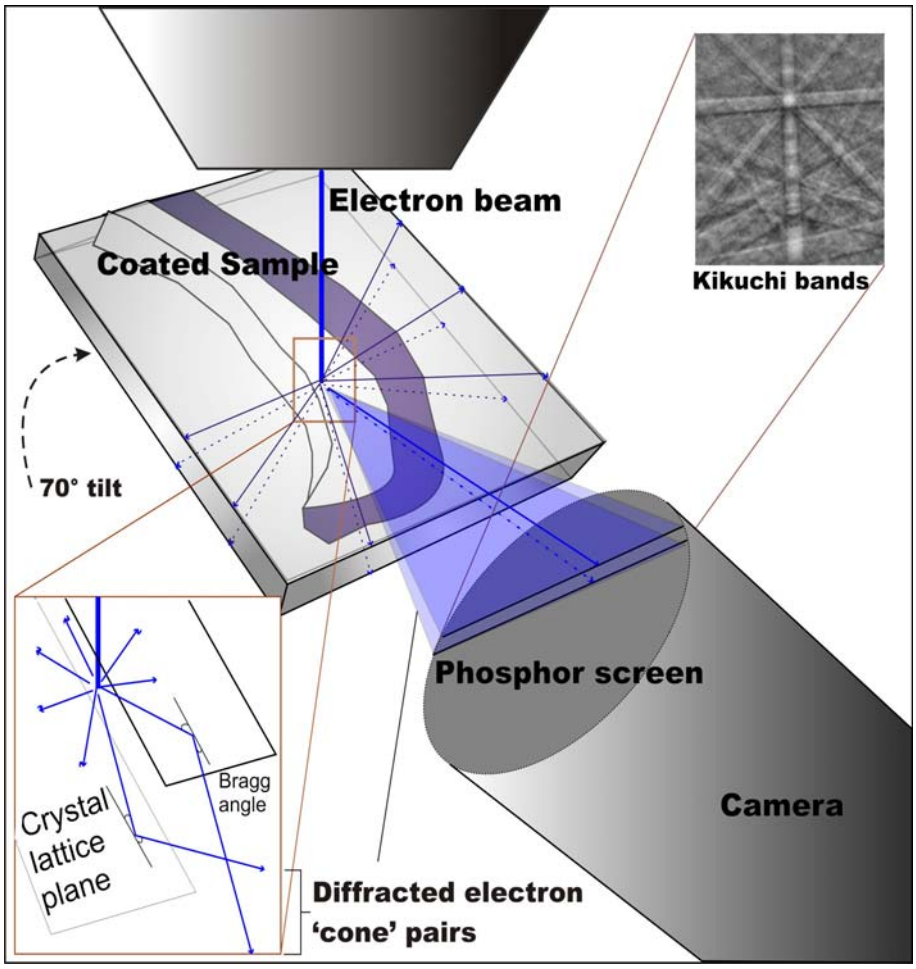

Figure 2.3 – Assembly for EBSD analysis. A polished and coated sample is tilted to 70° toward the phosphor screen. A focused electron beam is directed at the sample surface. Interaction of the electrons with the initial lattice planes (lower left inset) produces a flattened pair of diffracted electron cones. The cone pairs interact with the phosphor screen producing a diffraction (Kikuchi) band. These Kikuchi bands produce a pattern (upper right inset) used to determine crystallographic phase, texture and orientation.

An overview of the mineralogy and crystallographic orientation and texture of the material is enabled through various maps of material properties displayed as Orientation Imaging Microscopy (OIM) maps (Wright & Adams, 1992). The beam is scanned across the surface to produce point-to-point data which can be used to construct the OIM maps. From this, crystal orientation, grain misorientations, and phase identification are determined. Additionally, local orientation variations within a single crystal can be revealed.

2.2.2 Preparation of samples for EBSD analysis

Three specimens were selected from each ontogenic size range. Valves were cut into two halves as described in section 2.1.2, and half the valve used for EBSD analysis. The shell halves were mounted in Araldite resin blocks. To facilitate surface charge dissipation and to decrease the

working distance for EBSD, the size of the resin blocks was minimised as much as possible by cutting off excess resin. Specimens from group E (4.4-5cm) & F (5-6cm) were cut into 3 sub-sections after resin mounting. Specimens from group C (2.6-3.5cm) & D (3.6-4.3cm) were cut into 2 sub-sections. Specimens from group A (<1cm) & B (1cm-2.5cm) were kept fully intact.

EBSD is a surface analysis technique. In order to produce accurate diffraction patterns it is essential that the surface is completely free of topography and surface damage. The mounted samples are polished through a series of grinding and polishing discs. Initially the sample surface is ground down using diamond impregnated papers at 74µm and then 20 µm, diamond slurry at 8 µm and 6 µm are then used followed by a compound diamond pad at 6 µm and 3 µm. The polishing stages are performed with alpha aluminium oxide at 1 µm and 0.3 µm on with a final treatment with 0.06µm colloidal silica on a short nap disc. The colloidal silica stage is essential for EBSD analysis to remove any residual damage surface layers with local stress and deformity produced by the harder compound grinding and polishing (Prior *et al.*, 1999; Nowell *et al.*, 2005).

Carbonate materials are insulators and surface charging of specimens during EBSD analysis can result in weaker Kikuchi pattern quality. Silver paint is applied to the edges of the sample and used as a strong adhesive between the sample block and the aluminium stub providing a conduit for charge dissipation during EBSD analysis.

Carbon coating provided further reduction of excess surface charging. Coating thickness is critical with the requirements for a sufficiently thin coat to enable the diffracted beam to be backscattered while the carbon coat must be sufficiently thick to dissipate charge (Prior *et al.*, 1999). Coating in a carbon evaporator overnight to obtain a minimal coat produced the best results.

Preliminary assessment of conductive Buehler resin for mounting the samples indicated that the shells did not adhere well to the resin and therefore any potential benefits were lost. Shell samples embedded in regular Buehler Araldite resin used with silver paint and carbon coating was effective.

2.2.3 EBSD terminology

EBSD data and maps are interpreted and presented by way of confidence index (CI), fit, and image quality (IQ) of data points, misorientation, crystal orientation, pole figures (PF) and inverse pole figures (IPF) which are explained below.

Confidence Index (CI) of a data point is the reliability of an orientation solution produced during EBSD. This is calculated through the OIM analysis software during scanning of the sample. A number of structure file diffraction patterns may correlate with the Kikuchi pattern produced from

the scanned sample. Therefore, a ranking system using a voting scheme is required to select the best correlation. Confidence Index is calculated as follows (Field, 1997):

$$CI = \frac{(V_1 - V_2)}{V_{ideal}}$$

Where

CI - Confidence Index

V_1 - Number of votes for 1st diffraction solution

V_2 - Number of votes for 2nd diffraction solution

V_{ideal} – Total number of possible votes from detected bands

Multiphase materials produce separate CI calculations for the individual phases. The CI ranges from 0 to 1 with 1 being most desirable and points given as CI = -1 are omitted from the resultant maps.

Fit is derived by comparing the data to a 'best fit' prediction where the Kikuchi bands should appear referring to the voting system as used in CI calculation, and then quantifying the angle of deviation from that best fit for the diffraction pattern produced. Therefore, values closer to zero are desirable, showing smaller deviation from the best fit.

Image quality (IQ) of a data point refers to the intensity of the diffraction pattern produced from that point. Areas where the pattern is poor will be displayed as a darker area of an IQ map. Factors affecting the quality of an EBSD pattern in localised areas can be crystal inhomogeneity, organic presence, and crystal edges.

Misorientation can be used to describe the relative orientation between two neighbouring grains (Frank, 1988). Two differently oriented crystal lattices always have one crystallographic axis in common (Figure 2.4). Therefore, it is possible to describe this misorientation in terms of a common axis and the angle of orientation about that axis which will bring the two lattices into co-incidence. Grains misorientated more than a specified number of degrees from their neighbour, are distinguished on misorientation maps by different colours designated by the software.

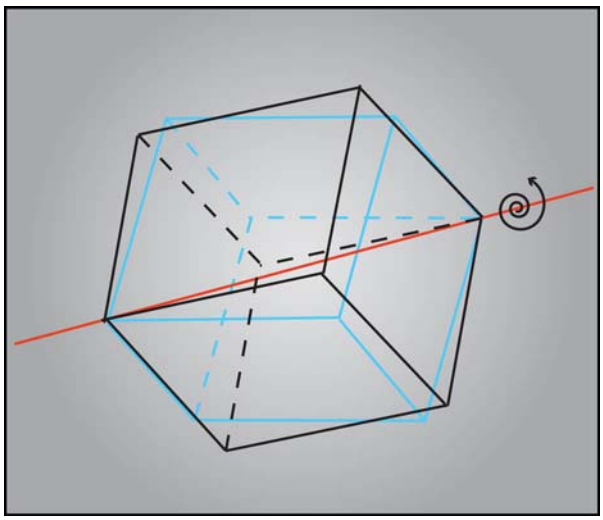

Figure 2.4 Misorientation of two crystal lattices rotated around a fixed common axis (marked in red). Misorientation is the angle of rotation around the fixed axis required to bring the two lattices into agreement.

Crystal orientation of the crystal lattice is displayed with respect to the sample reference frame. Orientation, Pole figure plots (Figure 2.5) and Inverse Pole Figure plots are all given with reference to three orthogonal reference directions; ND, normal direction (normal to the sample surface), RD, reference direction (parallel to the direction of sample tilt) and TD transverse direction (running horizontally across the sample surface).

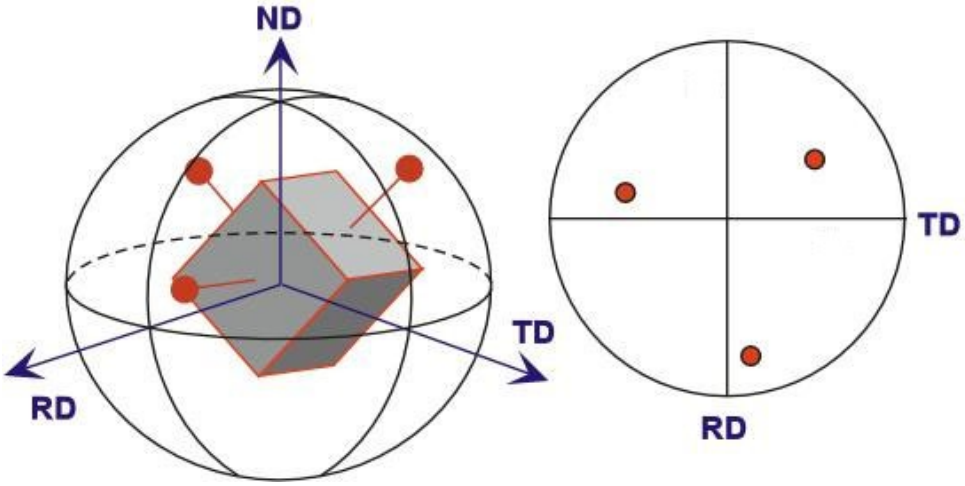

Figure 2.5. The three symmetrically equivalent planes of a cubic crystal in 3D space each produces a perpendicular pole to the crystallographic plane which plot as a single point on a hemispheric projection (left). This can be viewed as a 2-D stereographic projection (right) with ND perpendicular to the field of view. Taken from OIM User's Manual (Mahway, 2005)

Inverse Pole Figure (IPF) data are produced using the same reference frame with the crystallographic orientation reported here relative to Normal Direction (ND). Using this frame reference, crystal faces parallel to the field of view (poles normal to field of view) will be coloured according to the IPF colour key (Figure 2.6).

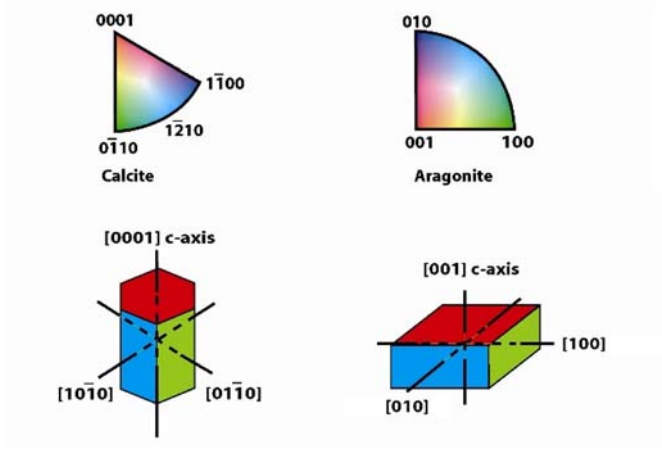

Figure 2.6 Inverse pole figure (IPF) colour keys (upper images) for calcite and aragonite with reference to the normal direction (ND). The respective wire frames (lower images) show a simplified view of the individual crystal faces of the unit cells and how they are coloured in an IPF map.

Use of the IPF triangle reduces the number of symmetrically equivalent planes that may be represented in a standard pole figure plot. For PFs and IPFs, crystal poles and planes are reported using Miller indices; {hkl} for aragonite, and {hkil} for calcite. Through these interpretation features of EBSD, *in situ* crystallographic information is collected, interpreted and presented in here.

2.2.4 EBSD analysis settings

EBSD analyses were carried out using a FEI Quanta 200F field emission scanning electron microscope (SEM) equipped with a TSL EBSD system running OIM software version 4 within the Department of Geographical & Earth Sciences at Glasgow University.

The angle of tilt is important for EBSD analysis. Nowell & Wright (2005) demonstrated the variation on Kikuchi pattern intensity at varying angles of tilt with a 70° angle producing optimal pattern intensity.

The phosphor screen camera control settings were set to collect the clearest Kikuchi patterns that could be quickly indexed, therefore producing a sufficient frame rate for quicker scans to be performed. The resolution of the camera screen (binning size) was set to 4x4. Exposures of 0.30s were used which resulted in varying frame rates of 4-6.5 frames per second. Scan rates were dependent on frame rate and step size and both are dependent on magnification of the scanning area. At lower magnifications, larger step sizes were employed to cover the areas. Smaller step sizes were used to produce high resolution maps at higher magnifications.

The distance of the sample to the electron gun, the working distance (WD), is another important factor in EBSD analysis. The optimum range was for pattern collection was established between 6-12mm.

Preliminary analyses were conducted on low vacuum mode but diffraction intensity was superior in high vacuum mode.

The beam aperture was set at size 4 with spot size 4 and an accelerating voltage of 20kV. This yielded a sufficiently strong beam but with surface charge effects minimised resulting in optimal Kikuchi patterns. Additionally, increasing the accelerating voltage thinned the Kikuchi bands facilitating pattern indexing and stronger signal production, resulting in increased scan rates. In samples where the carbon coating was too thin, settings were changed to aperture 3 to reduce sample charging.

The Kikuchi patterns were indexed using the OIM Data Collection database, which contains structure files of calcite and aragonite. Additional structure files for different calcite and aragonite lattice structures were obtained from the American Mineralogical Society of America crystal structure database for further indexing reference. The structure files were tested against a calcite and aragonite standard thin sections prepared using the above method of mounting and polishing. In testing the structure files, a confidence index of >0.5 and pattern fit of <2 over an average of 10 trial spot analyses was required to ensure accuracy of indexing. Hough parameters were set to a minimum peak magnitude of 2, minimum peak distance of 19, and peak symmetry of 0.80 and a binned pattern size of 120.

2.2.5 EBSD data analysis

EBSD data were interpreted and maps produced through OIM Analysis v4 software. OIM maps were subject to two clean-up algorithm procedures to ensure reliable data was displayed (Mahway, 2005). Grain Confidence Index (CI) Standardization was applied with a Grain Tolerance Angle of 5° and minimum grain size of 2 pixels and Neighbour Confidence Index (CI) Correlation of CI 0.2. Further partitioning of data was applied, with only grains of CI $\geq$0.2, Fit $\leq$2.9 and IQ $\geq$19 displayed in the resultant OIM map. This removed unreliable data from the final data set and individual data points not belonging to a neighbouring grain and points with unreliable confidence index were either removed or were related to the average orientation of neighbouring points and incorporated to that grain.

2.2.6 EBSD resolution

Beam diameters for a FEG source can achieve 2nm providing good spatial resolution with accurate indexing of grains ~10nm able to be identified. The accuracy of orientation determination depends on the angular resolution which is typically within 0.5-2° (Troost, 1993; Humphreys, 1999; Humphreys *et al.*, 1999; Humphreys, 2001, , 2004; El-Dasher & Rollett, 2005).

2.3 Trace Element Analysis

2.3.1 Sample preparation

The samples described in Section 2.2.2 for EBSD were also used for trace element analysis. These samples were reset in Araldite Buehler resin to create circular blocks which were repolished and recoated with carbon and then analysed using Electron Probe Micro Analysis (EPMA). Further treatment was required for Secondary Ion Mass Spectrometry (SIMS). The resin blocks were thinned to less than 1cm thickness and were then repolished and coated using a gold sputter coater. SIMS sample preparation is covered in further detail in Allison *et al.* (1996).

2.3.2 Electron Probe Micro Analysis (EPMA)

Electron Probe Micro Analysis (EPMA) allows non-destructive, fully quantitative analysis of trace element concentration of a material obtained through bombarding a specific micron-scale site of a sample with a focused electron beam (defocused for carbonates) and collecting the X-ray photons generated and emitted by the trace elemental species within the polished sample surface. The X-rays generated are characteristic of the emitting trace element species; the sample composition can then be identified by recording WDS spectra (Wavelength Dispersive Spectroscopy). WDS advantages over standard SEM/EDS (Energy Dispersive X-ray Spectroscopy) systems are increased sensitivity, analysis of light elements, spectral resolution and detector dead time (Maurice, 1979; Herrington, 1985). The risk of interpretation error to that of EDS is also reduced (Merlet, 1994; Newbury, 1998). As a result, the sensitivity of this method is at the level of ppm, elements in low concentrations are better detected and reproducibility to 1% can be obtained.

EPMA line analyses perpendicular to the line of section were produced using a Cameca SX50 Electron Microprobe operating at 15kV with a 10 nA current and using a 10 μm defocused beam. X-rays were detected from the sample surface through four wavelength dispersive spectrometers: TAP, LIF, TAP and PET crystals attached to the Cameca SX50. Matrix corrections used an online PAP correction procedure and provided a more accurate calculation of x-ray generation within the specimen. The electron microprobe was calibrated using mineral standards for Na (jadite: 11.3% Na, 27.8% Si, 13.2% Al, 0.2% Fe, 47.4% O), Mg (periclase: 60.3% Mg, 39.7% O), S (pyrite:

46.6% Fe, 53.4% S), Ca (calcite: 40.0% Ca, 12.0% C, 48.0% O), and Sr (celestite: 44.4% Sr, 16.7% S, 3.2% Ba, 0.1% Ca, 0.8% Si, 34.4% O). Some samples were calibrated for Mn & Fe analysis but derived totals were below the detection limit (see equation below) and were omitted from later analyses. Detection limits for each element in EPMA were calculated as follows:

$$\text{Detection limit} = \frac{3}{m}\sqrt{\frac{Rb}{Tb}}$$

m = counts/second/% element in the standard

Rb =counts per second on the background

Tb = count time on the background

Data errors for EPMA were calculated as follows:

$$\%\text{Error} = \frac{100}{\sqrt{T}\left(\sqrt{Rp} - \sqrt{Rb}\right)}$$

T = count time on the peak

Rp = counts per second on the peak

Rb = counts per second on the background

Background counting times were half of the count times on peaks, which were as follows: Na and Mg, 40 sec; Ca, 30 sec; Sr, 60 sec. Calculated detection limits are as follows: Na (0.023 wt%), Mg (0.027 wt%), S (0.033 wt%) and Sr (0.032 wt%). Some spot analyses for these elements in each specimen fall below detection limits but are included to retain continuity in each individual line traverse and comparisons between different areas of the samples.

The same sections used for EBSD analyses (section 2.3.2) were used in EPMA analysis; three specimens from each length category in the ontogenetic range used in this study. Line analyses were made in the umbo section, the mid section and posterior edge section of each specimen.

2.3.3 Secondary Ion Mass Spectrometry (SIMS) analysis

Additional trace element profiles for single specimens from stages A (<1cm) – E (4.4-5cm) were produced through SIMS analysis. SIMS is carried out by sputtering a polished, coated sample surface using a charged primary ion beam. The charge of the element being measured determines the charge of the ion beam used, with a negatively charged beam of O^- ions used for analysis of positive ionic species and a positively charged Cs^+ beam for negative species. The sputtered secondary ions ejected from the sample surface are accelerated through a double focusing mass spectrometer system for direct ion counting. This technique, the precision and the error corrections in carbonate analysis are covered in detail by Allison *et al*. (1996; 2005; 2007).

SIMS line analyses perpendicular to the line of section were carried out using a Cameca ims-4f ion microprobe with Charles Evans and Associates interface and computer control running Control-PXT v1.0. SIMS analysis was carried out at the School of Geosciences at the University of Edinburgh. Thin sections were analysed with a $^{16}O^-$ ion beam, accelerated at 14.5kV. The primary beam (O-) current was set at 5nA, and focused through electrostatic lenses to produce an image field of 25μm. An energy offset of 75eV was used to reduce the effect of interference species, a contrast aperture 3 was used to reduce angular spread of the ion beam and field aperture 3 was used to restrict the analysis area on the sample surface to ~8μm.

Trace element count rates for ^{26}Mg, ^{88}Sr and ^{23}Na are normalised to a reference species, in this case ^{44}Ca. Concentrations are then calculated relative to the carbonatite OKA standard of known composition.

EPMA and SIMS data were interpreted, graphs produced and trends determined using Microsoft Excel and Minitab v13.

2.4 Stable Isotope analysis

2.4.1 Conventional Mass Spectrometry

2.4.1.1 Preparation of samples for isotopic analysis

Corresponding valve halves from those analysed for crystallography and trace element were prepared for isotopic analysis through conventional mass spectrometry. The organic periostracum was removed using a variable speed mini-drill with a grinding wheel on the lowest rotation speed. Low drill speeds prevent over-heating of the drill and possible alteration of the crystal polymorphs. Samples were then collected by drilling the individual polymorphs at selected areas on the shell: the umbo (calcite and aragonite), the mid region (calcite and aragonite) and the very outer posterior edge of the shell (calcite). Aragonite was less abundant at the posterior edge and calcite was often worn away at the umbo region through previous mechanical or predation abrasion while the animal was alive. Scraping off material using a scalpel or razor blade was necessary where more delicate removal was required to avoid breaking the shell and contaminating the sample with the other polymorph. Larger mussels yielded 3-9mg of sample; smaller size ranges only yielded 0.5-2mg as thickness of the polymorph layers varied between specimens. Powdered samples were collected on aluminium foil and transferred to Eppendorf tubes.

Different methods of sample collection were assessed using test specimens before initialing the ontogenetic survey. Shell material was fragmented from the specimen using small dental tools to investigate any difference from that of drilling on the isotopic signature of the sample. The

difference was negligible and fragmenting the sample was time-consuming and increased the likelihood of cross-polymorph contamination. Test samples were collected via micromilling at the Scottish Universities Environmental Research Centre (SUERC). The size of the drill-bit was 0.25mm and did not allow any improved resolution across the shells which were 0.5 - 1mm thick. The time taken to obtain small sample sizes at the limits of mass spectrometer analyses was ineffective for a survey of this scale.

Samples between 0.2-2.5mg were carefully weighed into small glass buckets and transferred to a plasma asher. An oxygen plasma was set up under vacuum to cold burn and remove any organic matter from the samples for 20-24 hours to ensure an effective loss of organic material. Ashed samples were then reweighed immediately to determine the loss of organic material before being analysed in the mass spectrometer.

2.4.1.2 Isotopic analysis – Mass spectrometer

The isotopic analyses were carried out at the Scottish Universities Environmental Research Centre (SUERC) on a VG ISOCARB automated preparation system integrated with a VG ISOGAS PRISM II isotope ratio mass spectrometer. A modified version of McCrea's (1950) method was employed to determine the $^{18}O/^{16}O$ and $^{13}C/^{12}C$ ratios, with each individual sample (0.2–2.5 mg) reacted with 103% phosphoric acid (H_3PO_4) at 90°C to produce carbon dioxide (CO_2) which was then analysed. The mass spectrometer results for oxygen isotopes are corrected for isotopic fractionation between calcium carbonate and CO_2 using a fractionation factor ($10^3 \ln\alpha$) of 7.904 for the reaction with 103% H_3PO_4 at 90°C. Corrections were applied using the methods prescribed by Craig (1957) accounting for presence of ^{17}O and other interference in the system. Isotopic results are reported using the conventional δ‰ notation, with reference to the Vienna Pee Dee Belemnite (VPDB) international standard (Coplen, 1995; Gonfiantini *et al.*, 1995). Precision of each analysis was calculated through addition of internal laboratory marble (MAB2B) standards. The MAB2B standard was tested during analysis against the International Atomic Energy Agency's (IAEA) intercomparison material, IAEA CO-1, CO-2, CO-8 & NBS-18 producing acceptable values for the respective known compositions of the standards. For each batch of analyses, reproducibility between MAB2B standards for both $^{18}O/^{16}O$ and $^{13}C/^{12}C$ better than 0.1‰ at 1σ was required to ensure accuracy.

Individual analyses were replicated up to three times; the number of replicate analyses was dependent on the amount of sample available. A minimum of 0.2mg sample was required to obtain a reliable result which meant that triplicate analyses were not always possible in some samples. Variability between replicate analyses was, on average, <0.3‰ at 1σ. Higher incidences of variability in some sample replicates were attributed to possible remaining organic matter,

contamination within the shell structure, slight contamination between samples and occasional sample heterogeneity.

2.4.2 Isotopic analysis – SIMS Ion Probe

2.4.2.1 Preparation of sample for SIMS analysis

The same circular sample blocks used for Section 2.3.1 were used for SIMS stable isotope analysis. Each sample was highly polished to ensure the sample surface was optically flat with no relief. Samples were mounted as close to the centre of the blocks as possible. Areas within 2mm of the block edge could not be analysed. The resin blocks were reduced to 1cm thickness to decrease degassing time of the chamber prior to analysis. Samples were coated using a gold sputter coater.

2.4.2.2 Isotopic analysis - SIMS

Further isotopic analysis was carried out on a Cameca 1270 Ion Microprobe employing Secondary Ion Mass Spectrometry (SIMS). The Cameca 1270 allows *in situ* isotopic 'surface' analysis of solid targets by bombarding the sample with a charged ion beam with a diameter of several microns in the same technique as described for element analysis in section 2.3.3. This allows for improved spatial resolution in analyses and can analyse small volumes of material. Secondary Ion Mass Spectrometry (SIMS) bombards the surface of the sample, under vacuum, with a finely focused beam of primary ions (Cs^+, O^+, O^- or Ar^+). A collision cascade effect is produced with atoms and ions ejected from the sample surface. These secondary ions are accelerated into a double focusing mass spectrometer where they are separated according to their energy and mass/charge ratio before being detected.

The advantages of SIMS over conventional methods have been described in detail by Treble *et al.*(2007). Only minute quantities (1-2ng) of sample are removed by beam damage for each spot analysis, spatial resolution is greatly improved and allow accurate measurement of $\delta^{18}O$ in conjunction with minor element profiles from further *in situ* analyses such as the EPMA and SIMS trace element data described in section 2.3. However, the precision obtained in SIMS is generally lower than that obtained through conventional mass spectrometry (Treble *et al.*, 2005).

Stable oxygen isotope data were acquired at the University of Edinburgh with a Cameca ims 1270, using a ~5 nA primary $^{133}Cs^+$ beam and charge compensation by a normal-incidence electron gun. Secondary ions were extracted at 10 kV, and $^{18}O^-$ (~8.0 x10^6 cps) and $^{16}O^-$ (~4.0 x10^9 cps) were monitored simultaneously on dual Faraday cups. Each analysis involved a pre-sputtering time of 60 seconds, followed by data collection in two blocks of five cycles, amounting to a total count time of 45 seconds. To correct for instrumental mass fractionation (IMF), all data were normalised to an internal standard, University of Wisconsin Calcite (UWC $\delta^{18}O$ 23.28 ±0.06‰ VSMOW, J. Valley

pers comm.), which was assumed to be homogeneous and was measured throughout the analytical sessions. The internal precision of each analysis is +/- 0.2 per mil.

External reproducibility is shown through repeated analysis on the UWC standard of known composition (Figure 2.7). Variations greater than ±1‰ can therefore be discussed with respect to the profiles produced from the sample.

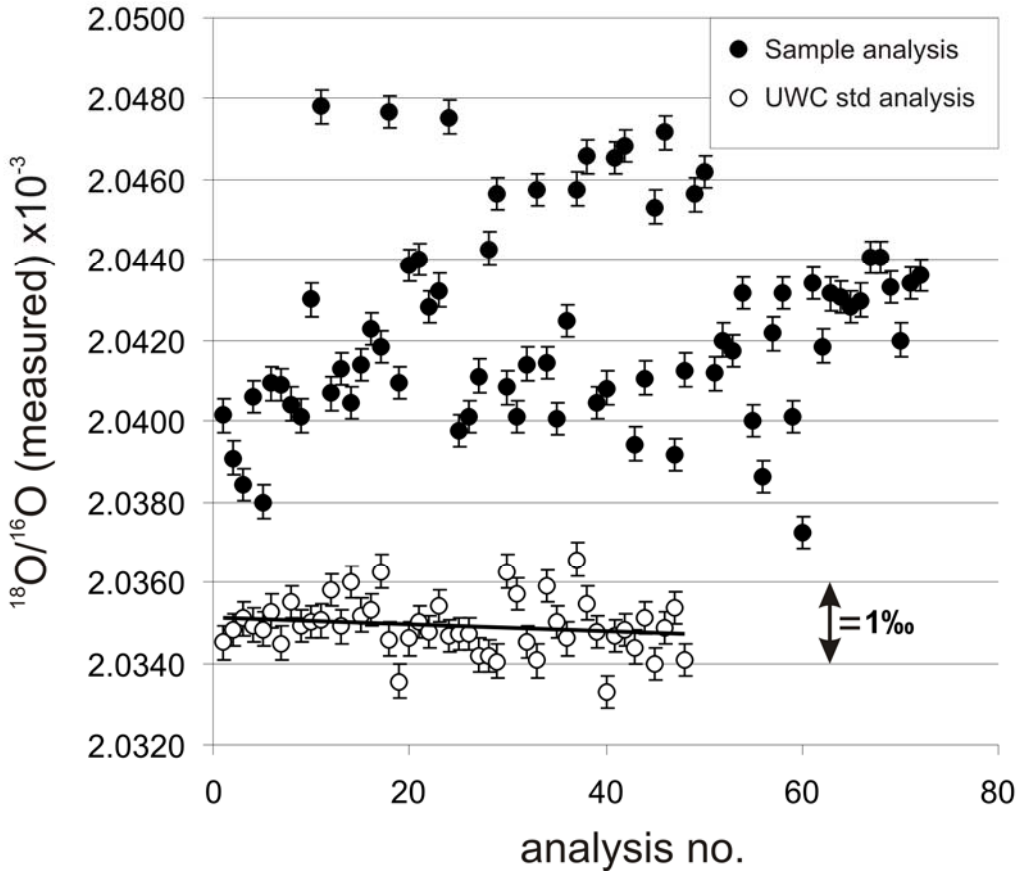

Figure 2.7 External precision for SIMS isotopic analysis. Sample analysis (n=48) and UWC standard (n=72) for a single SIMS session. Variations in the sample analysis greater than those on the homogenous UWC standard shown here can therefore be discussed.

Line scans perpendicular to the line of section were conducted using evenly spaced point analyses. Three line traverses were produced in three sections of the shell; umbo, mid region and posterior edge for a specimen from the A stage (<1cm) and C stage (1.6-3.5cm) of ontogeny. Three line traverses were also produced from the umbo region of a specimen from the F stage (5-6cm) of ontogeny. Profiles of $\delta^{18}O$ isotopic variation were therefore produced through the shell thickness. Stable isotopic ratios are reported using the conventional δ‰ notation, with reference to the Vienna Pee Dee Belemnite (VPDB) international standard (Coplen, 1995; Gonfiantini *et al.*, 1995).

2.4.3 SIMS vs Conventional offset

An offset was observed between the SIMS data and conventional mass spectrometry data consistent with other reported offsets for carbonate analysis (Rollion-Bard *et al.*, 2003). The offset can be accounted for through differences in trace element composition between the sample and the UWC standard. This affects matrix corrections in the SIMS technique. Data have been presented with the SIMS mean and the conventional mean displaying the offset. Discrete offsets are produced for calcite and aragonite accounting for the different trace element composition of the polymorphs.

2.4.4 Isotopic equilibrium calculation

To assess relationships between the stable isotopic signature of the carbonate and the surrounding water, a range of isotopic equilibrium was determined. Water temperature and salinity measurements spanning the growing period of the mussels (March to October) were taken from work by Stirling & Okumus (1995) conducted on Loch Etive. Salinity was used to calculate $\delta^{18}O$ values for the seawater using equation published by Austin & Inall for west coast Scottish waters including Loch Etive (2002):

$$\delta^{18}O_{water} = 0.18*S - 6.0$$

where S is the salinity of the loch water per mil (‰)

Values of $\delta^{18}O_{water}$ and the respective water temperature, T, were used to calculate a predicted range of equilibrium values for $\delta^{18}O$ of calcite and aragonite using equations published by Epstein *et al*. (1953) and Grossman (1982) respectively:

$$\delta^{18}O_{(calcite)} = \delta^{18}O_{(water)} + \left(\left[4.38 - \sqrt{19.18 - 0.4(16.9 - T)}\right] / 0.20\right)$$ (Epstein *et al.*, 1953)

$$\delta^{18}O_{(aragonite)} = \delta^{18}O_{(water)} + \left(\left[4.56 - \sqrt{20.79 - 0.76(20.19 - T)}\right] / 0.38\right)$$ (Grossman, 1982)

This produced a mean expected equilibrium value of -1.13‰ $\delta^{18}O$ for calcite and -0.32‰ $\delta^{18}O$ for aragonite. This produces an offset of ~0.8‰ $\delta^{18}O$ between the polymorphs which has been reported in previous studies, with aragonite enriched in $\delta^{18}O$ relative to calcite (Tarutani *et al.*, 1969; Rye & Sommer, 1980; Grossman & Ku, 1986; Rahimpour-Bonab *et al.*, 1997).

2.5 SEM imaging

Single specimens from the reserved samples not used in further analysis as described in section 2.1.2 were selected for imaging purposes. These were fractured, etched for 30 seconds in 10% HCl acid and mounted directly onto an aluminium stub using carbon adhesive and silver paint. These

were then gold coated for use in the FEI Quanta FEG scanning electron microscope using spot size 4, aperture 3 and an accelerating voltage of 20kV.

Imaging on the sample blocks used in EBSD, SIMS and EPMA analysis were performed using scanning electron microscope imaging with the same conditions as above. The sample blocks were coated using a carbon evaporator prior to image acquisition.

3

Ultrastructure in the context of ontogeny

3.1 Introduction

Biogenic carbonates comprise the largest proportion to the biosphere's carbon contribution, and is therefore of great significance for ocean chemistry (Berner *et al.*, 1983; Longhurst, 1991; Watson & Liss, 1998). In conjunction with this, Lowenstam (1981) discussed the importance of Ca-bearing minerals in biogenic systems and that they are the most abundant biominerals produced. Further to this is the exquisite control exerted by carbonate secreting systems to produce specialised structures tailored to a variety of functions as well as providing structural strength and durability. Therefore the importance of understanding how calcareous marine shells are constructed has implications for understanding biomineralisation and oceanic and global chemistry.

Ultrastructural analysis of biomineralised carbonate structures offers valuable insight to how these constructions are arranged, nucleated and grown to produce designs tailored to specific functions with optimal efficiency. In order to advance our understanding of the processes involved in carbonate biomineralisation it is necessary to determine the variety of mechanisms through which these mineralised fabrics are produced. This requires investigation into nucleation and growth of biominerals and the control exerted on the resultant crystal morphology and polymorphism. This process can be complex as environmental variation also influences the production of carbonate biominerals (Lowenstam, 1954; Dodd, 1964, 1966). This is further complicated by the effect that may occur through the animal's life and how biological variation in a dynamic system can affect biomineral production. Ontogenic effects on mineral structure have been investigated in other carbonate biominerals previously (Lowenstam, 1981; Legeros *et al.*, 1987; Whitehead & Wilson, 1992) and have been outlined in Section 1.3. This study aims to further the understanding of the role of ontogeny in biomineral production.

The ultrastructure of the shells encompassing six ontogenetic stages of the blue mussel *Mytilus edulis* is reported in this study. Ultrastructure was determined using secondary electron microscopy (SEM). Specifically, secondary electron imaging to view structures and electron back scatter diffraction (EBSD) to identify polymorph distribution and crystallographic orientation. *Mytilus*

edulis contains two polymorphs of calcium carbonate, each of which is produced in a distinctive crystal morphology. The mussels were selected from a Scottish sea loch and therefore have experienced the same environmental conditions. All the mussels were selected from the same location, a mussel farm, at the same time and were prepared in an identical manner (section 2.1). By selecting specimens from a single location where the shells will have been produced in similar environmental conditions through growth, and therefore any ultrastructural differences based on ontogeny alone can be assessed.

The ultrastructure of each specimen was analysed through *in situ* quantitative Electron Back Scatter Diffraction (EBSD) in an SEM. Mapping areas were carried out on the umbo region, mid section and the posterior edge on each shell cross-section. The data is presented as inverse pole figure maps, pole figure plots (section 2.3.1) as well as imposed wire frames representing crystal axis directions to establish correlations between each stage of ontogeny and the resultant crystal morphology and overall structural texture.

3.2 Previous work

The control exerted in producing biomineralised carbonate structures has been of great interest for materials scientists as the structures are produced using simple materials yet produce highly specialised structures (Weiner *et al.*, 2000).

The molluscan shell structure including that of *Mytilus edulis* has been investigated for over a century with pioneers in the field such as Carpenter (1848), Schmidt (1923) and Böggild (1930) describing molluscan shell microstructures and textures. More recent widescale investigations have been made by Taylor *et al*. (1969), Wilbur & Saleuddin (1983) and Chateigner *et al.* (2000). These found the molluscan shell structure to be a composite material consisting of matrix material and polycrystalline of calcium carbonate, $CaCO_3$, normally with the crystal c-axes showing a preferred alignment (Watabe, 1981).

The shell of *Mytilus edulis* is composed of two main polymorphs of $CaCO_3$; calcite and aragonite. The calcite prismatic layer which forms the outer layer has been investigated previously in a number of studies (Kobayashi, 1969; Carriker *et al.*, 1980; Nakahara *et al.*, 1980; Pojeta *et al.*, 1987; Feng *et al.*, 2000b; Checa *et al.*, 2005) with both the mineral phase and the associated organic framework of this layer considered. Aragonite forms the nacreous layer which has been subject to intensive study due to the fact that it is restricted to the Mollusca but also because of control involved and the resultant material properties (Jackson *et al.*, 1988; Addadi & Weiner, 1997; Feng *et al.*, 2000a). In bivalves, nacre forms a distinct brick and mortar-style (Watabe, 1965a; Weiner & Traub, 1984) construction, called “treppen pattern” (Schmidt, 1923) which has

been investigated in bivalved molluscs (Wada, 1961; Wise, 1970b) and grows in a terraced arrangement with the lowest tier of the terrace protruding as the growth front of the nacre down the shell length (Erben & Watabe, 1974; Checa *et al.*, 2006). Similarity in the growth of mollusc gastropod nacre has also been investigated with the arrangement of nacre found to be in conical stacks with a central c-axis alignment penetrating the height of the stack (Wada, 1961; Wise, 1970a; Manne *et al.*, 1994). Individual nacre tablets are shown to grow through screw dislocation (Wada, 1960; Wise & Devilliers, 1971; England *et al.*, 2007).

The orientation of calcite and nacre has been investigated via a variety of techniques (Manne *et al.*, 1994; Schaffer *et al.*, 1997; Feng *et al.*, 1999; Feng *et al.*, 2000b; DiMasi & Sarikaya, 2004; Checa & Rodriguez-Navarro, 2005; Cartwright & Checa, 2006; Dalbeck *et al.*, 2006) and each demonstrate that the c-axes are aligned in both gastropod and bivalve nacre but show differences between the alignment of the a- and b- axes. Investigations into correlating this with the organic matrix to suggesting a hetero-epitaxial growth model between organic and mineral have been undertaken by Weiner and Traub (1980; 1984) and others (Addadi & Weiner, 1986; Addadi *et al.*, 2006) but the extent of the need for continued renucleation on an organic substrate has been debated, (Manne *et al.*, 1994; Schaffer *et al.*, 1997; Hou & Feng, 2003; Checa *et al.*, 2006; Dalbeck *et al.*, 2006) suggesting that a mineral-mineral epitaxial growth mechanism may be an equally important growth strategy in nacre. The orientation of both calcite prisms and aragonite has also been investigated for mechanical strength (Feng *et al.*, 2000b) and promotion of nucleation and growth between the two polymorphs (Feng *et al.*, 2000b; Thompson *et al.*, 2000; DiMasi & Sarikaya, 2004).

The development of *Mytilus edulis* from the organic larval stage to the point of mineralisation has been investigated in a number of studies. *Mytilus edulis* shells develop from larvae consisting wholly of protein and organic material (Bayne, 1976). The individual stages of the *Mytilus* larval development has been summarised by Sprung (1984) with the initial mineral development discussed by Humphreys (1969) and other studies in mollusc larval mineralization (Kniprath, 1980, , 1981; Weiss et al., 2002). These indicate that the selection of polymorph may be more erratic in the initial stages of shell development than in later stages which will be investigated in this study.

The mineralogy of *Mytilus edulis* has also been assessed as an environmental indicator. The proportions of calcite and aragonite in *Mytilus edulis* shells has also been previously investigated as possible indicators of changes in temperature, salinity and latitude (Lowenstam, 1954; Dodd, 1964, , 1966) and productivity levels (Hubbard *et al.*, 1981). This study will develop further insight into this through determining any mineralogical variation between specimens collected at the same locality which have experienced similar environmental conditions.

3.3 Results

3.3.1 Phase proportions and overall structure

In each size range in the ontogenetic survey (Figure 2.3) the general structure comprising an outer layer of calcite and an inner layer of aragonite is apparent in the umbo, mid and posterior edge region of the shells with minimal or absence of aragonite at the growing posterior edge. Figure 3.1 shows phase maps obtained by electron back scatter diffraction (EBSD) of single specimens from each ontogenetic stage highlighting the dual-layered structure maintained through the shell. The thickness of both polymorph layers varies between specimens in each of the regions analysed with some specimens showing a thinning or absence of calcite in the umbo region with consistent thickening of the calcite layer towards the shell posterior.

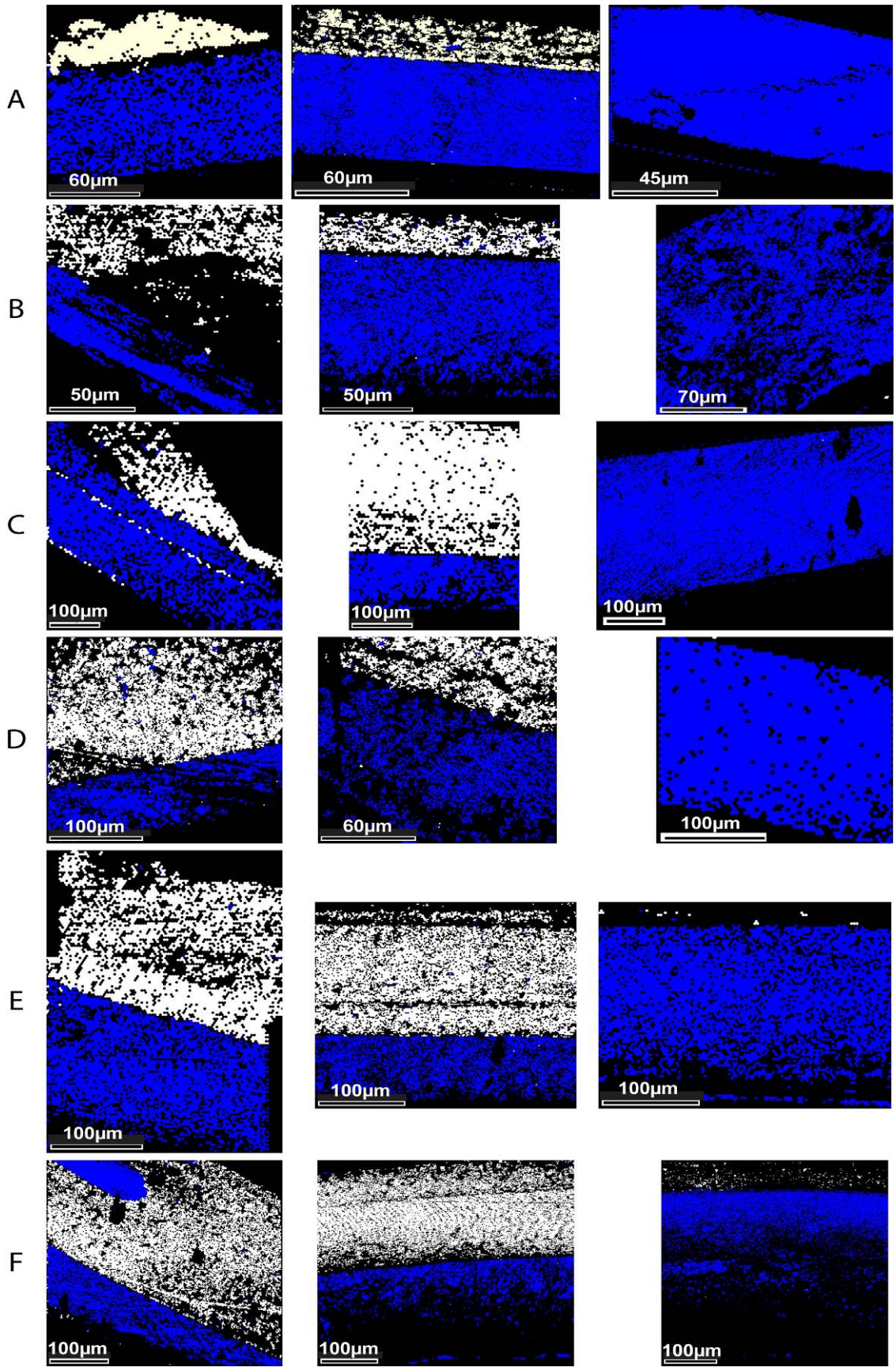

Figure 3.1 Phase maps showing the calcite (blue) and the aragonite (white) polymorph phases for the umbo (left), Mid section (centre) and posterior edge section (right) for the 6 stages of ontogeny A (top) to F (bottom). For all maps, the outer surface of the shell is to the bottom

In the majority of specimens, the dual-layered arrangement of polymorphs is well defined throughout the shell structure. However, the umbo section from the F range in Figure 3.1 shows that lenses of one polymorph can protrude into the other. This occurrence is observed in other specimens through ontogeny. An erratic distribution of calcite and interspersion with aragonite in the umbo region while loosely maintaining the outer layer of calcite and inner aragonite layer structure as shown in Figure 3.2

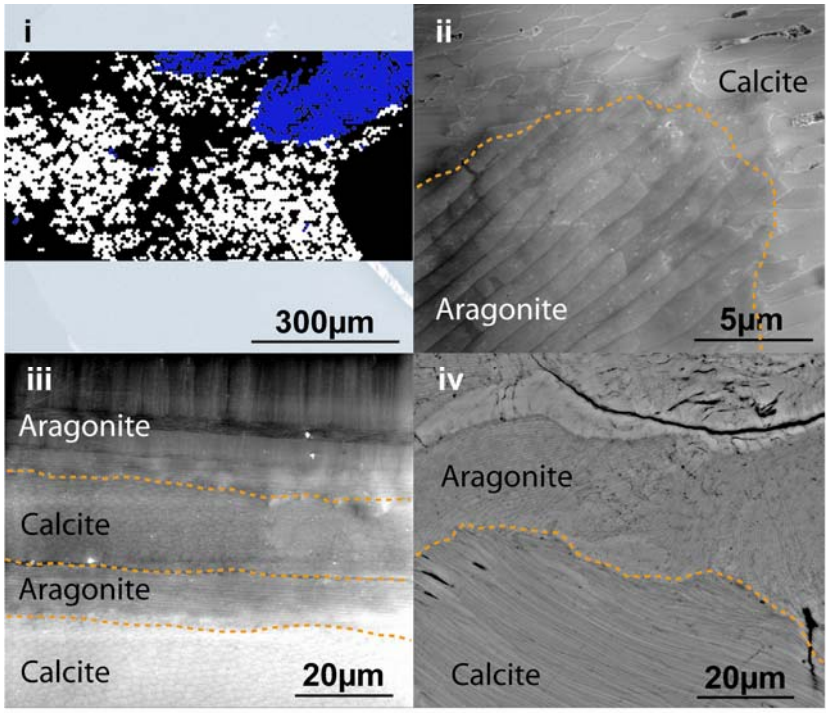

Figure 3.2 i - EBSD phase map of a specimen umbo, aragonite highlighted as white and calcite shown in blue. ii, iii, iv – scanning electron microscope (SEM) images of areas of distorted polymorph interfaces. The orange dashed lines show the polymorph interfaces.

Figure 3.2 shows undulating boundaries between the two polymorphs in the umbo region that are not seen in the rest of the shell in any stage of ontogeny. A section from the umbo of a specimen from the C stage of ontogeny (2.6-3.5cm) is displayed as an EBSD phase map in Figure 3.2i. This shows aragonite (white) that persists from the innermost to the outermost surface of the shell punctuated by two lenses of calcite (blue) protruding into the aragonite. These lenses are common in the umbo region and Figure 3.2ii and 3.2iv show two of these lenses and how the two polymorphs are juxtaposed. Figure 3.2iii shows an alternation between the two phases producing a multi-layered structure of varying layer thicknesses and crystal morphologies. However, such multi-layered structures are rare and were only observed in a couple of specimens from the entire ontogenetic set.

3.3.2 Crystal habit

3.3.2.1 Calcite

The crystal habit of calcite and aragonite retains, for the most part, uniformity through the shell in all stages of ontogeny. Figure 3.3 shows the common calcite habit through the shell with calcite prisms extending from an outer organic coating, the periostracum (P), toward the inner surface of the shell. The long axes of the prisms are normally inclined towards the polymorph interface/outer shell surface.

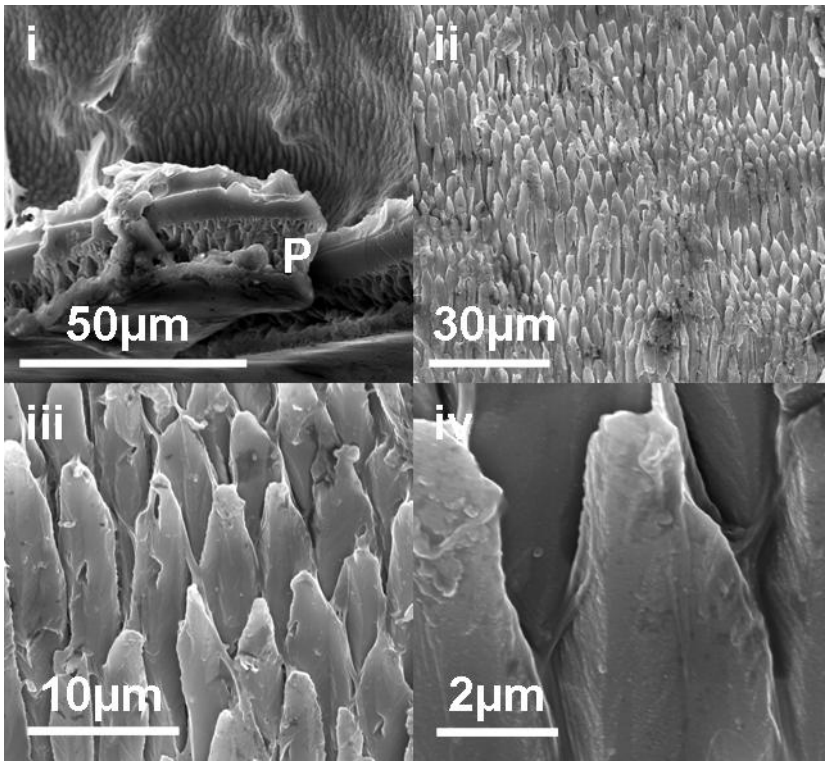

Figure 3.3 Scanning electron microscope images of fractured surface in the shell profile of *M. edulis*. i – the outermost calcite with the periostracum, the organic outer coating of the shell indicated 'P'. ii – clusters of needle-like calcite prisms uniformly oriented toward the shell interior. iii & iv show increasing detail of the individual prisms. The interior of the shell is to the top in each image.

However, variation is observed in each layer and especially in the umbo region of all stages of ontogeny which can also be observed in Figure 3.4 where different crystal morphologies can be observed in the same area. Figure 3.5 shows further evidence for differences in habit of the calcite in the umbo region of the shells in each stage of ontogeny.

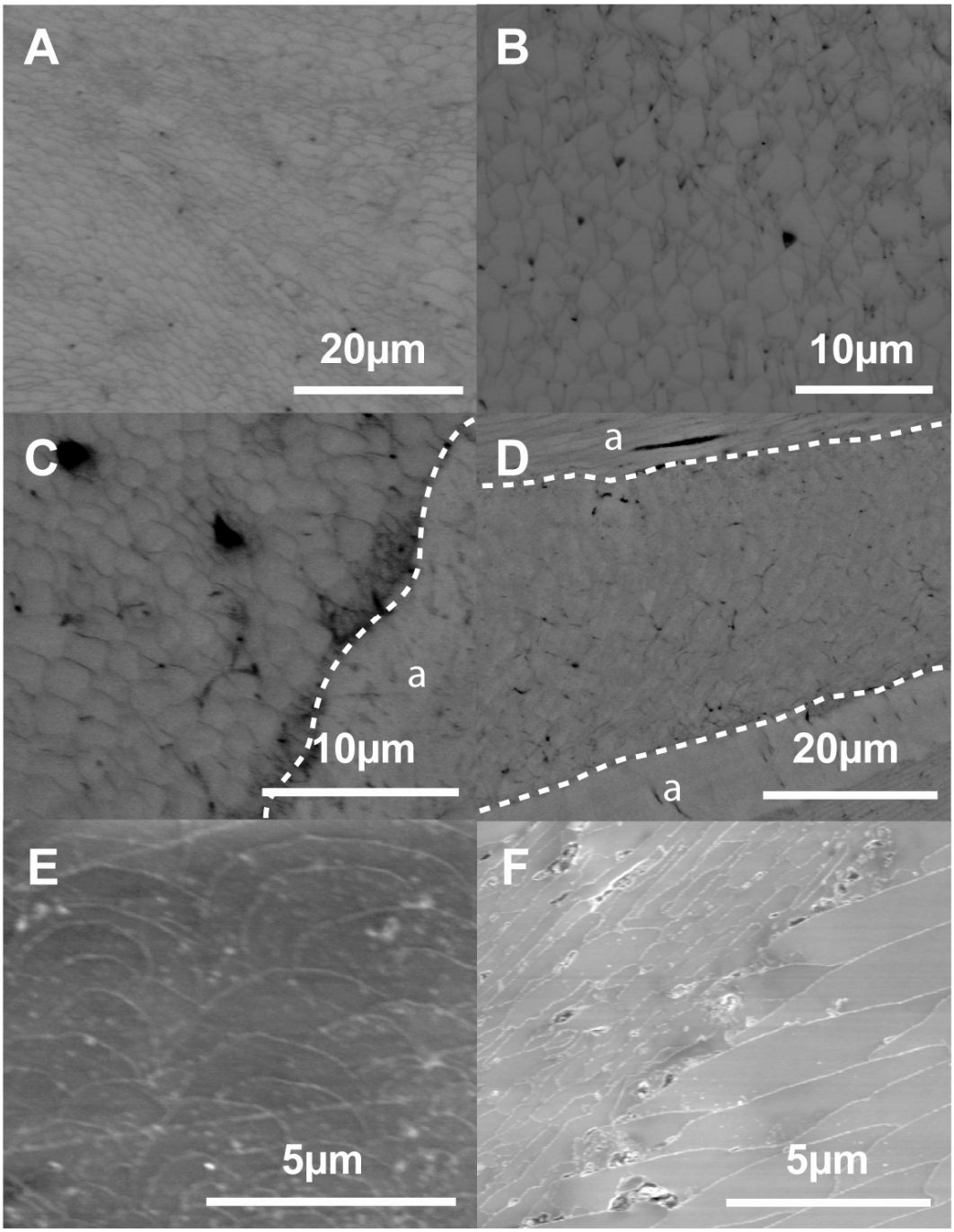

Figure 3.4 Scanning electron microscope images of variation in calcite size and shape in the umbo region of all the ontogenetic stages (A-F). The white dashed lines indicate boundaries with aragonite (a).

Each stage shown in Figure 3.4 displays size variation of the calcite crystals as well as variation in the general crystal shapes over a small area in the umbo. In the rest of the shell structure a similar distortion can be seen in the outermost calcite near the periostracum boundary at the outer surface of the shell which also shows crystal shape distortion and size variation (Figure 3.5) compared with calcite crystals nearer the polymorph interface where the morphology appears very uniform and tightly constrained with the calcite crystal shapes very well defined in Figure 3.6.

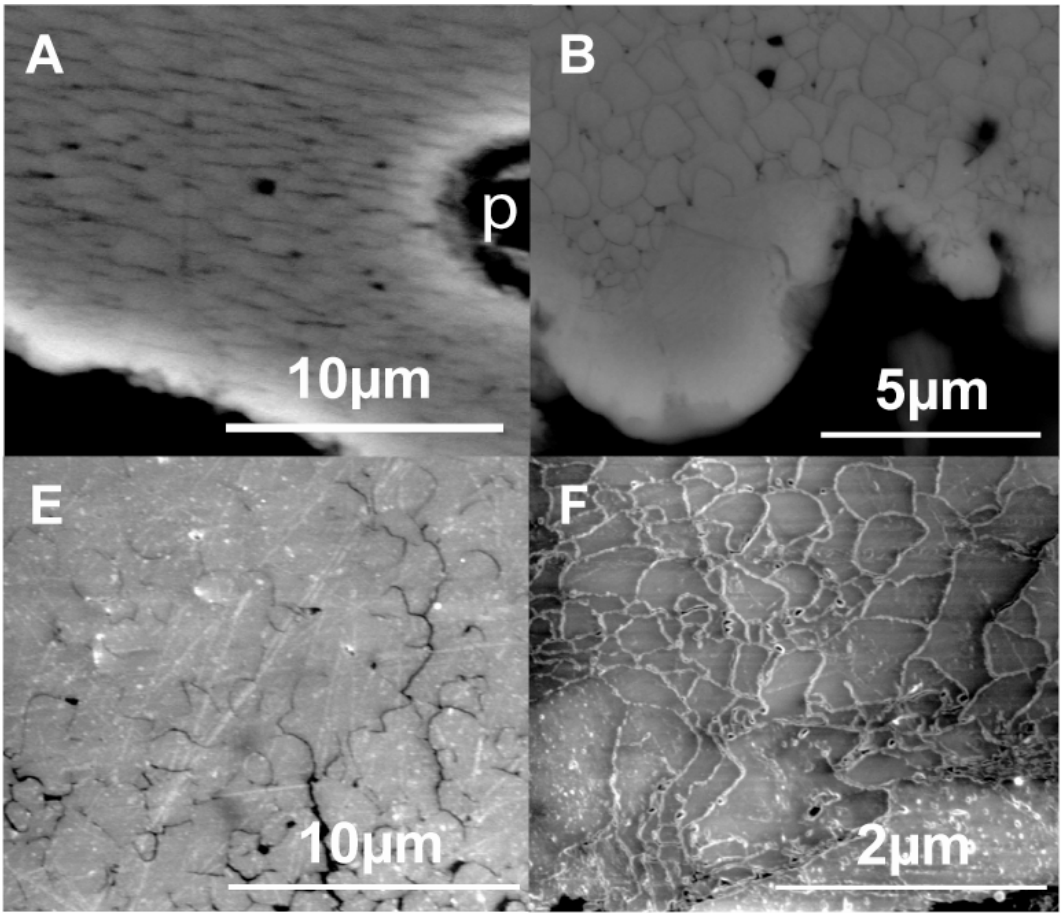

Figure 3.5. Scanning electron microscope images of the outermost calcite in 4 of the ontogenetic stages, A, B, E & F. Distinct variation of calcite shape and size at the outer edge of the shell (bottom of each image).'p' indicates an electron microprobe analysis spot.

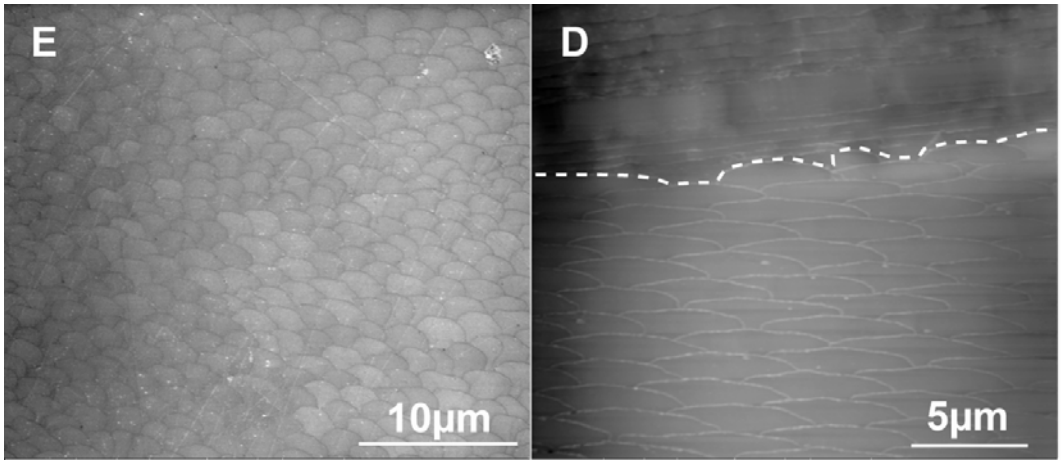

Figure 3.6 Scanning electron microscope images from the D and E stages showing uniform calcite shape and size within the calcite layer (E) and at the polymorph interface (D).

The outermost calcite appears to be considerably less well structured (Figure 3.5) than subsequent calcite. No discernable crystal shape can be distinguished which contrasts with the regular calcite crystal shape and structure especially viewed at the interface (Figure 3.6). Figure 3.7 shows more regularity and uniformity in calcite habit in the posterior edge section of each of the shells. This is

present in all stages of ontogeny with the calcite crystals becoming more steeply inclined than previously observed in the rest of the shell.

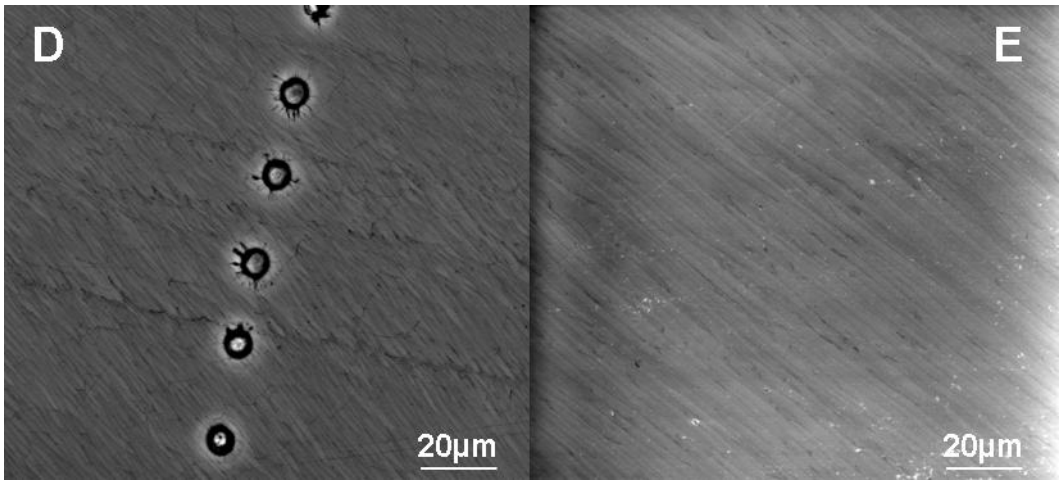

Figure 3.7 Scanning electron microscope images from the D and E stages showing uniform calcite shape and size within the calcite layer at the posterior edge. The calcite crystals all appear more steeply inclined than in the umbo and mid region. The large holes in the left image are electron microprobe analysis spots.

3.3.2.2 Aragonite

The aragonite shows greater variation in morphology with both nacreous and prismatic morphology present in each ontogenetic stage, with varying proportions in different areas of the shell (Figure 3.8).

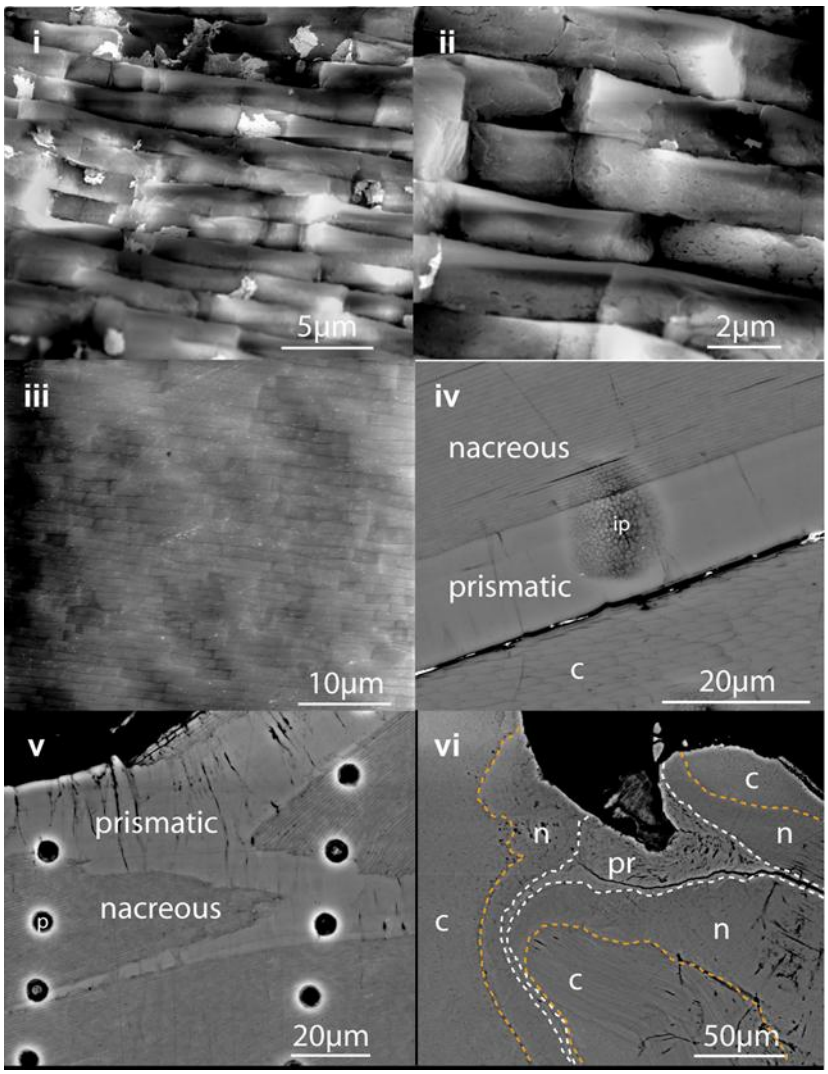

Figure 3.8 Scanning electron microscope images of variation in aragonite habit. i, ii & iii - nacreous aragonite and uniformity between each layer of tablets. iv & v - prismatic aragonite and nacreous aragonite. vi - aragonite at the umbo, with irregular prismatic aragonite bounded by the white dashed lines and nacreous aragonite in contact with calcite at the orange dashed lines. ip and p indicate damage spots from ion probe and electron microprobe analysis respectively.

Figure 3.8 shows the different morphologies of aragonite within the shell. The highest amount of variation in crystal habit is observed in the umbo region as shown in Figure 3.8vi where fine nacreous tablets of aragonite occur with prismatic aragonite, which also shows irregularity in the crystal habit. The nacreous tablet morphology of aragonite is the most common through the shell and, away from the umbo region, shows uniformity in size and shape with only some variation in

the thickness of the tablets from those closest to the polymorph interface which are <1µm thick while the tablets in the majority of the nacreous layer are 1-1.5µm thick. The occurrence of prismatic aragonite is most abundant in the umbo region of the shell with thick bands formed within the nacre. Away from the umbo, bands of prismatic aragonite, 10-15µm thick, occur often close to the polymorph switch as seen in Figure 3.8iv. These bands of prismatic aragonite persist along the length of the shell posteriorly, maintaining proximity to the polymorph interface which can be observed in all stages of ontogeny.

3.3.3 Crystal orientation

To observe possible changes in crystal orientation, each stage of ontogeny is observed through analysis of the umbo region, mid region and posterior edge region of the shell. The variance of the crystal habit discussed above corresponds with increased variance in orientation nearer the umbo, greater variation in crystallographic orientation occurs for the calcite and the aragonite and generally more uniformity prevailing towards the posterior in all stages of ontogeny.

3.3.3.1 Umbo region

The umbo region is the first formed part of the shell and investigation of the crystal habit has revealed greater variation in crystal shape and morphology than other regions of the shell. Variation in crystallographic orientation is also observed in this region through different stages of ontogeny. Figure 3.9 reveals the patchy distribution of calcite and variation in the calcite orientation.

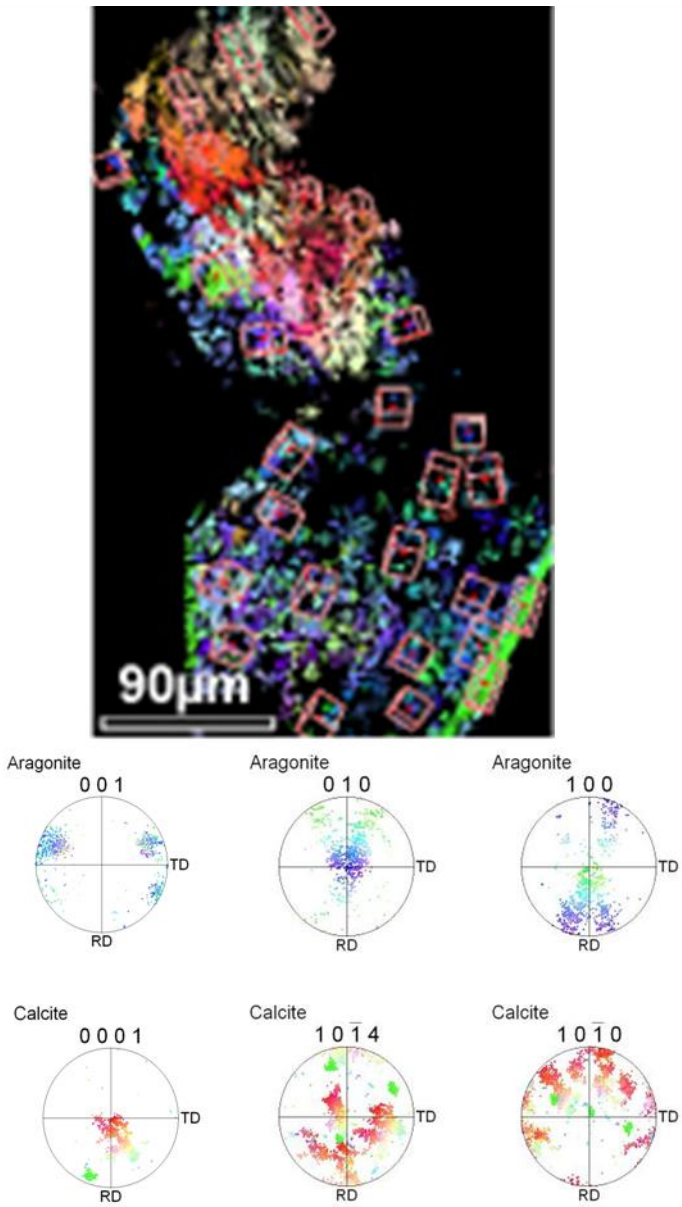

Figure 3.9 Inverse pole figure map and pole figure plots of crystal orientation in the umbo region of the A (<1cm) stage of ontogeny. The colours represent the crystal plane parallel to the field of view as discussed in Section 2.2.1. The IPF map also shows wire frames indicating the orientation of calcite and aragonite at selected points. The inner surface of the shell is to the left of the IPF map.

Variation of orientation of around 45° of the c-axis of calcite is apparent. In some cases the c-axis is perpendicular to the direction of growth and in some regions it follows the curvature of the shell. The thin layer of calcite in the bottom right, coloured bright green, indicates that moving away from the umbo, the c-axis now follows the curvature of the shell, parallel to the polymorph interface and the shell surface. The main cleavage planes of calcite, the {1014} planes, and the {1010} planes show a mutual variation on the same scale as the c-axis. The blue and green colours dominating the aragonite portion of the IPF map show a consistent alternation between the a- and the b-axes of aragonite normal to the field of view and, in turn, are parallel with the direction of growth. The {010} and {100} pole figures show that this alternation follows the shell curvature and

maintains this despite variation in orientation of the neighbouring calcite. The {001} pole figure displays a concentration of data points forming a distinct cluster representing c-axes perpendicular to the inner and outer surface of the shell and the polymorph interface. A similar pattern can also be observed in Figure 3.10.

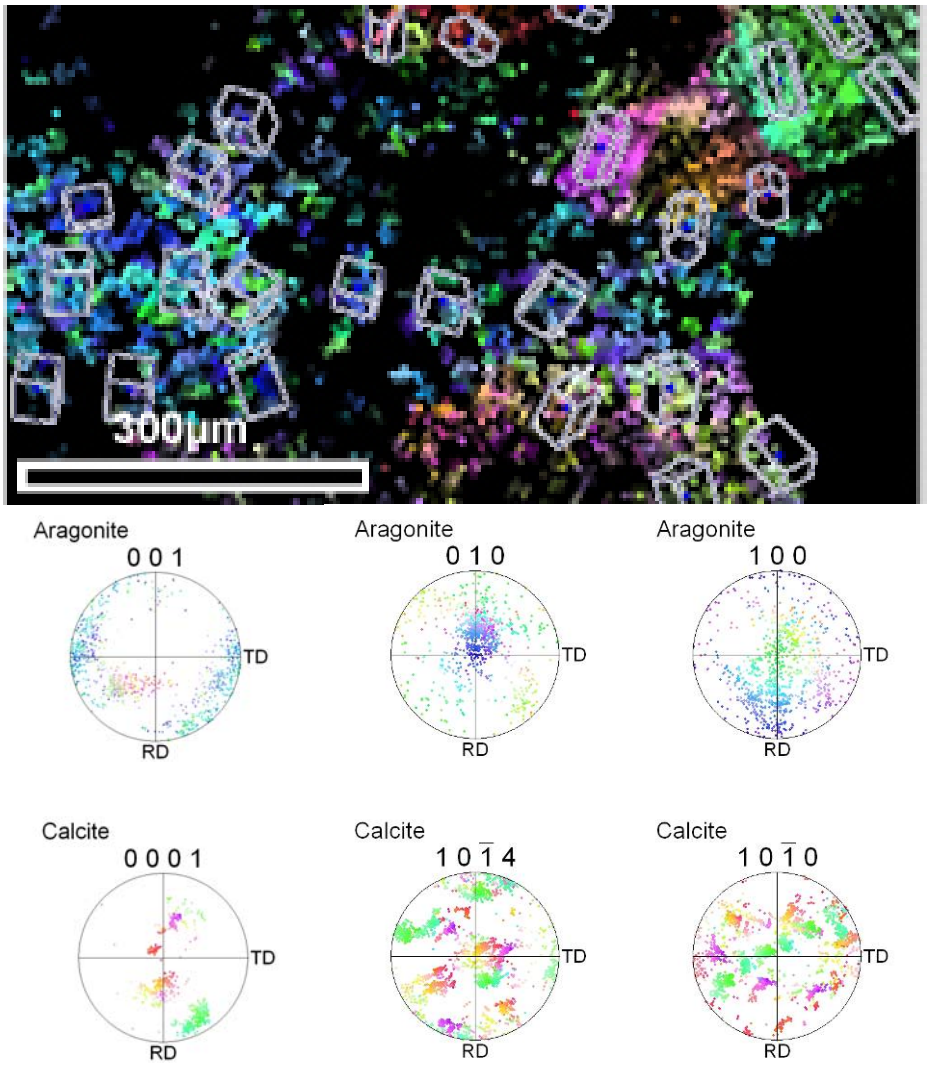

Figure 3.10 Inverse pole figure map and pole figure plots of crystal orientation in the umbo region of the C (2.6-3.5cm) stage of ontogeny. The colours represent the crystal plane parallel to the field of view as discussed in Section 2.2.1. The IPF map also shows wire frames indicating the orientation of calcite and aragonite at selected points. The inner surface of the shell is to the right of the IPF map

In the umbo region of the C (2.6-3.5cm) stage of ontogeny the patchy distribution of calcite is evident, showing clear variations in the orientation of the c-axis, {1014} and {1010} planes. The aragonite maintains a fixed c-axis position perpendicular to the shell surface with growth of new aragonite crystals showing rotation around this fixed axis. Both the calcite and aragonite layers show greater variation in crystallographic orientation than the earlier stage of ontogeny, probably as a result of analysing an area of greater curvature.

.

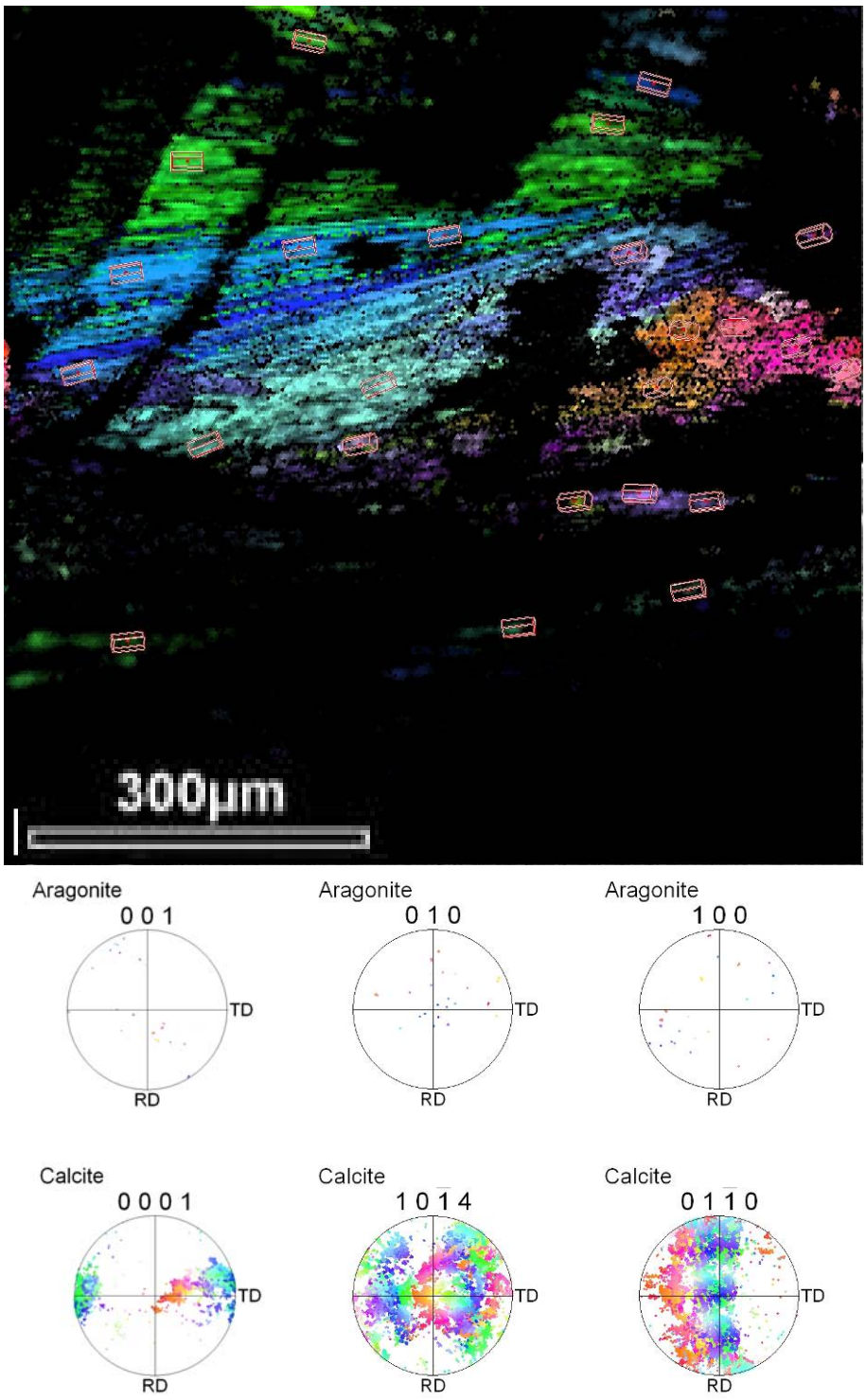

Figure 3.11 Inverse pole figure map and pole figure plots of crystal orientation in the umbo region of the F (5.1-6cm) stage of ontogeny. The colours represent the crystal plane parallel to the field of view as discussed in Section 2.2.1. The IPF map also shows wire frames indicating the orientation of calcite and aragonite at selected points. The inner surface of the shell is to the top left of the IPF map.

A section of calcite in the umbo region shown in Figure 3.11, from the F (5.1-6cm) stage of ontogeny reveals a similar variation in crystallographic orientation. The majority of calcite in this area has strong c-axis orientation in the direction of growth with morphological elongation of the calcite crystals in the same direction, with the region highlighted in red, orange & pink showing an

orientation difference of around 45° to that of the surrounding area. Both the {1014} and the {0110} planes show a wide spread of orientation with rotation around the c-axes and some vertical movement resulting in the wide clusters of data points in the pole figure plots (Figure 3.11).

The umbo region also bears more prismatic aragonite than any other sections of the shell and this prismatic layer that forms the muscle attachment (Taylor *et al.*, 1969) is present in all stages of ontogeny. Prismatic aragonite near the umbo region of two specimens from ontogenetic set 'A' (<1cm) is shown in Figure 3.12.

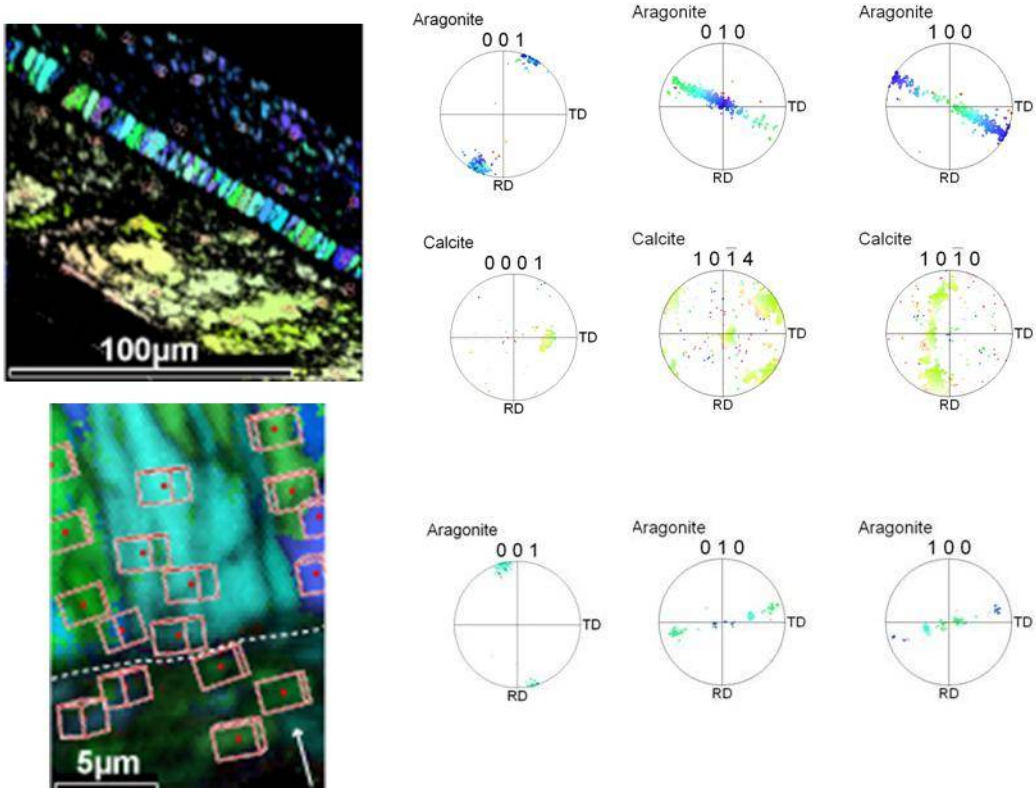

Figure 3.12 Inverse pole figure maps and their corresponding pole figure plots showing prismatic aragonite near the umbo region of two specimens from the earliest ontogenetic stage 'A' (<1cm). In the upper map, the inner shell surface is to the top right. In the lower map, the dotted line indicates the boundary between the nacre and the prismatic aragonite, the white arrow indicates the direction of the inner shell surface. The wire frames show crystal orientation for selected points on the IPF maps.

The distinctly strong highlighted colour represents strong electron beam diffraction compared with that of the neighbouring nacre which bounds it on either side. For much of this survey, the nacre nearest the polymorph interface diffracts the electron beam weakly compared to nacre at least 30µm from the interface. Both morphologies, however, show almost identical orientation, with the c-axes perpendicular to the shell surface and a rotation around the fixed c-axis revealing the a- or b-crystal face in a regular alternation. The calcite in this region has very uniform crystal orientation, with variation of only a few degrees over the entire region, especially for the c-axis. The cluster of poles-to-planes in the pole figure plots (Figure 3.12) suggest that there may be a relationship with

the {001} plane of aragonite with one of the three symmetrical cleavage planes {1014} or the {1010} planes of calcite. However, lack of consistent observation of this relationship between these crystal planes in other specimens and regions such as that displayed in Figure 3.13 means that any relationship may be co-incidental. Figure 3.13 also shows uniformity developing in calcite orientation and the continuation of orientation from one morphological form of aragonite to the next. However, in this example, the nacre laid down after the prismatic aragonite shows a slight tilt of the c-axis away from the field of view creating a mild discrepancy in crystallographic continuity.

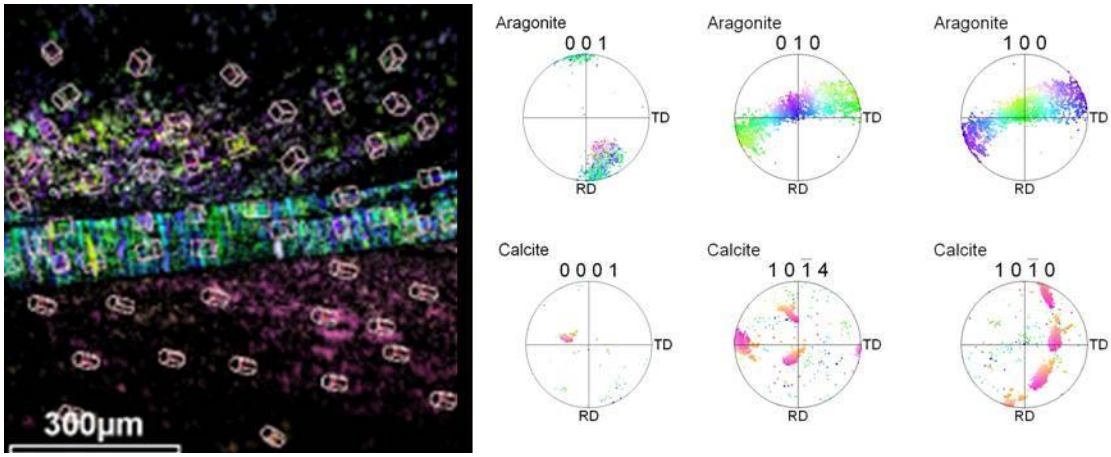

Figure 3.13 IPF map and the corresponding pole figure plots showing prismatic aragonite near the umbo region from ontogenetic stage 'E'. The inner shell surface is to the top. The wire frames show crystal orientation for selected points on the IPF maps.

3.3.3.2 Mid section

Moving from the umbo to the mid section of the shell, uniformity in crystallographic orientation develops in all stages of ontogeny. Figures 3.14 and 3.15 show IPF maps from each stage of ontogeny and display this uniformity in crystallographic orientation.

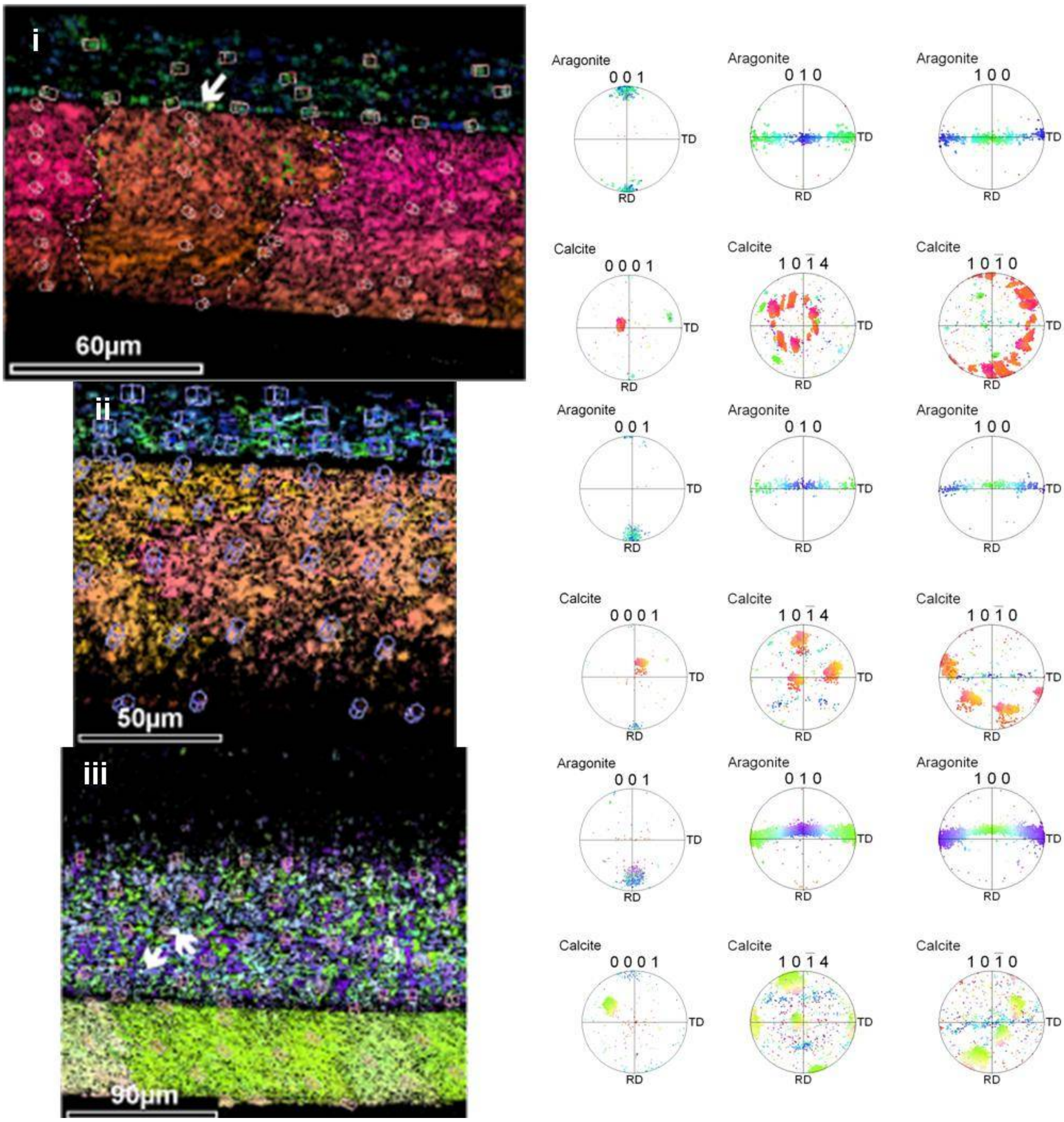

Figure 3.14 IPF maps and their corresponding pole figure plots showing the orientation of calcite and aragonite in the mid section from specimens from the earlier ontogenetic stages 'A(i), B (ii) & C(iii)'. In all the maps the inner shell surface is to the top. In maps (i) and (iii) the white arrows show bands of prismatic aragonite. The white dotted lines in (i) highlight a boundary within the calcite. The wire frames show crystal orientation for selected points on the IPF maps.

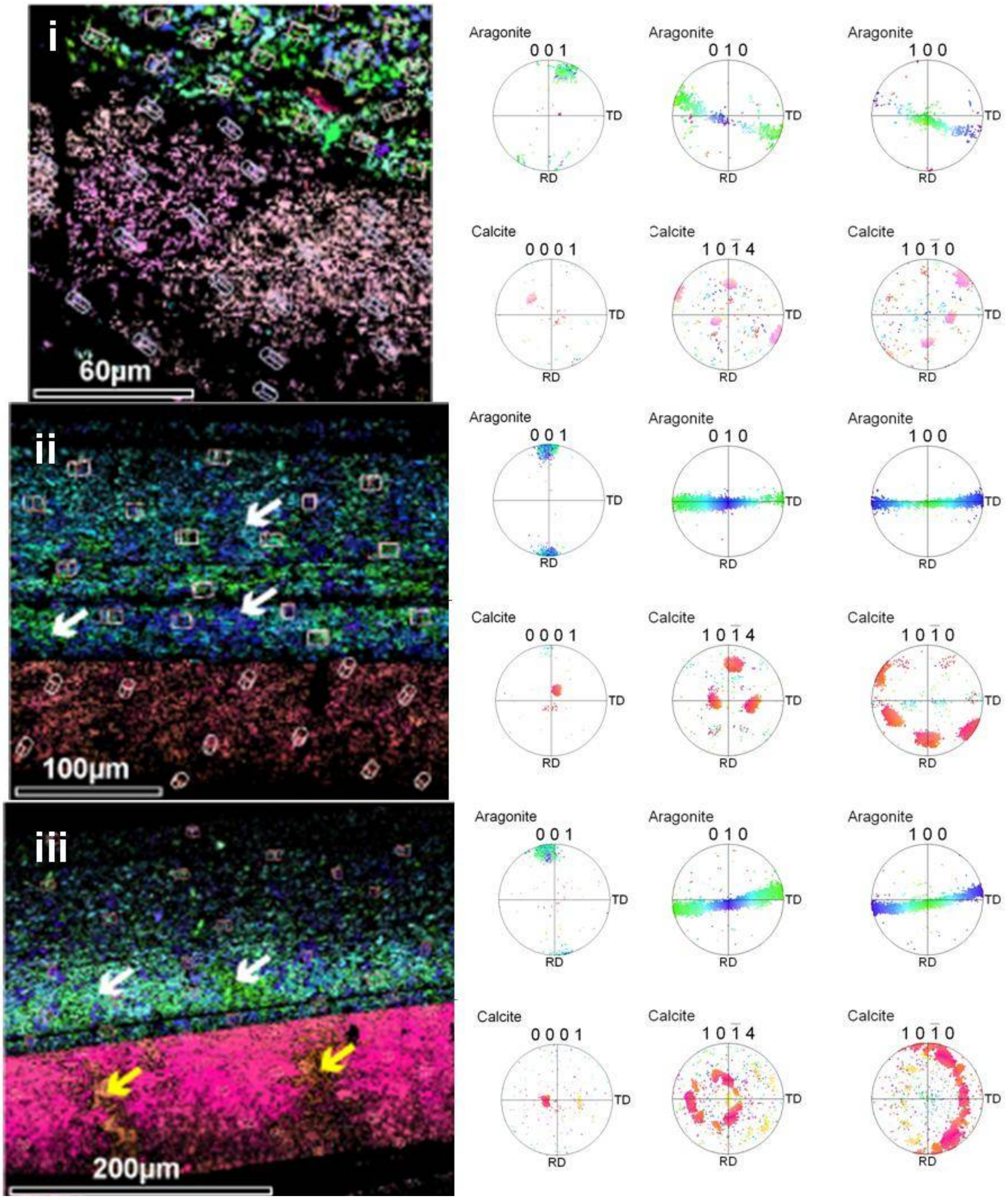

Figure 3.15 IPF maps and their corresponding pole figure plots showing the orientation of calcite and aragonite in the mid section nearest the umbo from specimens from the later ontogenetic stages 'D(i), E (ii) & F(iii)'. In all the maps the inner shell surface is to the top. In maps (ii) and (iii) the white arrows show regions of adjacent nacreous aragonite with identical orientation. The yellow arrows in (iii) highlight 'wedges' of differing orientation within the calcite layer. The wire frames show crystal orientation for selected points on the IPF maps.

Well constrained crystallographic orientation dominates the mid region in all ontogenic stages. Figures 3.14 & 3.15 also highlight discrete zoning within the calcite layer with large areas (60-80µm) of calcite crystals with uniform crystallographic orientation creating a discernible boundary with another crystal zone of different orientation. Adjacent regions of aragonite nacre showing uniform orientation are also apparent here.

3.3.3.3 Posterior edge

The posterior edge is the most recent deposit of shell material in the animal's life and is produced by the outer mantle folds. Only calcite is produced here as a result, with the growing front of aragonite still further along the shell anteriorly. Areas of the posterior edge in all stages of ontogeny and their crystal orientation are displayed in Figures 3.16 & 3.17.

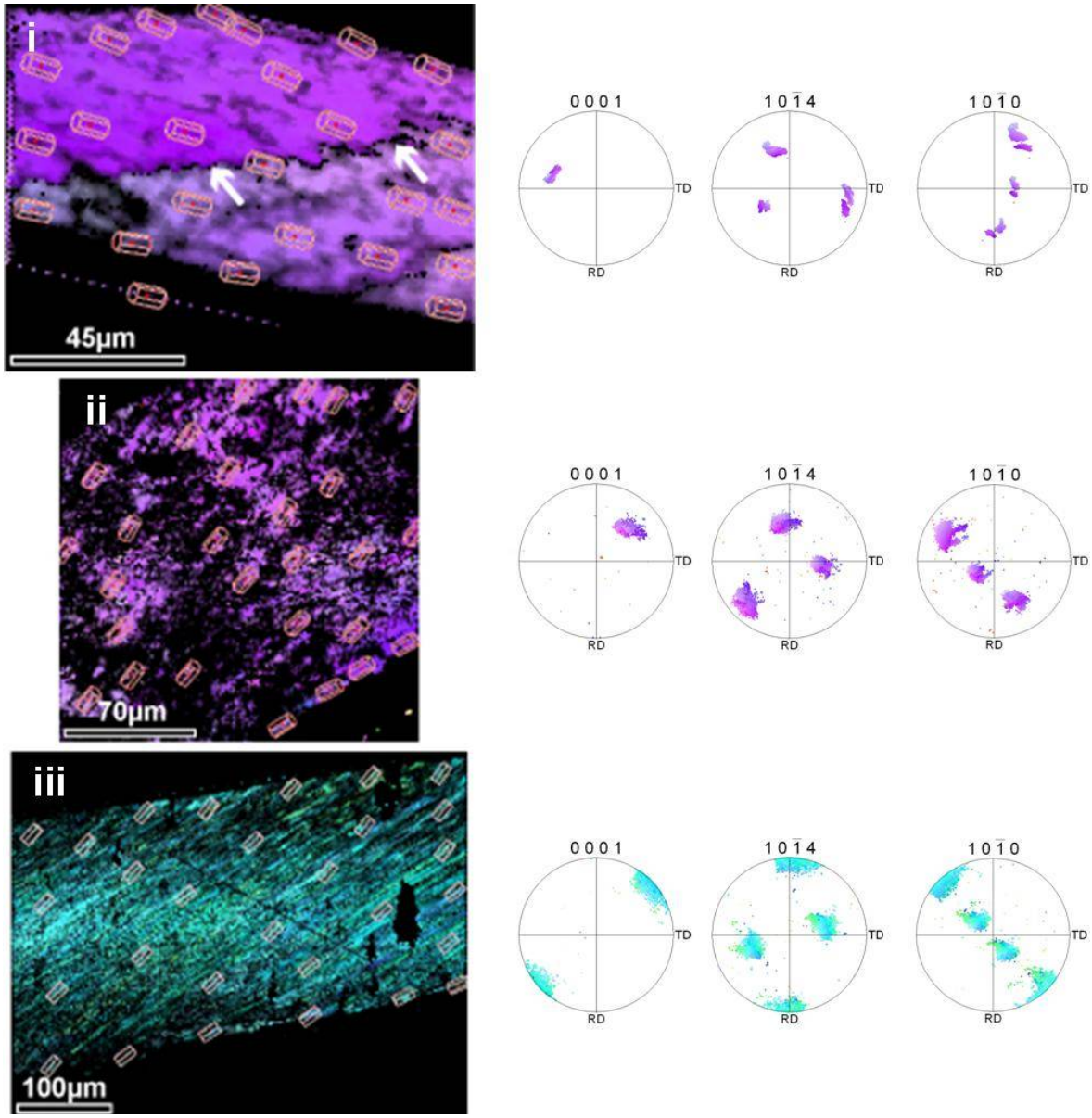

Figure 3.16 Inverse pole figure maps and their corresponding pole figure plots showing the orientation of calcite in the posterior edge section from specimens from the early ontogenetic stages 'A(i), B (ii) & C(iii)'. In all the maps the inner shell surface is to the top. The wire frames show crystal orientation for selected points on the IPF maps. The white arrows in (i) indicate a distinct boundary within the calcite layer.

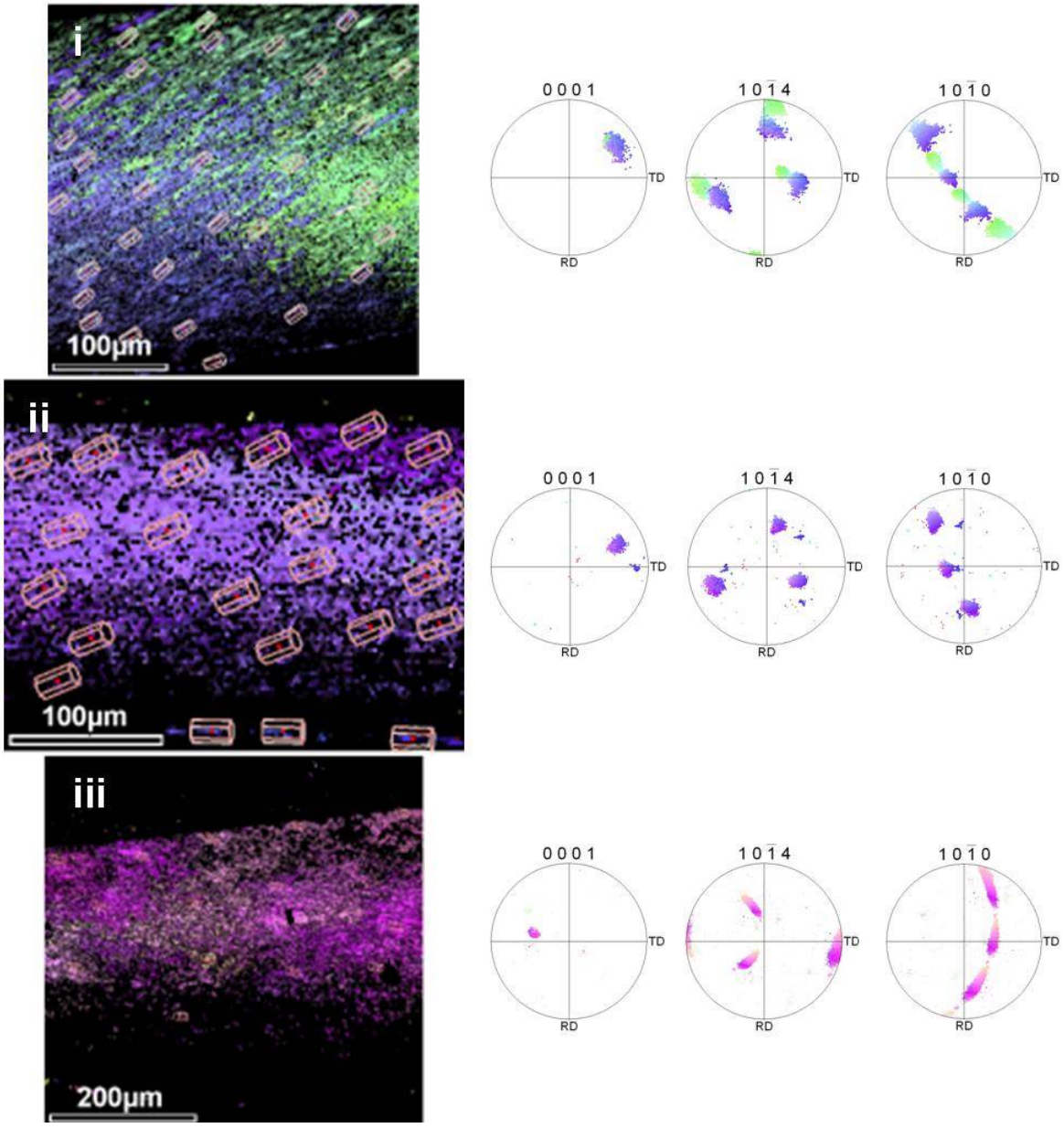

Figure 3.17 IPF maps and their corresponding pole figure plots showing the orientation of calcite in the posterior edge section from specimens from the older ontogenetic stages 'D(i), E (ii) & F(iii)'. In all the maps the inner shell surface is to the top. The wire frames show crystal orientation for selected points on the IPF maps.

The morphology of calcite crystals consistently shows steep inclination and here the c-axes orientation show the similar angles of inclination in all stages of ontogeny. Crystallographic orientation of the {0001} c-axis appears to trend in the growth direction of the shell and arrives at the inner shell surface at a shallow angle. The c-axis position is fixed very rigidly and the overall crystallographic pattern is very uniform compared with previous sections. The pole figure 'clusters', moving through the ontogenetic stages indicates that the c-axis orientation becomes more tightly constrained as well as the {1014} and the {1010} plane axes, with more rotation around the fixed c-axis as the data clusters for {1014} and {1010} are stretched laterally.

3.3.3.4 Cross-section profile

Tightening of calcite orientation similar to that observed in Figures 3.16 & 3.17 is also evident in samples analysed perpendicular to the line of section, ie from exterior to interior, through the calcite layer as shown in Figure 3.18.

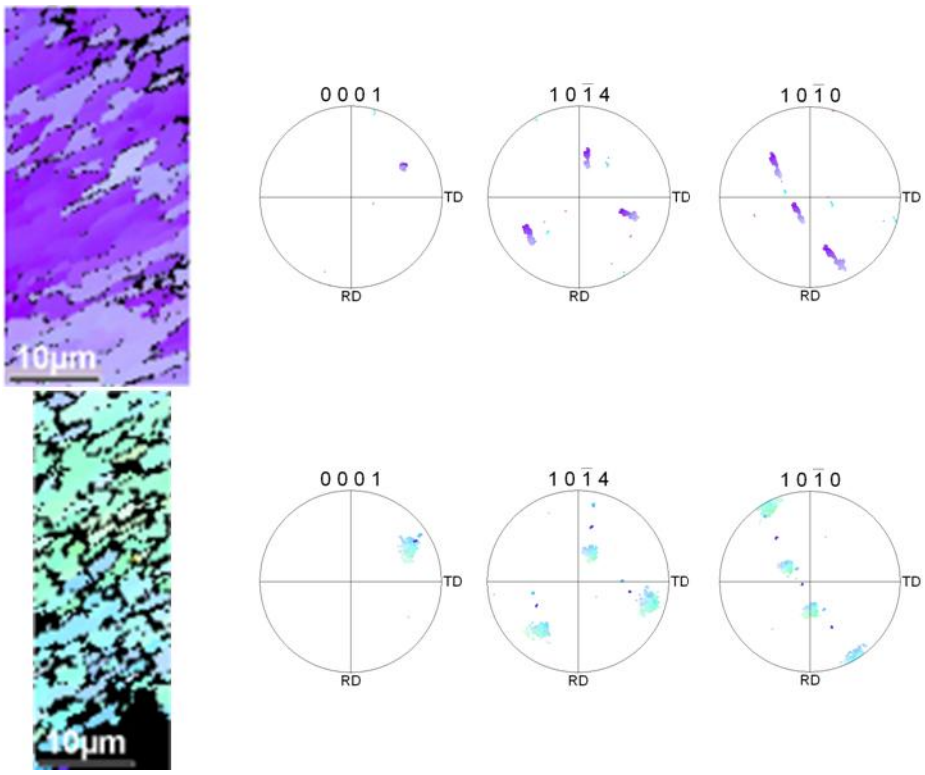

Figure 3.18 IPF maps and their corresponding pole figure plots showing the orientation of calcite in the posterior edge section from a specimen from the oldest ontogenetic stage 'F'. The maps were collected in the same region, the top map representing innermost calcite, the bottom map representing calcite at the outer shell edge. In both maps the inner shell surface is to the top.

Moving from the outer calcite to the innermost calcite nearest the polymorph interface, there appears to be a refinement in crystallographic orientation with the data clusters for all poles-to-planes plotted here showing a tighter constraint (Figure 3.18). More lateral movement of the {1014} and the {1010} planes indicate increased rotation around a more strongly fixed c-axis. The outermost edge of the calcite layer diffracts electrons more weakly than the remainder of the calcite layer. The same pattern is observed in the aragonite layer with the aragonite nearest the polymorph interface showing the poorest electron diffraction intensity which improves toward the shell interior. Figure 3.19 shows a full section through the shell thickness.

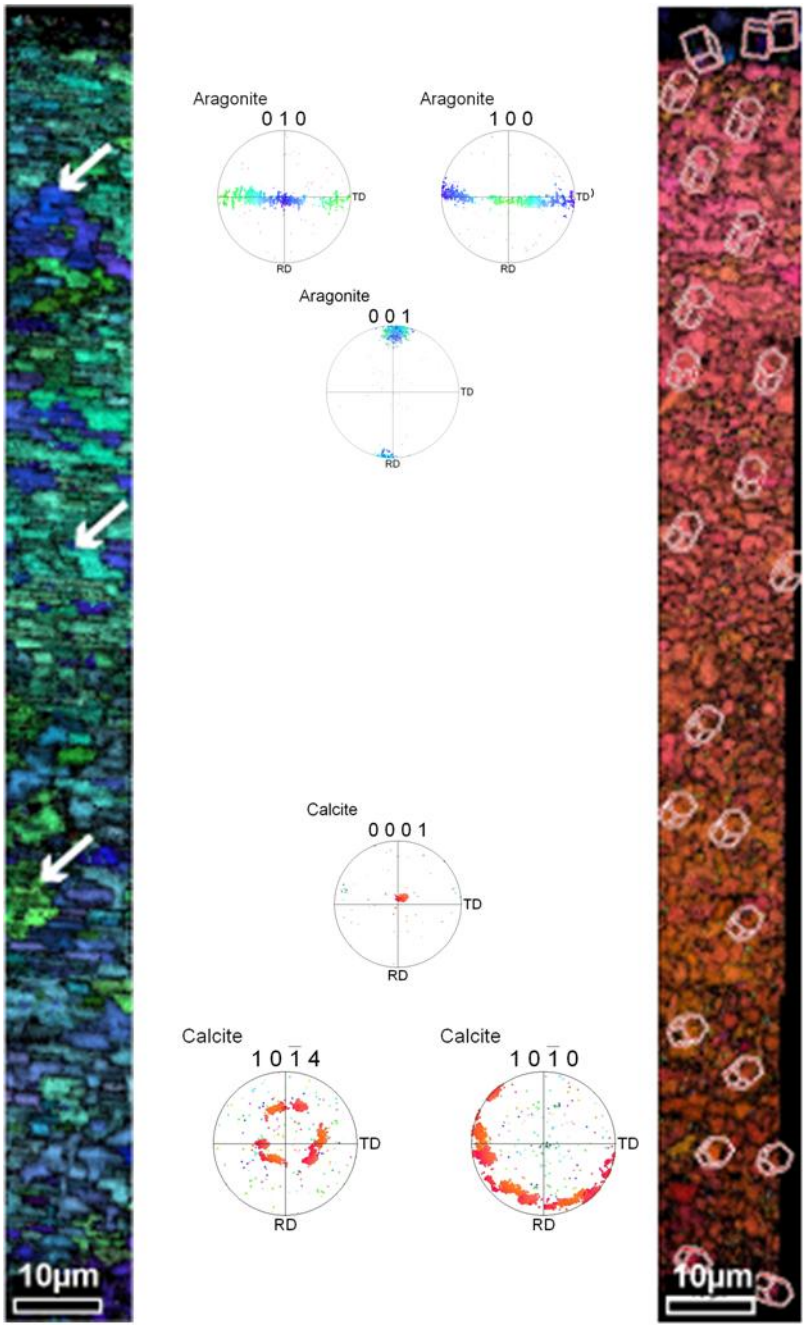

Figure 3.19 A sequence of combined IPF maps allowing a view of the full thickness near the umbo region of a specimen of *Mytilus edulis* from the 'F' stage of ontogeny with the respective pole figure plots. The inner shell surface is to the top, the inner aragonite layer and the outer calcite layer are represented in the left and right map respectively. The white arrows in the left map show areas of crystallographic continuity between adjacent nacreous layers.

Figure 3.19 shows that crystallographic orientation is well constrained through the shell thickness, with only some minor variations in the calcite layer as observed in Figure 3.18. Within the calcite layer, there is a trend of the c-axis to become more inclined as it reaches the polymorph interface. The wire frames imposed on the calcite IPF map, display the migration of the c-axis direction towards the interface. This appears to be a common feature and can be observed in a number of examples, with some specimens showing the calcite c-axes in the outermost calcite running parallel to the shell surface and becoming more inclined towards the interface. In the aragonite layer,

distinct crystallographic continuity between adjacent nacre tablets in the same layer and neighbouring layers is observed. In the calcite layer, a similar effect is observed with clusters of neighbouring calcite crystals showing identical orientation, and a slight difference in orientation to other crystallite clusters (Figure 3.18).

3.4 Discussion

3.4.1 Phase distribution

The mussels in this survey were collected from a single rope, all at the same time. The mussels had been cultured, cultivated and had received the same treatment. Thus environmental influences were as uniform between specimens. Thus, any variations in shell ultrastructure, crystal habit or crystallographic orientation between specimens can be considered to be biological rather than environmental.

The thickness and distribution of the calcium carbonate phases in the umbo region of the shell and through the shell have been the subject of much study because the calcite:aragonite ratio in the shell is an environmental indicator (Lowenstam, 1954; Dodd, 1963; Dodd, 1964). It was suggested that the ratio of aragonite to calcite in some molluscan species increases with increasing temperature, with Dodd, (1964) proposing that the structure *Mytilus californianus* umbo region is strongly affected by latitude and therefore temperature, with proportions of prismatic aragonite and nacreous aragonite in the umbo also being an environmental indicator. In this study, the proportion of calcite and aragonite varied between specimens of the same ontogenetic group, with much of the variation in the umbo area where there was notable absence of calcite in the outer layer and aragonite that persisted from inner to outermost surface of the shell. Presence of prismatic aragonite also varied between specimens as did its location in the umbo. Additionally, some specimens showed variability between calcite and aragonite in a multi-layered structure (Figure 3.2 iii). This may suggest that other controlling factors may influence aragonite and calcite deposition rather than merely temperature or salinity which concurs with previous work by Hubbard *et al.* (1981) in which the variation of aragonite and calcite ratios occurred in *Mytilus edulis* specimens in areas of comparable temperature and salinity in the Tay Estuary in Scotland. The variation in the layered structure in the umbo, which is not observed in the rest of the shell length, with patches of calcite found within the nacreous layer and vice-versa (Figure 3.2), may represent some disarray in the earliest stages of shell mineralisation where the dominant phase which is formed can alternate. This has been observed in other molluscan species (Stenzel, 1964; Carriker & Palmer, 1979; Medakovic *et al.*, 1997). However, as the larval stages of ontogeny were not available for this study, this cannot be confirmed.

3.4.2 Calcite in *M. edulis*

Through analysing six ontogenetic stages of *Mytilus edulis*, a regularity and uniformity of crystal morphology and orientation is consistent between each stage with local variations in certain regions that are also consistent in each stage of ontogeny. Each ontogenetic stage shows distinct distortion of both polymorphs in the umbo region of the shell.

Calcite morphology can be described as prismatic (Taylor *et al.*, 1969; Wilbur & Saleuddin, 1983; Pojeta *et al.*, 1987; Chateigner *et al.*, 2000) throughout the shell with elongate prisms of calcite with the long c-axis oriented in the direction of crystal growth (Berman *et al.*, 1993) and inclined away from the periostracum of the shell exterior as shown in the unpolished section in Figure 3.3. This structure has previously been termed as 'fibrous prismatic' (Kobayashi, 1969) in *Mytilus*.

However, the calcite prisms can show distortion in morphology (Figures 3.4 & 3.5) and significant variation in crystal orientation (Figures 3.9-11) in the umbo region, described in other *Mytilus* species as 'beak' calcite (Dodd, 1963), compared with other regions of the shell. Despite the distortions observed here, the overall orientation of the calcite c-axis {0001} trends in the main anterior-posterior axis of shell growth, with calcite orientation and crystal growth being regulated at an early stage in the shell development. The presence of this pattern in all six stages of ontogeny suggests that there has been no modification in this region to the calcite structure through the animal's life. However, the larval stages of growth were not obtained for this study and so there may be crystal modification and orientation changes at an earlier stage, but this cannot be investigated here but has been considered in *Mytilus edulis* (Humphreys, 1969) and other *Mytilus* and molluscan species (Kniprath, 1978, , 1980; Eyster, 1982, , 1983; Weiss *et al.*, 2002). Regions of calcium carbonate nucleation occur at the hinge region of larval shells of *Mytilus galloprovincialis* (Kniprath, 1980), which appear similar to the patchy distribution of calcite in the umbo observed here (Figure 3.9 & 3.10). Therefore, the orientation of calcite in this region may represent the earliest stages of growth, or may represent a relict structure which has been re-worked once the shell reaches a critical age.

Calcite appears to quickly become uniform, in terms of crystal habit and crystallographic orientation, from the umbo to the posterior (Figures 3.14 & 3.15). The orientation of the calcite c-axis at an angle towards the shell surface becomes more rigidly fixed over large areas of the calcite layer and polymorph interface with large portions of the calcite layer in crystallographic continuity. Areas of poor diffraction have been used previously to determine variation in strain, topography and grain boundaries (Wright & Nowell, 2006). Individual calcite prism outlines can be discerned in EBSD scans (Figures 3.18 & 3.19) due to areas of poor diffraction quality surrounding each crystal. This may indicate the layer of organic conchiolin (Gregoire, 1961) surrounding the

individual prisms with the organic material providing no diffraction pattern. Poorer diffraction may help identify areas of increased organic content in these mineralised structures. Conversely, areas of poorer diffraction quality can be produced by overlapping diffraction patterns at grain boundaries in EBSD. Diffraction patterns from two crystals create a difficulty in indexing resulting in an area of low diffraction quality displayed on an EBSD map (Humphreys, 2001). Areas of poor diffraction quality could simply be a result of increased grain boundaries with smaller grain size, such as the sub-micron sized grains observed at the outermost calcite layer and the aragonite immediately succeeding the polymorph interface.

Calcite orientation and morphology from the outer to inner shell (Figures 3.5, 3.6, 3.18 & 3.19) may be explained by a decrease in organic content. Grigorev (1965) and Taylor *et al.* (1969) describe calcite nucleation in the bivalves occurring as spherulites on the organic periostracum with the prisms growing and thickening from these nucleation centres in a fan-like pattern displacing surrounding organic material until abutting against neighbouring prisms. At this point, crystal regulation and orientation may be more mineral controlled than organically controlled and the organic material is merely pressed between (Carriker *et al.*, 1980) and included into prisms (Nakahara *et al.*, 1980) at this early stage becoming intercrystalline matrix. This mechanism may account for the refinement of morphology and orientation observed here and also account for the presence of regions of poorly defined calcite morphology (Figures 3.5), representing possible nucleation centres. If this correlates with increased organic influence then this may also account for the poor diffraction quality in this region in all the EBSD analysis undertaken here. A similar pattern of calcite prism nucleation, orientation and growth has been discussed previously in other molluscan species (Ubukata, 1994; Checa & Rodriguez-Navarro, 2001), in other specimens of *Mytilus edulis* (Dalbeck *et al.*, 2006) (Figure 3.20) and in other biomineralised structures (Dalbeck & Cusack, 2006) .

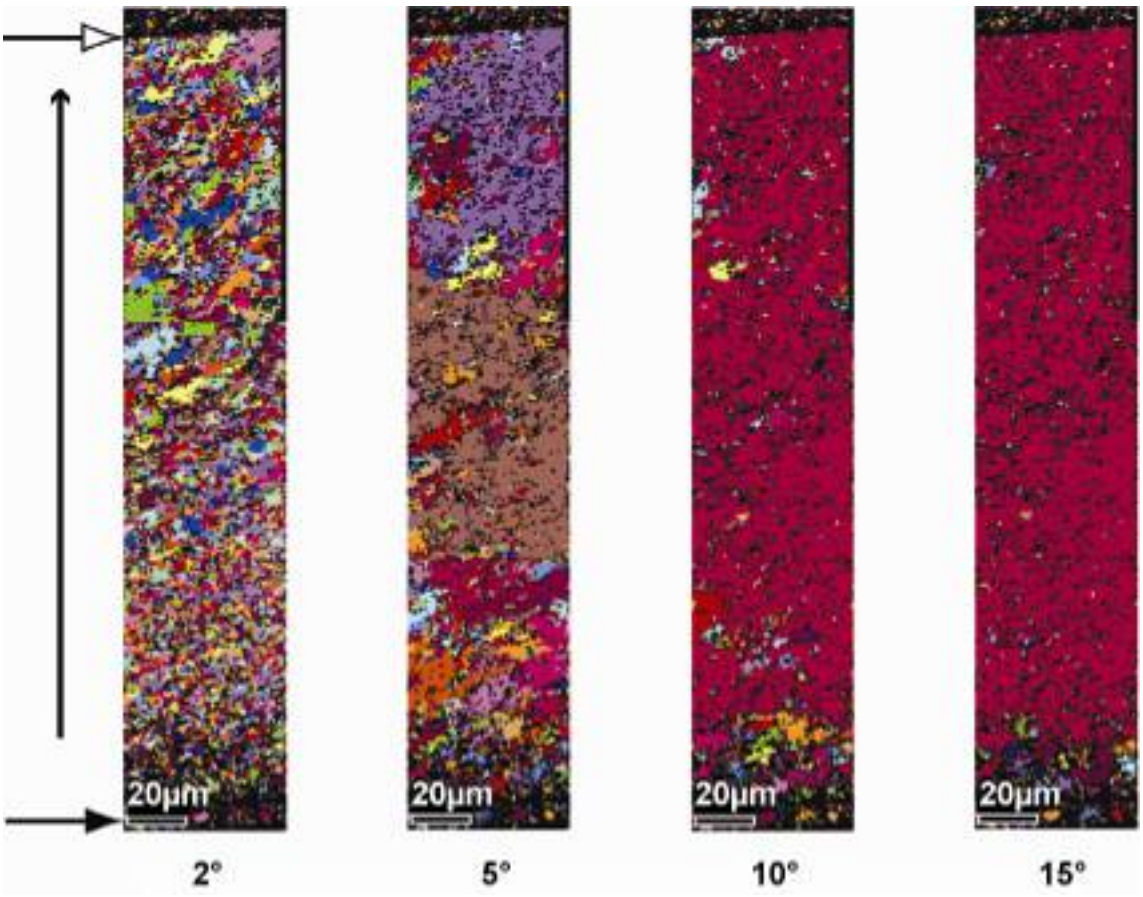

Figure 3.20 Misorientation OIM maps from Dalbeck *et al.* (2006) showing large areas of neighbouring calcite showing increasing crystallographic agreement by increasing in the angle of misorientation in each grain map. This means that apart from the outermost 40µm of the calcite layer, all the calcite in this region is within 15° misorientation showing uniformity through the layer. The white arrow indicates the polymorph interface; the black arrow shows the outer shell surface. The vertical arrow is normal to the inner shell surface.

Figure 3.20 highlights the uniformity in the calcite layer of *Mytilus edulis* showing agreement between neighbouring crystals to within 10-15° except for the outermost calcite which shows some disorder. This may support the hypothesis of the calcite growth in this layer as proposed above, with nucleation and fanning of calcite occurring in the outermost region. However, the explanation for the increased rotation of the calcite crystals, represented by the lateral movement of the {1014} and the {1010} poles of calcite, around an increasingly fixed c-axis as the crystallography appears to refine remains uncertain. Trace element partitioning and other factors in these areas remain to be fully investigated for any possible relationships (Dalbeck *et al.*, 2006).

A similar explanation may be derived for the progressive ordering of calcite from shell anterior to posterior. Higher organic content may be required for initial calcite nucleation at the earliest stage of shell growth, as a wholly organic shell (Humphreys, 1969; Kniprath, 1981; Eyster & Morse, 1984) provides the foundation for mineralised construction to then occur. With an existing mineral

framework then in place, it may then be easier to nucleate new calcite layers on the mineral scaffold, with the need for organic influence lessened towards the posterior of the shell.

Within the calcite layer, discrete zoning (Figures 3.14i, 3.15iii, 3.16i) is discerned through areas of poor diffraction intensity which outline boundaries between regions of calcite crystals which also marks a change in orientations. Judging by the scale of these regions, 60-80μm, these possibly indicate growth bands of the shell (Richardson, 1989) with variation in thickness such as Figure 3.15iii representing possible seasonal variation in growth with thinner bands representing growth in winter months (Richardson *et al.*, 1990). With the boundary line of poor indexing possibly indicating an organic-rich border between these regions and the crystallography showing a mild orientation change, this may represent a new nucleation and growth period after an interruption of growth but with the general trend of orientation and morphology still maintained throughout.

The discrete zoning of calcite crystal clusters within the calcite layer (Figure 3.18, 3.19 & 3.20) observed here may correlate with previous observations of calcite 'domains' (Feng *et al.*, 2000b) and may represent the growth of identically oriented prisms from the individual spherulitic nucleation centres as previously discussed above, until growth is delimited by another cluster impinging on the prism growth.

3.4.3 Aragonite in *M.edulis*

Aragonite in the umbo shows a greater degree of variation than the calcite, the main morphology being aragonite nacre as micron-sized tablets (Figure 3.8 i-iv), forming the distinctive brick and mortar-style construction. In EBSD maps, the diffraction intensity of this region is poorer than in the calcite layer. As already discussed with respect to calcite (Section 3.4.2), lower EBSD diffraction intensity most likely indicates higher amounts of grain boundaries due to smaller crystal size. As the thickness of the nacre tablets is thinner than the calcite prisms, this can account for lower diffraction intensity from the aragonite. However, the nacreous section of the shell is considered to be more organic-rich than the calcite (England, 2005) with organic material forming the boundaries between tablets. As with the calcite, the poor diffraction could be attributed to increased organic presence. This remains to be fully tested, and the smaller grain-size is most likely the significant factor.

The pole figure orientations for aragonite relate closely with previous investigations into molluscan nacre orientation (Wada, 1961; Wise, 1970b; Feng *et al.*, 1999; Feng *et al.*, 2000a; Hou & Feng, 2003; Checa & Rodriguez-Navarro, 2005; Checa *et al.*, 2006), the c-axis orientated perpendicular to the surface of the shell and the a- and b-axes of the parallel to the surface of the laminae. However, the *in situ* observations made here differ from the same previous studies that have

considered the b-axis of aragonite to follow the growth direction. Regular alternations between the {100} and {010} axes of aragonite were observed in the same cross-sections and neither axis showing considerable abundance over the other. This is the case for the nacre of all stages of ontogeny of *Mytilus edulis* and in all regions of the shell analysed here. Checa *et al.* (2006) also describe progressive ordering of the b-axis in the direction of growth as more laminae are successively deposited. A dominant axis orientation of nacre other than the fixed c-axis is not observed here with {100} and {010} axes alternations seen consistently through the entire thickness of the nacreous layer (Figure 3.13-3.15 & 3.19).

The progressive refinement of crystallographic orientation through the thickness of the shell and along the shell profile, from anterior to posterior, observed in the calcite layer does not appear in aragonite nacre. The only discernable difference is the crystal morphology immediately succeeding the polymorph interface, where the laminae are thinner than that of the rest of the shell. This area does not diffract as well as adjacent crystal layers. Again, this may be a result of the smaller crystal size or may indicate a higher proportion of organic material which assists with nucleation of the nacre and the switch in polymorph type (Fritz *et al.*, 1994; Belcher *et al.*, 1996; Falini *et al.*, 1996; Addadi *et al.*, 2006). Overall, nacre appears uniform in crystallographic orientation and morphology through the layer and along the shell throughout all stages of ontogeny with the c-axis <001> remaining fixed perpedicular to the shell surface. However, poles to the <001> and the <010> planes show a greater degree of rotation than the rotation around the c-axis in calcite. This may be explained by the screw dislocation model for crystal growth of nacre (Schmidt, 1923; Wada, 1960, , 1961; Wise & Devilliers, 1971; England *et al.*, 2007) where the crystal growth steps form spiral structures due to dislocations at the apex of growth hillocks and allow growth in the c-axis direction to continue.

Crystallographic continuity between nacre tablets is observed (Figure 3.19) with regions of adjacent tablets showing the same crystallographic orientation extending over several laminae. This suggests a physical mineral-mineral contact that may cause growth of a new nacre tablet, maintaining the crystal orientation without the need for a re-nucleation event on an organic substrate (Weiner & Hood, 1975; Weiner & Traub, 1980, , 1984). Despite the presence of organic material between tablets, physical mineral-mineral epitaxy has been discussed in previous studies of nacre (Manne *et al.*, 1994; Schaffer *et al.*, 1997; Feng *et al.*, 1999; Hou & Feng, 2003; Cartwright & Checa, 2006; Checa *et al.*, 2006) with the term ‘mineral bridging’ used to describe nucleation of a new tablet in a subsequent nacreous layer or even within the same layer by the penetration of growing mineralised material through pores in the organic matrix. The EBSD results observed here and previously published (Dalbeck *et al.*, 2006; England *et al.*, 2007) emphasise the

occurrence of this possible mineral bridging effect and may help to explain formation of bivalve nacre which is still debated.

The prismatic crystals that comprise the second morphology of aragonite appear in 20-30µm thick bands in which the individual crystal shapes are not as readily discernable as the nacre tablets. The prisms form conical structures (Figures 3.2iii, 3.12 & 3.13) corresponding with previous observations of molluscan prismatic aragonite (Dodd, 1964; Taylor *et al.*, 1969; Pojeta *et al.*, 1987) which was described as the myostracum, the site where internal muscles have been attached. The myostracum has previously been determined to lack conchiolin (Pojeta *et al.*, 1987), the organic sheaths that surround the crystals in mollusc shells, and this lack of organic content may explain the stronger diffraction intensity with that of the surrounding nacre. Taylor *et al.* (1969) describe the myostracum being found as being either pallial, pedal or adductor with the majority of the prismatic aragonite observed here in the umbo likely to be the anterior adductor muscle attachment site. Pojeta *et al.* (1987) describe the peripheral movement of the muscle locations as the animal grows and this may account for occasional emergence of prismatic aragonite throughout the shell sections observed in this survey.

The orientation of the prismatic aragonite correlates with the orientation of the surrounding nacre with the c-axis maintained perpendicular to the shell surface and alternation of the <100> and <010> axes of aragonite shown between prisms (Figure 3.12 & 3.13). This may suggest some form of continuation of the nacre growth in formation of the myostracum. Nacre is thought to normally develop due to limitation of growth in the c-axis direction by overlying organic matrix sheets (Watabe, 1965b; Wada, 1968) and therefore growth is then lateral along the a- and b- axes. Due to the similarity in orientation of the prismatic myostracal layer to the surrounding nacre, it is possible that a similar method of lateral growth is involved to allow the prisms to develop a lateral width similar to that of the nacre. However, the interaction with the muscle cells in this region must allow the myostracum the ability to grow uninhibited along the c-axis.

3.4.4 Polymorph interface

Through each ontogenetic stage and through the shell profile, there are no distinctive morphological and crystallographical relationships between the two calcium carbonate polymorphs. In the umbo region of the shell, the orientation of calcite can vary quite notably, whereas aragonite orientation remains fixed and shows the same pattern of orientation as in other areas of the shell, with the c-axis perpendicular to the inner shell surface. The distribution of both polymorphs in this region can be somewhat random, with nacre morphology following the curvature of the umbo (Figure 3.2iv & 3.8vi) whereas calcite morphology and orientation can be quite disordered. This

may suggest that the two polymorphs do not rely on each other to provide a mineralised substrate or scaffold in the early stages of development and can orient themselves independently of the other.

Moving through the shell profile and at different stages of ontogeny, aragonite crystallographic orientation and morphology does remain relatively constant, while the calcite can show variation in the orientation of the prisms from one region to the next with some areas showing the c-axis highly inclined towards the interface, and in others, a different crystal face can be revealed for large regions of the calcite (Figure 3.14i & iii). In previous analyses through the shell of *M. edulis* (Dalbeck et al., 2006), the {1014} plane of calcite coincided with the {001} plane of aragonite (Figure 3.14 & 3.15). The implications of this have been discussed in previous studies with calcite 'domains' having the {1014} faces parallel to the interface and the shell surface (Feng *et al.*, 2000b). The {1014} planes in calcite are the most thermodynamically stable (Weiner & Addadi, 1997). Therefore, it was proposed that nucleation and termination of the calcite prisms may be facilitated on the plane of minimal growth energy. It has also been discussed for other biomineralised structures that, due to the {1014} being the main cleavage plane of calcite, it would be beneficial to maintain the highest angle possible to any stress applied to the shell by keeping these planes parallel to the shell surface (Feng *et al.*, 2000b; Schmahl *et al.*, 2004; Cusack *et al.*, (in press)). Previous works also cited the possibility of direct aragonite <001> nucleation on the {1014} planes of calcite (Thompson *et al.*, 2000; DiMasi & Sarikaya, 2004) and while this seems plausible in some cases (Dalbeck *et al.*, 2006), it has not been consistently observed in this ontogenetic survey. Thus, both polymorphs can nucleate and orientate independently of each other with the function for the dual-layered arrangement still open to debate (Harper, 2000).

3.5 Summary

The shell of *Mytilus edulis* shows an overall uniformity in crystal habit and crystallographic orientation between ontogenetic stages, specimens within those stages, and regions along the shell profile. The {0001} c-axis of calcite inclines away from the nucleation area on the outer periostracum towards the shell interior with the crystals forming long prisms along that axis. Large areas of calcite prisms reveal the same crystal face. The aragonite {001} axis is perpendicular to the inner and outer shell surface (Figure 3.21). Rotation around the fixed c-axis occurs in both polymorphs, distinctly in the aragonite due to the screw dislocation model of growth. Rotational movement also occurs in the calcite layer as the c-axis becomes more strongly fixed towards the posterior and interior of the shell. This may be due to more mineral-influenced growth than organically influenced growth moving from the outer shell and the umbo which may contain more organic components. Strong alignment between neighbouring crystals in both polymorph layers is apparent with calcite 'domains' and growth line regions showing very uniform orientation and

aragonite mineral bridges showing a possible mineral-mineral epitaxial method of growth in the nacreous layer. No clear relationship between polymorphs can be distinguished with a constant relationship between crystal planes not being consistent between and within specimens.

No distinct differences can be discerned through ontogeny. Of the six stages analysed here no significant differences in crystal habit or crystallographic orientation were observed. Neither the calcite nor aragonite shows any evidence of reworking, refinement or mineral resorption between stages. Despite ontogenic effects reported in other biominerals (Lowenstam, 1981; Legeros *et al.*, 1987; Whitehead & Wilson, 1992), no considerable change with ontogeny was identified.

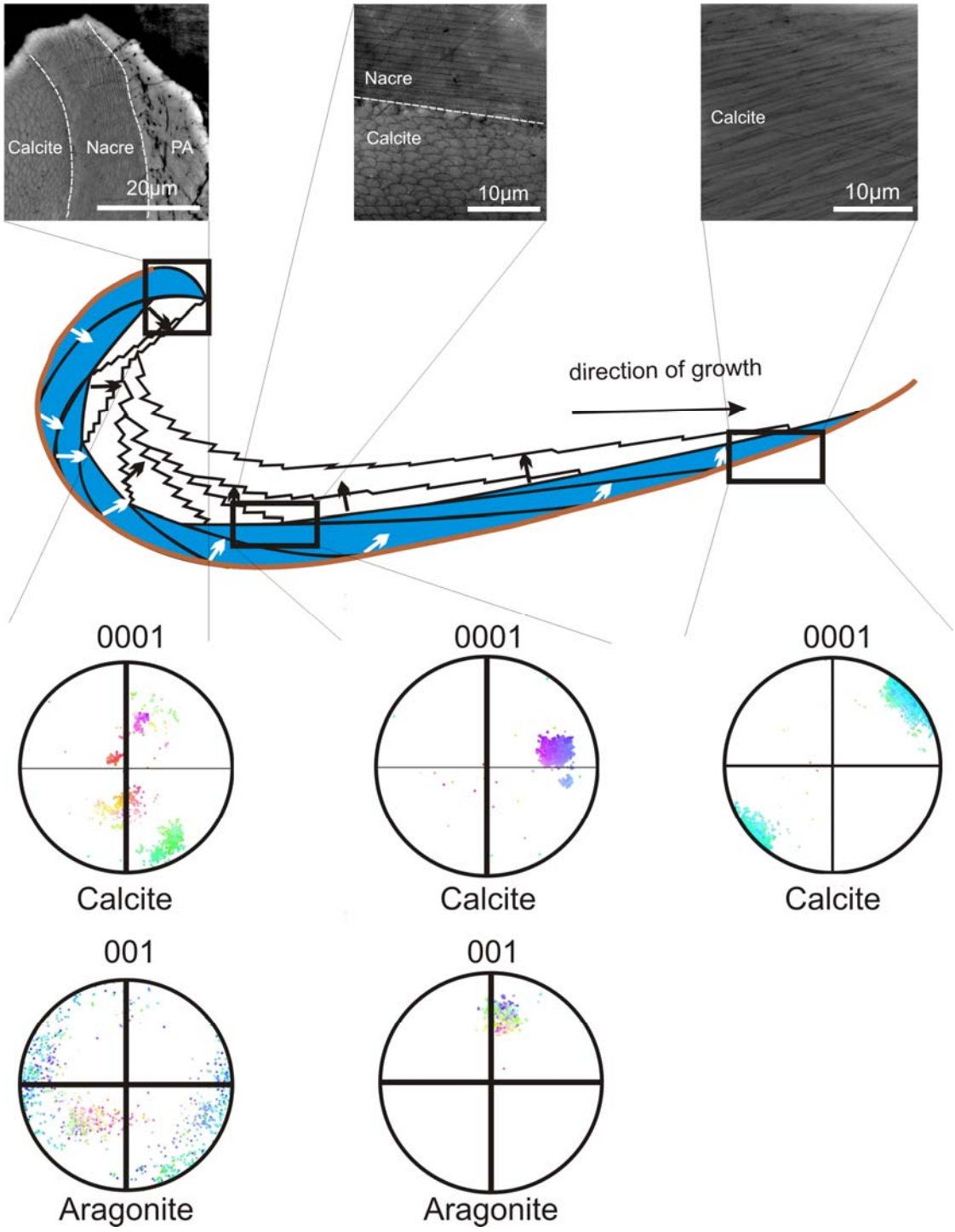

Figure 3.21. Summary of crystallography along the shell length. Refinement in crystallographic orientation of the and aragonite is shown in the pole figure plots for the *c*-axis of the respective polymorphs. SEM images indicate refinement in layering and crystal habit of the crystals moving from the umbo towards the shell posterior. PA indicates prismatic aragonite.

4

Trace element concentration in the context of ontogeny

4.1 Introduction

Chemical analysis of biologically produced minerals can yield vital information on the processes involved in biomineralisation and the interaction between the mineralising system and the surrounding environment. Trace elements are incorporated into biogenic carbonate systems at significantly lower quantities (~0.1wt%), to the major elements Ca, C and O. While these elements do not form crystal phases, their presence can be used to provide a better understanding of biomineralisation processes. Trace element composition can allow insight to the conditions in which mineralisation occurred, how these 'foreign' elements can affect the growth of biominerals and how they themselves may also be affected by mineral growth. To improve the understanding of partitioning of these trace elements in a dynamic system, a number of factors have to be considered as crystallography, biology and environmental factors can influence biomineral composition and these may be further influenced as the animal ages. This study aims to assess whether trace element chemistry is consistent at any stage of growth in the animal's life and whether trace element may be altered through periods of animal maturation, crystal maturity or resorption. Thus, implications this has for application of trace element chemistry to environmental proxies can be further considered.

A detailed account of six stages of ontogeny of *Mytilus edulis* are reported here to investigate the influence of ontogeny and the role of environmental conditions on the chemistry of the resultant carbonate shell. The farmed mussels were collected from one location at the same time. Thus, the mussel samples were all exposed to the same environmental conditions reducing the number of variables that may influence trace and minor element composition. Details of the location of the collection site and preparation are provided in Section 2.1. By studying specimens from a single location where the shells have been subject to the same fluctuations in environmental conditions through growth, any notable differences in trace element chemistry between ontogenic stages can therefore be attributed to variations other than environmental.

Minor and trace element chemistry for each stage of ontogeny was determined through quantitative analysis by electron probe micro analysis (EPMA) and secondary ion mass spectrometry (SIMS) as described in Section 2.3. Lines of spot analyses were made through the shell profile perpendicular to the line of section (anterior-posterior) at the umbo, mid and posterior margin regions. Data are presented through line graphs of element concentrations through the shell profile, scatterplots are used to determine any possible statistical correlations between elements in *Mytilus edulis* and ANOVA boxplots are used to further determine any relationships in the chemistry of the two carbonate polymorphs, regions of the shell and the different stages of ontogeny.

4.2 Previous work

Calcite is one of the most abundant minerals formed in biogenic systems (Lowenstam, 1981). Calcite can be produced in an *in vitro* system containing merely Ca^{2+} and CO_3^{2-} ions in solution. However, this simple chemistry results in a range of forms in the biomineralised world. Following the pioneering geochemical work of Goldschmidt (1926; 1927), where the minor elements substituted for the major components of an ionic crystal lattice affecting the resultant structure of the mineral produced, greater importance is given to understanding the other chemical components associated with what appears to be a simple reaction in producing carbonate biominerals.

For calcium carbonate minerals, a number of previous studies concluded that magnesium (Mg) is vitally important in modifying growth of $CaCO_3$ in abiotic systems (Chave, 1954b; Degroot & Duyvis, 1966; Berner, 1975; Smallwood, 1977). The ability of Mg^{2+} and other divalent cations to substitute for Ca^{2+} in the calcium carbonate crystal lattice has been investigated previously (Reeder, 1983). This impurity can affect the dynamics of calcite crystal growth of the lattice e.g. Davis *et al.* (2000) on step edges resulting in elongation of crystal habit along the c-axis. Therefore, determination of crystal morphology and polymorphism has been attributed to Mg (Deleuze & Brantley, 1997; Sugawara & Kato, 2000; Rautaray *et al.*, 2005) and this control has been emphasised through further investigation of biogenic carbonate systems (Chave, 1954a; Waddell *et al.*, 1991; Hincke & St. Maurice, 2000; Cusack *et al.*, 2003; Herfort *et al.*, 2004). In the presence of elevated concentrations of Mg^{2+} ions in solution, calcite crystals grown *in vitro* showed altered crystal morphologies rather than the typical calcite rhombohedral shape (Meldrum & Hyde, 2001; Rautaray *et al.*, 2005). Indeed, high-Mg calcite is often the resultant composition (Kitano & Hood, 1965). In cases where concentrations of Mg in solution were raised sufficiently, aragonite, the metastable form of $CaCO_3$, was produced (Kitano & Hood, 1965; Fernandez-Diaz *et al.*, 1996; Sugawara & Kato, 2000). Precursor phases such as amorphous calcium carbonate (ACC), thought to be important in the formation of biomineral structures, were more stable in systems with higher Mg contents (Loste *et al.*, 2003). The importance of Mg control in these biogenic systems is

emphasised with the evidence of a physiological regulation of Mg in the calcite of *Mytilus edulis* (Lorens & Bender, 1977).

In *M. edulis* and other carbonate systems, other trace elements also create similar modifications to the resulting crystal lattice and also affect shell growth. The incorporation of these elements themselves is affected by the kinetics of the crystal growth (Rimstidt *et al.*, 1998). While magnesium is the primary element substituting for Ca^{2+} in calcite, strontium is also an important trace component (Pingitore *et al.*, 1992), and has been investigated in inorganic (Holland *et al.*, 1964; Katz *et al.*, 1972a; Lorens, 1981; Mucci & Morse, 1983) and biogenic systems (Cronblad & Malmgren, 1981; Lea *et al.*, 1999). Strontium affects, and is itself affected, by the dynamics of calcite growth. Incorporation of Sr can increase with an increase in calcite growth rate (Lorens, 1981), and at low concentrations, promotes faster growth of calcite with higher concentrations in solution slowing crystal growth through the pinning of kink sites and step edges (Wasylenki *et al.*, 2005b). This was determined, like Mg, to cause modification of calcite crystal morphology with SR affecting the $\{01\bar{1}0\}$ face causing flatter, tablet-like crystals. Similarly to elevated magnesium concentrations, large quantities of Sr^{2+} in solution cause a switch from calcite to aragonite growth (Reeder, 1983). However, growth modification by Sr incorporation are difficult to determine in natural systems as high Sr concentrations are normally associated with high Mg concentrations and so any modification by Sr will be obscured by the effect of Mg on the system.

Additional trace elements that can be present in biological carbonates systems are sulphur and monovalent sodium (Na^{+}). Due to the nature of biomineral systems, the minerals are closely associated with organic components, incorporated in the ultrastructure and within the individual crystals as soluble and insoluble macromolecules. This close association means that the chemistry of the organic material may impact on the crystals produced. This has led to the investigation of sulphur as an indicator of the presence of organic material in biomaterials in the form of sulphated sugars and polysaccharides (Dauphin *et al.*, 2003b; England, 2005). It has been suggested that sulphur can be present in biomineral systems as sulphate (SO_4^{2-}) which can become incorporated into the $CaCO_3$ lattice distorting the lattice parameters (Kontrec *et al.*, 2004). As a result, this affects the kinetics of the biomineral system and creates impurities in the calcite lattice (Kralj *et al.*, 2004) that can cause greater uptake of other impurities such as Mg^{2+}. The same study demonstrated that sulphate ions alone can create variations in calcite morphology. Therefore, determining the location and nature of sulphur in calcium carbonate biominerals is essential to understanding the role and influence of sulphur on the biomineral formation and also on the uptake of other trace elements.

The incorporation of sodium (Na^{+}) into biogenic carbonate systems remains unclear. In calcium carbonate, Mg^{2+} substitutes for Ca^{2+} and anions like sulphate (SO_4^{2-}) can substitute for carbonate

(CO_3^{2-}), the behaviour of monovalent ions is more difficult to determine (Ishikawa & Ichikuni, 1984; Okumura & Kitano, 1986). In biogenic marine carbonates and abiotic carbonate sediments Na^+ may substitute for Ca^{2+} in the $CaCO_3$ crystal lattice (Billings & Ragland, 1968; Amiel *et al.*, 1973; Land & Hoops, 1973) with incorporation into the aragonite lattice being easier than into the calcite structure.

Despite the uncertainty about the nature and location of trace elements in biomineral systems, biogenic carbonate shells produced by molluscan species such as *Mytilus* (Dodd, 1965; Malone & Dodd, 1967; Dodd & Crisp, 1982), can record the temperature and salinity of the environment in which they form. The environmental data is interpreted through the trace element composition of the biominerals which then serve as proxies of the environmental conditions (Lea, 2003).

Mg/Ca ratios in $CaCO_3$ skeletons of coccoliths, Foraminifera (Nurnberg, 1995; Elderfield & Ganssen, 2000), brachiopods (Lowenstam, 1961; Mii & Grossman, 1994) and molluscs (Klein *et al.*, 1996a) are controlled by seawater temperature. Positive correlations occur in each of these cases. However, further investigations have shown that the relationship is complicated with variations in trace element concentrations within shells (Erez, 2003; Eggins *et al.*, 2004), physiological controls (Lorens & Bender, 1977), other environmental controls (Bender *et al.*, 1976) and ontogenic effects (Buening & Carlson, 1992; Hintz *et al.*, 2006) with some biomineral systems producing no definite correlation (Vander Putten *et al.*, 2000). Variation in Mg/Ca ratios have even been investigated in biominerals produced in constant temperature environments like the avian eggshell (Cusack *et al.*, 2003; Dalbeck & Cusack, 2006). Sr/Ca ratios are also employed as environmental indicators (Dodd, 1965; Dodd & Crisp, 1982; Klein *et al.*, 1996b; Stoll *et al.*, 2002) even though growth rate (Stecher *et al.*, 1996), metabolic factors (Rosenberg & Hughes, 1991; Klein *et al.*, 1996b; Purton *et al.*, 1999) and ontogeny (Purton-Hildebrand *et al.*, 2001) may influence Sr uptake. Such factors may also contribute to distributions of Na and S which have been proposed to be associated with organic material that is intimately associated with the mineral phase (Lorens & Bender, 1980; Vander Putten *et al.*, 1999). The true nature of Na and S incorporation must also be deduced as attempts to apply Na as a climate proxy have also been carried out (Veizer *et al.*, 1977; White, 1977).

4.3 Results

4.3.1 Chemical profiles

Lines of spot analyses across the shell profile were obtained through Electron Probe Micro Analysis (EPMA) and Secondary Ion Mass Spectrometry (SIMS) as described in Section 2.3.2 and 2.3.3 respectively. Line analyses by EPMA were made in the umbo section, the mid section and

posterior edge section of three specimens from the six ontogenic stages, A-F. Line analyses by SIMS were also performed in the umbo, mid and posterior region for single specimens from stages A-E of ontogeny, with the exception of stage E where only the umbo section was analysed. In some stages, two profiles were produced for the umbo region of some specimens due to variation in mineralogy distribution and to provide sufficient data points for each polymorph. Details of the ontogenic stages and their respective ages are given in Section 2.1.2. The line profiles are presented in Figures 4.1-4.8 for each stage of ontogeny and the specimens analysed in each stage. Calculated detection limits for EPMA are as follows: Na (0.023wt%), Mg (0.027wt%), S (0.033wt%) and Sr (0.032wt%). Some spot analyses for these elements in each specimen fall below detection limits but are included to retain continuity in each individual line traverse and comparisons in element distribution between different areas of the samples.

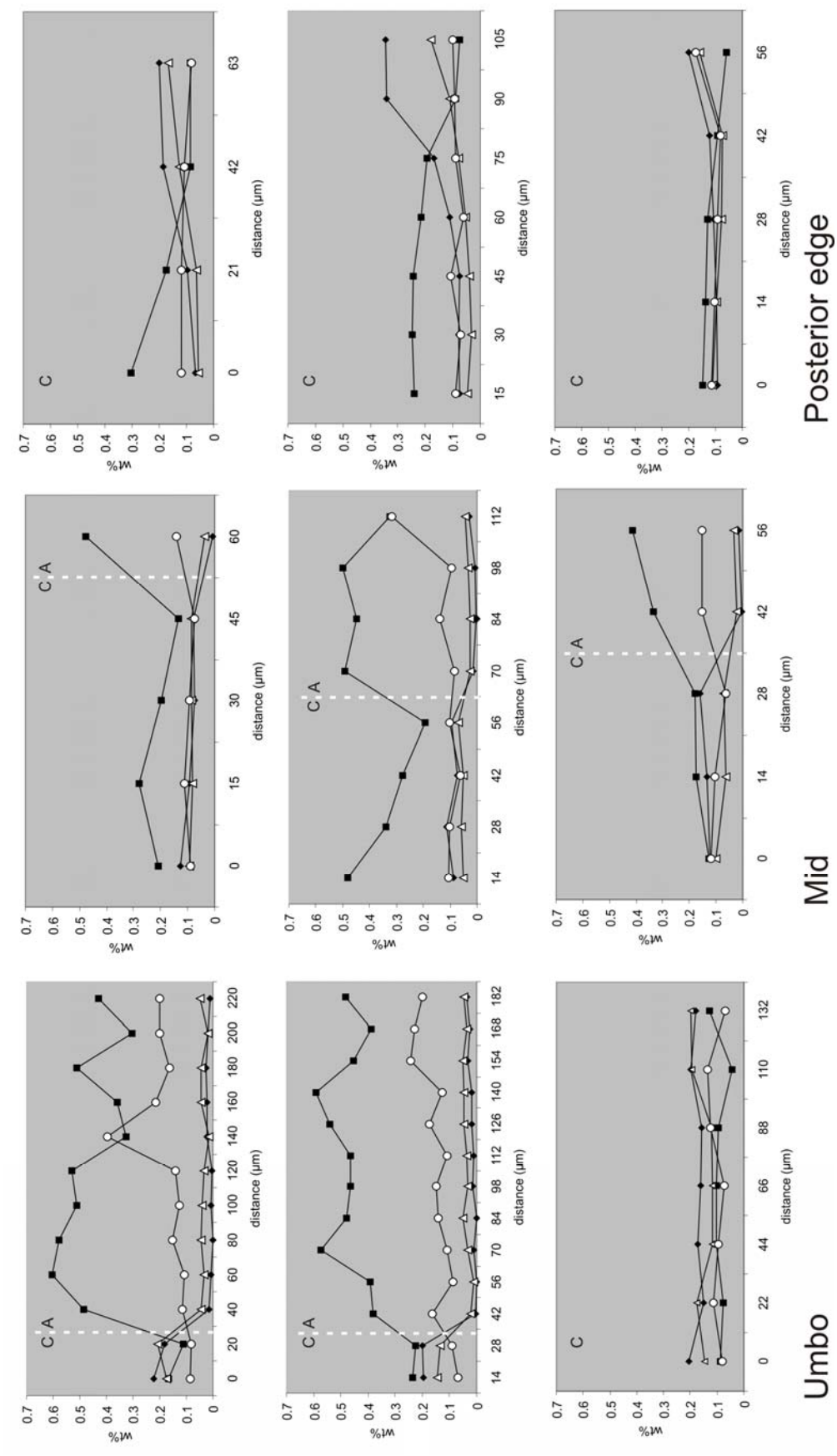

Figure 4.1. Trace element profiles for three specimens from the A stage of ontogeny (<1cm, 10-12months). Line graphs showing the element profile through the shell from the outer surface (left of each graph) to the inner surface (right of each graph) in three sections of the shell; umbo, mid region and the posterior edge. The switch between the $CaCO_3$ polymorph is marked for each profile with a white dashed line. Calcite is denoted by 'C' and aragonite 'A'. Elements are labelled as follows: Na (black squares), Mg (black diamonds), S (white triangles), Sr (white circles). Data were collected via EPMA.

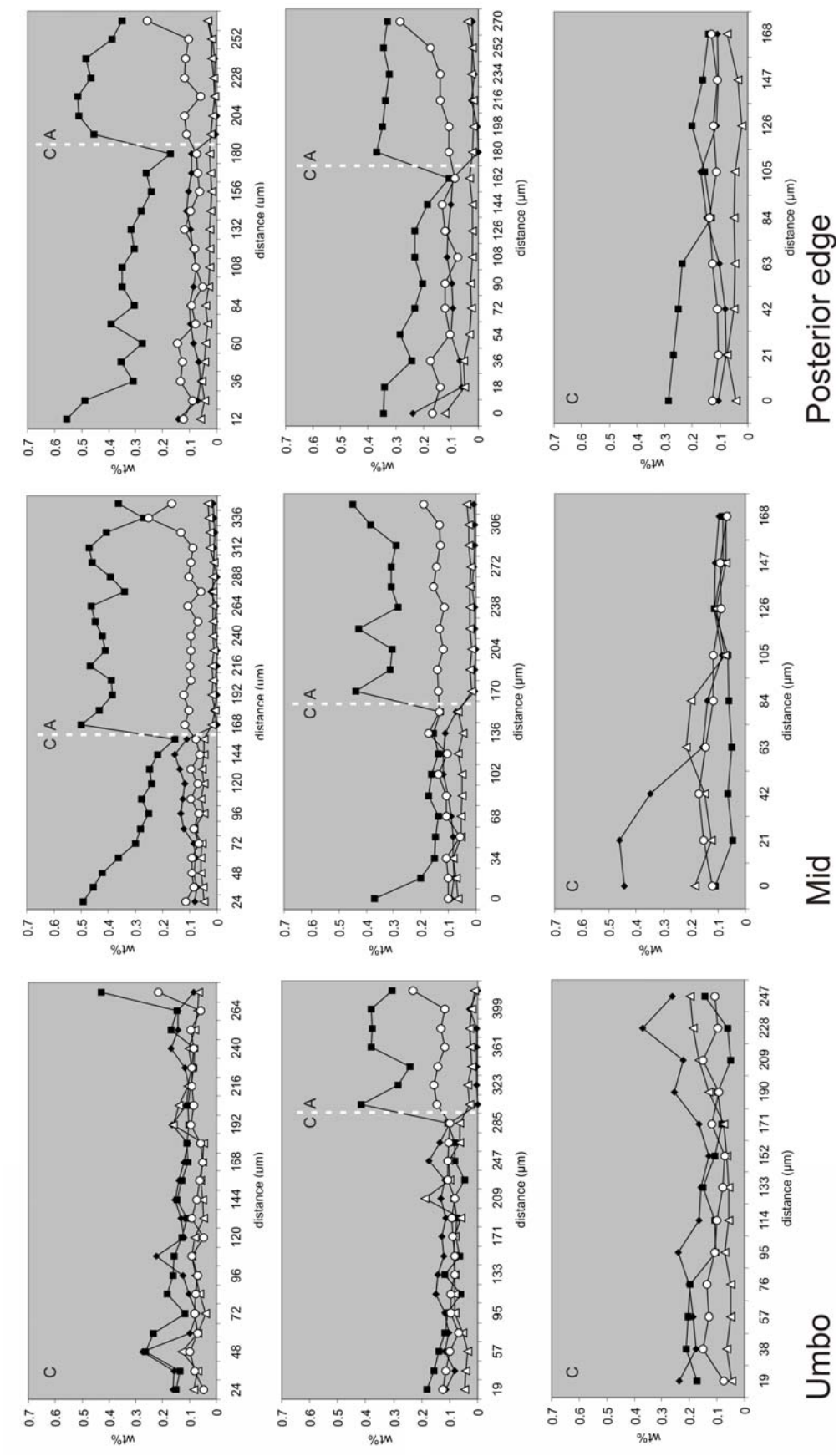

Figure 4.2. Trace element profiles for three specimens from the B stage of ontogeny (1-2.5cm, 12-14 months). Line graphs showing the element profile through the shell from the outer surface (left of each graph) to the inner surface (right of each graph) in three sections of the shell; umbo, mid region and the posterior edge. The switch between the $CaCO_3$ polymorph is marked for each profile with a white dashed line. Calcite is denoted by 'C' and aragonite 'A'. Elements are labelled as follows: Na (black squares), Mg (black diamonds), S (white triangles), Sr (white circles). Data were collected via EPMA.

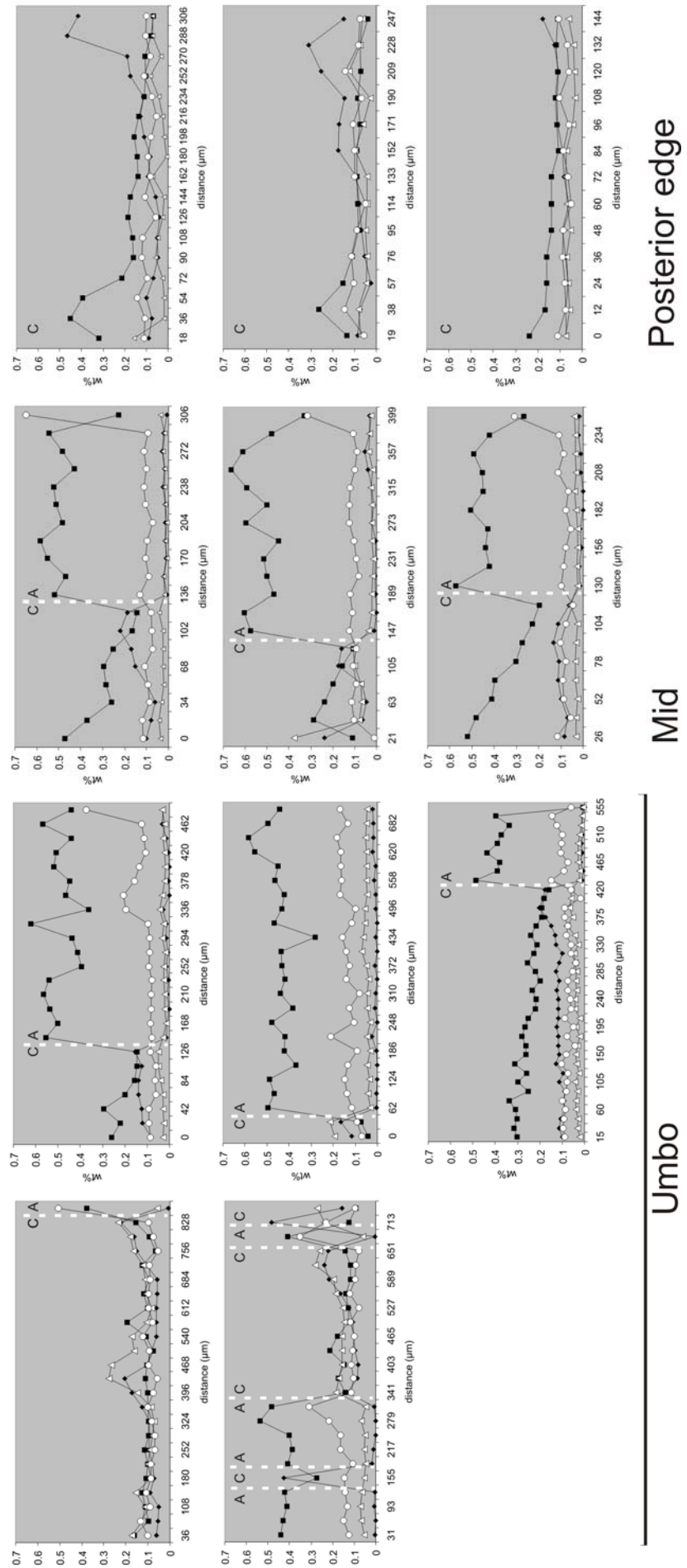

Figure 4.3. Trace element profiles for three specimens from the C stage of ontogeny (2.6-3.5cm, 22-24 months). Line graphs showing the element profile through the shell from the outer surface (left of each graph) to the inner surface (right of each graph) in three sections of the shell; umbo, mid region and the posterior edge. Where two profiles are present in the umbo region, the left profile is the closest to the shell anterior. The switch between the $CaCO_3$ polymorph is marked for each profile with a white dashed line. Calcite is denoted by 'C' and aragonite 'A'. Elements are labelled as follows: Na (black squares), Mg (black diamonds), S (white triangles), Sr (white circles). Data were collected via EPMA.

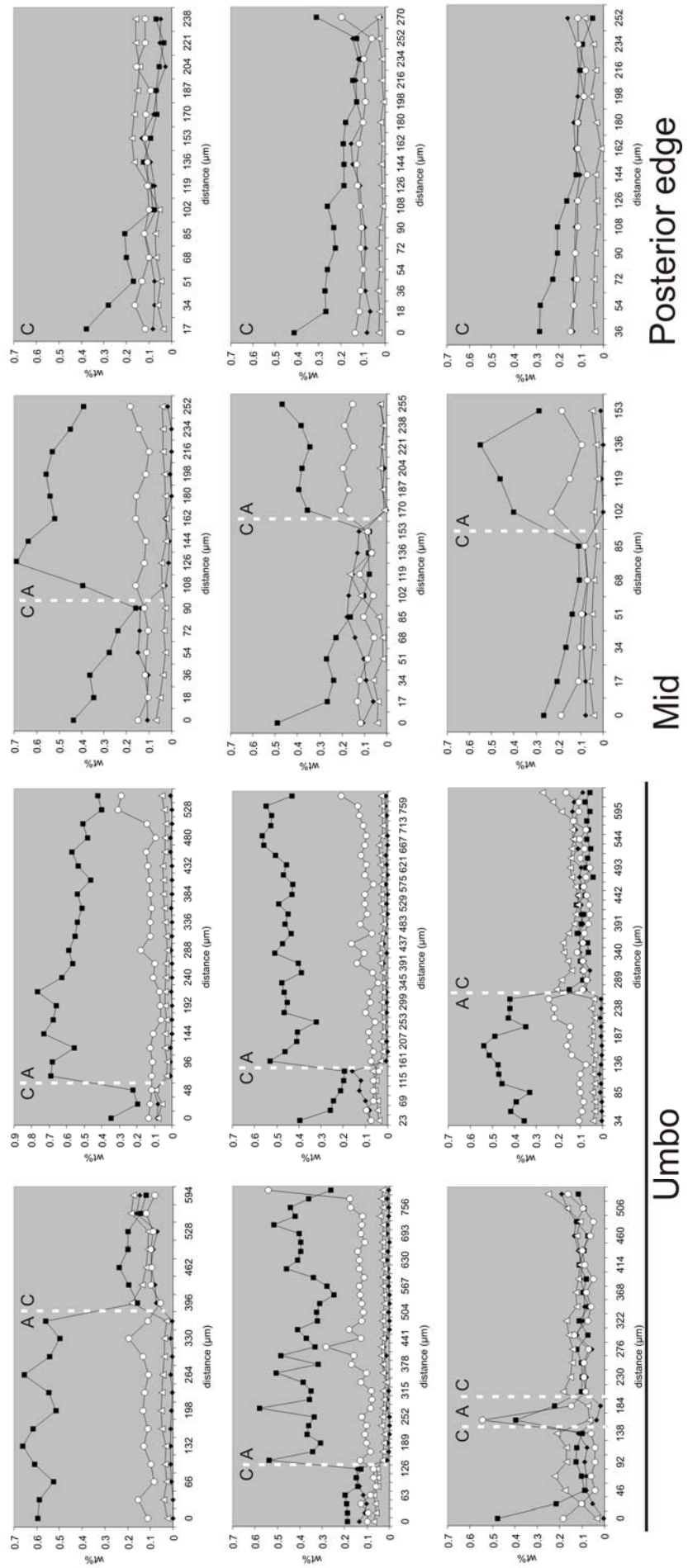

Figure 4.4. Trace element profiles for three specimens from the D stage of ontogeny (3.6-4.3cm, 24-26 months). Line graphs showing the element profile through the shell from the outer surface (left of each graph) to the inner surface (right of each graph) in three sections of the shell; umbo, mid region and the posterior edge. Where two profiles are present in the umbo region, the left profile is the closest to the shell anterior. The switch between the $CaCO_3$ polymorph is marked for each profile with a white dashed line. Calcite is denoted by 'C' and aragonite 'A'. Elements are labelled as follows: Na (black squares), Mg (black diamonds), S (white triangles), Sr (white circles). Data were collected via EPMA.

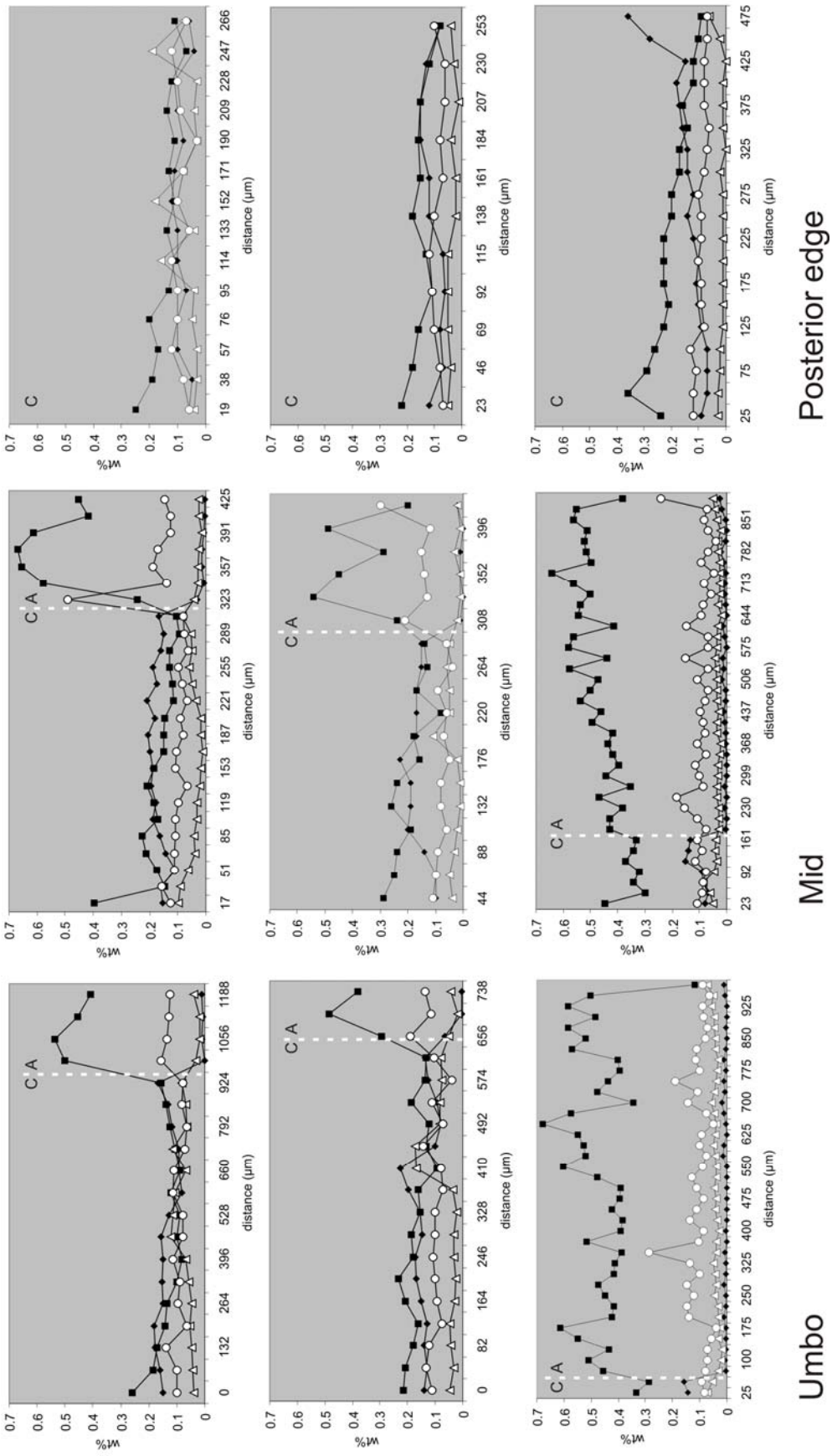

Figure 4.5. Trace element profiles for three specimens from the E stage of ontogeny (4.4-5cm, 34-36 months). Line graphs showing the element profile through the shell from the outer surface (left of each graph) to the inner surface (right of each graph) in three sections of the shell; umbo, mid region and the posterior edge. The switch between the $CaCO_3$ polymorph is marked for each profile with a white dashed line. Calcite is denoted by 'C' and aragonite 'A'. Elements are labelled as follows: Na (black squares), Mg (black diamonds), S (white triangles), Sr (white circles). Data

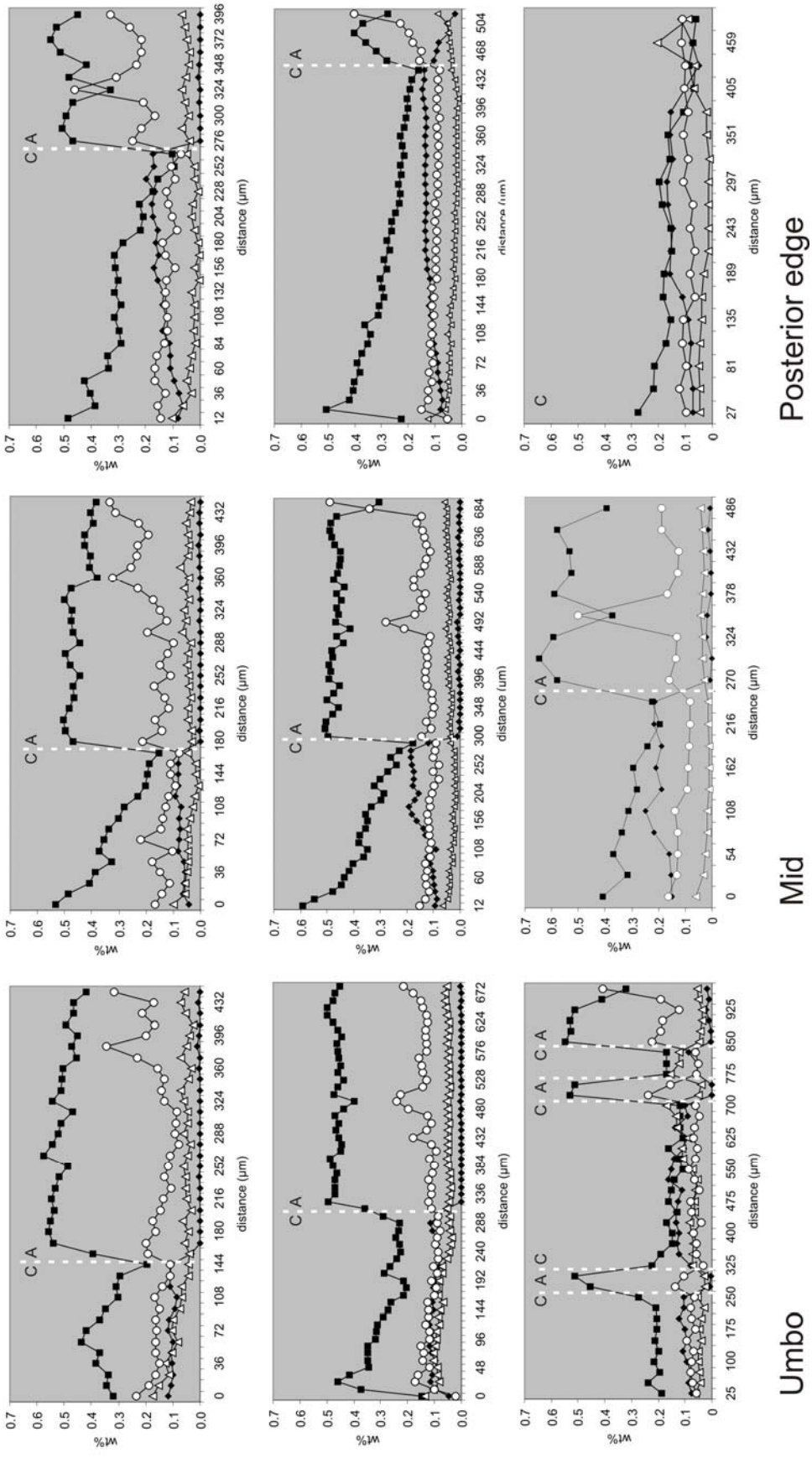

Figure 4.6. Trace element profiles for three specimens from the F stage of ontogeny (5.1-6cm, 36+ months). Line graphs showing the element profile through the shell from the outer surface (left of each graph) to the inner surface (right of each graph) in three sections of the shell; umbo, mid region and the posterior edge. The switch between the $CaCO_3$ polymorph is marked for each profile with a white dashed line. Calcite is denoted by 'C' and aragonite 'A'. Elements are labelled as follows: Na (black squares), Mg (black diamonds), S (white triangles), Sr (white circles). Data were collected via EPMA.

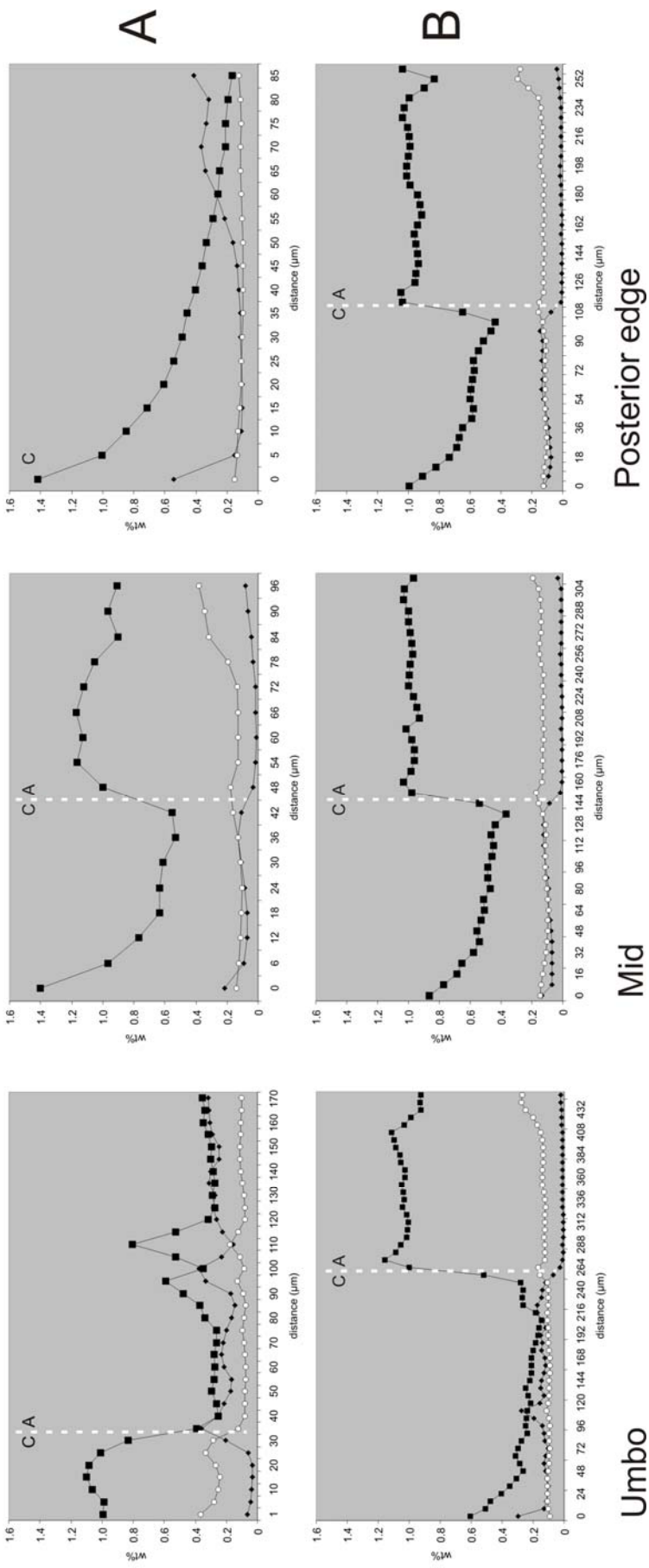

Figure 4.7. Trace element profiles obtained via SIMS for stage A (top row) and B (bottom row) of ontogeny. Line graphs showing the element profile through the shell specimens from the outer surface (left of each graph) to the inner surface (right of each graph) in three sections of the shell; umbo, mid region and the posterior edge. The switch between the $CaCO_3$ polymorph is marked for each profile with a white dashed line. Calcite is denoted by 'C' and aragonite 'A'. Elements are labelled as follows: Na (black squares), Mg (black diamonds), Sr (white circles).

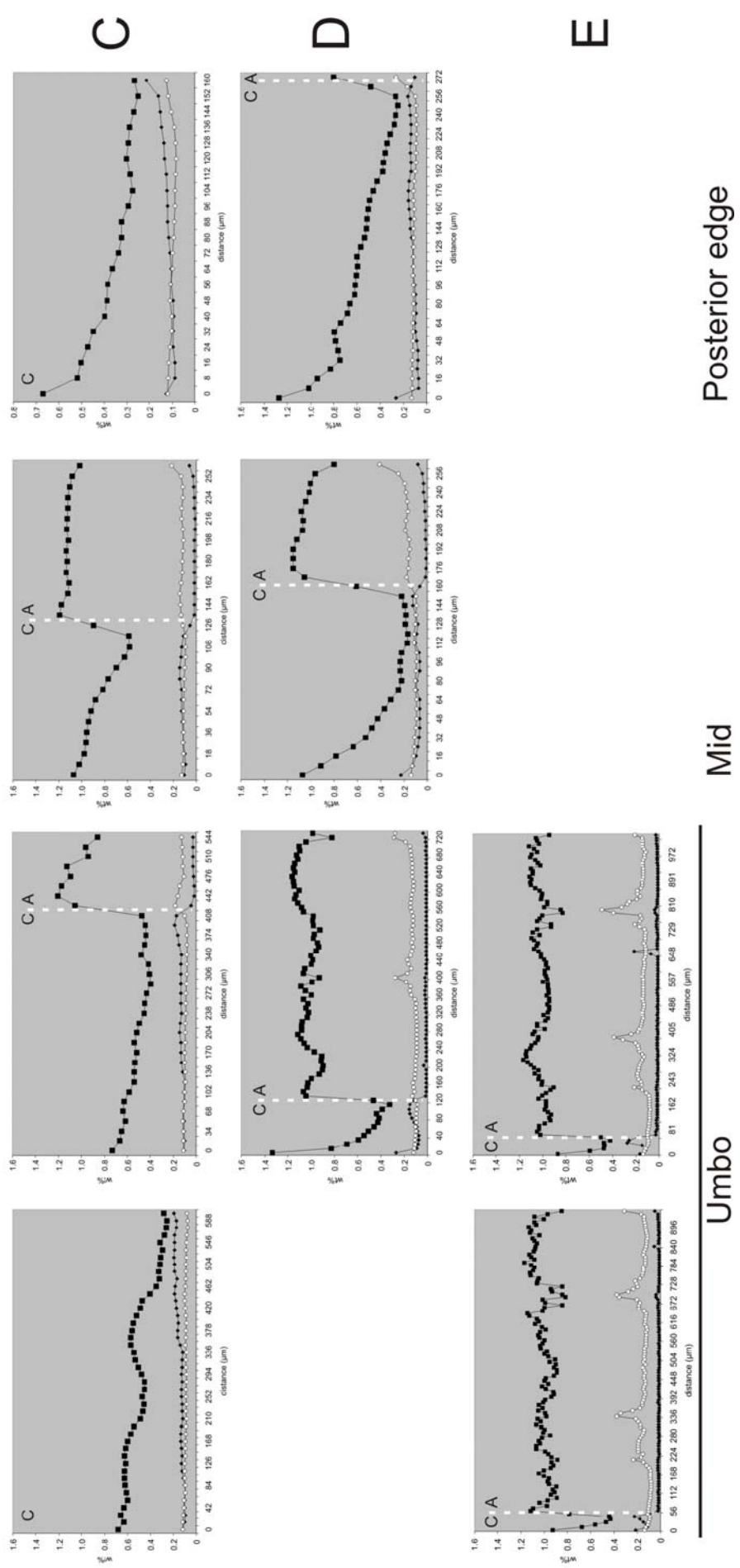

Figure 4.8. Trace element profiles obtained via SIMS for stage C (top row), D (middle row) and E (bottom row) of ontogeny, line graphs showing the element profile through the shell specimens from the outer surface (left of each graph) to the inner surface (right of each graph) in three sections of the shell; umbo, mid region and the posterior edge. Where two profiles are present in the umbo region, the left profile is the closest to the shell anterior. The switch between the CaCO3 polymorph is marked for each profile with a white dashed line. Calcite is denoted by 'C' and aragonite 'A'. Elements are labelled as follows: Na (black squares), Mg (black

The profiles obtained by EPMA show a distinct and common pattern in all stages of ontogeny, with similar distribution patterns observed in the umbo, mid and posterior regions. This is also observed in the data obtained via SIMS. The difference in element concentrations between the polymorphs is clearly evident with profiles of Na and Sr showing clear distinctions between the polymorph layers and almost an absence of Mg and S often falling below detection limits for EPMA in the aragonite layer.

Sodium concentration decreases from the outer surface of the calcite layer towards the polymorph interface, with a marked recovery in concentration in the aragonite, often greater than the initial concentration in the calcite. This recovery in Na^+ concentration is followed by a relatively constant Na^+ concentration through the nacreous aragonite layer. Na^+ concentration ranges from 0.1-0.8wt% in EPMA data and 0.2-1.4wt% for SIMS data. The reason for this marked difference is unknown but can possibly be attributed to uncertainty of the Na concentration of the OKA standard used in SIMS. Sharp drops in Na^+ concentration within the nacreous aragonite layer are often accompanied by correspondingly sharp rises in Sr concentration, observed more notably in Figure 4.1 & 4.8 in the umbo region of A and E stages of ontogeny and Figure 4.6 in all regions in the F stage of ontogeny.

Strontium concentrations are relatively invariant through most profiles apart from the 'spikes' in the aragonite layer in some sections as mentioned above. Sr concentrations range between 0.05wt%-0.6wt% in both SIMS and EPMA data. In a number of the profiles, an initial increase in Sr concentration is observed when crossing the polymorph interface with Sr concentration in the aragonite layer commonly higher than in the calcite layer. Also, an increase in Sr concentration can often be observed at the innermost points of the profiles in all three areas in all stages of ontogeny.

Magnesium concentrations vary between 0.05-0.25wt% in the calcite layer but Mg is almost absent in the aragonite layer. The Mg profile remains invariant through the calcite layer in all stages of ontogeny, however, in many of the profiles (Figures 4.1-4.8), an increase in Mg concentration can be observed moving from the outer edge towards the polymorph interface, where concentrations fall abruptly in the aragonite layer.

The profile of sulphur through the shell is not as distinctive as that of the other elements analysed here, with S concentrations often showing similar behaviour to that of Mg with an increase in concentration in the calcite layer preceding the change in polymorph. This is followed by very low S concentrations in the aragonite layer. Frequently, a sharp decrease in S concentration is observed in the outermost part of the calcite layer, in the initial spot analyses of the profiles. However, this pattern is inconsistent between specimens and in some profiles the difference observed between

polymorphs is almost indiscernible. However, the range in S concentration in the calcite layer is between 0.02wt%-0.3wt% and between 0.02wt%-0.1wt% in the aragonite layer.

In the three sections analysed in each specimen, the umbo region shows the most deviation from the typical element profile described here, compared to the rest of the shell. In some sections, only calcite is present but the profiles appear more irregular to that of other wholly calcitic areas such as profiles from the posterior edge region. Also, in some specimens, changes in polymorph occurs a number of times across the shell, producing erratic changes in the profile.

4.3.2 Element concentration through ontogeny

The mean concentrations and range of element concentrations for data collected via EPMA and SIMS were investigated using ANOVA boxplots to determine the differences in concentration between the different areas of the shell analysed, the differences between the polymorphs in each section and how this varies throughout ontogeny are displayed in Figures 4.9-4.14.

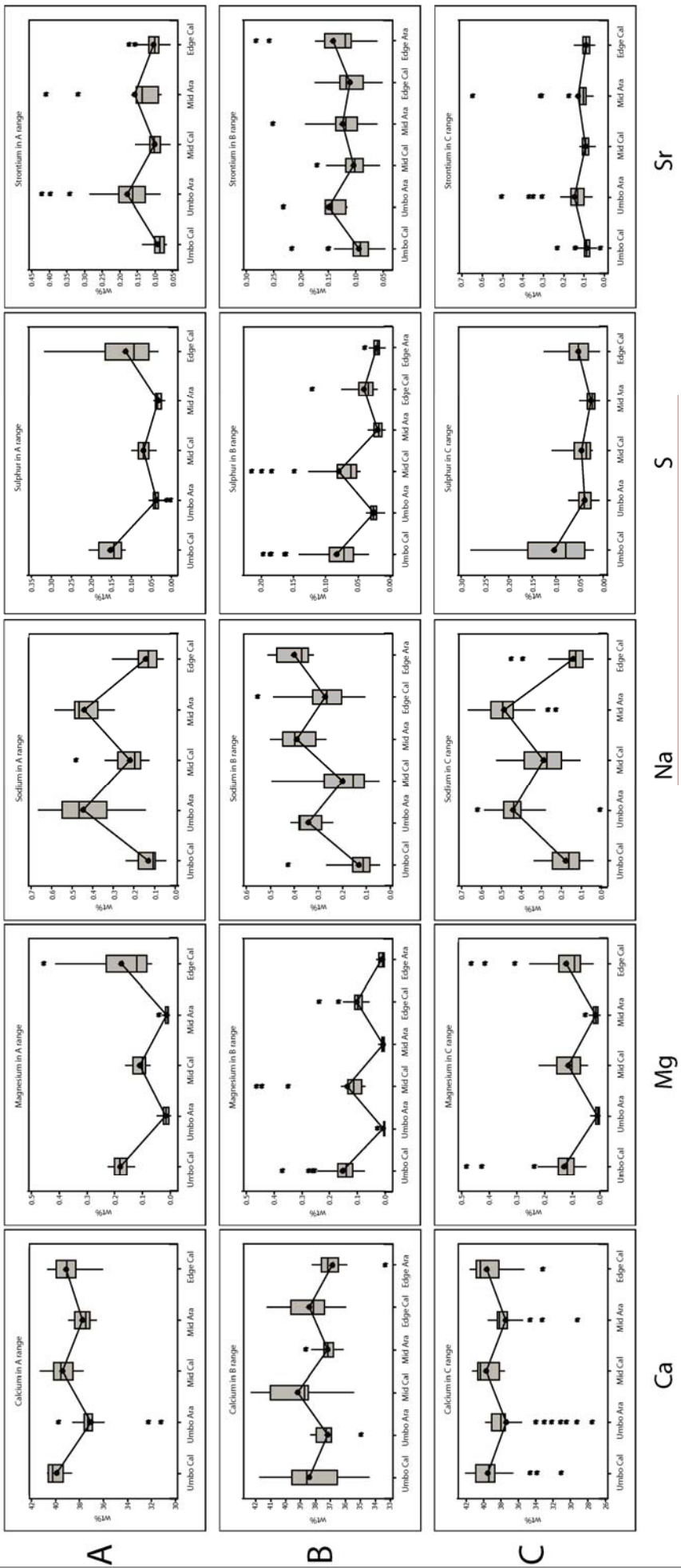

Figure 4.9. ANOVA box plots comparing mean element concentrations in the calcite and aragonite layers of *M. edulis* in three stages of ontogeny: A (top row), B (middle row) & C (bottom row). In each graph, moving left to right, the boxes represent data for the calcite in the umbo, aragonite in the umbo, calcite in the mid region, aragonite in the mid region, calcite in the posterior edge and aragonite in the posterior edge in the B stage of ontogeny. Each box represents the interquartile range (IQR) of the sample set (i.e. Q1–Q3). Top and bottom whiskers extend from the box to the highest and lowest values within Q1+1.5*IQR. Values outside the range of the whiskers are marked as an asterisk (*). Mean values are displayed as circles. The median value is represented by a horizontal line bisecting the box. Note that Mg is below detection limit in aragonite but has been included for continuity in comparing the polymorphs. Data were collected via EPMA.

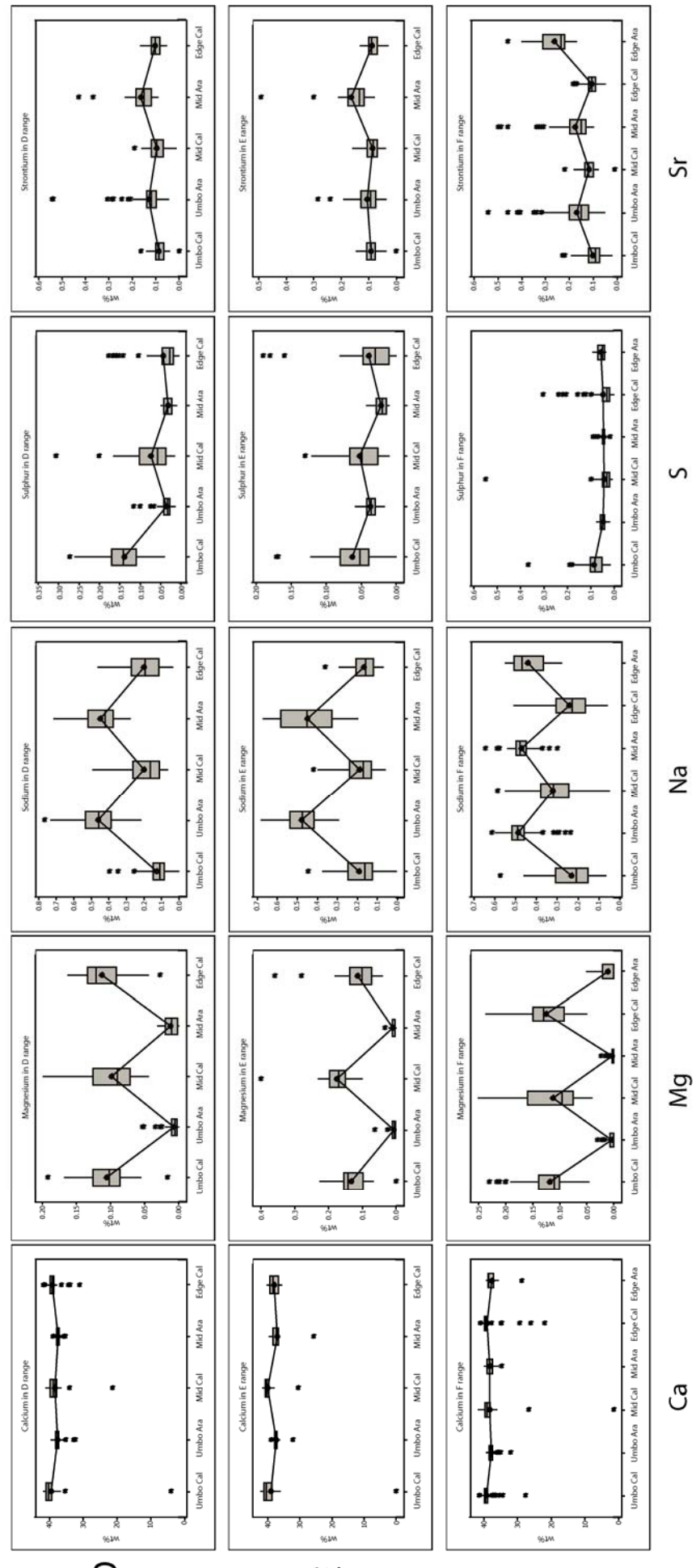

Figure 4.10. ANOVA box plots comparing mean element concentrations in the calcite and aragonite layers of *M. edulis* in three stages of ontogeny: D (top row), E (middle row) & F (bottom row). In each graph, moving left to right, the boxes represent data for the calcite in the umbo, aragonite in the umbo, calcite in the mid region, aragonite in the mid region, calcite in the posterior edge and aragonite in the posterior edge in the F stage of ontogeny. Each box represents the interquartile range (IQR) of the sample set (i.e. Q1–Q3). Top and bottom whiskers extend from the box to the highest and lowest values within Q1+1.5*IQR. Values outside the range of the whiskers are marked as an asterisk (*). Mean values are displayed as circles. The median value is represented by a horizontal line bisecting the box. Note that Mg is below detection limit in aragonite but has been included for continuity in comparing the polymorphs. Data were collected via EPMA.

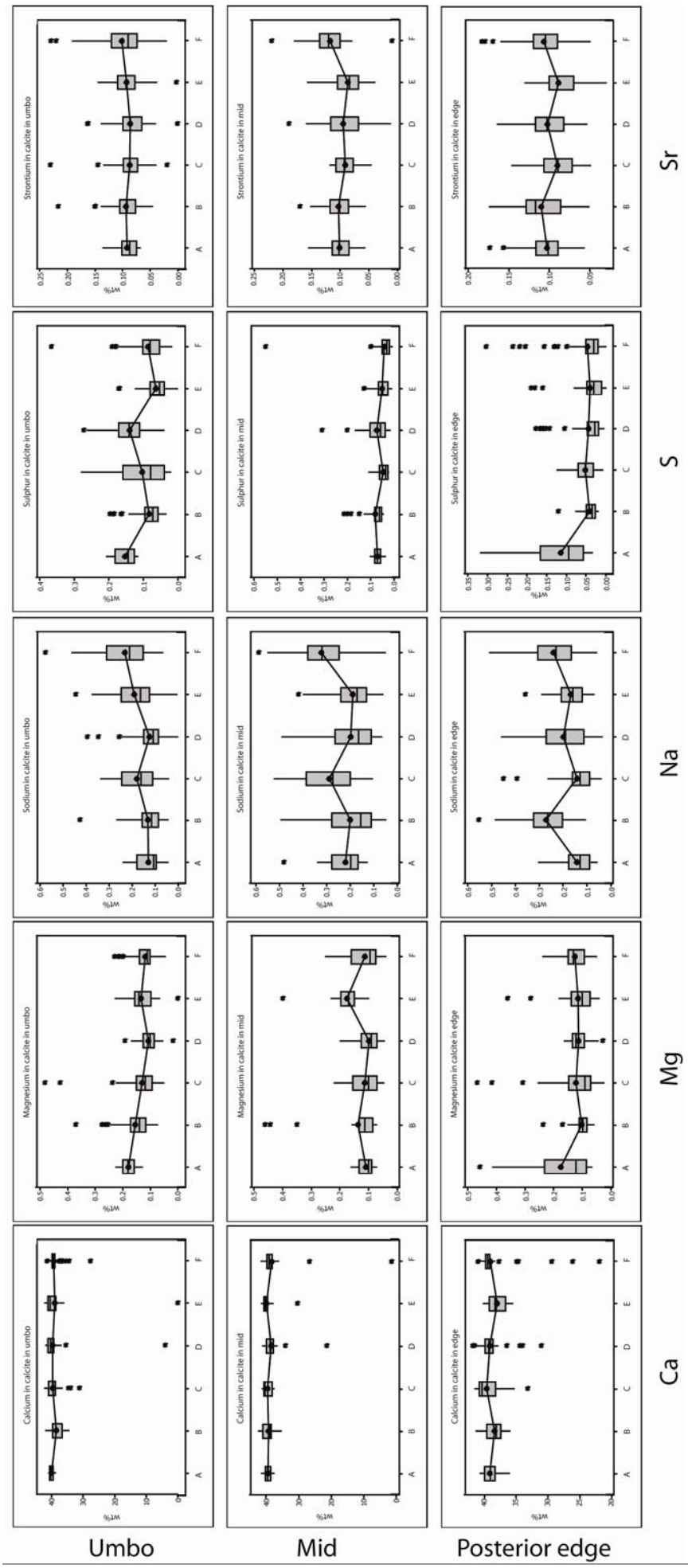

Figure 4.11. ANOVA box plots comparing mean element concentrations in the calcite layers of *M. edulis* through all stages of ontogeny in three different sections of the shell: umbo (top row), mid region (middle row) & posterior edge (bottom row). In each graph, moving left to right, the boxes represent data for the A, B, C, D, E & F stages of ontogeny. Each box represents the interquartile range (IQR) of the sample set (i.e. Q1–Q3). Top and bottom whiskers extend from the box to the highest and lowest values within Q1+1.5*IQR. Values outside the range of the whiskers are marked as an asterisk (*). Mean values are displayed as circles. The median value is represented by a horizontal line bisecting the box. Data were collected via EPMA.

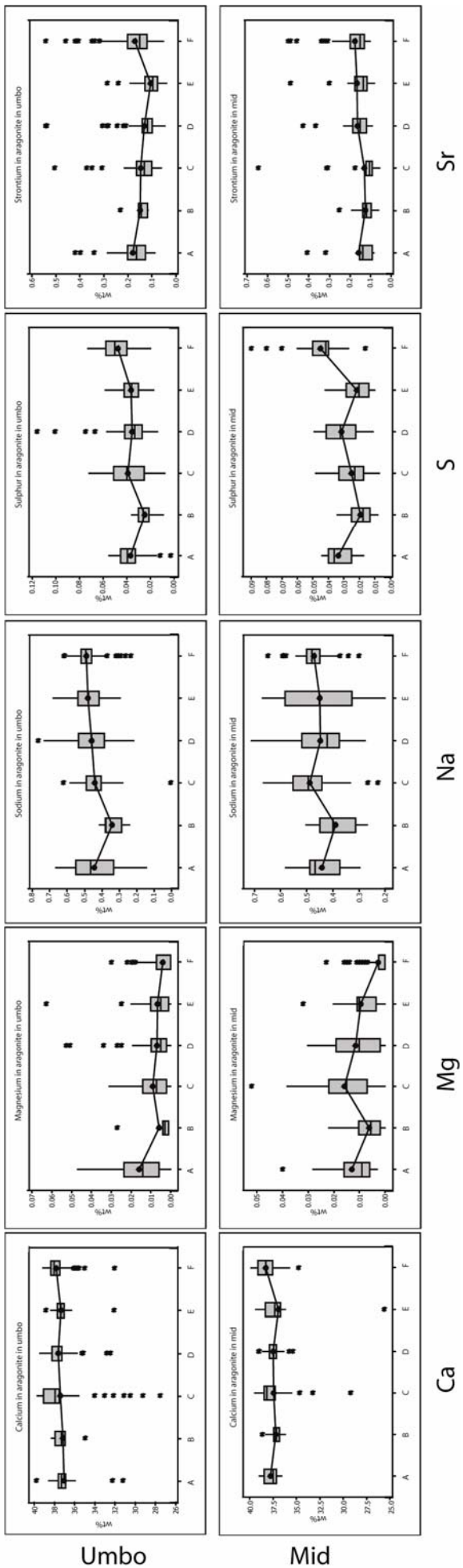

Figure 4.12. ANOVA box plots comparing mean element concentrations in the aragonite layers of *M. edulis* through all stages of ontogeny in two different sections of the shell: umbo (top row) & mid region (bottom row). In each graph, moving left to right, the boxes represent data for the A, B, C, D, E & F stages of ontogeny. Each box represents the interquartile range (IQR) of the sample set (i.e. Q1–Q3). Top and bottom whiskers extend from the box to the highest and lowest values within Q1+1.5*IQR. Values outside the range of the whiskers are marked as an asterisk (*). Mean values are displayed as circles. The median value is represented by a horizontal line bisecting the box. Note that Mg is below detection limit in aragonite but has been included for continuity in comparing the polymorphs. Data were collected via EPMA.

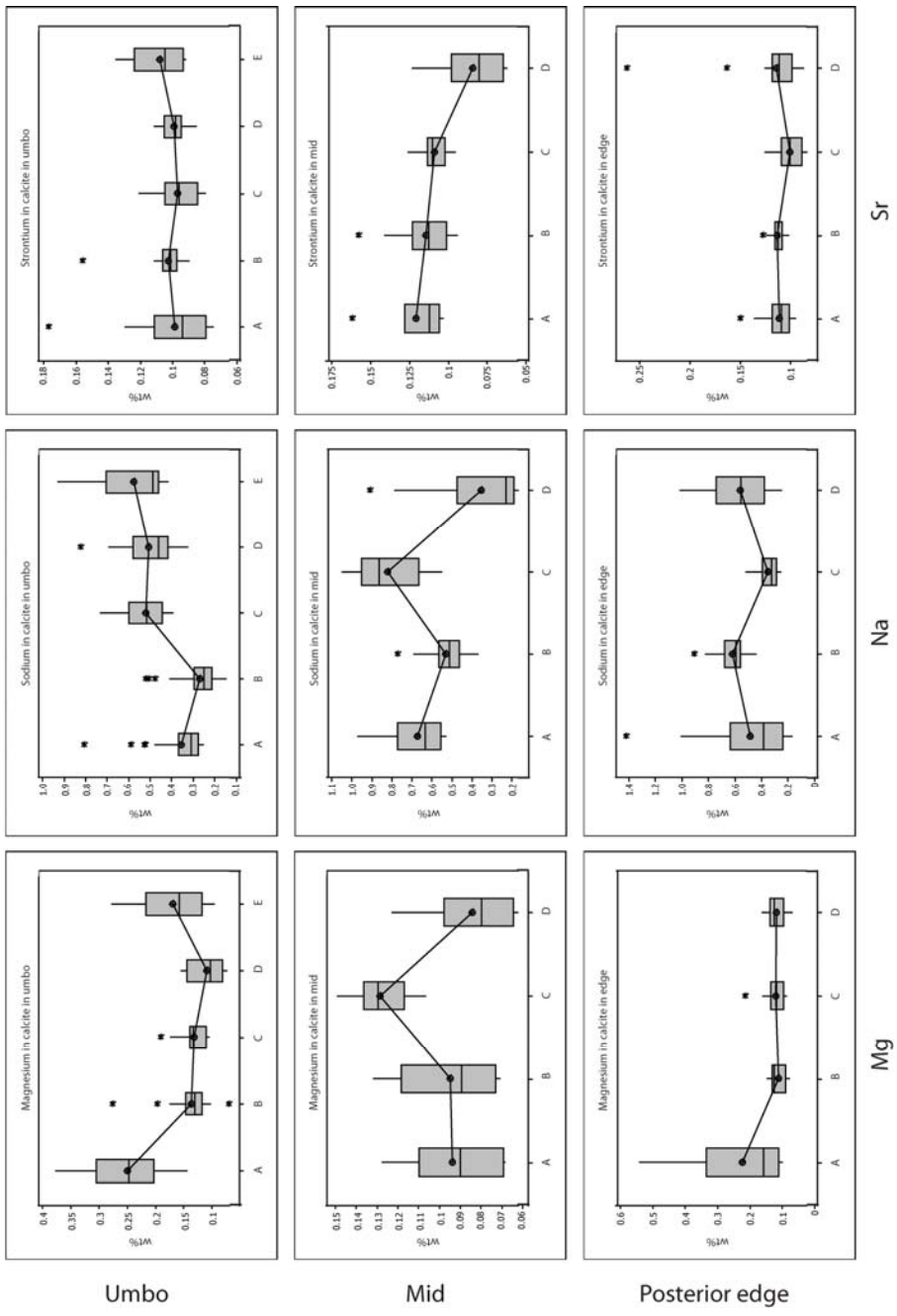

Figure 4.13. ANOVA box plots comparing mean element concentrations in the calcite layers of single specimens of *M. edulis* through 5 stages of ontogeny in three different sections of the shell: umbo (top row), mid region (middle row) & posterior edge (bottom row). In each graph, moving left to right, the boxes represent data for the A, B, C, D & E stages of ontogeny. Each box represents the interquartile range (IQR) of the sample set (i.e. Q1–Q3). Top and bottom whiskers extend from the box to the highest and lowest values within Q1+1.5*IQR. Values outside the range of the whiskers are marked as an asterisk (*). Mean values are displayed as circles. The median value is represented by a horizontal line bisecting the box. Data were collected via SIMS analysis.

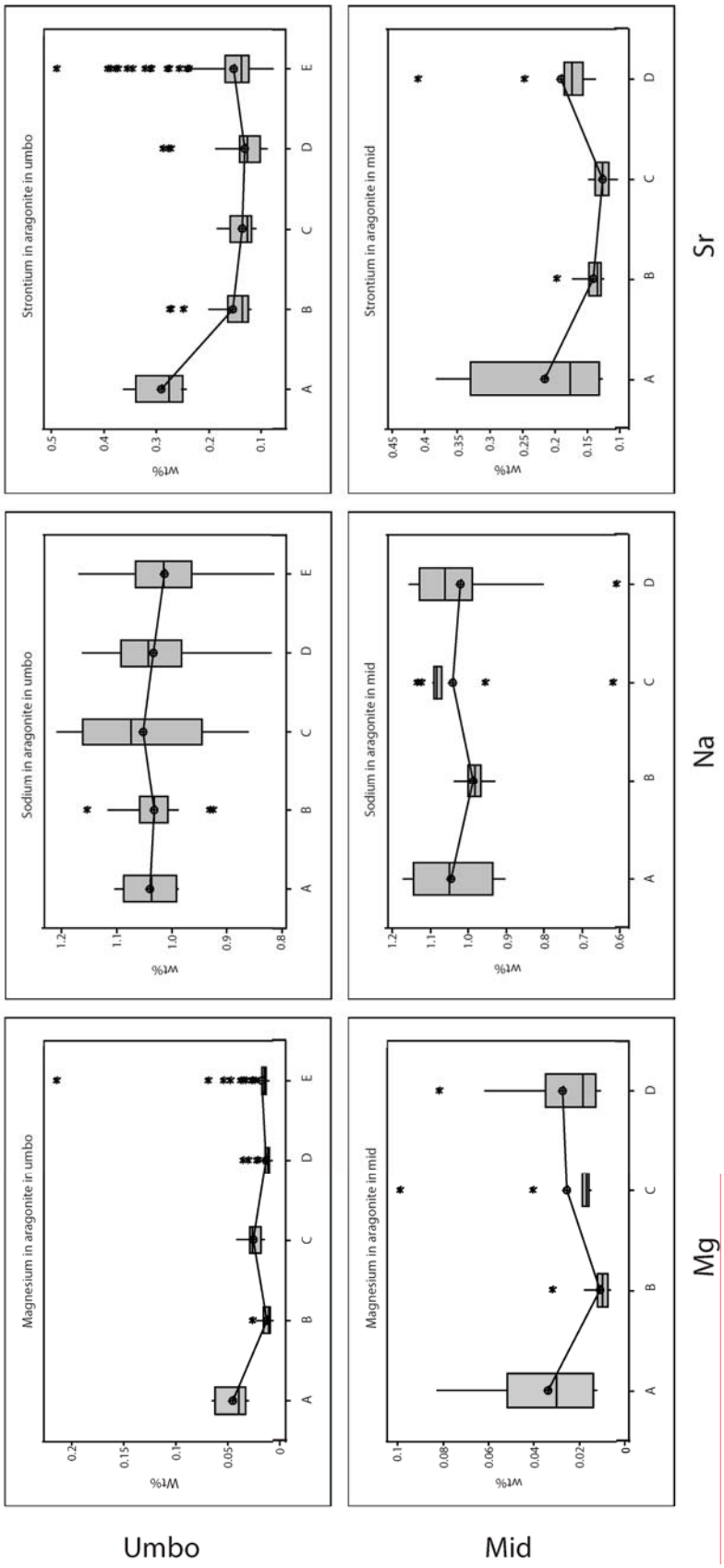

Figure 4.14. ANOVA box plots comparing mean element concentrations in the aragonite layers of single specimens of *M. edulis* through 5 stages of ontogeny in two different sections of the shell: umbo (top row) & mid region (bottom row). In each graph, moving left to right, the boxes represent data for the A, B, C, D & E stages of ontogeny. Each box represents the interquartile range (IQR) of the sample set (i.e. Q1–Q3). Top and bottom whiskers extend from the box to the highest and lowest values within Q1+1.5*IQR. Values outside the range of the whiskers are marked as an asterisk (*). Mean values are displayed as circles. The median value is represented by a horizontal line bisecting the box. Note that Mg is below detection limit in aragonite but has been included for continuity in comparing the polymorphs. Data were collected via SIMS.

For each element, the distribution patterns already discussed is emphasised in the ANOVA boxplots. The marked difference in Mg and Na concentrations between the calcite and the aragonite layer in all specimens is apparent and the greater concentration of S in calcite compared to aragonite is more well-defined.

For many of the elements, the spread of the data ranges represented by the boxes shows significant overlap and so differences between the umbo, mid and posterior regions analysed are minor, although some general trends are observed, as described below.

Ca concentrations are slightly lower in the aragonite layer compared to the calcite layer in all regions and all stages of ontogeny (Figure 4.9 & 4.10). Ca concentration in the calcite layer is uniform throughout ontogeny in all stages, with only some slight variation in the posterior edge (Figure 4.11). In the aragonite layer, Ca concentration for the most part also shows uniformity between ontogenic stages and in the different regions (Figure 4.9 & 4.10) analysed but shows more outlying data points than the calcite layer (Figure 4.12).

Aside from the obvious difference between the polymorphs, Mg does not show any significant change in concentration moving posteriorly down the shell length in the calcite layer. The exact behaviour of Mg and any pattern in the aragonite layer is difficult to determine as many of the data points are below EPMA detection limits. However, the SIMS data provide little evidence for any major differences in mean Mg concentrations between different areas of the shell (Figure 4.14). Through ontogeny the mean Mg concentrations decrease in the umbo region in the calcite layer (Figure 4.11 & 4.13) and also the aragonite layer (Figure 4.14). However, this pattern is not consistent between different regions of the shell. The SIMS data suggest that the youngest ontogenic stage (stage A <1cm) has a higher mean concentration of Mg for both polymorphs and in all regions apart from the calcite in the mid region.

The mean concentration of Na does not decrease or increase significantly, moving posteriorly down the shell in the three major regions analysed here for either polymorph. No distinct pattern can be discerned in any ontogenic stage that can be said to recur in each subsequent ontogenic stage except for the greater concentration of Na in the aragonite layer than the calcite layer. However, the SIMS data obtained for the calcite in the umbo region of the shell indicates that the younger stages of ontogeny, A and B, show lower mean values of Na than older stages (Figure 4.13).

Mean sulphur concentrations in the calcite layer do fall from the umbo region to the posterior edge (Figures 4.10 & 4.11). S concentrations in the aragonite layer are often below EPMA detection limits and so significant trends are difficult to deduce for the nacre layer but from the data obtained here no significant pattern can be easily discerned. Through ontogeny, the earliest stage, A, shows

higher concentrations of sulphur in the calcite region of the umbo and the posterior edge, with the mean concentrations in the mid regions very uniform through all stages of ontogeny in the calcite layer (Figure 4.11).

The EPMA data shows that the range in data and the mean concentration of Sr through the shell regions in each stage of ontogeny (Figure 4.9 & 4.10) and the Sr concentration through ontogeny in each of the regions (Figure 4.11 & 4.12) investigated is relatively uniform. However, there are notable differences in Sr concentration between the polymorphs in each individual stage with higher mean Sr concentrations in the aragonite layer. The SIMS data for Sr in the aragonite layer show that higher concentrations exist in the youngest stage of ontogeny, the A stage, with a decrease in the older stages (Figure 4.14). This trend is also visible in the mid region of the calcite layer (Figure 4.13) but is not clearly seen in the other regions for the calcite layer in either the SIMS or EPMA data.

4.3.3 Trace Element Correlations

To establish any statistical correlation between specific trace elements, Pearson correlation co-efficients for the EPMA data were determined (Tables 4.1-4.3) and linear relationships and R^2 values were calculated for the SIMS data (Figure 4.15-4.18). The R^2 values in the scatterplots represent the squared value of the Pearson co-efficient; a value closer to 1 indicates a greater statistical correlation.

Group A	Umbo	Mid	Edge	Polymorph	Group B	Umbo	Mid	Edge	Polymorph
Ca/Mg	-0.377	0.248	0.002	Calcite	Ca/Mg	0.442	0.349	0.174	Calcite
Ca/Na	-0.795	-0.396	-0.343	Calcite	Ca/Na	0.166	-0.453	-0.321	Calcite
Ca/S	0.371	0.415	0.326	Calcite	Ca/S	-0.021	0.621	0.621	Calcite
Ca/Sr	0.044	0.234	0.278	Calcite	Ca/Sr	0.250	0.038	0.038	Calcite
Mg/Na	0.430	-0.344	-0.645	Calcite	Mg/Na	-0.060	-0.397	-0.099	Calcite
Mg/S	0.211	0.192	0.741	Calcite	Mg/S	0.525	0.587	0.587	Calcite
Mg/Sr	-0.042	0.434	0.287	Calcite	Mg/Sr	0.135	0.458	0.458	Calcite
Na/S	-0.693	-0.502	-0.571	Calcite	Na/S	-0.266	-0.512	-0.512	Calcite
Na/Sr	-0.138	-0.158	-0.273	Calcite	Na/Sr	0.435	-0.359	-0.359	Calcite
Sr/S	0.078	0.056	0.579	Calcite	Sr/S	0.087	0.464	0.464	Calcite
Ca/Mg	-0.012	0.056		Aragonite	Ca/Mg	-0.068	0.069	-0.203	Aragonite
Ca/Na	-0.151	0.249		Aragonite	Ca/Na	-0.028	-0.468	-0.102	Aragonite
Ca/S	-0.209	0.103		Aragonite	Ca/S	0.716	-0.280	-0.253	Aragonite
Ca/Sr	0.014	-0.085		Aragonite	Ca/Sr	-0.724	-0.154	-0.227	Aragonite
Mg/Na	-0.340	-0.676		Aragonite	Mg/Na	0.286	-0.213	-0.572	Aragonite
Mg/S	0.269	0.396		Aragonite	Mg/S	-0.078	0.220	0.488	Aragonite
Mg/Sr	0.538	0.868		Aragonite	Mg/Sr	-0.425	0.060	0.694	Aragonite
Na/S	0.421	-0.062		Aragonite	Na/S	0.250	-0.263	-0.665	Aragonite
Na/Sr	-0.638	-0.770		Aragonite	Na/Sr	-0.414	-0.411	-0.557	Aragonite
Sr/S	-0.168	0.310		Aragonite	Sr/S	-0.626	0.688	0.866	Aragonite

Table 4.1. Correlation co-efficients for two stages of ontogeny; A (left) and B (right) showing the Pearson co-efficients in both polymorphs and in three different areas of the shell; the umbo, mid region and posterior edge. A value closer to 1 represents a strong statistical correlation. Stronger correlations (±0.5-1) are highlighted in red and moderate correlations (±0.35-0.5) highlighted in blue. Data were collected via EPMA.

Group C	Umbo	Mid	Edge	Polymorph	Group D	Umbo	Mid	Edge	Polymorph
Ca/Mg	-0.009	0.298	0.208	Calcite	Ca/Mg	0.297	-0.423	-0.025	Calcite
Ca/Na	-0.433	-0.447	-0.106	Calcite	Ca/Na	0.151	0.155	-0.279	Calcite
Ca/S	0.345	0.300	-0.257	Calcite	Ca/S	0.250	-0.657	0.191	Calcite
Ca/Sr	0.182	0.265	0.199	Calcite	Ca/Sr	0.317	0.324	0.306	Calcite
Mg/Na	-0.020	-0.460	-0.398	Calcite	Mg/Na	-0.076	0.025	-0.208	Calcite
Mg/S	0.280	-0.006	0.358	Calcite	Mg/S	0.027	0.279	-0.390	Calcite
Mg/Sr	0.390	-0.089	0.134	Calcite	Mg/Sr	0.306	-0.033	-0.125	Calcite
Na/S	-0.693	-0.501	-0.342	Calcite	Na/S	-0.504	-0.377	-0.461	Calcite
Na/Sr	-0.138	0.235	0.335	Calcite	Na/Sr	0.096	0.588	-0.038	Calcite
Sr/S	0.365	0.204	0.228	Calcite	Sr/S	0.305	-0.234	0.332	Calcite
Ca/Mg	-0.149	0.025		Aragonite	Ca/Mg	-0.019	-0.470		Aragonite
Ca/Na	0.296	0.314		Aragonite	Ca/Na	-0.262	-0.038		Aragonite
Ca/S	0.275	-0.559		Aragonite	Ca/S	0.108	0.235		Aragonite
Ca/Sr	0.137	0.025		Aragonite	Ca/Sr	-0.089	-0.418		Aragonite
Mg/Na	0.152	0.175		Aragonite	Mg/Na	-0.263	-0.144		Aragonite
Mg/S	-0.128	0.073		Aragonite	Mg/S	0.547	0.000		Aragonite
Mg/Sr	0.123	-0.009		Aragonite	Mg/Sr	0.213	0.123		Aragonite
Na/S	0.030	-0.465		Aragonite	Na/S	-0.125	-0.055		Aragonite
Na/Sr	-0.015	-0.654		Aragonite	Na/Sr	-0.213	-0.468		Aragonite
Sr/S	0.383	0.344		Aragonite	Sr/S	0.246	0.138		Aragonite

Table 4.2 Correlation co-efficients for two stages of ontogeny; C (left) and D (right) showing the Pearson co-efficients in both polymorphs and in three different areas of the shell; the umbo, mid region and posterior edge. A value closer to 1 represents a strong statistical correlation. Stronger correlations (±0.5-1) are highlighted in red and moderate correlations (±0.35-0.5) highlighted in blue. Data were collected via EPMA.

Group E	Umbo	Mid	Edge	Polymorph	Group F	Umbo	Mid	Edge	Polymorph
Ca/Mg	0.535	-0.586	-0.049	Calcite	Ca/Mg	0.274	0.237	-0.062	Calcite
Ca/Na	0.151	-0.334	-0.669	Calcite	Ca/Na	-0.290	0.221	-0.094	Calcite
Ca/S	0.316	-0.468	0.496	Calcite	Ca/S	-0.140	-0.954	-0.513	Calcite
Ca/Sr	0.499	-0.056	-0.109	Calcite	Ca/Sr	-0.303	0.310	0.015	Calcite
Mg/Na	-0.016	-0.219	-0.289	Calcite	Mg/Na	-0.093	-0.257	-0.317	Calcite
Mg/S	0.017	0.215	-0.188	Calcite	Mg/S	0.098	-0.209	-0.147	Calcite
Mg/Sr	0.262	-0.207	-0.360	Calcite	Mg/Sr	-0.061	-0.360	-0.176	Calcite
Na/S	-0.283	-0.113	-0.412	Calcite	Na/S	-0.311	-0.125	-0.023	Calcite
Na/Sr	0.300	0.305	0.261	Calcite	Na/Sr	0.565	0.666	0.538	Calcite
Sr/S	0.076	0.164	0.287	Calcite	Sr/S	0.073	-0.256	0.192	Calcite
Ca/Mg	0.020	0.000		Aragonite	Ca/Mg	-0.386	-0.085	0.064	Aragonite
Ca/Na	0.259	0.205		Aragonite	Ca/Na	0.110	-0.094	0.394	Aragonite
Ca/S	-0.100	0.079		Aragonite	Ca/S	0.178	0.031	-0.394	Aragonite
Ca/Sr	-0.224	-0.039		Aragonite	Ca/Sr	-0.276	-0.190	-0.185	Aragonite
Mg/Na	-0.282	-0.470		Aragonite	Mg/Na	-0.006	0.170	-0.293	Aragonite
Mg/S	0.226	0.574		Aragonite	Mg/S	-0.240	-0.162	-0.147	Aragonite
Mg/Sr	0.334	0.842		Aragonite	Mg/Sr	0.210	0.160	-0.172	Aragonite
Na/S	-0.064	-0.223		Aragonite	Na/S	-0.025	-0.283	-0.580	Aragonite
Na/Sr	-0.577	-0.483		Aragonite	Na/Sr	-0.448	-0.604	-0.608	Aragonite
Sr/S	0.188	0.586		Aragonite	Sr/S	0.341	0.140	0.664	Aragonite

Table 4.3 Correlation co-efficients for two stages of ontogeny; E (left) and F (right) showing the Pearson co-efficients in both polymorphs and in three different areas of the shell; the umbo, mid region and posterior edge. A value closer to 1 represents a strong statistical correlation. Stronger correlations (±0.5-1) are highlighted in red and moderate correlations (±0.35-0.5) highlighted in blue. Data were collected via EPMA.

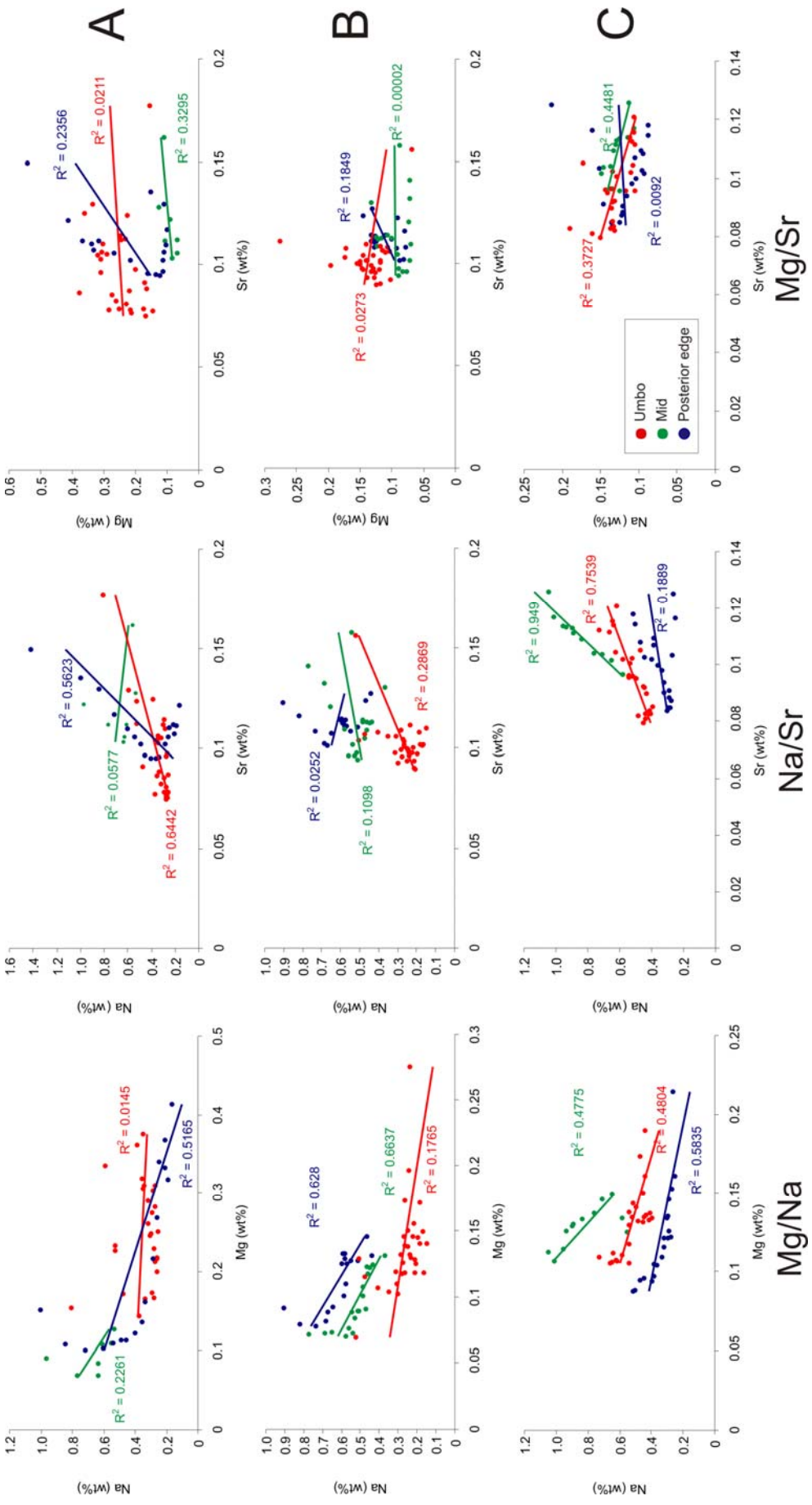

Figure 4.15. Scatterplots for SIMS element data for Mg, Na and Sr obtained from 3 stages of ontogeny, A (top row), B (middle row) & C (bottom row) in the calcite layer. In each plot the area of the shell where the data points were obtained are coloured red (umbo), green (mid region) & blue (posterior edge) with their respective trendlines and R^2 values coloured accordingly.

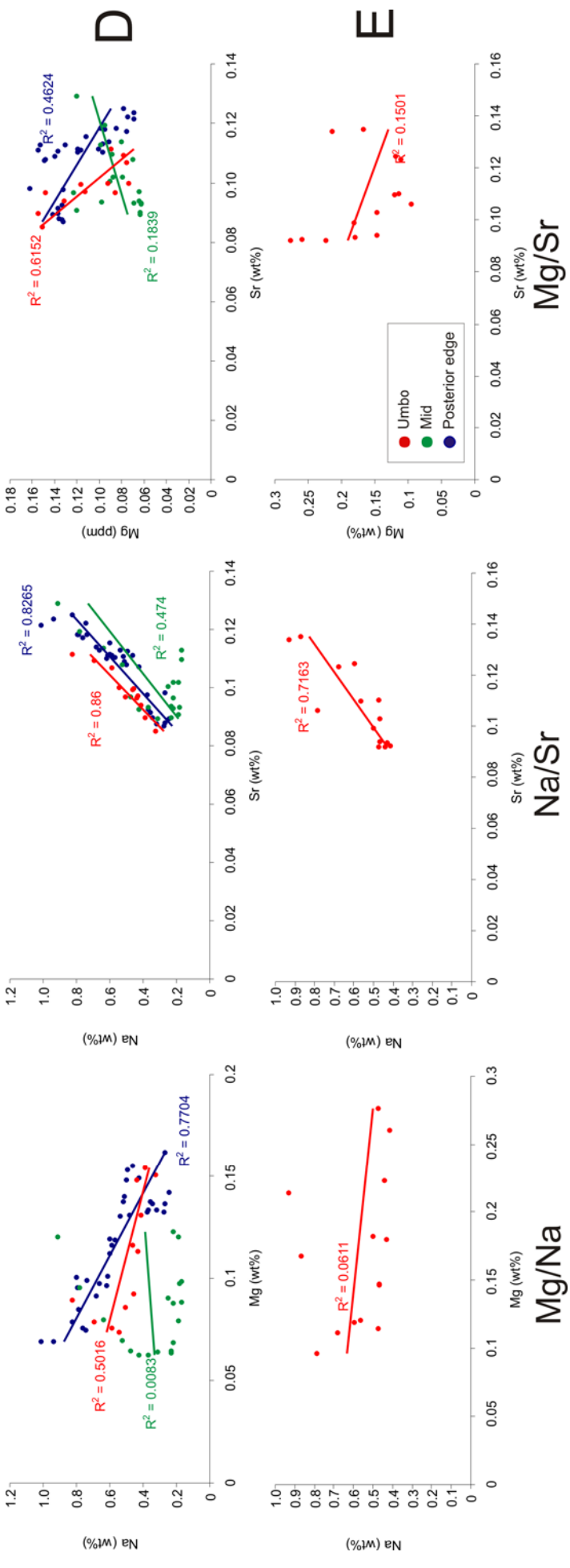

Figure 4.16. Scatterplots for SIMS element data for Mg, Na and Sr obtained from 2 stages of ontogeny, D (top row) & E (bottom row) in the calcite layer. In each plot the area of the shell where the data points were obtained are coloured red (umbo), green (mid region) & blue (posterior edge) with their respective trendlines and R^2 values coloured accordingly.

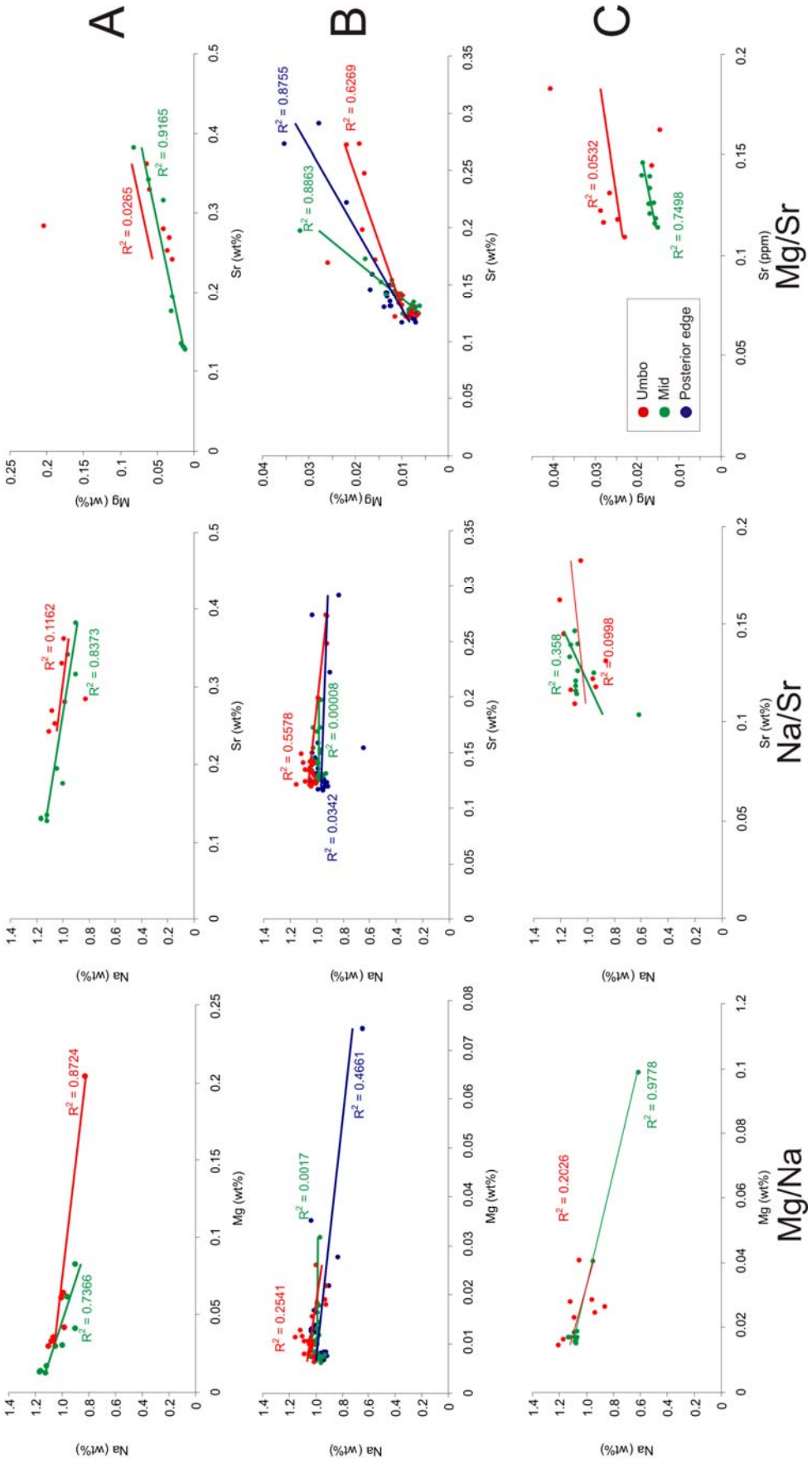

Figure 4.17. Scatterplots for SIMS element data for Mg, Na and Sr obtained from 3 stages of ontogeny, A (top row), B (middle row) & C (bottom row) in the aragonite layer. In each plot the area of the shell where the data points were obtained are coloured red (umbo), green (mid region) & blue (posterior edge) with their respective trendlines and R^2 values coloured accordingly

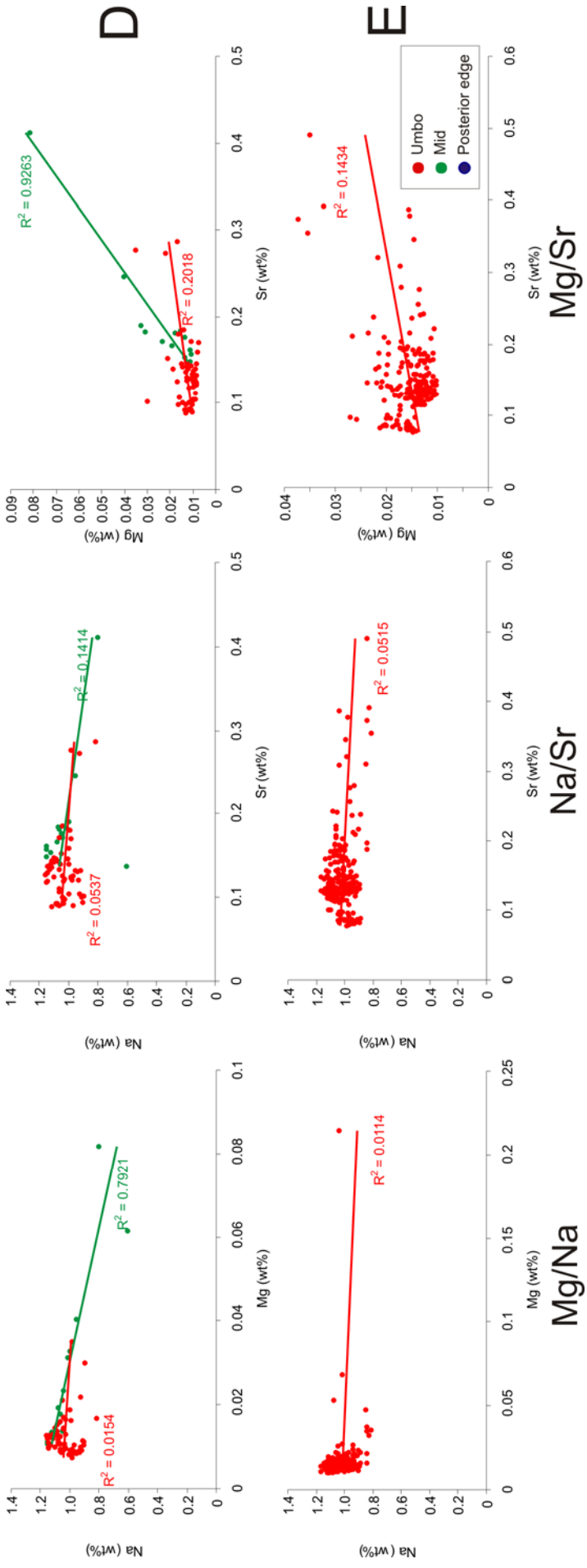

Figure 4.18. Scatterplots for SIMS element data for Mg, Na and Sr obtained from 2 stages of ontogeny, D (top row) & E (bottom row) in the aragonite layer. In each plot the area of the shell where the data points were obtained are coloured red (umbo), green (mid region) & blue (posterior edge) with their respective trendlines and R^2 values coloured accordingly.

Through the different regions within the shell and through ontogeny, there does not appear to be a consistent pattern in the correlations produced in Tables 4.1-4.3. The correlation co-efficient between Na and S in the calcite layer does appear to be significant for the stages of ontogeny A-D and throughout ontogeny the correlation of Na and Sr in the aragonite layer shows a consistent negative trend. Ca and S show a considerable correlation in the calcite layer through ontogeny through the shell, more notably away from the umbo. Sr and S also show a moderate correlation in the aragonite layer at various stages of ontogeny. However, many of the data points for S and Mg in the aragonite layer are below detection limits for EPMA and so conclusions derived from the statistical correlations in Tables 4.1-4.3 for Mg or S in the aragonite layer are tenuous. No further significant correlation between all stages of ontogeny is present for the EPMA data obtained here, although there are stronger correlations in the data for the youngest stages, A & B, in the ontogenic set (Table 4.1).

However, the scatterplots and statistical linear correlations shown in Figures 4.15-4.18 for the SIMS data show further relationships between Mg, Sr and Na in the calcite and aragonite layers. Many of the linear correlations drawn show a similar trend between regions of the shell and through ontogeny. However, the strength of the correlation based on the R^2 value varies considerably. The most striking correlation in the calcite layer is that between Na and Sr which appears to strengthen through ontogeny (Figure 4.15 & 4.16). This strong correlation is not the same in the aragonite layer (Figure 4.17 & 4.18). The R^2 values of the Mg/Na correlation in the calcite layer show no regular pattern between regions of the shell analysed but do appear stronger in ontogenic stages B, C & D (Figure 4.15 & 4.16), and the trend of the line is very similar for the majority of the regions and ontogenic stages analysed. No such patterns of R^2 values or trends of lines can be easily discerned for a relationship between Mg and Sr in the calcite layer. However, in the aragonite layer, the Mg/Sr relationship does show significance in the mid regions of the A, B, C & D stages of ontogeny and the trend of the data is similar between regions of the shell and stages of ontogeny (Figure 4.17 & 4.18). The mid region also shows stronger correlations between Mg and Na and for Mg/Na, the linear correlations drawn follow on a similar trend.

4.4 Discussion

From the chemical profiles produced by EPMA and SIMS (Figure 4.1-4.8) it is evident that the dstribution of the minor and trace elements in the *Mytilus edulis* system is a function of the polymorph produced as the standard profile and concentration ranges for each element are noticeably different, moving from the calcite layer to the nacreous aragonite layer. This is consistent between shell regions and through all stages in ontogeny. Therefore, the crystal structure

of the polymorph produced plays a central role in determining the uptake of certain minor and trace elements, i.e. Mg and S are present in higher concentrations in calcite than in aragonite.

4.4.1 Magnesium

The crystal structure of $CaCO_3$ governs the behaviour of certain elements as discussed previously Mg^{2+} is able to substitute for Ca^{2+} in calcite (Reeder, 1983) but not in orthorhombic aragonite. The covariance of Mg with Ca through the shell and ontogeny for the calcite layer does not produce a consistent pattern in the Pearson coefficients displayed here (Tables 4.1-4.3) but some areas do show a moderate correlation. However, if Mg and Sr compete for the Ca^{2+} site in calcite, then the correlation strength for Mg/Ca will be expected to vary if other element substitutions, such as Sr, occur. The uptake of Mg or Sr is affected by either temperature or rate of crystal growth respectively (Lea *et al.*, 1999). Any variation in environmental conditions or mussel growth rate may favour substitution of one trace element over the other. However, if this were a significant factor in this case, then the correlation in Sr/Ca could be expected to be stronger at the expense of a weak Mg/Ca correlation, or a significant Mg/Sr correlation. This is not observed consistently here.

In a number of the profiles, the Mg concentration often shows a rise from the outermost calcite, through the prismatic layer to the aragonite interface. This is similar to the pattern observed in other calcitic biomineral systems such as the avian eggshell. Here the profile of Mg^{2+} shows initial high concentration followed by a sharp decrease after nucleation of the calcite prisms, a gradual increase in Mg is coupled with the main stage of growth and finally, termination of calcite crystal growth is accompanied by a return to the initial high levels of Mg (Dalbeck & Cusack, 2006). In the avian system Mg may be involved in both the nucleation of calcite growth and the termination of calcite growth (Hincke & St. Maurice, 2000). Mg has been discussed previously as a modifier of calcite growth and is also considered to be a stabilizing component of amorphous calcium carbonate (ACC) (Loste *et al.*, 2003) which may be a pre-requisite for nucleation and growth of crystalline $CaCO_3$ (Beniash *et al.*, 1997). Thus, controlled Mg incorporation could aid biomineral production. Although the concentrations of Mg involved in the avian eggshell profile are higher than those observed for *M. edulis*, but still the *Mytilus* system may employ a similar selectivity of Mg incorporation to facilitate growth of the calcite layer.

Other studies have found that elevating concentrations of Mg in solution (Sugawara & Kato, 2000) will result in the precipitation of aragonite, the growth kinetics of which, is not affected by Mg^{2+} (Deleuze & Brantley, 1997). Thus, it may be necessary in the *Mytilus* system to elevate Mg concentration sufficiently to allow aragonite growth to begin. A similar mechanism was suggested by Lorens and Bender (1980) where the solution chemistry effects on *Mytilus edulis* calcite and aragonite were investigated. Mg incorporated into shell calcite increased exponentially when Mg

concentrations in solution were elevated to sufficient levels to breach the threshold of Mg regulation in the *Mytilus* system (Lorens & Bender, 1977). The physiological exclusion of Mg from *Mytilus edulis* would explain why the calcite in the system normally has lower Mg concentrations from those expected if the system were to passively record the Mg/Ca ratio found in modern seawater like other organisms such as echinoids (Hardie, 1996; Ries, 2004). Therefore, if the *Mytilus* system can regulate Mg incorporation, this may explain the lack of regularity in the correlation co-efficients of Mg/Ca in the calcite (Tables 4.1-4.3) in specimens taken from a single location, which has been subject to the same environmental conditions. This reinforces the idea proposed by Lorens and Bender (1980) and Vander Putten *et al*.(2000) that Mg in *Mytilus* cannot be used reliably as an environmental proxy as other factors may control the Mg incorporation.

Changes through ontogeny may be significant in interpreting Mg incorporation. SIMS data (Figure 4.13 & 4.14) do show a trend of decreasing mean Mg concentrations in the calcite and aragonite layers towards older stages of ontogeny and a similar trend can be seen in the EPMA data for the calcite in the umbo region. It may be that the younger specimen had a greater uptake of trace elements due to a higher metabolism in the earlier stages of the animal's life. Rosenberg and Hughes (1991) suggested that areas of higher shell curvature, such as the umbo, require greater metabolic expenditure resulting in an increase in Mg and S uptake. In this present study, sulphur is also found to be higher in concentration in the umbo (Figure 4.9-4.10) and also shows higher mean values in the earliest stage of ontogeny (Figure 4.11). This supports the idea of a higher metabolic rate and thus higher trace element uptake in the younger specimens. Sr in aragonite also has higher mean values in the youngest (A) stage of ontogeny (Figure 4.14). A greater incorporation of trace elements may also account for the more distorted profiles in the umbo region compared to the other regions of the shell (Figures 4.1-4.8) if this is due to higher metabolic requirements in this area.

Vander Putten *et al.* (2000) previously published an equation to describe the relationship between Mg/Ca in calcite of *M. edulis*:

$$(Mg/Ca*1000\ \{mmol/mol\} = 0.70\ (\pm 0.02) * T - 0.63\ (\pm 0.29).$$

Using a 40 wt% mean concentration of Ca^{2+}in calcite shells of *M. edulis*, T can be calculated from the Mg/Ca of the shell calcite (Figure 4.19).

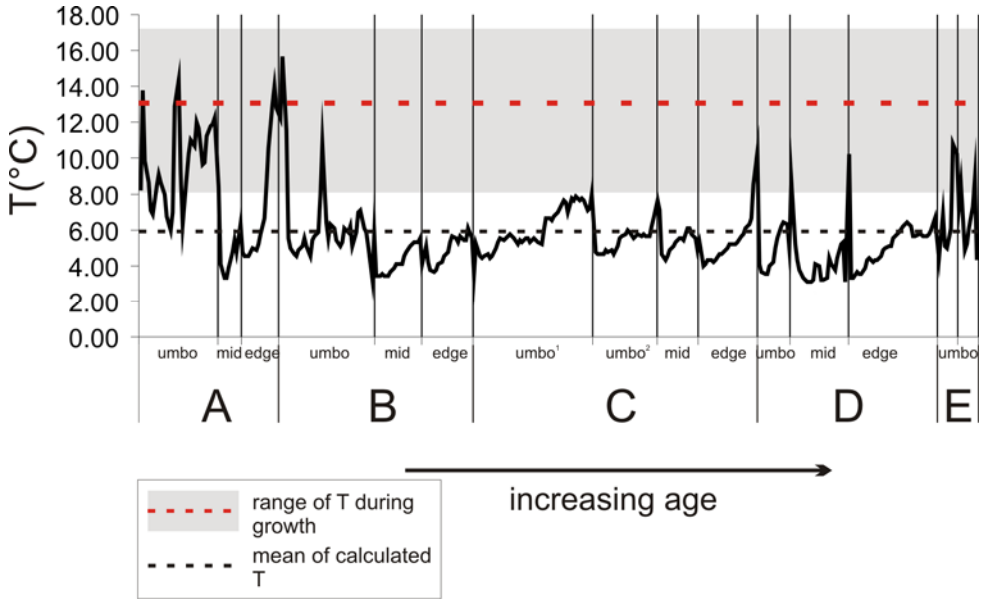

Figure 4.19. Calculated Temperature (T) in shell calcite through ontogeny. Line graph shows the profile of calculated T from Mg/Ca using the equation published by Vander Putten *et al*. (2000) through 5 stages of ontogeny in *M. edulis*. The umbo, mid and posterior edge regions are also indicated and each of these sub-profiles was obtained across the shell thickness. The estimated range of temperature (from Stirling and Okumus (1995)) during growth is highlighted in grey. The white dashed horizontal line indicates mean average T during growth. Mg/Ca were produced via SIMS.

The profile of T calculated from Mg/Ca shows a significant offset from the temperature range predicted from previous studies of Loch Etive (Stirling & Okumus, 1995). The mean value of calculated temperature (5.9°C) is offset from the average water temperature (13.2°C) during shell growth. Only the youngest specimens of ontogeny show values within the temperature range. The average variation of 4°C in the calculated profile does not reflect the extent of variation in actual temperature. Mg/Ca ratios in estuarine and sea loch environments only significantly offset from marine values when salinity is lower than 10‰ (Dodd & Crisp, 1982). Thus, salinity is not likely to explain the offset observed here. Similar observations have also been reported by Vander Putten *et al*. (2000). It would appear that Mg/Ca ratios in *M. edulis* cannot be explained by simply environmental variations. The difference observed through ontogeny could be related to a similar observation in Foraminifera (Hintz *et al.*, 2006). Age specific Mg/Ca ratios were observed by Hintz *et al*. in foram specimens through ontogeny, and Mg enrichments were noted in older specimens that were not attributed to environmental variation. In this present study, an enrichment of Mg is observed in the younger specimens (stage A) of *M. edulis* which produces significant offsets (4-12°C) in predicted temperature to older specimens.

Given that Mg/Ca ratios are considered to be important environmental temperature proxies in biocarbonates (Chave, 1954a) including the *Mytilus* system (Dodd, 1965; Klein *et al.*, 1996a) greater attention needs to be given to the factors affecting the incorporation of Mg in the system such as those discussed here.

4.4.2 Sodium

The Na profiles are consistent in all specimens. Na concentration decreases across the calcite layer towards the aragonite interface and recovers to greater concentrations to that of the calcite after immediately crossing the interface (Figure 4.1-4.8). This suggests a possible exclusion mechanism in the calcite for Na. Less Na is incorporated as the calcite layer grows towards the interface and this exclusion does not occur in the aragonite layer. A physiological exclusion of Na is a potential explanation. Alternatively, this could represent a refinement in the calcite crystal structure where defects in which Na can occupy are steadily reduced through the calcite layer. Relationships between element distribution profiles and crystallography will be discussed in Chapter 6.

As with Mg, the structure of $CaCO_3$ can account for the obvious difference between the polymorphs as Na^+ incorporation into the aragonite lattice is easier than into the calcite system for biogenic marine carbonates and abiotic carbonate sediments (Billings & Ragland, 1968; Amiel *et al.*, 1973; Land & Hoops, 1973). With Na^+ more able to compete with Ca^{2+} in the aragonite lattice, this may account for the lower mean concentrations of Ca observed in the aragonite layer compared to the calcite layer (Figure 4.10 & 4.11) if Ca is excluded at the expense of Na.

The bonding of Na in calcite is more difficult to determine than the other chemical species investigated here. Previous studies have shown that Na^+ has difficulty substituting for Ca^{2+} in calcite (Kitano *et al.*, 1975) and so Na^+ may occupy interstitial sites (Ishikawa & Ichikuni, 1984; Busenberg & Plummer, 1985; Okumura & Kitano, 1986). Kitano *et al.* (1975) suggested that uptake of SO_4^{2-} in aragonite enhanced Na uptake. However, the lack of S detected in the *M. edulis* system here suggests that this may not be the reason for the high levels of Na in aragonite through ontogeny. However, the Na/S data for younger stages of ontogeny, A-D (Table 4.1 & 4.2) shows that a moderate correlation exists in the calcite layer. If sulphate ions incorporated into the lattice can cause a lattice expansion (Kontrec *et al.*, 2004) then this may create interstitial space for Na. A similar lattice expansion could be used to explain the strong linear correlation for Na and Sr in the calcite layer (Figures 4.15 & 4.16) with the larger Sr^{2+} ion substituting for Ca^{2+} in the calcite lattice causing an expansion that could accommodate Na^+. White (1978) suggested that the presence of organic material may also be attributed to higher concentrations of Na in biogenic calcite. If the S concentration is attributed to the organics in the system, then the Na/S correlation suggests that Na may also be linked to the organic material in the system. However, the youngest specimens of the ontogenic survey have higher S contents in calcite than later stages of ontogeny (Figure 4.9 & 4.10), and the inverse is the case for Na in calcite (Figure 4.13). This would suggest that Na is associated more directly with the crystalline phase than the organic material.

Through ontogeny, Na is in lower concentrations in the youngest stages of ontogeny in the calcite of the umbo region (Figure 4.13). This is the converse of the situation with Mg. If Na occupies interstitial sites and so may have greater mobility than trace elements that are bonded more strongly in the crystal lattice. Na^+ and other monovalent ions can move through the calcite crystal lattice even once the system has become fully crystallised and is considered to be a static closed system. The mobility of these elements can have greater implications for the use of trace element distributions as paleoclimate proxies as the surface sites are renewed regularly due to this ionic mobility. (Stipp *et al.*, 1998).

If Na is to be used as an indicator of paleoclimate and salinity (Veizer *et al.*, 1977; White, 1977) then the speciation and bonding of Na in the lattice should be resolved in order to understand the mechanisms involved.

4.4.3 Strontium

The possible behaviour of strontium in the shell profile has been discussed above with respect to Mg and Na. Sr substitutes more readily for Ca^{2+} in aragonite than calcite (Reeder, 1983) and the contrasts in partition coefficients explain the greater mean concentrations in the aragonite than the calcite. Again, similar to Na^+ behaviour in the aragonite layer, if Sr^{2+} is more able to compete with Ca^{2+} in the aragonite lattice, this may explain the reduced mean Ca^{2+} concentrations in the aragonite layer compared to the calcite (Figure 4.9 & 4.10). The strong negative Pearson co-efficient for Na/Sr in the aragonite shown throughout (Table 4.1-4.3) suggests that there may be competition between the two for sites in the aragonite lattice. This is also reinforced with sharp decreases in Na concentration often coinciding with similar sharp rises in Sr concentration observed in the chemical profiles across the shell.

Klein *et al* (1996b) discussed the use of Sr/Ca as a possible proxy for seawater chemistry and found that the metabolic activity of the mantle in *Mytilus trossulus* primarily dictated the Sr/Ca ratio of the shell material. Metabolic effects on shell Sr/Ca have been shown in other studies (Purton *et al.*, 1999; Purton-Hildebrand *et al.*, 2001; Takesue & Van Geen, 2004). As discussed previously in comparison to Mg, S has a similar distribution pattern to Sr. The youngest stage of ontogeny, stage A, has higher mean concentrations of S and this is also the case for Sr in the aragonite of the umbo region. There is a significant correlation between Sr and S (Table 4.1-4.3). This suggests that the proposal of the metabolic model by Rosenberg & Hughes (1991) may explain the preference of Sr for areas of higher metabolic expenditure such as the umbo and younger, more metabolically active stages of ontogeny.

The reason for the strong linear correlations between Sr and Mg in the aragonite, (Figure 4.17 & 4.18) particularly the mid region, through ontogeny is unknown. However, it could be that, while Mg^{2+} is unable to enter the aragonite lattice, it may sufficiently inhibit other ions such as Ca^{2+} and Na^{+} to allow Sr^{2+} to be incorporated.

4.4.4 Sulphur

Sulphur is in greater abundance in calcite than aragonite, with many aragonite EPMA points falling below detection limits. Sulphur has often been considered as an indicator of organic material and yet the observations here would suggest this is not a good proxy as the aragonite layer in *M. edulis* contains greater quantities of organic material than the calcite layer (England, 2005). Thus, the organic matter may be different in the calcite layer or that S is incorporated into the calcite lattice more easily than the aragonite. A model for the incorporation of inorganic anions, such as SO_4^{2-}, into calcite producing a lattice expansion has previously been proposed (Kontrec *et al.*, 2004). This followed a previous investigation on the effect of inorganic anions on the calcite structure in which the presence of Mg facilitated the incorporation of these anions (Kralj *et al.*, 2004). Thus, S may be present as inorganic S if Mg is also present in the calcite layer. However, there is a lack of consistent statistical co-variation observed in the Pearson correlation values produced in Tables 4.1-4.3 with only the B stage of ontogeny showing a strong Mg/S correlation through the shell. Sulphur is associated with the organic matrix in the calcite prismatic layer of *M. edulis* (Dauphin *et al.*, 2003b). The affinity of S for the umbo region and younger stages of ontogeny may be due to elevated concentrations of organic material in metabolically expensive areas (Rosenberg *et al.*, 1989; Rosenberg & Hughes, 1991). This may then suggest that the nature of the organic material dictates S content.

4.5 Summary

A general profile can be described for the majority of the specimens in the ontogenic set: Na concentrations decrease from the outer shell surface through the calcite layer and dramatically increase to a relatively constant level in the aragonite layer (Figure 4.20).

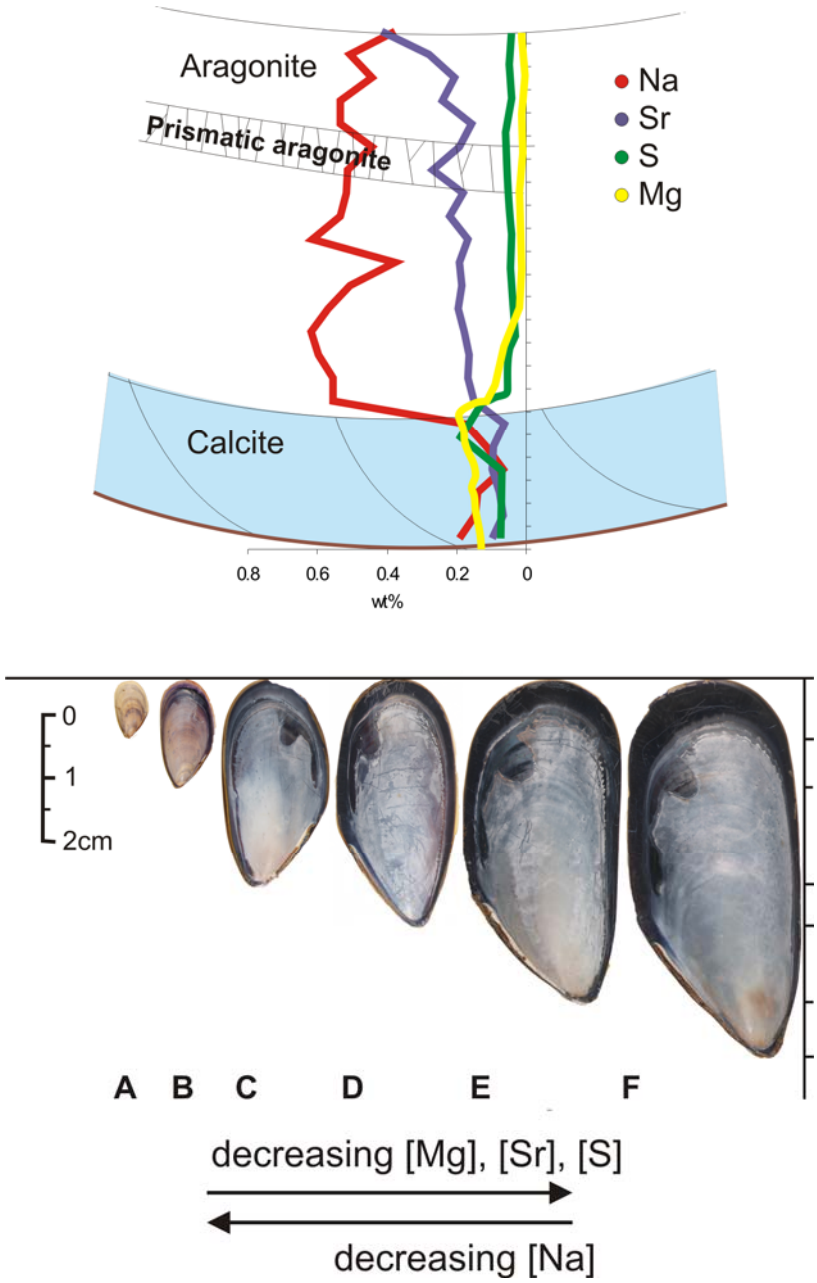

Figure 4.20 Summary of trace element chemistry observed in *M. edulis*. Top: Typical trace element profile through the shell thickness observed in all stages of ontogeny and different shell regions. Changes in element profiles are observed moving between crystal polymorphs and different crystal habit. Bottom: Ontogenetic range and the general pattern of trace element distribution observed

Mg is present in the calcite layer but is virtually absent in the aragonite layer and frequently an increase in Mg concentration occurs through the calcite layer towards the polymorph interface. S and Mg have similar distributions between polymorphs. Sr is relatively invariant in the calcite layer, and usually rises as the polymorph interface is crossed. As this typical trace element profile is observed between regions analysed, specimens and stages of ontogeny, while the shells analysed have been through different seasons, it is likely that there are other factors determining trace

element incorporation in the *M. edulis* system rather than simply passively recording ambient environmental conditions. The earliest stage of ontogeny (A) shows significant offset to older specimens when the Mg/Ca are used to calculate temperature. The reason for the uptake of certain elements may be more strongly determined by the metabolic requirements of the animal and the physiological regulation of these elements to control biomineral growth.

The shells used in this study were taken from the same location in order to minimise the variation of environmental factors between specimens. Each stage of ontogeny began growth at the same time each year and so seasonal variations between specimens are minimised. If *M. edulis* was a passive recorder of environmental conditions, the statistical correlations between specimens and stages of ontogeny and the concentrations of elements between the ontogenic stages would be more similar than those observed here. Younger stages of ontogeny and different regions of the shell have a greater affinity for Mg, Sr and S while also being relatively depleted in Na compared to older ontogenic stages. Therefore, a variation of trace element incorporation through ontogeny can be perceived even though the overall profile remains the same through ontogeny. The mobility of ions such as described by Stipp *et al.* (1998) discussed above may account for the differences between the ontogenic stages. However, this implies that the dynamic system is continually changing. More factors such as earlier stages of ontogeny, ionic mobility and metabolic features would ideally be considered in greater detail before applying trace element distribution as environmental indicators.

5

Stable isotope composition in the context of ontogeny

5.1 Introduction

Stable isotopic composition of marine biogenic carbonates provides insights into the environmental conditions during growth and the influence of biological control on biomineral formation. As carbonate secreting organisms grow, the elements Ca, C and O, which combine to produce $CaCO_3$ can yield valuable information through stable isotopes ratios, $^{18}O/^{16}O$ and $^{13}C/^{12}C$. These ratios are determined by the isotopic ratios in the surrounding system. From this, the basis for the use of stable isotopes in reconstructing past climates arises, similarly to the use of trace element composition discussed in Chapter 4. However, in a dynamic system such as a living system, a simplistic incorporation of isotopes becomes complicated. Lighter isotopes are often preferentially selected for mineral and organic production. Biological functions such as respiration, metabolism and faster growth periods of the animal also influence the stable isotope ratios. These biological functions are themselves influenced by ontogeny. Therefore, it becomes essential to consider the effects of growth and ontogeny of carbonate secreting organisms to gain clearer insight of the variables in the system. Thus, greater understanding will allow isotopic proxies to be applied more reliably for palaeothermometry and to understand the biological processes involved in these biomineralising systems.

This study examines the stable carbon and oxygen isotopic composition of *M. edulis* shells from a single location in the context of ontogeny. To reduce the environmental variables between specimens, the mussels were all collected from a mussel farm at the same time and were then immediately prepared for analysis via the same treatment methods (Section 2.1).

The $\delta^{18}O$ values for 3 stages of ontogeny, A (10-12 months), C (22-24 months) and F (36+ months) were determined using secondary-ion mass spectrometry analysis (SIMS). Further $\delta^{18}O$ and $\delta^{13}C$ data were produced for 5 stages of ontogeny, B (12-14 months), C (22-24 months), D (24-26 months), E (34-36 months) and F (36+ months), through conventional mass spectrometry using a

modified version of the phosphoric acid digestion method developed by McCrea (1950) which is detailed in Section 2.4.1.2.

This study aims to assess the influence of marine invertebrate aging on isotopic composition of the shell produced. This is determined through analysis of the stable isotopic composition produced in *M. edulis* in the context of ontogeny over a period of 3 years. $\delta^{18}O$ and $\delta^{13}C$ values will be expected to change as the animal ages. Understanding of vital effects on biomineralising systems is investigated through the behaviour of ^{18}O and ^{13}C expected to vary at different stages of ontogeny.

Further understanding of isotopic partitioning between calcium carbonate polymorphs, calcite and aragonite is developed. Calcite and aragonite are present in *M. edulis* shells and both polymorphs are expected to show differences in isotopic composition.

5.2 Previous work

The reconstruction of past climate conditions remains of great interest to earth scientists and climatologists with significant application to understanding modern and palaeoclimate patterns and predictions. However, the ability to quantify changes in past climates remained elusive until the pioneering work involving the use of stable isotopes, such as ^{18}O, (Urey, 1947, , 1948b; Urey *et al.*, 1948; Epstein *et al.*, 1951; Epstein *et al.*, 1953) gave palaeoclimatologists the ability to measure variations in environmental variables such as temperature recorded in ancient carbonate rocks (Urey *et al.*, 1950; Urey *et al.*, 1951).

As many of the Earth's carbonate sedimentary rocks are comprised of biogenic carbonate, this application of stable isotopes as a marine chemistry proxy generated a surge of interest in the use of biominerals as tools for deducing past climates.

Following on their work with Urey, Epstein and Lowenstam (1953) explored the use of mollusc carbonate to determine sea-surface temperature (SST) and this led to further research in applications of stable isotopes to mollusc carbonate (Valentine & Meade, 1960; Dodd & Stanton, 1975; Gustavson, 1976; Killingley & Berger, 1979; Wefer & Killingley, 1980; Donner & Nord, 1986; Brand, 1994; Weidman *et al.*, 1994; Elliot *et al.*, 2003).

Lowenstam (1961) further applied the use of $^{18}O/^{16}O$ ratios to other carbonate-secreting organisms such as brachiopods. Lowenstam demonstrated that brachiopods with low Mg-calcite produce $CaCO_3$ with stable isotopic ratios in equilibrium with the ambient environment. This finding combined with the large geological range of brachiopods makes them attractive as sources of palaeoclimate information (Popp *et al.*, 1986b, 1986a; Gruszczynski *et al.*, 1989; Bates & Brand, 1991; Grossman *et al.*, 1991; Grossman *et al.*, 1993; Mii & Grossman, 1994). Other studies on

palaeoclimate and modern climatic reconstructions have employed corals and planktonic organisms such as foraminifera and coccoliths, in stable isotope applications (Margolis *et al.*, 1975; Anderson & Steinmetz, 1983; Aharon, 1991). The application of the stable oxygen isotope proxy for SST relied on the precipitation of skeletal material in equilibrium with the ambient environment as reported by Lowenstam (1961).

Interpretation of stable isotopic information from these dynamic systems is complicated due to the metabolic, biological and kinetic growth effects often referred to collectively as 'vital effects'. This phenomenon was recognised by Urey (1951) and Epstein (1951). Due to vital effects, the isotopic signature of biogenic carbonate may be offset from equilibrium with the surrounding environment. This has been investigated for a number of biomineral systems e.g. molluscs (Krantz *et al.*, 1987; Krantz *et al.*, 1989; Klein *et al.*, 1996a, 1996b; Dettman *et al.*, 1999; Lecuyer *et al.*, 2004) brachiopods (Popp *et al.*, 1986a; Carpenter & Lohmann, 1995; RahimpourBonab *et al.*, 1997; Parkinson *et al.*, 2005) corals (McConnaughey, 1989b, 1989a; Heikoop *et al.*, 2000; McConnaughey, 2002, , 2003) and coralline sponges (Bohm *et al.*, 2000).

These vital effects have led to investigations into which phyla attain stable isotopic equilibrium (Wefer & Berger, 1991). However, even within a single phylum, variation occurs between species (Shackleton *et al.*, 1973), within different regions of single specimens (Weber & Raup, 1966; Auclair *et al.*, 2003; Parkinson *et al.*, 2005; Cusack *et al.*, (in press)) and through ontogeny of species (Spero & Lea, 1993, , 1996).

The shell production in the mollusc system is mediated through the extrapallial fluid (EPF) detailed in Section 1.1.3. The dissolved inorganic carbon content of this mineralising medium has implications for isotopic composition of the shell produced (Section 1.2.2). Debate surrounds the proportion of inorganic seawater dissolved inorganic carbon (DIC) (Mook & Vogel, 1968; Fritz & Poplawski, 1974) and that derived from metabolism (Tanaka *et al.*, 1986; McConnaughey *et al.*, 1997; Vander Putten *et al.*, 2000; Lecuyer *et al.*, 2004; Gillikin *et al.*, 2006) incorporated into the shell mineralised tissue. Spero and Lea (1996) described variation in $\delta^{18}O$ and $\delta^{13}C$ values of Foraminifera tests through ontogeny based on variation in metabolic CO_2 incorporation during mineralisation through the animal's life.

Further to this, McConnaughey (1989a; 1989b) demonstrated in corals, faster growing biomineralising regions display significant effects on incorporation of the both ^{18}O and ^{13}C. As the equilibration of the mineralising medium with the surrounding environment has not been fully completed, this kinetic effect creates offsets from expected carbonate equilibrium values.

A survey of *M. edulis* in the context of ontogeny over a 3 year period should assist in determining any changes in metabolic activity that would be expected as the animal ages and whether this has a

significant effect on the $\delta^{18}O$ and $\delta^{13}C$ within the mollusc shell. The ontogenic survey also allows for further investigation of any $\delta^{18}O$ and $\delta^{13}C$ offsets that could be induced by the kinetic effects described by McConnaughey during periods of increased shell growth of the animal's life.

5.3 Results

5.3.1 High-resolution $\delta^{18}O$ profile (SIMS)

Profiles of $\delta^{18}O$ for 3 stages of ontogeny, A (10-12 months), C (22-24 months) and F (36+ months) were determined through secondary ion mass spectrometry (SIMS) analysis as described in Section 2.4.2. SIMS analysis allowed for high-resolution investigation of the isotopic signature on a micron scale across the shell thickness. Three parallel transects were made in the umbo, mid region and posterior edge of single specimens from the earlier stages of ontogeny, A and C, with the umbo region of F also analysed with three transects. External precision of SIMS is detailed in Section 2.4.2.2. The offset between SIMS and the conventional data is detailed in Section 2.4.3 and displayed on the profiles are displayed in Figures 5.1-5.3. The predicted equilibrium range for calcite and aragonite, calculated in Section 2.4.4 is also indicated.

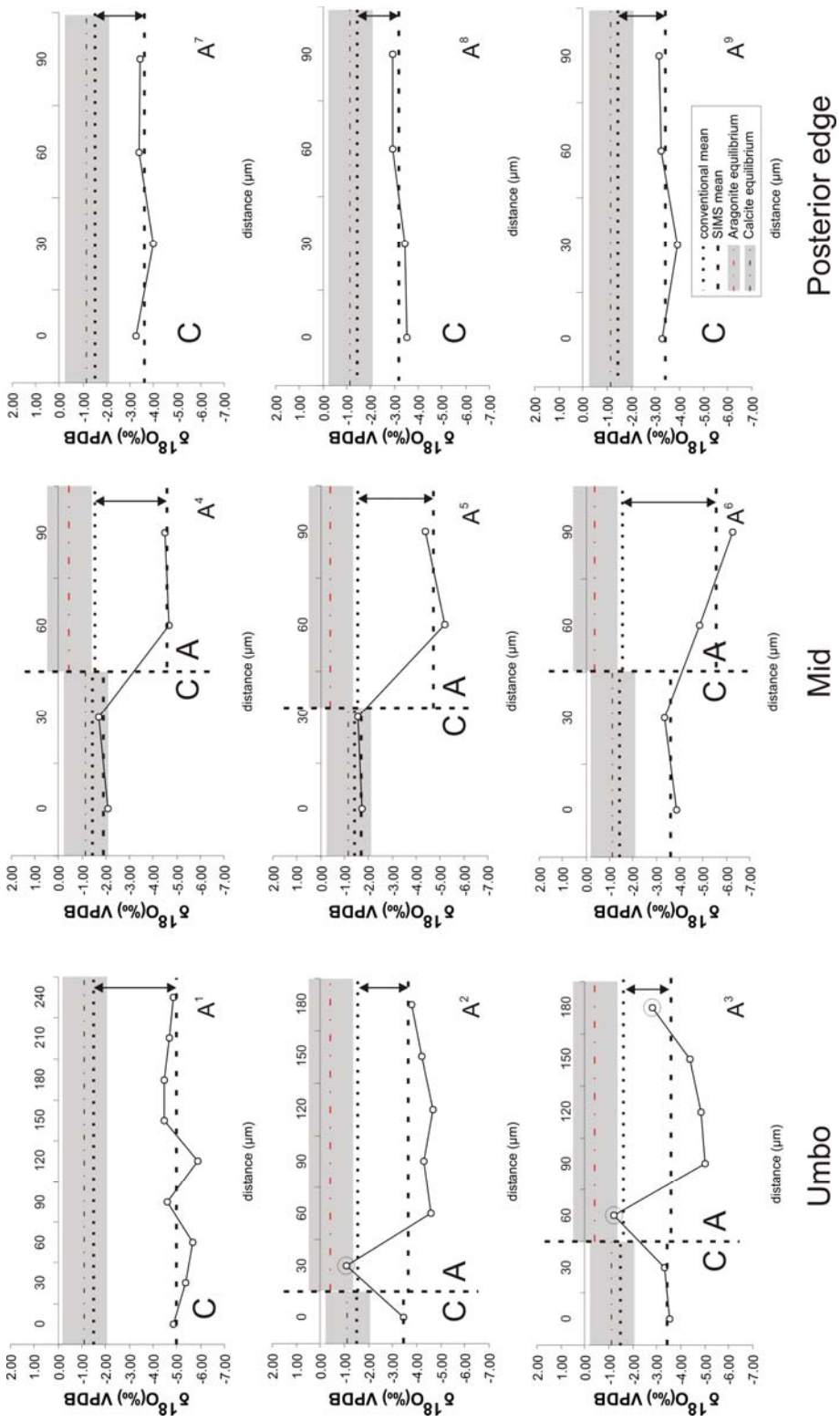

Figure 5.1. $\delta^{18}O$ profiles in A (10-12 months) stage of ontogeny. Line graphs showing three $\delta^{18}O$ profiles through the shell in three main regions of the shell, umbo, mid and posterior edge regions. Profiles taken from the outer surface (left of each graph) to the inner surface (right of each graph). The switch between calcite 'C' and aragonite 'A' is marked for each profile with a vertical dashed line. Profiles without vertical dashed lines represent areas of only calcite 'C'. Ringed data points are those in prismatic aragonite. Inset (bottom right) indicates the aragonite and calcite equilibrium respective means and ranges. Conventional values for A were estimated from the closest whole shell values 'D' (Figure 5.4). Conventional and SIMS means are also indicated, with the offset shown on graphs with vertical double arrows. The data were collected via SIMS analysis

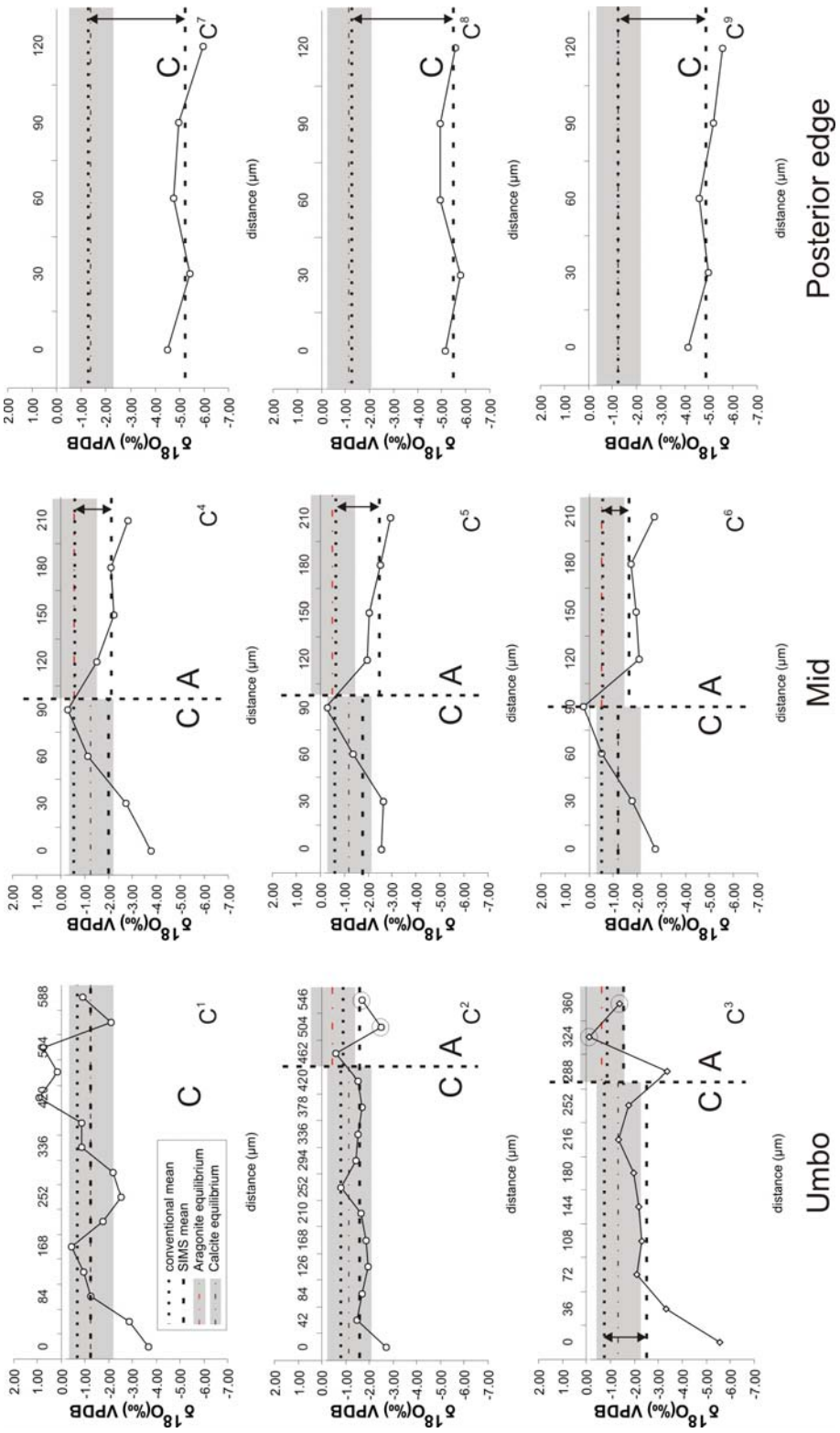

Figure 5.2. $\delta^{18}O$ profiles in C(22-24 months) stage of ontogeny. Line graphs showing three $\delta^{18}O$ profiles through the shell in three main regions of the shell, umbo, mid and posterior edge regions. Profiles taken from the outer surface (left of each graph) to the inner surface (right of each graph). The switch between calcite 'C' and aragonite 'A' is marked for each profile with a vertical dashed line. Profiles without vertical dashed lines represent areas of only calcite 'C'. Ringed data points are those in prismatic aragonite. Inset (top left) indicates the aragonite and calcite equilibrium respective means and ranges. Conventional and SIMS means are also indicated, with the offset shown on graphs with vertical double arrows. The data were collected via SIMS analysis

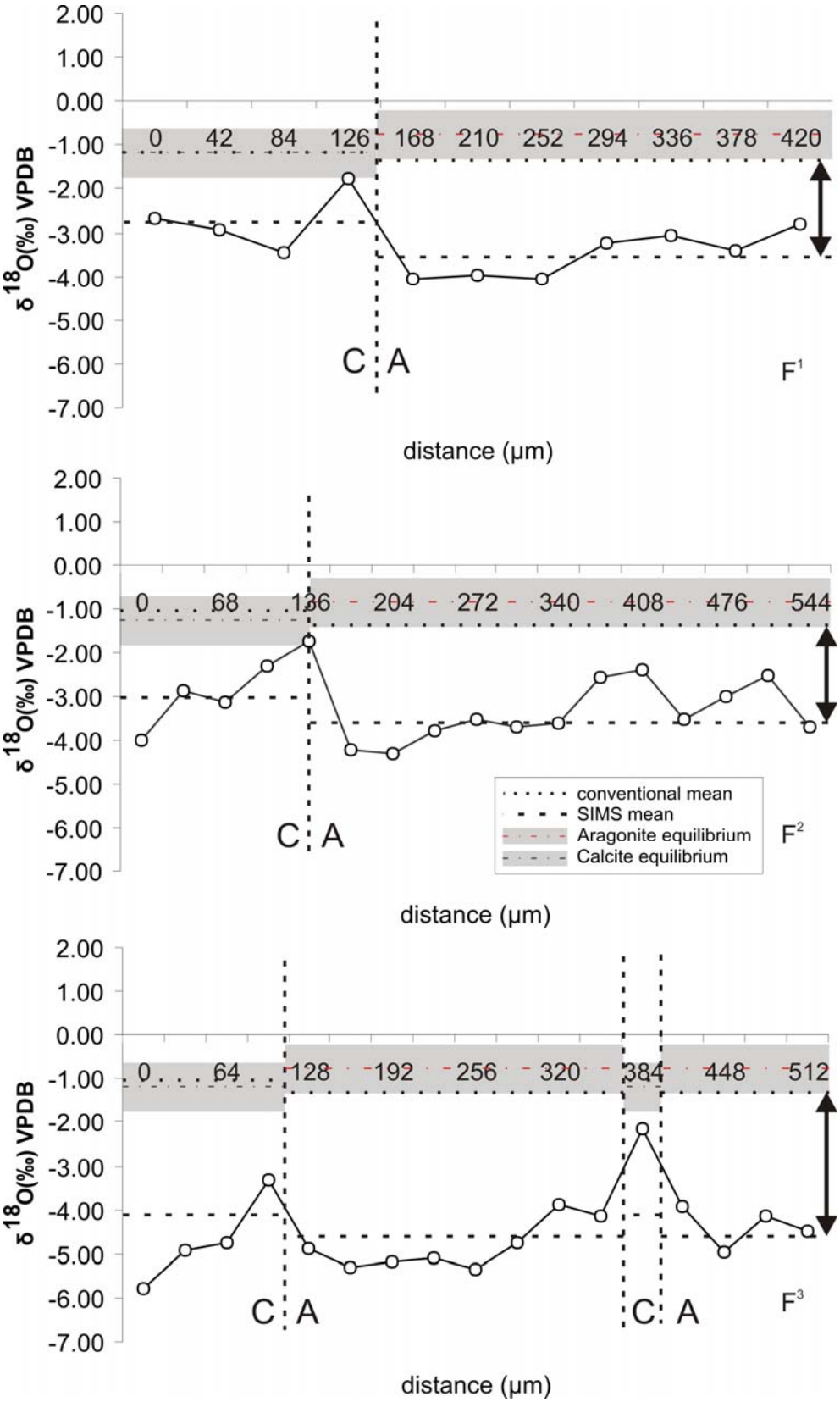

Figure 5.3. $\delta^{18}O$ profiles in F (36+ months) stage of ontogeny. Line graphs showing three $\delta^{18}O$ profiles through the shell in the umbo, region. Profiles taken from the outer surface (left of each graph) to the inner surface (right of each graph). The switch between calcite 'C' and aragonite 'A' is marked for each profile with a vertical dashed line. Inset indicates the aragonite and calcite equilibrium respective means and ranges. Conventional and SIMS means are also indicated, with the offset shown on graphs with vertical double arrows. The data were collected via SIMS analysis.

The profiles reveal common trends through all stages of ontogeny, and between different areas of the shell and well as similar $\delta^{18}O$ values. The outermost calcite has typically lower $\delta^{18}O$ values than the rest of the calcite layer in the umbo and mid region. The $\delta^{18}O$ values in the same regions become higher moving through the calcite layer towards the interface, $\Delta^{18}O‰$ typically on the scale of 2-3‰ with a maximum of 5‰ in one profile (Figure 5.2, C^1). Normalising the SIMS mean to the conventional mean brings these higher $\delta^{18}O$ points out of the expected equilibrium range for calcite.

Figures 5.1 & 5.2 also show that the wholly calcitic posterior edge has lower $\delta^{18}O$ values than the calcite in other regions of the shell. The $\delta^{18}O$ values in this region are relatively invariant with $\Delta^{18}O‰$ in the posterior edge commonly within 0.5‰. Normalising the SIMS mean to the conventional mean brings the data for this region of the shell within the expected equilibrium values.

In each profile, moving across the polymorph interface is accompanied by a sharp decrease in $\delta^{18}O$ values with $\Delta^{18}O$ as much as 4‰. Where lenses of calcite are present within the aragonite layer, a similar abrupt shift in the isotopic profile is observed, as shown in profile F^3 of Figure 5.3. However, $\delta^{18}O$ values in the aragonite layer are relatively invariant. Abrupt shifts to positive $\delta^{18}O$ values within the aragonite are typically associated with layers of prismatic aragonite (Figure 5.1, A^2 & A^3; Figure 5.2, C^3). Normalising the SIMS mean to the conventional mean for aragonite leaves many data points out of the predicted equilibrium range for aragonite.

In some regions of the umbo where calcium carbonate morphology is largely or wholly calcitic, (Figure 5.2, C^1 & C^2), the $\delta^{18}O$ profile shows a 'rise and fall' pattern twice through the calcite layer in a cyclical fashion. This pattern occurs while the overall profile still trends towards higher $\delta^{18}O$ values moving towards the inner shell surface.

The $\delta^{18}O$ profile in the thicker aragonite layer in the older stage of ontogeny F (36+months) (Figure 5.3) show a trend toward more positive $\delta^{18}O$ values moving towards the inner shell surface, with rises at polymorph interfaces also observed (Figure 5.3, F^3).

The general isotopic values between the ontogenic stages do not show any major differences, with no ontogenic stage showing a particular enrichment or depletion of $\delta^{18}O$ compared to another.

5.3.2 $\delta^{13}C$ & $\delta^{18}O$ through ontogeny

It is necessary to compare $\delta^{13}C$ values against $\delta^{18}O$ to determine relationships that could reveal metabolic or 'vital' effects within the shell through ontogeny. The presence of these vital effects has often been determined where the ratios of both isotopes have been affected by the same

changes to the micro-environment where the shell material has been produced (McConnaughey, 1989a, 1989b). During analysis of the ontogenetic stages, results for the younger stages of ontogeny (A & B) proved to be difficult. Smaller sample sizes yielded small mounts of carbonate making cross-contamination of carbonate polymorph material difficult to avoid. Therefore the isotopic composition of whole shells for the smaller shells (stages A and B) were determined and compared against the mean values of the older stages of ontogeny (Figure 5.4) in order to determine any significant deviations of whole shell values through ontogeny. Figure 5.5 shows a crossplots of data obtained through the ontogenic survey.

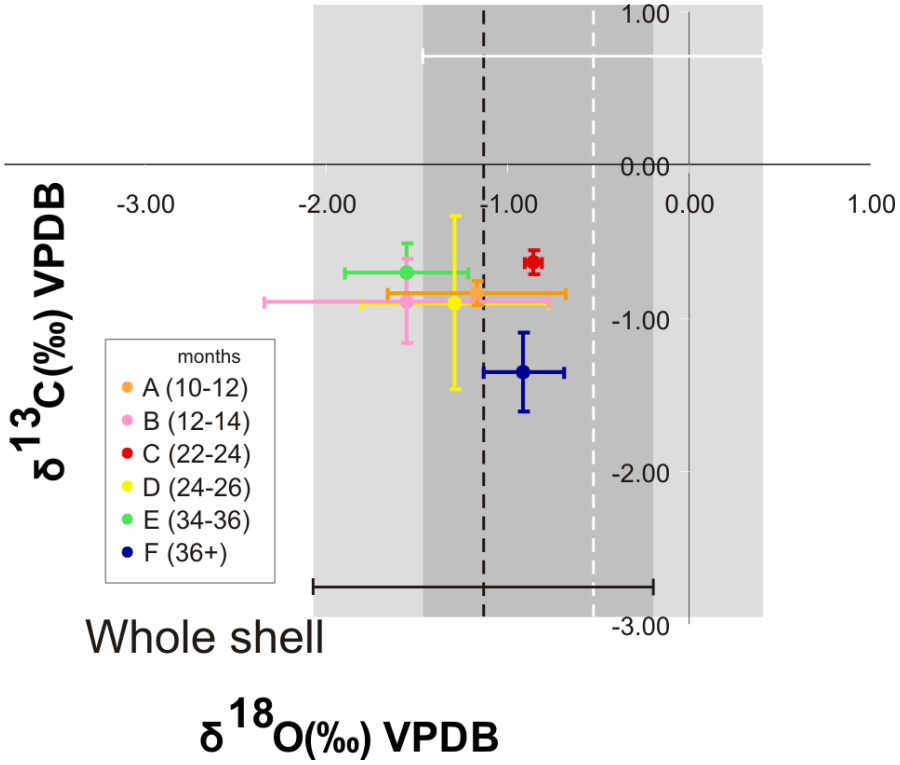

Figure 5.4 Cross plots from all stages of ontogeny (A-F). $\delta^{18}O$ is plotted against $\delta^{13}C$ showing the mean values of entire shell data combined for each ontogenic stage. Data points indicate mean values; error bars indicate 1σ. The vertical black dotted line indicates the mean expected equilibrium value for calcite. The shaded area with the black horizontal bar represents the range of expected $\delta^{18}O$ equilibrium values for calcite. The vertical white dotted line indicates the mean expected $\delta^{18}O$ equilibrium value for aragonite. The shaded area with the white horizontal bar represents the range of expected equilibrium values for aragonite. Data were collected via mass spectrometry through a modified version of McCrea's (1950) analysis technique. N values for the entire shells and the respective ontogenic stages are: 7 (A), 21 (B), 40 (C), 56 (D), 84 (E), 77 (F).

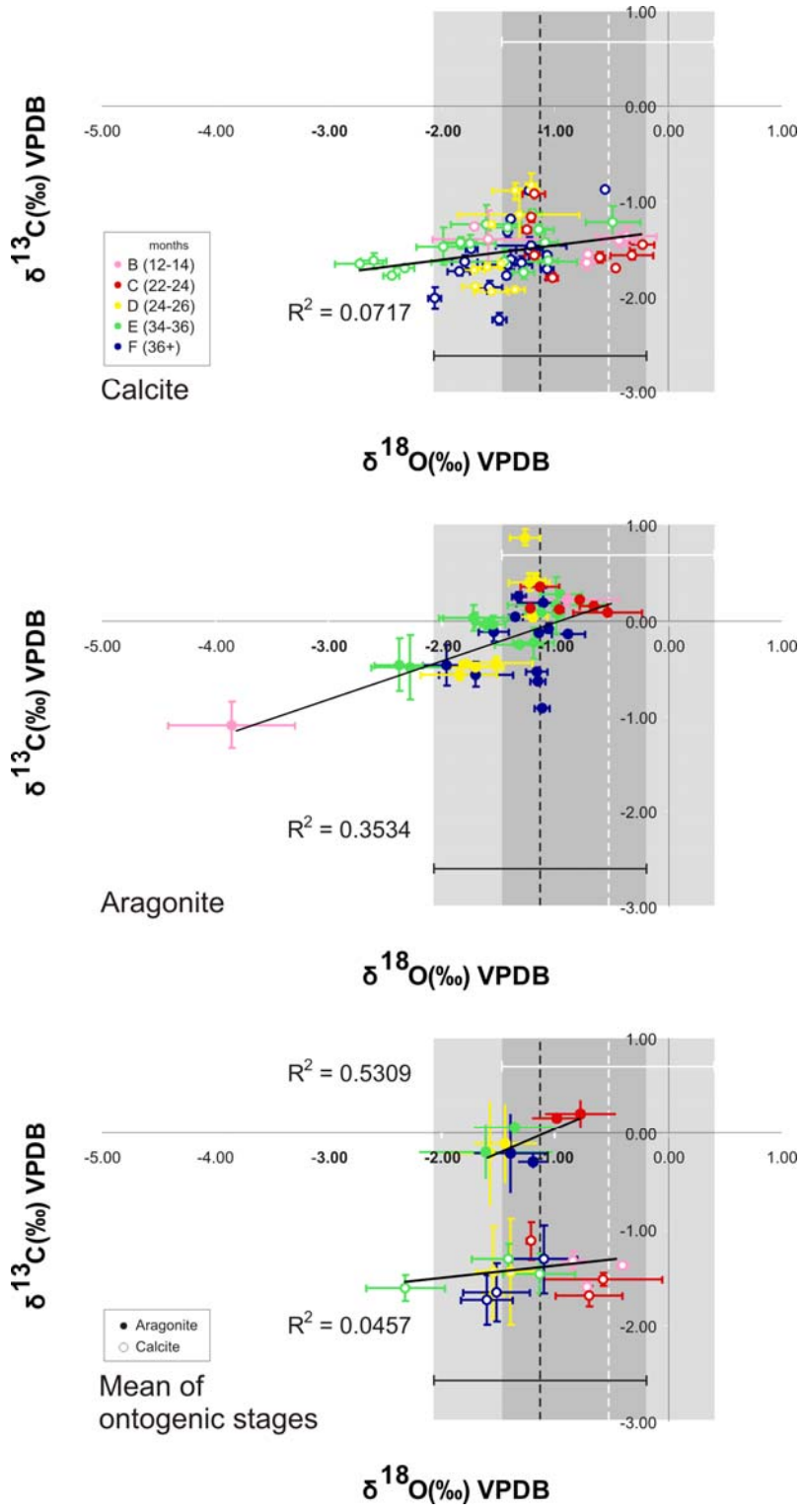

Figure 5.5 Cross plots showing all data from stages B-F of ontogeny. $\delta^{18}O$ is plotted against $\delta^{13}C$ showing the data in the two different polymorphs of calcium carbonate in the shell; calcite (top), aragonite (mid) with the mean values of all the data from each ontogenic stage in a combined plot (bottom). Data points indicate mean values; error bars indicate 1σ. The vertical black dotted line indicates the mean expected equilibrium value for calcite. The shaded area with the black horizontal bar represents the range of expected $\delta^{18}O$ equilibrium values for calcite. The vertical white dotted line indicates the mean expected equilibrium value for aragonite. The shaded area with the white horizontal bar represents the range of expected $\delta^{18}O$ equilibrium values for aragonite. Data were collected via mass spectrometry through a modified version of McCrea's (1950) analysis technique. Data for aragonite from B stage of ontogeny has been omitted in the last plot as insufficient data could be collected to give a reliable mean of the entire ontogenic stage. N values for the calcite layer and the respective ontogenic stages are: 10 (B), 24 (C), 32 (D), 49 (E), 47 (F). For the aragonite layer 7 (B), 16 (C), 24 (D), 35 (E), 30 (F)

The results of the whole shell (Figure 5.4) show a clustering of similar values. The SIMS data for the youngest (A) stage of ontogeny also shows similar values and trends in the oxygen signature to that of the C and F stages of ontogeny. Detailed conventional data is not available for the youngest stage of ontogeny. However, from the observations here it can be assumed that the youngest stage of ontogeny will not have significant deviations from the observations on conventional values obtained from the other ontogenic stages in this survey. The whole shell values all fall within the expected $\delta^{18}O$ equilibrium range for calcite, but some (B & E) show depletion with respect to the expected $\delta^{18}O$ equilibrium values for aragonite.

The data in Figure 5.5 show the distinct differences in isotopic composition between the two polymorphs of calcium carbonate in the *Mytilus* shell. The data from the aragonite layer shows enrichment of $\delta^{13}C$ compared to the calcite layer with the $\Delta^{13}C$ generally 1-1.5‰ between the data clusters. However $\delta^{18}O$ values in both polymorphs appear very similar, with a similar range in variation of the values. The data from the aragonite layer show a more significant positive correlation efficient than the calcite layer in the entire data set (R^2=0.5309) and the mean values (R^2=0.3534). No significant correlation is observed in the data of the calcite layer for the mean values (R^2=0.0717) or the entire data set (R^2=0.0457).

This pattern also occurs in the different regions of the shell length with samples from the umbo, mid and posterior edge region and the data presented for each region in Figure 5.6.

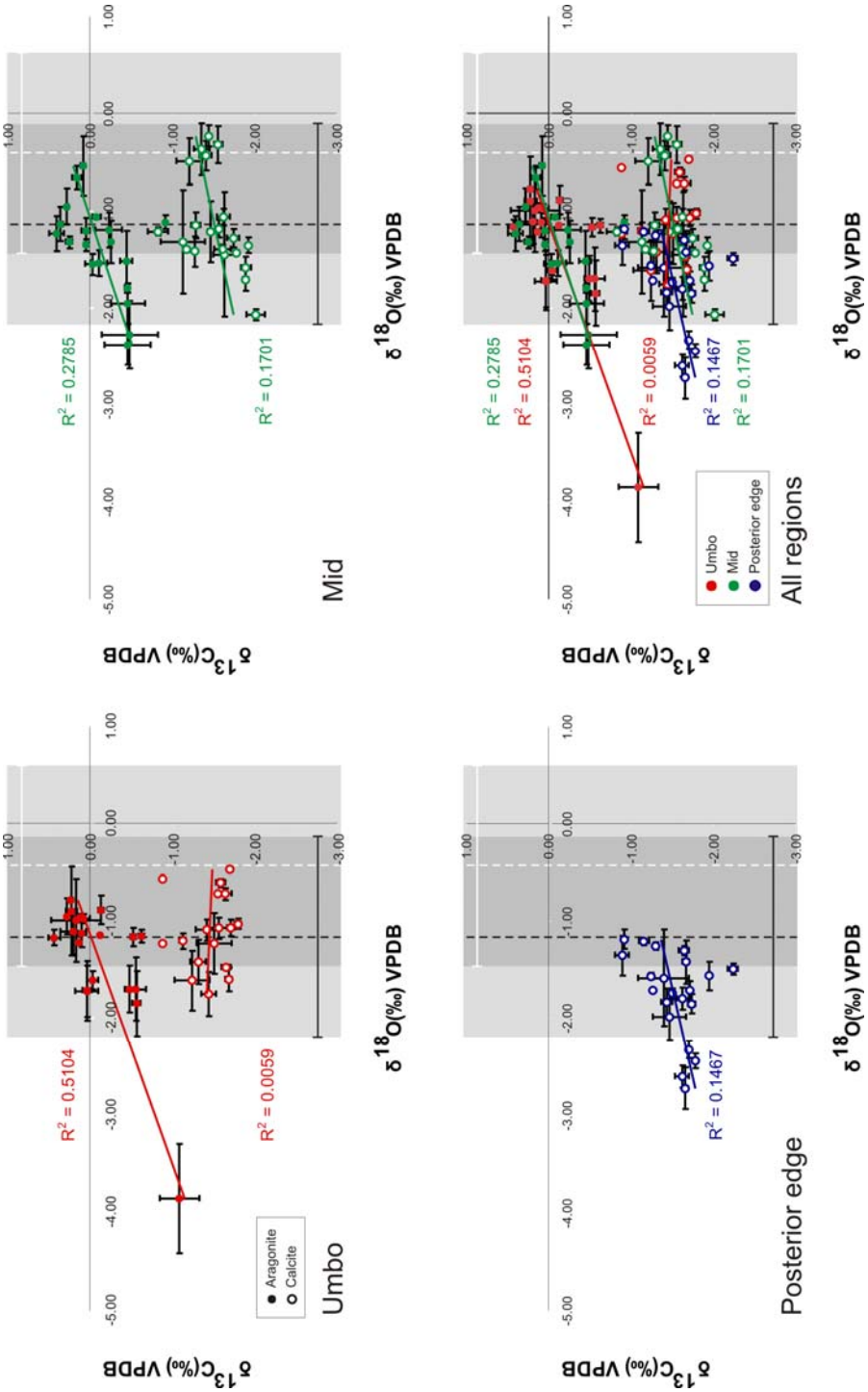

Figure 5.6. Cross plots from the different shell regions combining all stages of ontogeny. $\delta^{18}O$ is plotted against $\delta^{13}C$ representing data from the three different regions of the shell; Umbo (top left), Mid region (top right) and posterior edge region (bottom left). The vertical black dotted line indicates the mean expected equilibrium value for calcite. The shaded area with the black horizontal bar represents the range of expected $\delta^{18}O$ equilibrium values for calcite. The vertical white dotted line indicates the mean expected equilibrium value for aragonite. The shaded area with the white horizontal bar represents the range of expected $\delta^{18}O$ equilibrium values for aragonite. Data points indicate mean values; error bars indicate 1σ. Data were collected via mass spectrometry through a modified version of McCrea's (1950) analysis technique. N values for the calcite layer are 41 (umbo), 57 (mid), 58 (edge) and the aragonite layer: 56 (umbo), 56 (mid).

The stronger positive correlation coefficient between $\delta^{13}C$ and $\delta^{18}O$ values in the aragonite is present in both the umbo (R^2=0.5104) and the mid region (R^2=0.2785) of the shell, with the stronger relationship observed in the umbo region. However, the calcite layer is the converse with a weak correlations observed in all regions of the shell. The weakest is observed in the umbo region of the shell (R^2=0.0051) with the correlation improving moving posteriorly down the shell in the mid (R^2=0.1701) and posterior edge (R^2=0.1467) regions. The trend lines for the aragonite data in both the umbo and mid region produce very similar positive bearings. The calcite layer does not show the same strong agreement of correlation line between shell regions.

The data from the calcite layer in all regions fall within the predicted $\delta^{18}O$ equilibrium range for calcite. However, the values in the posterior edge calcite show more depletion in ^{18}O with some values falling out of the expected $\delta^{18}O$ equilibrium range for calcite. Similarly, data from the aragonite layer fall within the $\delta^{18}O$ equilibrium range for aragonite however some data points show depletion in ^{18}O and fall outside the expected equilibrium range.

Line graphs of the mean $\delta^{13}C$ and $\delta^{18}O$ values in both the calcite layer and aragonite layer through ontogeny are presented in Figure 5.7.

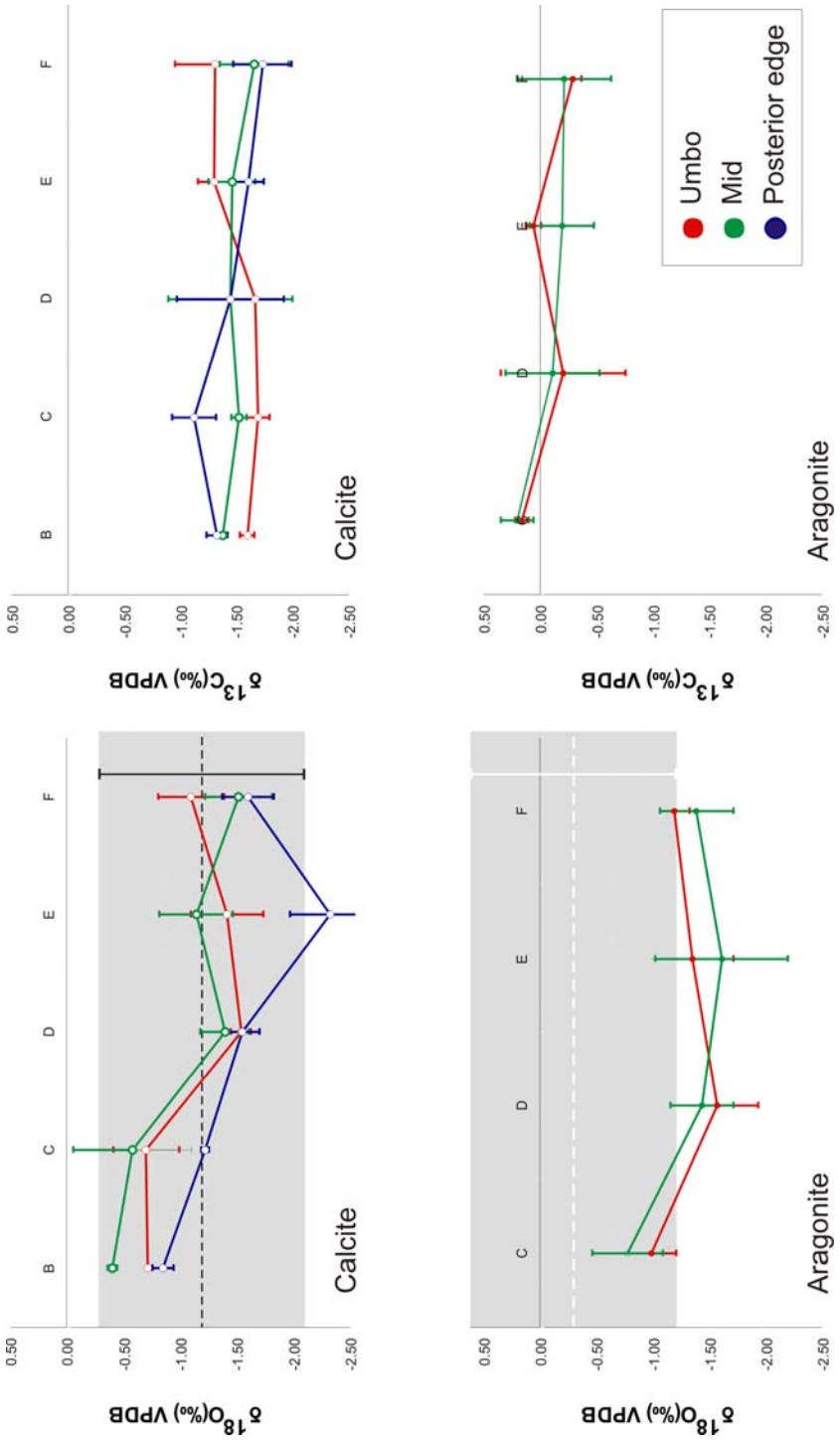

Figure 5.7. Line plots for $\delta^{18}O$ and mean $\delta^{13}C$ through ontogeny. Mean $\delta^{18}O$ values (left) and mean $\delta^{13}C$ values (right) through all stages of ontogeny with each line representing data from the three different regions of the shell; Umbo (red), Mid (green) and posterior edge (blue). Data points indicate mean values from entire ontogenic sets; error bars indicate 1σ. The B stage has been omitted from the aragonite profile as insufficient data could be collected to provide a reliable mean for the entire ontogenic stage B. The horizontal black dotted line indicates the mean expected $\delta^{18}O$ equilibrium value for calcite. The shaded area with the black horizontal bar represents the range of expected equilibrium values for calcite. The vertical white dotted line indicates the mean expected equilibrium value for aragonite. The shaded area with the white horizontal bar represents the range of expected $\delta^{18}O$ equilibrium values for aragonite. Data were collected via mass spectrometry through a modified version of McCrea's (1950) analysis technique. Data for aragonite from B stage of ontogeny has been omitted here as insufficient data could be collected to give a reliable mean of the entire ontogenic stage. N values for the calcite layer and the respective ontogenic stages are: 10 (B), 24 (C), 32 (D), 49 (E), 47 (F). For the aragonite layer: 16 (C), 24 (D), 35 (E), 30 (F)

Figure 5.7 show a trend toward a depletion of ^{18}O in the older stages of ontogeny in both polymorphs. More depletion of ^{18}O occurs in the posterior edge region in the calcite layer in all stages of ontogeny. Values of $\delta^{18}O$ in the aragonite layer are higher in the mid region compared to the umbo in stages C & D, while the converse is true for the older stages E & F. The $\delta^{13}C$ values show only minor fluctuations through ontogeny with no particular enrichment or depletion with respect to different stages of ontogeny.

5.4 Discussion

In comparing the overall trends in the oxygen isotope composition through the shell profile in SIMS and the overall $\delta^{18}O$ and $\delta^{13}C$ values in three regions of the shell through ontogeny, we can determine if the growth of the animal has a major effect on the isotopic composition of the shell. The analysis of *Mytilus edulis* allows an insight into a bi-mineralic biogenic structure which has implications for both calcitic and aragonitic organisms and from this to determine if ontogeny has a significant effect in such biomineral systems.

5.4.1 $\delta^{18}O$ values through ontogeny

5.4.1.1 Calcite layer

The earliest work on biogenic carbonate as an environmental indicator (Epstein *et al.*, 1953) has seen mollusc carbonate accepted as being deposited in isotopic equilibrium with the surrounding water. Further studies have confirmed this observation e.g. (Mook & Vogel, 1968; Killingley & Berger, 1979; Wefer & Berger, 1991). The conventional data obtained in this study supports this, as the majority of the mollusc calcite is produced within the expected $\delta^{18}O$ isotopic equilibrium range.

However, at higher resolution, the SIMS data obtained from transects through the shell reveal distinct isotopic composition patterns of the calcite layer where some values occur outside the expected $\delta^{18}O$ equilibrium values.

In the SIMS profiles, the increase in $\delta^{18}O$ values from the shell exterior towards the polymorph interface is observed in a number of the profiles. This trend suggests that there is a preferential uptake of ^{18}O towards the polymorph switch with the $\Delta^{18}O$ values typically ~2-3‰ suggesting that there are factors other than the environmental conditions affecting the oxygen isotope ratio of the calcite. If environmental conditions were the only factor, $\Delta^{18}O$ which reaches a maximum of 5‰ (Figure 5.2, C^1) would suggest a large shift in temperature of ~25°C, or salinity of ~28‰, or a combination of both in a relatively rapid period between initial growth of the calcite at the outermost surface and final deposition at the innermost surface.

As temperature and salinity ranges have been shown for the sampling site (Stirling & Okumus, 1995) such a significant environmental change is highly unlikely. Alternative explanations for this large shift are unknown, but could be due to factors such as the crystallography of the shell and the trace element profile through the shell which vary through the shell thickness (Chapters 3 & 4). The relationships between these factors will be discussed in more detail in Chapter 6.

However, the trends in the posterior edge calcite do not show the same scale of variation, only ~0.5‰, as the umbo or mid region (Figure 5.1 & 5.2). When the SIMS profile for the posterior region is normalised to the conventional mean, the data falls within the expected $\delta^{18}O$ equilibrium values for calcite.

This difference of $\delta^{18}O$ values between shell regions may indicate a variation of growth mechanism of the animal during ontogeny. When the first shell calcite is produced in the umbo region, the shell initially nucleates at the organic outer coating, the periostracum (Chapter 3). If shell nucleation requires rapid initial growth to provide the initial shell material in the umbo region, this could cause variation in the growth rate accounting for sharp increases of $\delta^{18}O$ observed at the outer shell surface and towards the interface. The calcite grown in the posterior edge has an existing mineralised framework when the shell has matured on which to continue growth. This could explain the invariance in the profiles from the most recently formed calcite.

As the specimens analysed here were collected at the same time from the same location, it can therefore be assumed that the most recently formed calcite on both A and C stages of ontogeny have been subject to the same environmental conditions. However, the difference in the posterior edge $\delta^{18}O$ values between the A and C (Figure 5.1 & 5.2) shows lower $\delta^{18}O$ values in the older stage (C) of ontogeny. This suggests that the most recently formed calcite, at the posterior edge of both specimens, has been subject to kinetic differences as the growth rate slows with the age of the specimen (Goodwin *et al.*, 2003). However, kinetic effects are often recognised by a linear correlation between $\delta^{18}O$ and $\delta^{13}C$ values (Swart, 1983; McConnaughey, 1989a, 1989b). No such strong correlation is observed here (Figures 5.5 & 5.6) but the weak correlation is greater in the posterior than the umbo. Poor correlations between $\delta^{18}O$ and $\delta^{13}C$ have been noted in other biogenic systems in the secondary layer of articulated brachiopods (Parkinson *et al.*, 2005). However, the calcite formed in the secondary layer was also where equilibrium carbonate was more likely to be formed and growth rates were likely to be slower. These observations in the brachiopods may be analogous to what is observed here, with regions such as the posterior edge becoming a slower growing area as the animal ages. In turn, the slower growth rate may offer more time for oxygen isotopic equilibrium to be achieved.

This concept of lower $\delta^{18}O$ values in calcite through ontogeny is emphasised in Figure 5.7. Here the posterior edge shows lower $\delta^{18}O$ values compared to the other shell regions in all stages of ontogeny, but also displays a trend towards lower $\delta^{18}O$ values through ontogeny. From the conventional mass spectrometer data, more points from the posterior edge are shown to be depleted with respect to the expected $\delta^{18}O$ equilibrium values for calcite than the other shell regions (Figure 5.6).

The variation of isotopic signature in different parts of the mollusc shell has been investigated previously (Klein *et al.*, 1996b) where the metabolic activity of the mantle at areas of greater curvature in the shell have been said to exert different metabolic demands (Rosenberg *et al.*, 1989; Rosenberg & Hughes, 1991). Klein *et al*. (1996b) noted that secretion of the calcite at the ventral margins of *Mytilus trossulus*, where growth rate was higher, had a mild enrichment in ^{18}O compared to the lateral margins of the shell where growth slowed and metabolic demands were higher. Here a similar effect may also explain the general pattern of ^{18}O depletion in the calcite layer from umbo to posterior as observed in both the SIMS and the conventional mass-spectrometer data.

5.4.1.2 Aragonite layer

The inner aragonite (nacreous) layer is often omitted from isotopic studies in molluscs (Margosian *et al.*, 1987; Vander Putten *et al.*, 2000; Gillikin *et al.*, 2006). The main reason for omitting the nacreous layer from isotope studies is the fact that the nacreous layer experiences prolonged direct contact with the tissues of the animal as well as the presence of the isolated micro-environment within the shell, the extrapallial space (Section 1.1.3). Different parts of the mantle are involved in the formation of the two polymorphs and so for environmental reconstructions, more metabolic and kinetic factors can obscure the signal.

As with the calcite, correcting for the offset between SIMS and conventional data brings much of the aragonite close to the expected range of $\delta^{18}O$ equilibrium for aragonite. However, the aragonite values produced in this study show a regular offset (~0.5-1‰) from the expected $\delta^{18}O$ mean equilibrium values for aragonite for both SIMS and conventional. This is consistent with reported offsets of ~0.6-0.8‰ for aragonite $\delta^{18}O$ values (Tarutani *et al.*, 1969; Rye & Sommer, 1980; Grossman & Ku, 1986; Rahimpour-Bonab *et al.*, 1997). When the data is further corrected for this offset, it brings the majority of data from the aragonite layer within the expected $\delta^{18}O$ equilibrium value for aragonite.

In higher resolution analysis, $\delta^{18}O$ profiles through the shell generated via SIMS are more invariant compared with the calcite layer. However, significant shifts in $\Delta^{18}O$ (2‰.) are still observed in the

aragonite layer (Figure 5.3). These shifts in ^{18}O content tend to be a gradual increase in ^{18}O towards the inner shell surface.

As for the posterior edge calcite, the generally invariant $\delta^{18}O$ profiles in aragonite may represent the different rates of growth between calcite and aragonite. As the rate of nacre deposition remains relatively constant, so do the $\delta^{18}O$ values in the aragonite similar to the invariant $\delta^{18}O$ profile observed in posterior edge calcite, but distinct to other regions of calcite.

The correlation between the $\delta^{18}O$ and $\delta^{13}C$ values is significantly stronger (Figure 5.5 & 5.6) in the aragonite layer than the calcite layer suggesting that it may be more strongly affected by kinetic effects than the calcite layer (McConnaughey, 1989a, 1989b). These observations may not be a consequence of kinetics, as the nacre is considered to accumulate more slowly than the calcite layer.

The suggestion that aragonite may be influenced by kinetic effects here may also be reinforced by the observation that where significant enrichment of ^{18}O occurs in the aragonite layer is often associated with the aragonite prismatic myostracal bands compared to the surrounding nacre (Figure 5.2, C^2 & C^3). If these prisms have grown at a faster rate than the smaller nacre tablets, then this could result in an enrichment of the heavier isotope.

5.4.2 $\delta^{13}C$ values through ontogeny

The $\delta^{13}C$ values of the mollusc are often considered in environmental studies as they have been shown to reflect the environmental factors such as temperature (Mook & Vogel, 1968). However, the carbon isotope signature is thought to reveal more about changes in the mollusc system itself (Wefer & Berger, 1991; Vander Putten *et al.*, 2000; Owen *et al.*, 2002; Geist *et al.*, 2005; Gillikin *et al.*, 2006).

The most significant observation of the $\delta^{13}C$ values here is the discernable offset between the values in the calcite layer and the aragonite layer. The aragonite layer shows higher $\delta^{13}C$ values of ~1‰ on average. However, aragonite has been shown to have more enriched in ^{13}C compared with calcite when grown under the same conditions with an offset in $\delta^{13}C$ of around 1.2‰ (Gonzalez & Lohmann, 1985). Rahimpour-Bonab *et al*. (1997) investigated calcite and aragonite-secreting molluscs in the same cool-water environment and demonstrated that the 'vital' effect did not play a significant role in determining the $\delta^{13}C$ of the molluscs as the shell carbonate was precipitated in equilibrium with the ambient seawater. The offset in $\delta^{13}C$ values between the specimens was attributed to a difference in mineralogy and not a biological effect. Rahimpour-Bonab *et al*. (1997) recognized the cool-water conditions as a limiting factor of the growth rates to a sufficient level that allowed equilibrium to be reached. Cool water conditions could be an explanation for the offset

observed here rather than a vital effect. However, the linear correlation of the $\delta^{13}C$ with the $\delta^{18}O$ discussed previously suggests that a kinetic effect may exist here. When $\delta^{18}O$ and $\delta^{13}C$ co-vary, this implies that the CO_2 involved in the biomineralising process may not have reached equilibrium due to the rapid growth (Turner, 1982) causing an incomplete isotopic equilibration of the CO_2 in the extrapallial fluid.

Due to the lack of a linear correlation between $\delta^{18}O$ and $\delta^{13}C$ in the calcite, it can be suggested that the $\delta^{13}C$ here may be modified by metabolic influences since the $\delta^{13}C$ values of the CO_2 and the HCO_3^- in the extrapallial fluid can be affected by factors such as respiration in localised areas of the shell (Swart, 1983). This would cause a shift away from equilibrium as respiratory CO_2 is isotopically depleted with respect to carbon. The amount of metabolic carbon incorporated into the mussel system has been debated. Values ranging from 10% (McConnaughey *et al.*, 1997; Kennedy *et al.*, 2001) to as much as 85% has been reported (Tanaka *et al.*, 1986). Therefore, with other studies on the *Mytilus* system indicating that periods of increased metabolic activity in the mussel can be interpreted through identification of more depleted values (Klein *et al.*, 1996b; Geist *et al.*, 2005). Thus, it could be assumed that greater variation of $\delta^{13}C$ could be observed through ontogeny as metabolism varies as the animal ages (Krantz *et al.*, 1987). However that is not observed here, $\delta^{13}C$ values remains relatively invariant in both calcite and aragonite (Figure 5.7).

5.5 Summary

The overall mean values in the different regions along the shell show very little variation through ontogeny. The minor variations between the regions of the calcite layer with respect to the oxygen isotopes can possibly be considered as being influenced through kinetics as the rate of growth decreases with increasing age. The calcite in the posterior edge of the shell comprises lower values for $\delta^{18}O$ through ontogeny which continue to decrease with age (Figure 5.8)

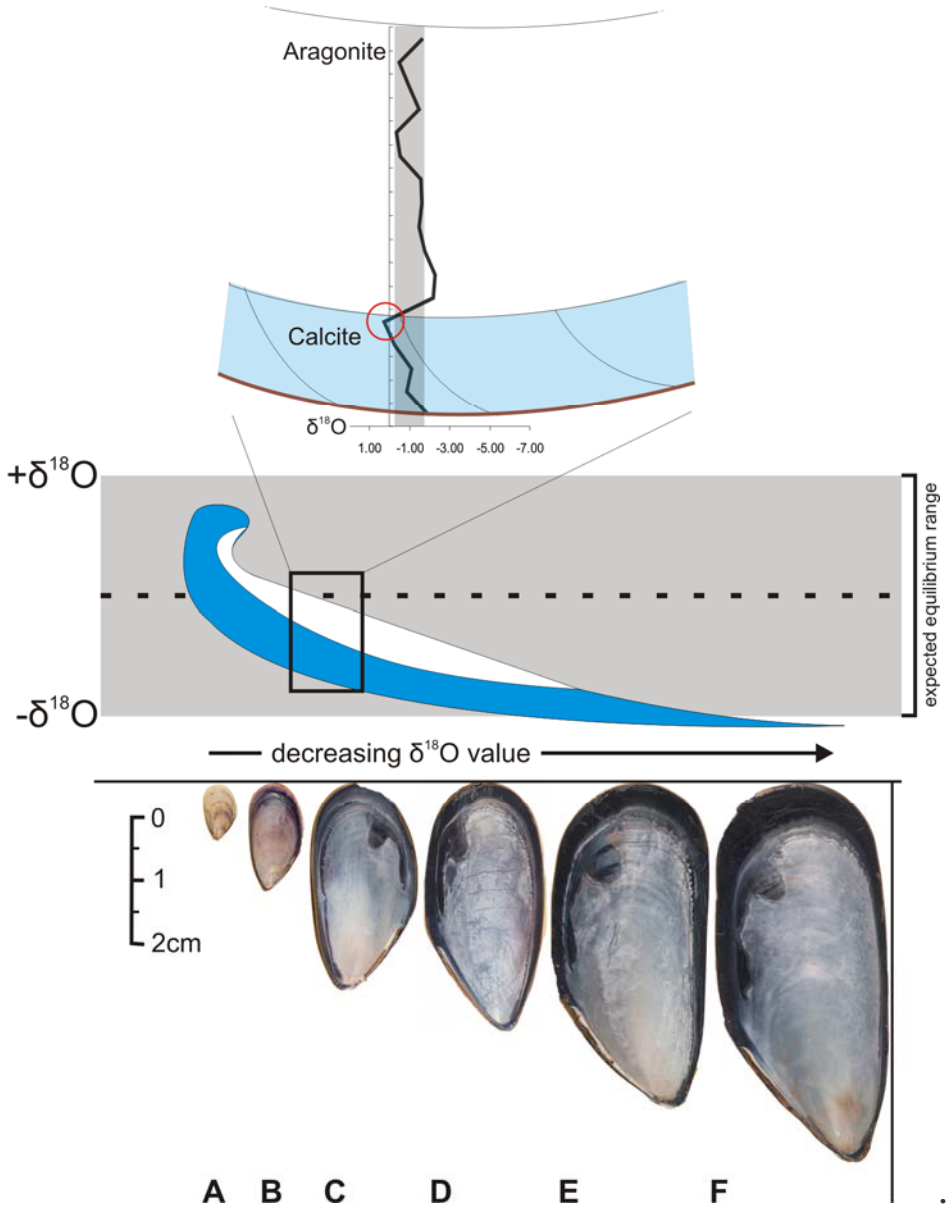

Figure 5.8 Summary of observations in stable isotopic composition in *M. edulis*. Top: typical profile through the shell thickness. Data is corrected for offset, but shows trend toward values (red circle) outside expected equilibrium values for calcite before polymorph switch. Middle: Shell cartoon with the majority of the shell carbonate produced within expected equilibrium range, however, some posterior edge values lie outside this range. Bottom, decrease in $\delta^{18}O$ values noted as animal age increases.

If the carbon isotopes reflect metabolic changes within the system, then the lack of any significant changes in the $\delta^{13}C$ signature suggests that the metabolism does not change significantly through the ontogenic range observed here and any differences may depend on the individual animal analysed. The offset of the $\delta^{13}C$ values between the calcite and the aragonite lies within the accepted range for previously determined offset values between the polymorphs (Rahimpour-Bonab *et al.*, 1997) indicating that the mineralogy may be more significant in determining the $\delta^{13}C$ composition.

The difference in the correlation trends between $\delta^{13}C$ and $\delta^{18}O$ in calcite and aragonite remains unresolved. There is a stronger linear correlation in the aragonite suggesting kinetic effects yet no significant effect is observed in the $\delta^{18}O$ values through ontogeny which would be susceptible to a kinetic effect. Calcite shows a weak correlation which is thought to be more typical of metabolic effects, however, the lack of variation in $\delta^{13}C$ do not suggest a metabolic shift.

Large shifts in $\Delta^{18}O$ in short periods which cannot be accounted for by environmental changes suggest a kinetic effect in both polymorphs. Faster growing calcite in early stages of shell development could prevent equilibrium being achieved in some regions across the shell thickness. Similarly, if prismatic aragonite grows faster than nacre, this could account for aragonite deposited outside expected equilibrium values.

For the ontogenic range of *M.edulis* observed here, the oxygen and carbon isotope composition show similar values between shell regions and through ontogeny. A minor effect on $\delta^{18}O$ composition is exerted by the age of the animal. Despite this, mean values generally form within expected equilibrium values. Significant variation observed here is more likely determined by differences in mineralogy and the rate of crystal growth through the shell.

6

Discussion & Further Work

6.1 Aim of investigation

This investigation was undertaken to determine any significant changes in shell chemistry and crystallographic ultrastructure through different stages of ontogeny of the mussel *Mytilus edulis*. Identifying changes in shell chemistry and crystallography and any relationship between them will contribute to our understanding of biomineralisation as well as the interpretation of climate proxies. The crystallography of the shell has been examined through Electron Back Scatter Diffraction (EBSD) in the umbo, mid and posterior edge of the shell along the main growth axis of the animal for each of the six stages of ontogeny to determine any differences in the crystallography of the shell as it ages. The minor and trace element chemistry and stable isotopic signature has been investigated in conjunction with the crystallography through Secondary Ion Mass Spectrometry (SIMS), Electron Probe Micro Analysis (EPMA) and conventional mass spectrometry. These analyses were performed to identify any significant relationships between chemistry, isotope composition and crystallography through the animal's life. Studying *Mytilus edulis* has provided an insight into a bimineralic system, with calcite and aragonite, and this has allowed further insight into the extent of which polymorphism and crystal habit of calcium carbonate in *M. edulis* influences shell chemistry.

The following chapter summarizes the main findings of this study and investigates any relationships between the crystallography, trace element concentration and stable isotopic composition. Each of these components has been dealt with separately in more detail in Chapter 3, 4 and 5 respectively.

6.2 The growth stages

Each of the specimens of *Mytilus edulis* used in this study was from a single collection of farmed mussels from a cluster of mussels grown on a rope immersed in the waters of Loch Etive (Section 2.1.1). Thus, each specimen was subject to the same environmental conditions during development. The continuous immersion reduces the effects of hiatus of growth during tidal events, observed in

specimens of *M. edulis* found in near-shore environments, which may distort effects produced through ontogeny. Thus, one advantage of using farmed mussels is the ability to estimate age based on shell length. The entire cluster was removed from the water at the same time on 15/3/05. Therefore, handling and transportation was the same for all samples as detailed in Section 2.1. This process of collection therefore ensured a degree of control over environmental parameters and stresses possibly experienced through laboratory conditions. Therefore, any significant differences in the characteristics investigated here between the life stages can be more reliably attributed to ontogenic effects.

6.3 Relationships between crystallography, trace element and stable isotopes

The crystallography of the shell through ontogeny was covered in detail in Chapter 3 and was analysed in the umbo, mid and posterior edge region of the shell along the main axis (anterior-posterior) of growth. The general observation in the calcite layer for all stages of ontogeny is uniformity of crystal habit (Section 3.3.2.1) and crystal orientation (Section 3.3.3). Prismatic crystals were observed with the *c*-axis inclined towards the shell surface. Moving down the shell from the umbo region to the posterior edge, the crystallographic orientation and crystal habit becomes more constrained (Figures 3.4, 3.7, 3.9 & 3.16). This same refinement in morphology and crystallographic orientation occurs when comparing the outermost calcite at the periostracum to the calcite at the polymorph interface (Figures 3.5, 3.6 & 3.18). The umbo region has more distortion of crystal morphology and polymorph layering (Figures 3.2 & 3.4).

The aragonite layer also showed regularity in orientation and crystal habit (Figures 3.8i-iii, 3.14 & 3.15) with the *c*-axis of the nacreous tablets orientated perpendicular to the shell surface with regular alternations between the {100} and {010} crystal faces presented at the analysis surface. However, the nacreous layer is occasionally punctuated by layers of prismatic aragonite with crystals much larger than the nacreous tablets (Figure 3.8iv & v). However, the same pattern of crystallographic orientation is maintained throughout these prismatic aragonite bands (Figure 3.12).

The trace element composition was discussed in Chapter 4 with a consistent pattern between all sections of the shell through all stages of ontogeny. The average element concentration shows little variation between the different areas along the shell. However, individual element profiles through the calcite layer have a distinctive recurring pattern in each of the three areas of the shell in each stage of ontogeny. Na concentration decreases steadily across the calcite layer from high initial concentrations at the outermost calcite to the polymorph interface. Mg and S concentration profiles often increased in concentration preceding the polymorph switch. Sr concentrations are relatively consistent through the entire calcite layer with only minor variations.

The aragonite layer has more uniform minor element concentrations through the shell thickness, with distinctly high concentrations of Na and Sr, and very low concentrations of S and Mg compared to the calcite layer. Distinct 'spikes' in the element profiles coincide with the prismatic bands indicating a difference in element distribution based on crystal habit. There are no major differences in trace element content between ontogenic stages. However, younger stages of ontogeny and the umbo region do show a minor increase in Mg, Sr and S concentrations while also being relatively depleted in Na concentration compared to older ontogenic stages.

Stable isotopic signatures also show regular $\delta^{18}O$ profile patterns through the shell thickness and values for both $\delta^{18}O$ and $\delta^{13}C$ are consistent through each stage of ontogeny. However, some increased irregularity in the profiles occurs in the umbo region, similar to the irregularity in trace element profiles and crystallography in this region of the shell. Accounting for offsets between analysis techniques and differences in isotopic partitioning between the two polymorphs brings most of the $\delta^{18}O$ data within expected equilibrium values for the respective polymorphs.

The calcite layer shows a trend toward higher $\delta^{18}O$ values moving from the outermost calcite to the polymorph interface. Also the $\delta^{18}O$ values found in the calcite of the posterior edge were increasingly negative compared to the calcite of the umbo and mid region. Increasing age of the animal also yields slightly more negative $\delta^{18}O$ values. The aragonite layer did not show the same distinct patterns, with $\delta^{18}O$ and $\delta^{13}C$ values relatively constant between ontogenic stages and areas of the shell.

Large offsets in the $\delta^{18}O$ profiles of both polymorph layers, maximum $\Delta^{18}O$ ~5‰ for calcite and ~4‰ for aragonite, are observed that cannot be explained by merely variation in environmental conditions. The large offsets in the aragonite layer are typically associated with prismatic aragonite, showing more positive $\delta^{18}O$ values than the aragonite nacre.

From the patterns observed in all aspects investigated here, suggestions can be made about the relationship between the crystallography and the resultant shell chemistry. The uniformity in crystallography for the majority of the shell coincides with the regular recurrence of the trace element and stable isotope profiles. Where the shell chemistry and isotopic pattern is more distorted, at the umbo region, the crystallography also has more disorder. Regularity in crystallographic orientation, crystal habit and shell chemistry increases from the umbo region to the posterior. Similarly, the improvement in crystallographic orientation and morphology moving from the outermost calcite to the calcite at the polymorph interface coincides with the fall in Na and often an increase in Mg and S and an increase in $\delta^{18}O$ values. Abrupt changes of crystal habit in the aragonite layer between nacre and prismatic aragonite are accompanied by significant differences in the stable isotope signature and trace element concentrations despite crystallographic orientation

being maintained. The factors that may account for any relationships are difficult to isolate as there are various aspects that occur simultaneously which can affect the system. These have been considered through this study and are summarized below.

6.3.1 Animal growth and growth kinetics

6.3.1.1 Calcite layer

Crystal growth and trace and minor element incorporation for carbonates has been investigated previously under laboratory conditions (Tsusue & Holland, 1966; Kinsman & Holland, 1969; Katz *et al.*, 1972b; Katz, 1973; Kontrec *et al.*, 2004; Kralj *et al.*, 2004). The main aim of such studies being the determination of the distribution of elements in the crystal lattice and determining how the elements affect crystal growth. These investigations have shown that, in analysis of trace and minor element incorporation in carbonates, kinetics of the system have a significant effect on the resultant composition of calcite (Lorens, 1981; Mucci & Morse, 1983; Pingitore & Eastman, 1986; Burton & Walter, 1987; Morse & Bender, 1990; Major & Wilber, 1991; Rimstidt *et al.*, 1998; Nehrke *et al.*, 2007) with increased growth rate often resulting in greater trace element incorporation.

Trace element chemistry has been investigated in conjunction with stable isotope chemistry in the mussel (Stecher *et al.*, 1996) and other carbonate systems for kinetic effects (Devilliers *et al.*, 1995). Other studies have also revealed kinetic effects on the stable isotopic signature in biomineralising systems with faster growing regions having marked differences to expected 'equilibrium' carbonate values of $\delta^{13}C$ and $\delta^{18}O$ (Land *et al.*, 1975; McConnaughey, 1989a, 1989b; Allison *et al.*, 1996; Guzman & Tudhope, 1998).

This kinetic influence on isotopic and chemical composition has implications for *Mytilus edulis* analysed here. It can be expected that the mussels may have different rates of growth at different stages through ontogeny (Coe & Fox, 1942; Coe, 1945; Pannella & MacClintock, 1968; Seed, 1969; Bayne & Newell, 1983) and different seasonal growth. If growth kinetic effects in periods of increased shell production during specific stages in ontogeny, such as early growth, periods of reproduction and sexual maturation, then it may possibly be expected that this would be evident in the crystallography and shell chemistry profiles.

The banding in the EBSD data caused by minor variation in crystal orientation, which was noted in Section 3.3.3.2 & 3.3.3.3, almost certainly represents the incremental additions of shell material during periods of variation of growth (Clark, 1974). The thinner bands indicate growth possibly at night (Pannella & MacClintock, 1968) or during metabolically slower periods (Rodland *et al.*, 2006). However, the pattern in the trace element distribution does not appear to vary significantly

as expected from significant kinetic effects. In fact mean concentrations of trace elements are constant between ontogenic stages.

Shell precipitation rate has been considered as a factor in trace element incorporation previously with Sr/Ca ratios found to be strongly affected by growth kinetics in other carbonate producing systems such as coccoliths (Rickaby *et al.*, 2002) and other bivalve systems (Lorrain *et al.*, 2005). Comparison studies involving other biomineralising systems (England, 2005) contrasted the fast growing *M. edulis* against the slower growing marine brachiopod, which also secretes calcite, have further investigated the kinetic effect. The Mg concentration was lower in the mussel system, which is counterintuitive if kinetics is to explain the trace element variation and suggests that the kinetic effects may be species specific.

For ontogenic effects on isotopic values, Goodwin *et al*. (2003) modelled and observed varying growth rates of mollusc development. They found that the earliest stages of growth provided the best range of values for use in environmental proxies with slower growing, older stages more difficult to apply to reconstructing climate conditions. Also changes in trends of isotopic mean values were thought to represent a change in growth rate rather than changes in the environmental conditions. This seems in agreement with what is observed here, with a trend towards more negative $\delta^{18}O$ values in older ontogenic stages, which could represent the slowing of shell growth. A greater range of ontogenic stages than analysed here, would be needed to fully investigate this for *M. edulis*.

The refinement of the calcite crystal morphology and orientation posteriorly and in older stages of ontogeny occurs in tandem with the trend toward negative $\delta^{18}O$ values. This suggests that with slower growth, calcite formation with an 'improved' structure is formed with selective isotope uptake. However, strict interpretation of this is complicated with the converse being observed through the thickness of the calcite layer with refinement in crystallography coinciding with trends toward more positive $\delta^{18}O$ values. Further factors must be considered here rather than simply the kinetics of the system.

6.3.1.2 Aragonite layer

The aragonite layer is considered to be slower growing than the calcite layer (Seed, 1969) with greater control exerted on the construction of the 'brick and mortar' design of nacre. As well as this, the nacre is deposited by different mantle cells with the isolated extrapallial space, filled with fluid, responsible for nacre deposition (Taylor *et al.*, 1969; Wise, 1970b; Erben & Watabe, 1974; Wilbur & Saleuddin, 1983; Addadi *et al.*, 2006).

If aragonite nacre grows at a slower rate than the calcite crystals, it can possibly be assumed that the aragonite crystals have more time to achieve equilibrium and can exclude more foreign ions. However, the trace element data suggests otherwise, with higher concentrations of Sr and Na throughout the aragonite layer compared to the faster growing calcite layer.

Distinct changes occur in trace element and stable isotope profiles where layers of prismatic aragonite are produced. Increases in Sr concentration and $\delta^{18}O$ values in these areas suggest a kinetic effect in the faster growing aragonite prisms. These changes are also coupled with a decrease in Na concentration. This suggests that Sr and Na are competing in the aragonite crystal lattice in the prismatic crystals. While the nature of the ions is different with monovalent Na^{+} compared to divalent Sr^{2+}, as discussed previously in Chapter 4, Na^{+} can substitute for Ca^{2+} in the aragonite lattice easier than in calcite (Amiel *et al.*, 1973; Land & Hoops, 1973). Therefore, direct competition for the Ca^{2+} site in the prismatic aragonite can explain the abrupt spikes in the trace element profile, and kinetics can possibly account for the greater Sr uptake previously correlated with faster growing carbonate (Lorens, 1981). Sr/Ca ratios have been correlated with shell growth rates in aragonitic shells (Takesue & Van Geen, 2004).

With respect to the stable isotopic values, as discussed with the calcite layer above, a kinetic influence on the isotopic signature may occur in faster growing calcium carbonate (McConnaughey, 1989a; 1989b; 2002; 2003). This kinetic influence may account for elevated $\delta^{18}O$ values in the prismatic aragonite layers. A kinetic influence in the aragonite prismatic layer may also account for the linear correlation between $\delta^{18}O$ and $\delta^{13}C$, which normally indicates kinetic effects, observed in the aragonite layer.

The differences between the calcite and aragonite $\delta^{18}O$ and $\delta^{13}C$ values observed in this study, fall within the region for offset between the isotope behaviour for the polymorphs (Tarutani *et al.*, 1969; Gonzalez & Lohmann, 1985; Rahimpour-Bonab *et al.*, 1997). If aragonite nacre accumulates at a more regular, slower rate than calcite, this may account for the more regular $\delta^{18}O$ values in the aragonite nacre. A variable rate of growth in the calcite layer may produce the increased variation observed in the data produced via SIMS (Chapter 5). Overall, for the nacreous majority of the aragonite layer, the crystallography shows little variation in habit or orientation, and this coincides with very consistent uniform values of Na, Sr and $\delta^{18}O$ and $\delta^{13}C$ values through the shell and through ontogeny. With the slower growth rate, it would appear that the aragonite layer is not affected by kinetic effects except the prismatic bands, which therefore has implications for the importance of crystal habit in applications of biominerals in climate proxies.

6.3.1.3 Sector zoning

The concept of sector zoning in carbonates (Reeder & Grams, 1987; Reeder & Paquette, 1989; Paquette & Reeder, 1990; 1995) means that non-equivalent crystallographic faces can accumulate significantly different concentrations of trace elements within the same crystal, with intrasectoral zoning also producing distribution variation within the same crystal face (Staudt *et al.*, 1994). Thus, interpretation of kinetic effects on trace element partitioning into the crystal structure can be complicated, through preferential concentration of certain elements to different crystal faces. Distinct changes in crystal orientation have coincided with abrupt shifts in trace element profiles in other calcite-secreting organisms such as brachiopods (A. Pérez-Huerta, pers comm). The EBSD data obtained in this study shows that the crystallographic orientation of the calcite remains constant with the same crystal face presented for analysis by EPMA and SIMS. Therefore, sector zoning does not account for the variation observed in the profiles in this study. In conjunction with this, in cases where slight deviation in general orientation occurs between regions analysed, thus different crystal faces are analysed, the profiles still retain the typical pattern of element distribution. The aragonite layer shows consistent alternation between the {100} and {010} faces being presented for analysis and the chemical profile remains constant through the nacre and so there does not appear to be any significant effect of element partitioning here.

Changes in crystal orientation have corresponded to changes in the isotopic signature in calcite-secreting biological systems (Cusack *et al.*, (in press)). Sector zoning has been previously attributed to disequilibrium and isotopic variation in other minerals such as quartz (Onasch & Vennemann, 1995) but has not been found to affect carbonates in the same manner (Klein & Lohmann, 1995). The observations in this study support the idea that sector zoning is not involved in the variation in the isotopic signature and is more likely affected by other factors.

6.3.2 Metabolic and biological controls

A further complication in interpreting the trace element and isotopic signature, with respect to the crystallography, is the extent of the regulation that metabolism exerts over the system. Rosenberg et al. (1989; 1991) demonstrated that different metabolic rates in different parts of the mantle were needed to produce specific areas of the shell. More metabolically ‘expensive’ regions had greater trace element incorporation, normally in areas of greater curvature like the umbo region. In this survey, the umbo region does show differences in crystallographic orientation, crystal habit, polymorph layering, trace element chemistry and stable isotopic ratios compared to other parts of the shell. Therefore, the metabolic model could explain the variation observed here. It would, however, be expected that the stable isotopic and trace element values would show more differences between the ontogenic stages.

Lorens & Bender (1977) demonstrated a physiological exclusion of Mg in *M. edulis*. Therefore, the trace element signature could be considered as an indicator of biological functions. If Mg is an essential component and modifier of biomineral growth (Reddy & Wang, 1980; Davis *et al.*, 2000; Meldrum & Hyde, 2001; Han & Aizenberg, 2003; Loste *et al.*, 2003) and polymorph selection (Fernandez-Diaz *et al.*, 1996; Sugawara & Kato, 2000; Kitamura, 2001) then it could be that *M. edulis* controls the Mg concentration to develop the shell. A similar system has been proposed for controlling avian eggshell growth (Hincke & St. Maurice, 2000; Cusack *et al.*, 2003; Dalbeck & Cusack, 2006). This may account for the recurring pattern in the Mg profile, with an increase in Mg concentration towards the polymorph interface in many of the specimens, and the regularity in the profile in each region of the shell in all stages of ontogeny.

Klein *et al*. (1996b) established that Sr also reflects metabolic activity in *M. edulis*. Sr reflects the rate of metabolic pumping of ions through the mantle tissue to the isolated extrapallial fluid (Klein *et al.*, 1996b). When metabolism was most active, more Ca^{2+} was pumped across the mantle reduing the Sr/Ca of the extrapallial fluid. Further investigations have also shown that Mg/Ca and Sr/Ca ratios also show effects from biological functions and also changes through ontogeny in bivalves (Purton *et al.*, 1999; Vander Putten *et al.*, 2000; Purton-Hildebrand *et al.*, 2001; Gillikin *et al.*, 2005; Freitas *et al.*, 2006). Dick *et al*. (2007) described enrichments of trace elements in the umbo of *Laternula elliptica* followed by a decrease in concentrations posteriorly along the shell. This was attributed to a decrease in respiration mass as the animal aged and the change in metabolism that resulted. Similar decreases in the metabolism and oxygen consumption of the animal increase with age (Zeuthen, 1953; Sukhotin & Portner, 2001). Therefore, trace element chemistry differences should be apparent between the stages of ontogeny if the biology of the system, and ultimately the growth rate, change concurrently with this. Freitas *et al*. (2005) showed a marked decrease in Mg/Ca correlation with temperature with increasing age in *Pinna nobilis*, and also distinct differences compared to other neighbouring bivalve species. This study also reports difference This suggests a metabolic effect with increasing ontogeny as well as further emphasis on species specificity for metabolic effects in biomineralising systems. Richardson *et al*. (2001) also reported a decrease in trace element incorporation of lead (Pb) in *Modiolus modiolus* shells as animal age increased.

The metabolic model from Klein *et al*. (1996b) was also used to account for changes in $\delta^{13}C$ in *Mytilus trossulus*. Respiratory and biological functions create offsets in predicted equilibrium values for carbon (McConnaughey *et al.*, 1997; Heikoop *et al.*, 2000; Kennedy *et al.*, 2001). Therefore, changes in ontogeny and slowing of metabolic rates with increased age should be reflected in the carbon isotopic values. Such patterns in $\delta^{13}C$ composition have often been used to indicate periods of maturation in bivalves (Wefer & Berger, 1991). Metabolic functions are not

considered to affect the $\delta^{18}O$ values (Klein *et al.*, 1996a) and so the variation in the oxygen isotope profiles through the shell are not attributed to metabolism in the present study.

However, little evidence of these metabolic effects is observed in the ontogenic survey performed here. Crystallography, chemistry and the isotopic signature showing little change through the 3 year span investigated here. Only the umbo shows evidence that may affirm the metabolic expenditure model of Rosenberg and Hughes (1991), and the umbo does show increased affinity for trace elements as suggested by Dick *et al.* (2007). However, further indications of metabolic activity are not reinforced by expected changes through ontogeny. Later stages of ontogeny may need to be investigated to develop further insight into the effect of ontogeny on metabolism and ultimately the shell produced by *Mytilus edulis*.

6.3.3 Presence and influence of organic material

Organic material is of considerable interest in biomineralising systems, since it modifies the crystal growth, morphology and polymorphism (Kitano & Hood, 1965; Aizenberg *et al.*, 1996; Albeck *et al.*, 1996; Belcher *et al.*, 1996; Meldrum & Hyde, 2001). In other mineralising systems, trace elements are strongly associated with the organic material in producing carbonate (Hincke & St. Maurice, 2000). Organic material must therefore be considered to determine if the chemistry of the system is associated with the organic material rather than the crystal lattice directly (Lingard *et al.*, 1992), which has implications for applying these proxies to fossil examples as palaeoclimate indicators.

Growth of calcite is inhibited by organic molecules coating the surface (Lebron & Suarez, 1996; 1998; de Leeuw & Cooper, 2004; De Yoreo & Dove, 2004; Volkmer *et al.*, 2004) altering the kinetics of the system. Pokroy *et al* (2004; 2006a; 2007) investigated the effect of organic material on the atomic structure of biogenic aragonite, which revealed elongation of the *a*- and *c*-axes with shortening of the *b*-axis associated with the presence of organic molecules. This was followed by investigation into the effect of the organic material on biogenic calcite (Pokroy *et al.*, 2006b; 2006c) and similar elongations on the *a*- and *c*-axes were produced. With these macromolecules closely associated with the crystal lattice (Addadi *et al.*, 1994) and the effect they have on the atomic structure, this may produce greater interstitial sites for monovalent ions such as Na^+ and other ions to be more easily incorporated into the lattice.

If the organic molecules can affect and distort the growth of the crystallites with greater uptake of ions into expanded lattices, trace element chemistry could reflect organic activity (White, 1978). In *M. edulis*, the distortion of size and shape of the outermost calcite crystals, where the calcite nucleates on the organic periostracum, decreases towards the polymorph interface as the orientation

and morphology become more refined. This refinement could represent a decreasing organic effect with a reduction in organic material through the calcite layer that could explain the consistent pattern in the trace element and stable isotope signature.

In the umbo region there is a greater range of crystal sizes and shapes and more variable chemistry. The umbo is an area of higher curvature. The metabolic model by Rosenberg and Hughes (1991) would predict more organic material in the umbo region and therefore the increased organic concentration could again account for variation in trace element and isotopic signatures. Increased amounts of shell matrix in the umbo region was proposed by Dick *et al.* (2007) as the explanation for greater trace element concentrations.

If organic material production is related to metabolic function then evidence of this from trace element concentrations or isotope composition would be expected through ontogeny. Mg concentrations are higher in younger stages of ontogeny and Na concentration is also shown to decrease through ontogeny. However, Sulphur concentration increases through ontogeny. If S is to be considered as an indicator of organic material in carbonate biomineral systems (Crenshaw & Ristedt, 1976; Lorens & Bender, 1980; Cuif *et al.*, 2003; Dauphin *et al.*, 2003a) this suggests that more organic material is produced as the animal ages which is counter-intuitive as this is more metabolically expensive. However, given the lack of S in the organic-rich aragonite layer compared to the calcite layer in *M. edulis* , it seems likely that S may be associated with the crystal lattice (Kontrec *et al.*, 2004; Kralj *et al.*, 2004).

However, if the differences in S concentration between the two polymorphs represents a difference in the nature of the organic material, this has further implications if the trace element chemistry is associated with the organic components. While sulphated material has been found to be common in carbonate biomineralising systems (Dauphin *et al.*, 2003a), the detailed protein make-up is different between species (England, 2005). Any species-specific organic material may therefore have specific trace element signatures associated. Further investigation of the organic material through a more extensive range of ontogeny would be required to fully consider this.

6.3.4 Environmental controls

Trace element and isotopic signatures in calcium carbonate biominerals have previously been considered to reflect the environment in which they were formed (Wefer & Berger, 1991; Lea *et al.*, 1999). The effects of the ambient surroundings have been interpreted using trace element and isotope proxies in *Mytilus* and other bivalve molluscs (Dodd, 1965; Mook & Vogel, 1968; Killingley & Berger, 1979; Dodd & Crisp, 1982; Klein *et al.*, 1996a). Mineralogy and proportions of calcium carbonate polymorphs produced in bimineralic systems have also been studied

(Lowenstam, 1954; Dodd, 1964; Eisma, 1966; Checa *et al.*, 2007). Using the mineralogy of the shell to indicate environmental variation in salinity and temperature, this study found distinct variation in proportions of calcite and aragonite between specimens and ontogenic stages (Section 3.3.1). Hubbard *et al*. (1981) also showed that *Mytilus* mineralogy proportions varied when salinity and temperature were constant with other biological factors as a possible explanation for the differences.

Using the Mg/Ca temperature equation from Vander Putten *et al.* (Vander Putten *et al.*, 2000) with the results obtained from the shell calcite in this survey yielded a significant offset (Section 4.4.1) from a measured temperature range previously been reported in mussel farms in Loch Etive (Stirling & Okumus, 1995). Only the youngest stage of ontogeny A showed a similar range in values compared to actual temperature measurements, but was still offset from the measured mean temperature during the growing months. Freitas *et al*. (2005; 2006) previously stated that the use of Mg/Ca ratios from bivalves in palaeo-proxies is unreliable, which further emphasised what Vander Putten *et al*. (2000) reported for *Mytilus edulis*. Vander Putten *et al*. (2000) also affirmed what Klein *et al*. (1996b) had reported with respect to the Sr/Ca ratio with metabolic effects and changes in the extrapallial fluid thought to be responsible as Sr/Ca did not reflect environmental conditions. In this survey, the difference in Sr content between the two polymorphs and the greater Sr concentration in the prismatic aragonite suggest influences other than the ambient water temperature.

The range of $\delta^{18}O$ values obtained through conventional mass spectrometry and SIMS in this study generally fall within expected $\delta^{18}O$ equilibrium values for both calcite and aragonite. However, lower $\delta^{18}O$ values were observed in calcite of the shell posterior in all stages of ontogeny and $\delta^{18}O$ values decreased with increasing age, with some values falling outside equilibrium range. If this trend continues in older stages of ontogeny not analysed here, then an expected offset from equilibrium could result caused by shell aging which has implications for proxy applications. Further analysis would be required to fully investigate the extent of this possible offset. Also, reasons for regions within the calcite and aragonite layer that are produced out of equilibrium are still unaccounted for. Crystal habit may be responsible, but this remains to be fully resolved. This reinforces the need for thorough ultrastructural investigation of biomineral systems prior to applying proxies. With this minor isotopic offset and the offset shown for the Mg/Ca predicted temperature range, and the variation in shell mineralogy proportions, this study agrees with others (Vander Putten *et al.*, 2000; Freitas *et al.*, 2005; Freitas *et al.*, 2006) that more detailed investigation into the biological factors and kinetics of any biomineral system should be made before applying biomineral systems to environmental proxies.

6.4 *Mytilus edulis* in the context of ontogeny

The three major factors of crystallography, trace element and stable isotope signatures are regarded as fundamentals in determining the growth evolution of the *Mytilus* system as well as its interaction with the surrounding environment. All three have been considered here in the context of ontogeny, with a suite of specimens encompassing a three year span used to identify possible variation through six different age ranges. Suggestions for variation within stages and specimens have also been proposed in the context of ontogeny and the biomineralising method employed in the *Mytilus edulis* system.

Common patterns in crystallography, stable isotopes and trace element chemistry were observed in all stages of ontogeny, with the umbo region showing a degree of disorder compared to other sections of the shell. The trace element and isotope profiles show a recurring pattern through the shell thickness in both polymorphs of calcium carbonate with a refinement in calcite crystallography in conjunction with this. Minor trends were noted through ontogeny with Mg and Na concentrations and $\delta^{18}O$ values decreasing through ontogeny. However, S concentrations increased with age.

Other studies performed in the context of ontogeny have only noted significant changes in much older stages of ontogeny, e.g. *Mytilus* reaching 17 years (Sukhotin *et al.*, 2007). The ontogenic range surveyed here was restricted by the fact that farmed mussel grow quickly over a short period of time. Additionally, spat samples are handled by suppliers other than the mussel farmers. Thus, the lower end of the ontogenetic range was also unavailable for this study. Despite this, the main advantage of using *M. edulis* from such a source was, of course, consistent environmental conditions between ontogenetic stages and ability to estimate the age of each specimen. Thus, although a full ontogenetic suite was not available for this work, all analyses were done with separate ontogenetic stages to allow any ontogenetic trends to be revealed. This also offered the opportunity of detecting any resorption, ionic mobility and thus any changes in the first formed shell over time. Although such changes were not significantly apparent, by keeping the ontogenetic stages separate, this possibility has been investigated.

However, this study has developed further insight into chemistry, mineral and environmental interaction and the application of such systems in environmental proxies. This study agrees with other investigations into the reliability of applying the bivalve system directly to predicting past climate conditions without fully investigating the numerous other factors involved in the production of the mineralised shell. Variations in crystal polymorph, size and shape have coincided with marked changes in the shell chemistry and isotopic signature and should be more fully

considered as well as the kinetics and biology of the system before undertaking an environmental study.

6.5 Further work

The investigation of a greater age range should permit a better understanding of the magnitude of the effect of ontogeny on the system. This was outside the scope of this study since a limited ontogenetic suite was available from farmed mussels.

Investigations into the mineralising extrapallial fluid through ontogeny would provide a better insight to how the metabolism of the animal may change through growth and how this impacts on the shell chemistry. This would entail a detailed study of the chemistry of the fluid at different stages of ontogeny and protein composition. The quantity of specific proteins in the fluid and how these relate to what proportion of protein that is then incorporated into the mineralised tissue in different sections of the shell and in each ontogenic stage.

The use of Mg/Ca and Sr/Ca ratios assume that Mg or Sr is ideally substituted for Ca in the carbonate lattice. X-ray Absorption Near Edge Structure (XANES) and Extended X-Ray Absorption Fine Structure (EXAFS) mapping would be ideal to determine whether Mg and Sr are strictly associated with the mineralised component or is actually a component of the organic matrix.

Studies on the protein structure of extrapallial fluid proteins should be pursued to aid further understanding of biomineralising processes. This should be investigated, possibly with changes that may occur to protein structure through ontogeny and the impact this has on the resultant shell structure and carbonate chemistry produced.

Ontogenetic changes in material properties could be assessed using nano-indentation. Building on this current data set, the relationship between material properties, organic content, crystallographic orientation, structure and shell chemistry could then be determined.

Appendix A

A.1 Electron Microprobe analyses expressed as carbonates

Onto. Stage	Shell Area	Point	Line	$Ca(CO_3)$	$Mg(CO_3)$	$Na_2(CO_3)$	$S(CO_3)_2$	$Sr(CO_3)$	Total
A	Umbo	1	1	97.74	0.91	0.72	0.54	0.10	100.00
A	Umbo	2	1	98.10	0.72	0.46	0.62	0.09	100.00
A	Umbo	3	1	97.43	0.06	2.23	0.14	0.14	100.00
A	Umbo	4	1	97.02	0.03	2.72	0.11	0.13	100.00
A	Umbo	5	1	97.03	0.00	2.64	0.15	0.18	100.00
A	Umbo	6	1	97.36	0.04	2.32	0.13	0.15	100.00
A	Umbo	7	1	97.27	0.02	2.42	0.12	0.17	100.00
A	Umbo	8	1	97.85	0.10	1.51	0.05	0.49	100.00
A	Umbo	9	1	97.87	0.10	1.63	0.14	0.25	100.00
A	Umbo	10	1	97.23	0.11	2.32	0.15	0.20	100.00
A	Umbo	11	1	98.33	0.08	1.31	0.06	0.23	100.00
A	Umbo	12	1	97.50	0.05	2.03	0.17	0.25	100.00
A	Umbo	1	2	97.60	0.82	1.04	0.46	0.08	100.00
A	Umbo	2	2	97.65	0.83	0.99	0.43	0.10	100.00
A	Umbo	3	2	98.02	0.02	1.70	0.06	0.19	100.00
A	Umbo	4	2	98.13	0.00	1.74	0.04	0.10	100.00
A	Umbo	5	2	97.17	0.05	2.55	0.10	0.13	100.00
A	Umbo	6	2	97.43	0.00	2.23	0.17	0.18	100.00
A	Umbo	7	2	97.47	0.06	2.18	0.11	0.18	100.00
A	Umbo	8	2	97.21	0.06	2.45	0.13	0.15	100.00
A	Umbo	9	2	97.02	0.08	2.53	0.16	0.21	100.00
A	Umbo	10	2	96.90	0.08	2.71	0.15	0.15	100.00
A	Umbo	11	2	96.85	0.17	2.45	0.19	0.35	100.00
A	Umbo	12	2	97.71	0.11	1.79	0.12	0.27	100.00
A	Umbo	13	2	97.28	0.16	2.18	0.15	0.24	100.00
A	Umbo	1	3	98.28	0.82	0.37	0.44	0.09	100.00
A	Umbo	2	3	98.41	0.60	0.33	0.54	0.13	100.00
A	Umbo	3	3	98.41	0.70	0.43	0.35	0.11	100.00
A	Umbo	4	3	98.48	0.65	0.44	0.36	0.08	100.00
A	Umbo	5	3	98.41	0.65	0.42	0.38	0.14	100.00
A	Umbo	6	3	98.26	0.80	0.19	0.60	0.15	100.00
A	Umbo	7	3	98.07	0.71	0.55	0.59	0.08	100.00
A	Mid	1	4	98.20	0.51	0.90	0.29	0.10	100.00
A	Mid	2	4	98.04	0.38	1.20	0.25	0.13	100.00
A	Mid	3	4	98.49	0.30	0.85	0.26	0.10	100.00
A	Mid	4	4	98.77	0.32	0.57	0.26	0.08	100.00
A	Mid	5	4	97.53	0.02	2.16	0.12	0.17	100.00
A	Mid	1	5	97.22	0.36	2.13	0.16	0.12	100.00
A	Mid	2	5	97.74	0.47	1.49	0.18	0.12	100.00

A	Mid	3	5	98.21	0.32	1.24	0.16	0.07	100.00
A	Mid	4	5	98.41	0.39	0.86	0.22	0.12	100.00
A	Mid	5	5	97.51	0.06	2.25	0.08	0.10	100.00
A	Mid	6	5	97.66	0.01	2.08	0.08	0.17	100.00
A	Mid	7	5	97.48	0.03	2.27	0.11	0.11	100.00
A	Mid	8	5	97.82	0.12	1.52	0.15	0.39	100.00
A	Mid	1	6	98.57	0.48	0.53	0.30	0.13	100.00
A	Mid	2	6	98.43	0.53	0.74	0.19	0.12	100.00
A	Mid	3	6	98.25	0.67	0.79	0.22	0.07	100.00
A	Mid	4	6	98.19	0.02	1.53	0.07	0.19	100.00
A	Mid	5	6	97.81	0.07	1.84	0.10	0.18	100.00
A	Edge	1	7	98.12	0.27	1.31	0.17	0.14	100.00
A	Edge	2	7	98.38	0.44	0.82	0.21	0.15	100.00
A	Edge	3	7	98.37	0.75	0.37	0.38	0.12	100.00
A	Edge	4	7	98.22	0.81	0.36	0.52	0.09	100.00
A	Edge	1	8	98.36	0.31	1.07	0.15	0.11	100.00
A	Edge	2	8	98.36	0.34	1.11	0.11	0.09	100.00
A	Edge	3	8	98.33	0.32	1.10	0.13	0.13	100.00
A	Edge	4	8	98.31	0.47	0.97	0.18	0.07	100.00
A	Edge	5	8	98.07	0.70	0.87	0.26	0.10	100.00
A	Edge	6	8	97.71	1.42	0.40	0.36	0.11	100.00
A	Edge	7	8	97.53	1.45	0.33	0.57	0.12	100.00
A	Edge	1	9	98.53	0.37	0.64	0.34	0.13	100.00
A	Edge	2	9	98.62	0.38	0.58	0.30	0.12	100.00
A	Edge	3	9	98.68	0.43	0.55	0.24	0.10	100.00
A	Edge	4	9	98.80	0.50	0.39	0.22	0.09	100.00
A	Edge	5	9	98.28	0.80	0.24	0.48	0.19	100.00
B	Umbo	1	1	98.13	0.76	0.75	0.30	0.06	100.00
B	Umbo	2	1	98.42	0.66	0.60	0.22	0.09	100.00
B	Umbo	3	1	97.19	1.14	1.15	0.41	0.11	100.00
B	Umbo	4	1	98.25	0.41	1.04	0.22	0.08	100.00
B	Umbo	5	1	98.94	0.31	0.52	0.13	0.09	100.00
B	Umbo	6	1	98.48	0.43	0.80	0.20	0.09	100.00
B	Umbo	7	1	98.44	0.52	0.72	0.25	0.08	100.00
B	Umbo	8	1	98.00	0.93	0.68	0.29	0.11	100.00
B	Umbo	9	1	98.65	0.50	0.56	0.25	0.05	100.00
B	Umbo	10	1	98.69	0.55	0.49	0.15	0.11	100.00
B	Umbo	11	1	98.46	0.65	0.65	0.16	0.09	100.00
B	Umbo	12	1	98.60	0.59	0.56	0.18	0.07	100.00
B	Umbo	13	1	98.77	0.52	0.48	0.17	0.06	100.00
B	Umbo	14	1	98.80	0.47	0.51	0.15	0.07	100.00
B	Umbo	15	1	98.20	0.70	0.46	0.52	0.11	100.00
B	Umbo	16	1	98.48	0.48	0.47	0.46	0.10	100.00
B	Umbo	17	1	98.68	0.44	0.43	0.34	0.11	100.00
B	Umbo	18	1	98.72	0.50	0.37	0.30	0.11	100.00
B	Umbo	19	1	98.53	0.70	0.35	0.32	0.10	100.00
B	Umbo	20	1	98.27	0.60	0.76	0.26	0.11	100.00
B	Umbo	21	1	98.46	0.61	0.64	0.22	0.07	100.00
B	Umbo	22	1	97.32	0.34	1.88	0.21	0.25	100.00
B	Umbo	1	2	98.51	0.45	0.77	0.14	0.14	100.00
B	Umbo	2	2	98.60	0.37	0.75	0.15	0.14	100.00
B	Umbo	3	2	98.59	0.52	0.65	0.12	0.13	100.00
B	Umbo	4	2	98.70	0.46	0.57	0.19	0.09	100.00
B	Umbo	5	2	98.59	0.52	0.50	0.28	0.12	100.00
B	Umbo	6	2	98.72	0.63	0.27	0.27	0.11	100.00
B	Umbo	7	2	98.42	0.64	0.55	0.28	0.10	100.00
B	Umbo	8	2	98.77	0.54	0.30	0.29	0.10	100.00
B	Umbo	9	2	98.66	0.58	0.37	0.29	0.11	100.00

B	Umbo	10	2	98.80	0.52	0.36	0.21	0.11	100.00
B	Umbo	11	2	98.29	0.58	0.40	0.63	0.10	100.00
B	Umbo	12	2	98.77	0.53	0.22	0.35	0.13	100.00
B	Umbo	13	2	98.34	0.78	0.40	0.35	0.13	100.00
B	Umbo	14	2	98.66	0.61	0.39	0.21	0.13	100.00
B	Umbo	15	2	98.72	0.44	0.50	0.22	0.12	100.00
B	Umbo	16	2	97.87	0.00	1.86	0.10	0.17	100.00
B	Umbo	17	2	98.38	0.01	1.30	0.12	0.19	100.00
B	Umbo	18	2	98.68	0.01	1.08	0.07	0.17	100.00
B	Umbo	19	2	98.01	0.01	1.75	0.08	0.14	100.00
B	Umbo	20	2	97.99	0.02	1.74	0.10	0.16	100.00
B	Umbo	21	2	97.91	0.12	1.76	0.07	0.14	100.00
B	Umbo	22	2	98.17	0.00	1.50	0.03	0.30	100.00
B	Umbo	23	2	67.68	1.88	3.08	27.35	0.02	100.00
B	Umbo	1	3	98.04	0.97	0.76	0.15	0.09	100.00
B	Umbo	2	3	98.04	0.70	0.90	0.20	0.17	100.00
B	Umbo	3	3	98.08	0.76	0.87	0.15	0.14	100.00
B	Umbo	4	3	98.08	0.80	0.82	0.15	0.15	100.00
B	Umbo	5	3	98.30	0.94	0.43	0.21	0.11	100.00
B	Umbo	6	3	98.61	0.65	0.45	0.18	0.11	100.00
B	Umbo	7	3	98.48	0.63	0.63	0.17	0.09	100.00
B	Umbo	8	3	98.76	0.52	0.46	0.19	0.08	100.00
B	Umbo	9	3	98.62	0.66	0.36	0.23	0.13	100.00
B	Umbo	10	3	98.12	1.00	0.40	0.38	0.10	100.00
B	Umbo	11	3	98.27	0.87	0.22	0.49	0.16	100.00
B	Umbo	12	3	97.62	1.46	0.26	0.56	0.11	100.00
B	Umbo	13	3	97.42	1.14	0.66	0.65	0.13	100.00
B	Mid	1	4	97.21	0.34	2.18	0.15	0.13	100.00
B	Mid	2	4	97.39	0.31	2.04	0.17	0.10	100.00
B	Mid	3	4	97.52	0.35	1.84	0.18	0.11	100.00
B	Mid	4	4	97.79	0.33	1.59	0.19	0.11	100.00
B	Mid	5	4	98.06	0.36	1.33	0.18	0.08	100.00
B	Mid	6	4	97.89	0.51	1.24	0.27	0.10	100.00
B	Mid	7	4	98.09	0.56	1.11	0.16	0.08	100.00
B	Mid	8	4	97.94	0.53	1.22	0.19	0.11	100.00
B	Mid	9	4	98.20	0.50	1.07	0.16	0.08	100.00
B	Mid	10	4	98.04	0.58	1.09	0.18	0.11	100.00
B	Mid	11	4	98.16	0.65	0.97	0.16	0.07	100.00
B	Mid	12	4	98.60	0.47	0.69	0.15	0.09	100.00
B	Mid	13	4	97.46	0.00	2.33	0.06	0.14	100.00
B	Mid	14	4	97.83	0.04	1.98	0.03	0.12	100.00
B	Mid	15	4	98.02	0.00	1.78	0.06	0.15	100.00
B	Mid	16	4	98.00	0.03	1.80	0.05	0.12	100.00
B	Mid	17	4	97.66	0.00	2.15	0.06	0.12	100.00
B	Mid	18	4	97.96	0.00	1.89	0.03	0.11	100.00
B	Mid	19	4	97.89	0.02	1.93	0.04	0.12	100.00
B	Mid	20	4	97.80	0.04	2.03	0.05	0.08	100.00
B	Mid	21	4	97.67	0.01	2.15	0.04	0.13	100.00
B	Mid	22	4	98.22	0.10	1.57	0.05	0.07	100.00
B	Mid	23	4	97.99	0.00	1.85	0.04	0.13	100.00
B	Mid	24	4	97.72	0.05	2.09	0.04	0.12	100.00
B	Mid	25	4	97.59	0.05	2.18	0.08	0.11	100.00
B	Mid	26	4	97.86	0.03	1.88	0.08	0.16	100.00
B	Mid	27	4	98.31	0.05	1.24	0.10	0.30	100.00
B	Mid	28	4	97.92	0.06	1.70	0.11	0.20	100.00
B	Mid	1	5	97.67	0.37	1.64	0.21	0.12	100.00
B	Mid	2	5	98.47	0.32	0.87	0.22	0.12	100.00
B	Mid	3	5	98.64	0.34	0.65	0.26	0.12	100.00

B	Mid	4	5	98.78	0.35	0.65	0.17	0.06	100.00
B	Mid	5	5	98.63	0.40	0.65	0.19	0.13	100.00
B	Mid	6	5	98.43	0.45	0.82	0.17	0.13	100.00
B	Mid	7	5	98.41	0.52	0.74	0.17	0.16	100.00
B	Mid	8	5	98.50	0.53	0.63	0.22	0.13	100.00
B	Mid	9	5	98.36	0.51	0.74	0.16	0.22	100.00
B	Mid	10	5	98.75	0.31	0.58	0.20	0.16	100.00
B	Mid	11	5	97.75	0.02	2.03	0.05	0.16	100.00
B	Mid	12	5	98.36	0.01	1.40	0.07	0.16	100.00
B	Mid	13	5	98.46	0.00	1.35	0.04	0.14	100.00
B	Mid	14	5	97.81	0.01	1.95	0.07	0.16	100.00
B	Mid	15	5	98.51	0.02	1.27	0.07	0.14	100.00
B	Mid	16	5	98.27	0.06	1.41	0.07	0.19	100.00
B	Mid	17	5	98.31	0.04	1.43	0.06	0.17	100.00
B	Mid	18	5	98.40	0.02	1.34	0.09	0.16	100.00
B	Mid	19	5	97.93	0.01	1.81	0.09	0.17	100.00
B	Mid	20	5	97.53	0.03	2.10	0.11	0.23	100.00
B	Mid	1	6	97.06	1.78	0.46	0.56	0.14	100.00
B	Mid	2	6	97.51	1.77	0.19	0.37	0.16	100.00
B	Mid	3	6	97.73	1.37	0.27	0.44	0.19	100.00
B	Mid	4	6	98.42	0.60	0.20	0.63	0.15	100.00
B	Mid	5	6	98.50	0.53	0.25	0.59	0.13	100.00
B	Mid	6	6	99.05	0.34	0.26	0.22	0.13	100.00
B	Mid	7	6	98.66	0.44	0.48	0.32	0.10	100.00
B	Mid	8	6	98.92	0.43	0.34	0.21	0.10	100.00
B	Mid	9	6	99.02	0.37	0.33	0.21	0.07	100.00
B	Edge	1	7	96.54	0.60	2.52	0.20	0.15	100.00
B	Edge	2	7	97.27	0.30	2.18	0.14	0.11	100.00
B	Edge	3	7	98.00	0.25	1.41	0.18	0.16	100.00
B	Edge	4	7	97.85	0.28	1.58	0.15	0.15	100.00
B	Edge	5	7	98.11	0.36	1.23	0.13	0.17	100.00
B	Edge	6	7	97.65	0.41	1.74	0.11	0.09	100.00
B	Edge	7	7	97.95	0.42	1.38	0.14	0.11	100.00
B	Edge	8	7	97.93	0.35	1.56	0.10	0.06	100.00
B	Edge	9	7	97.95	0.32	1.56	0.09	0.09	100.00
B	Edge	10	7	98.06	0.38	1.38	0.09	0.10	100.00
B	Edge	11	7	97.93	0.42	1.42	0.09	0.14	100.00
B	Edge	12	7	98.07	0.47	1.27	0.08	0.12	100.00
B	Edge	13	7	98.34	0.45	1.08	0.06	0.07	100.00
B	Edge	14	7	98.28	0.40	1.17	0.07	0.08	100.00
B	Edge	15	7	98.67	0.40	0.77	0.09	0.09	100.00
B	Edge	16	7	97.67	0.01	2.10	0.08	0.13	100.00
B	Edge	17	7	97.51	0.00	2.30	0.05	0.14	100.00
B	Edge	18	7	97.55	0.04	2.32	0.03	0.07	100.00
B	Edge	19	7	97.68	0.04	2.10	0.04	0.14	100.00
B	Edge	20	7	97.28	0.03	2.46	0.07	0.15	100.00
B	Edge	21	7	97.98	0.07	1.77	0.06	0.13	100.00
B	Edge	22	7	97.83	0.13	1.62	0.11	0.31	100.00
B	Edge	1	8	96.86	1.01	1.55	0.39	0.20	100.00
B	Edge	2	8	97.85	0.27	1.55	0.16	0.17	100.00
B	Edge	3	8	98.13	0.31	1.16	0.19	0.22	100.00
B	Edge	4	8	97.98	0.44	1.34	0.11	0.13	100.00
B	Edge	5	8	98.30	0.41	1.06	0.08	0.15	100.00
B	Edge	6	8	98.35	0.43	0.97	0.10	0.15	100.00
B	Edge	7	8	98.25	0.50	1.08	0.07	0.09	100.00
B	Edge	8	8	98.21	0.49	1.08	0.07	0.15	100.00
B	Edge	9	8	98.44	0.44	0.88	0.07	0.16	100.00
B	Edge	10	8	98.92	0.40	0.48	0.10	0.10	100.00

B	Edge	11	8	98.14	0.00	1.66	0.07	0.13	100.00
B	Edge	12	8	98.24	0.01	1.57	0.06	0.13	100.00
B	Edge	13	8	98.11	0.11	1.55	0.06	0.17	100.00
B	Edge	14	8	98.19	0.06	1.50	0.09	0.17	100.00
B	Edge	15	8	97.97	0.09	1.64	0.08	0.22	100.00
B	Edge	16	8	97.87	0.10	1.55	0.14	0.35	100.00
B	Edge	1	9	98.11	0.42	1.20	0.13	0.14	100.00
B	Edge	2	9	98.23	0.31	1.13	0.22	0.12	100.00
B	Edge	3	9	98.32	0.32	1.07	0.15	0.13	100.00
B	Edge	4	9	98.33	0.41	0.99	0.14	0.14	100.00
B	Edge	5	9	98.57	0.59	0.55	0.14	0.15	100.00
B	Edge	6	9	98.42	0.66	0.65	0.14	0.13	100.00
B	Edge	7	9	98.51	0.45	0.85	0.06	0.14	100.00
B	Edge	8	9	98.66	0.42	0.69	0.11	0.12	100.00
B	Edge	9	9	98.55	0.46	0.62	0.23	0.15	100.00
C	Umbo	1	1	98.44	0.24	0.68	0.53	0.11	100.00
C	Umbo	2	1	98.82	0.22	0.43	0.39	0.15	100.00
C	Umbo	3	1	98.90	0.20	0.46	0.34	0.10	100.00
C	Umbo	4	1	98.55	0.36	0.52	0.46	0.12	100.00
C	Umbo	5	1	98.91	0.28	0.46	0.26	0.10	100.00
C	Umbo	6	1	98.86	0.32	0.42	0.31	0.09	100.00
C	Umbo	7	1	98.79	0.38	0.49	0.27	0.07	100.00
C	Umbo	8	1	98.90	0.38	0.41	0.24	0.08	100.00
C	Umbo	9	1	98.90	0.38	0.42	0.22	0.09	100.00
C	Umbo	10	1	98.71	0.50	0.42	0.26	0.11	100.00
C	Umbo	11	1	98.37	0.68	0.42	0.44	0.09	100.00
C	Umbo	12	1	97.88	0.79	0.45	0.82	0.06	100.00
C	Umbo	13	1	98.24	0.41	0.44	0.80	0.11	100.00
C	Umbo	14	1	98.77	0.33	0.32	0.49	0.10	100.00
C	Umbo	15	1	98.61	0.25	0.47	0.54	0.14	100.00
C	Umbo	16	1	98.52	0.24	0.83	0.32	0.09	100.00
C	Umbo	17	1	99.00	0.24	0.42	0.24	0.11	100.00
C	Umbo	18	1	98.85	0.23	0.49	0.32	0.11	100.00
C	Umbo	19	1	98.94	0.23	0.39	0.34	0.10	100.00
C	Umbo	20	1	98.54	0.43	0.54	0.38	0.11	100.00
C	Umbo	21	1	98.58	0.60	0.26	0.50	0.06	100.00
C	Umbo	22	1	98.32	0.65	0.40	0.55	0.09	100.00
C	Umbo	23	1	97.42	0.97	0.71	0.78	0.12	100.00
C	Umbo	24	1	97.55	0.03	1.66	0.18	0.58	100.00
C	Umbo	1	2	98.09	0.38	1.31	0.11	0.11	100.00
C	Umbo	2	2	98.14	0.56	1.09	0.09	0.12	100.00
C	Umbo	3	2	97.95	0.54	1.32	0.09	0.11	100.00
C	Umbo	4	2	98.42	0.56	0.87	0.09	0.07	100.00
C	Umbo	5	2	98.59	0.56	0.67	0.12	0.07	100.00
C	Umbo	6	2	98.65	0.50	0.62	0.16	0.07	100.00
C	Umbo	7	2	98.52	0.61	0.62	0.15	0.09	100.00
C	Umbo	8	2	97.34	0.06	2.43	0.09	0.09	100.00
C	Umbo	9	2	97.66	0.04	2.16	0.04	0.10	100.00
C	Umbo	10	2	97.44	0.00	2.39	0.07	0.10	100.00
C	Umbo	11	2	97.25	0.04	2.54	0.07	0.09	100.00
C	Umbo	12	2	97.46	0.02	2.35	0.08	0.09	100.00
C	Umbo	13	2	98.03	0.06	1.73	0.08	0.11	100.00
C	Umbo	14	2	98.01	0.03	1.80	0.06	0.10	100.00
C	Umbo	15	2	97.81	0.06	1.92	0.10	0.10	100.00
C	Umbo	16	2	96.96	0.06	2.79	0.08	0.11	100.00
C	Umbo	17	2	97.88	0.12	1.63	0.13	0.23	100.00
C	Umbo	18	2	97.54	0.00	2.11	0.11	0.25	100.00
C	Umbo	19	2	97.73	0.02	2.00	0.06	0.18	100.00

C	Umbo	20	2	97.44	0.00	2.35	0.06	0.16	100.00
C	Umbo	21	2	97.54	0.02	2.26	0.07	0.12	100.00
C	Umbo	22	2	97.83	0.06	1.89	0.09	0.13	100.00
C	Umbo	23	2	97.08	0.13	2.57	0.07	0.15	100.00
C	Umbo	24	2	97.31	0.12	2.02	0.11	0.45	100.00
C	Umbo	1	3	97.58	0.02	2.06	0.18	0.15	100.00
C	Umbo	2	3	97.77	0.00	1.85	0.21	0.17	100.00
C	Umbo	3	3	97.49	0.04	2.05	0.26	0.17	100.00
C	Umbo	4	3	97.81	0.01	1.82	0.20	0.16	100.00
C	Umbo	5	3	96.73	1.75	1.19	0.16	0.17	100.00
C	Umbo	6	3	97.81	0.08	1.84	0.15	0.13	100.00
C	Umbo	7	3	97.93	0.04	1.68	0.17	0.19	100.00
C	Umbo	8	3	97.90	0.00	1.76	0.15	0.19	100.00
C	Umbo	9	3	97.11	0.00	2.42	0.22	0.26	100.00
C	Umbo	10	3	97.27	0.03	2.18	0.15	0.36	100.00
C	Umbo	11	3	98.18	0.54	0.60	0.56	0.13	100.00
C	Umbo	12	3	98.29	0.35	0.74	0.51	0.11	100.00
C	Umbo	13	3	98.49	0.32	0.60	0.46	0.12	100.00
C	Umbo	14	3	98.14	0.38	0.89	0.47	0.12	100.00
C	Umbo	15	3	98.28	0.40	0.75	0.47	0.11	100.00
C	Umbo	16	3	98.50	0.42	0.52	0.43	0.13	100.00
C	Umbo	17	3	98.45	0.49	0.53	0.45	0.09	100.00
C	Umbo	18	3	98.06	0.66	0.60	0.56	0.13	100.00
C	Umbo	19	3	97.90	0.88	0.50	0.60	0.11	100.00
C	Umbo	20	3	97.70	0.91	0.48	0.81	0.10	100.00
C	Umbo	21	3	97.59	0.90	0.62	0.80	0.09	100.00
C	Umbo	22	3	97.51	0.02	1.86	0.19	0.42	100.00
C	Umbo	23	3	96.68	1.87	0.51	0.70	0.25	100.00
C	Umbo	24	3	98.08	0.62	0.39	0.81	0.11	100.00
C	Umbo	1	4	98.31	0.60	0.22	0.77	0.10	100.00
C	Umbo	2	4	98.20	0.69	0.33	0.68	0.11	100.00
C	Umbo	3	4	97.57	0.01	2.19	0.10	0.13	100.00
C	Umbo	4	4	97.65	0.02	2.04	0.13	0.16	100.00
C	Umbo	5	4	97.53	0.00	2.19	0.11	0.17	100.00
C	Umbo	6	4	98.10	0.00	1.61	0.14	0.15	100.00
C	Umbo	7	4	97.96	0.02	1.83	0.10	0.10	100.00
C	Umbo	8	4	97.58	0.11	1.91	0.15	0.25	100.00
C	Umbo	9	4	97.66	0.00	2.12	0.11	0.12	100.00
C	Umbo	10	4	98.01	0.04	1.67	0.14	0.15	100.00
C	Umbo	11	4	97.85	0.03	1.89	0.14	0.09	100.00
C	Umbo	12	4	97.82	0.00	1.88	0.13	0.16	100.00
C	Umbo	13	4	97.68	0.05	1.96	0.16	0.15	100.00
C	Umbo	14	4	97.69	0.00	1.93	0.22	0.16	100.00
C	Umbo	15	4	98.39	0.03	1.21	0.20	0.18	100.00
C	Umbo	16	4	97.57	0.00	2.10	0.19	0.14	100.00
C	Umbo	17	4	97.73	0.03	1.94	0.18	0.12	100.00
C	Umbo	18	4	97.79	0.02	1.85	0.15	0.19	100.00
C	Umbo	19	4	97.51	0.06	2.09	0.16	0.19	100.00
C	Umbo	20	4	97.57	0.03	2.03	0.17	0.20	100.00
C	Umbo	21	4	97.07	0.09	2.48	0.16	0.19	100.00
C	Umbo	22	4	96.91	0.07	2.64	0.17	0.22	100.00
C	Umbo	23	4	97.38	0.08	2.22	0.16	0.16	100.00
C	Umbo	24	4	97.55	0.09	2.02	0.15	0.20	100.00
C	Umbo	1	5	98.02	0.43	1.38	0.08	0.11	100.00
C	Umbo	2	5	97.91	0.48	1.40	0.10	0.11	100.00
C	Umbo	3	5	98.01	0.45	1.35	0.09	0.11	100.00
C	Umbo	4	5	98.03	0.38	1.37	0.12	0.10	100.00
C	Umbo	5	5	97.90	0.38	1.48	0.12	0.12	100.00

C	Umbo	6	5	98.31	0.37	1.12	0.10	0.10	100.00
C	Umbo	7	5	97.95	0.48	1.34	0.14	0.09	100.00
C	Umbo	8	5	98.25	0.41	1.16	0.09	0.09	100.00
C	Umbo	9	5	97.83	0.54	1.39	0.11	0.12	100.00
C	Umbo	10	5	98.15	0.47	1.16	0.12	0.10	100.00
C	Umbo	11	5	98.21	0.49	1.16	0.10	0.05	100.00
C	Umbo	12	5	98.11	0.49	1.24	0.07	0.09	100.00
C	Umbo	13	5	98.13	0.52	1.17	0.12	0.06	100.00
C	Umbo	14	5	98.21	0.50	1.12	0.07	0.10	100.00
C	Umbo	15	5	98.34	0.49	0.96	0.14	0.07	100.00
C	Umbo	16	5	98.33	0.50	0.97	0.13	0.07	100.00
C	Umbo	17	5	98.23	0.53	1.04	0.12	0.09	100.00
C	Umbo	18	5	98.45	0.47	0.88	0.12	0.08	100.00
C	Umbo	19	5	98.32	0.53	0.98	0.11	0.06	100.00
C	Umbo	20	5	98.22	0.48	1.13	0.13	0.05	100.00
C	Umbo	21	5	98.37	0.41	1.01	0.14	0.07	100.00
C	Umbo	22	5	98.38	0.54	0.94	0.08	0.07	100.00
C	Umbo	23	5	98.16	0.55	1.06	0.14	0.10	100.00
C	Umbo	24	5	98.11	0.62	0.95	0.24	0.09	100.00
C	Umbo	25	5	98.15	0.72	0.85	0.18	0.10	100.00
C	Umbo	26	5	97.99	0.85	0.85	0.21	0.10	100.00
C	Umbo	27	5	98.23	0.77	0.79	0.19	0.02	100.00
C	Umbo	28	5	98.30	0.73	0.70	0.20	0.07	100.00
C	Umbo	29	5	97.45	0.05	2.23	0.09	0.18	100.00
C	Umbo	30	5	97.91	0.03	1.87	0.08	0.12	100.00
C	Umbo	31	5	97.63	0.08	2.07	0.11	0.11	100.00
C	Umbo	32	5	97.24	0.06	2.43	0.12	0.16	100.00
C	Umbo	33	5	97.23	0.08	2.40	0.12	0.17	100.00
C	Umbo	34	5	97.54	0.05	2.16	0.10	0.15	100.00
C	Umbo	35	5	97.92	0.06	1.79	0.05	0.18	100.00
C	Umbo	36	5	97.95	0.05	1.80	0.03	0.17	100.00
C	Umbo	37	5	99.85	0.00	0.03	0.03	0.09	100.00
C	Mid	1	1	97.40	0.40	1.97	0.11	0.13	100.00
C	Mid	2	1	97.84	0.32	1.58	0.13	0.13	100.00
C	Mid	3	1	98.45	0.25	1.10	0.10	0.10	100.00
C	Mid	4	1	98.26	0.39	1.19	0.07	0.10	100.00
C	Mid	5	1	97.91	0.61	1.27	0.08	0.12	100.00
C	Mid	6	1	98.12	0.67	1.06	0.08	0.08	100.00
C	Mid	7	1	98.28	0.86	0.70	0.08	0.08	100.00
C	Mid	8	1	98.45	0.73	0.60	0.14	0.09	100.00
C	Mid	9	1	97.46	0.03	2.30	0.06	0.15	100.00
C	Mid	10	1	97.67	0.09	2.07	0.07	0.11	100.00
C	Mid	11	1	97.37	0.04	2.45	0.02	0.12	100.00
C	Mid	12	1	97.18	0.06	2.60	0.04	0.12	100.00
C	Mid	13	1	97.71	0.06	2.12	0.03	0.08	100.00
C	Mid	14	1	97.51	0.06	2.25	0.05	0.12	100.00
C	Mid	15	1	97.45	0.10	2.26	0.06	0.13	100.00
C	Mid	16	1	97.86	0.08	1.89	0.05	0.12	100.00
C	Mid	17	1	97.54	0.12	2.13	0.08	0.13	100.00
C	Mid	18	1	97.26	0.10	2.47	0.06	0.11	100.00
C	Mid	19	1	98.08	0.03	1.02	0.12	0.76	100.00
C	Mid	1	2	73.23	9.90	4.89	11.88	0.11	100.00
C	Mid	2	2	98.18	0.26	1.21	0.24	0.12	100.00
C	Mid	3	2	98.49	0.19	1.00	0.20	0.13	100.00
C	Mid	4	2	98.55	0.28	0.85	0.22	0.10	100.00
C	Mid	5	2	98.21	0.70	0.67	0.30	0.12	100.00
C	Mid	6	2	98.48	0.64	0.45	0.33	0.10	100.00
C	Mid	7	2	97.15	0.04	2.55	0.12	0.14	100.00

C	Mid	8	2	97.13	0.00	2.67	0.07	0.13	100.00
C	Mid	9	2	97.69	0.02	2.08	0.07	0.14	100.00
C	Mid	10	2	97.58	0.04	2.23	0.06	0.10	100.00
C	Mid	11	2	97.53	0.02	2.30	0.05	0.11	100.00
C	Mid	12	2	97.81	0.01	1.99	0.07	0.12	100.00
C	Mid	13	2	97.05	0.08	2.65	0.08	0.15	100.00
C	Mid	14	2	97.52	0.06	2.21	0.06	0.14	100.00
C	Mid	15	2	96.98	0.10	2.70	0.08	0.14	100.00
C	Mid	16	2	96.69	0.16	2.97	0.06	0.12	100.00
C	Mid	17	2	96.83	0.22	2.73	0.11	0.11	100.00
C	Mid	18	2	97.48	0.14	2.16	0.11	0.13	100.00
C	Mid	19	2	97.92	0.14	1.49	0.09	0.37	100.00
C	Mid	1	3	97.09	0.35	2.32	0.10	0.14	100.00
C	Mid	2	3	97.39	0.30	2.15	0.10	0.07	100.00
C	Mid	3	3	97.57	0.42	1.83	0.08	0.10	100.00
C	Mid	4	3	97.53	0.47	1.78	0.11	0.11	100.00
C	Mid	5	3	97.98	0.46	1.35	0.12	0.09	100.00
C	Mid	6	3	97.97	0.57	1.24	0.10	0.12	100.00
C	Mid	7	3	98.31	0.48	1.03	0.08	0.09	100.00
C	Mid	8	3	98.60	0.27	0.89	0.18	0.06	100.00
C	Mid	9	3	97.18	0.05	2.58	0.07	0.12	100.00
C	Mid	10	3	97.82	0.07	1.91	0.09	0.11	100.00
C	Mid	11	3	97.52	0.04	2.25	0.09	0.11	100.00
C	Mid	12	3	97.68	0.06	2.11	0.08	0.07	100.00
C	Mid	13	3	97.47	0.00	2.33	0.11	0.09	100.00
C	Mid	14	3	97.75	0.00	2.05	0.12	0.08	100.00
C	Mid	15	3	97.62	0.05	2.09	0.11	0.13	100.00
C	Mid	16	3	97.37	0.04	2.36	0.12	0.11	100.00
C	Mid	17	3	97.58	0.09	2.07	0.13	0.14	100.00
C	Mid	18	3	98.18	0.07	1.24	0.13	0.38	100.00
C	Edge	1	9	97.00	0.46	1.77	0.62	0.16	100.00
C	Edge	2	9	97.63	0.30	1.90	0.06	0.12	100.00
C	Edge	3	9	97.72	0.40	1.67	0.05	0.16	100.00
C	Edge	4	9	98.64	0.27	0.91	0.08	0.11	100.00
C	Edge	5	9	98.82	0.19	0.69	0.17	0.14	100.00
C	Edge	6	9	98.84	0.20	0.69	0.14	0.13	100.00
C	Edge	7	9	98.93	0.16	0.78	0.07	0.06	100.00
C	Edge	8	9	98.86	0.23	0.74	0.05	0.12	100.00
C	Edge	9	9	98.75	0.36	0.59	0.22	0.09	100.00
C	Edge	10	9	98.96	0.32	0.60	0.02	0.10	100.00
C	Edge	11	9	98.74	0.45	0.67	0.06	0.09	100.00
C	Edge	12	9	98.79	0.51	0.57	0.07	0.06	100.00
C	Edge	13	9	98.88	0.45	0.46	0.12	0.08	100.00
C	Edge	14	9	98.50	0.69	0.44	0.25	0.12	100.00
C	Edge	15	9	98.62	0.75	0.45	0.09	0.09	100.00
C	Edge	16	9	97.52	1.84	0.32	0.21	0.11	100.00
C	Edge	17	9	97.72	1.67	0.29	0.21	0.11	100.00
C	Edge	1	10	98.56	0.41	0.69	0.26	0.08	100.00
C	Edge	2	10	98.11	0.32	1.15	0.26	0.17	100.00
C	Edge	3	10	98.99	0.10	0.66	0.14	0.11	100.00
C	Edge	4	10	99.05	0.22	0.47	0.13	0.13	100.00
C	Edge	5	10	99.13	0.28	0.34	0.15	0.10	100.00
C	Edge	6	10	99.16	0.31	0.35	0.13	0.06	100.00
C	Edge	7	10	99.00	0.38	0.39	0.13	0.11	100.00
C	Edge	8	10	98.54	0.69	0.37	0.29	0.11	100.00
C	Edge	9	10	98.71	0.68	0.31	0.18	0.12	100.00
C	Edge	10	10	98.87	0.59	0.37	0.09	0.08	100.00
C	Edge	11	10	98.14	1.02	0.30	0.38	0.16	100.00

C	Edge	12	10	98.15	1.22	0.32	0.22	0.09	100.00
C	Edge	13	10	98.95	0.60	0.17	0.19	0.08	100.00
C	Edge	1	11	98.12	0.32	1.15	0.27	0.14	100.00
C	Edge	2	11	98.66	0.32	0.75	0.19	0.09	100.00
C	Edge	3	11	98.70	0.27	0.73	0.21	0.09	100.00
C	Edge	4	11	98.63	0.32	0.72	0.23	0.11	100.00
C	Edge	5	11	98.73	0.38	0.62	0.18	0.10	100.00
C	Edge	6	11	98.86	0.25	0.62	0.21	0.06	100.00
C	Edge	7	11	98.70	0.35	0.63	0.24	0.08	100.00
C	Edge	8	11	98.81	0.39	0.47	0.23	0.10	100.00
C	Edge	9	11	98.82	0.47	0.51	0.14	0.07	100.00
C	Edge	10	11	98.76	0.48	0.54	0.10	0.12	100.00
C	Edge	11	11	98.87	0.45	0.50	0.11	0.07	100.00
C	Edge	12	11	98.74	0.54	0.52	0.13	0.08	100.00
C	Edge	13	11	98.43	0.75	0.50	0.19	0.13	100.00
D	Umbo	1	1	97.11	0.00	2.68	0.07	0.13	100.00
D	Umbo	2	1	97.04	0.00	2.64	0.14	0.18	100.00
D	Umbo	3	1	97.49	0.03	2.30	0.09	0.10	100.00
D	Umbo	4	1	96.97	0.04	2.76	0.12	0.11	100.00
D	Umbo	5	1	96.71	0.05	2.99	0.10	0.15	100.00
D	Umbo	6	1	96.85	0.05	2.82	0.16	0.13	100.00
D	Umbo	7	1	97.31	0.03	2.34	0.17	0.16	100.00
D	Umbo	8	1	97.23	0.01	2.46	0.16	0.15	100.00
D	Umbo	9	1	96.73	0.04	2.96	0.14	0.13	100.00
D	Umbo	10	1	97.22	0.02	2.48	0.12	0.16	100.00
D	Umbo	11	1	97.30	0.04	2.30	0.13	0.24	100.00
D	Umbo	12	1	97.20	0.01	2.57	0.09	0.14	100.00
D	Umbo	13	1	98.45	0.29	0.65	0.55	0.06	100.00
D	Umbo	14	1	98.33	0.32	0.83	0.41	0.11	100.00
D	Umbo	15	1	98.15	0.39	1.00	0.36	0.11	100.00
D	Umbo	16	1	98.40	0.35	0.82	0.33	0.11	100.00
D	Umbo	17	1	98.49	0.27	0.83	0.32	0.09	100.00
D	Umbo	18	1	98.02	0.66	0.61	0.57	0.14	100.00
D	Umbo	19	1	98.31	0.59	0.50	0.52	0.09	100.00
D	Umbo	1	2	97.82	0.34	1.46	0.24	0.15	100.00
D	Umbo	2	2	98.54	0.32	0.82	0.18	0.14	100.00
D	Umbo	3	2	98.26	0.40	0.93	0.28	0.13	100.00
D	Umbo	4	2	96.60	0.04	3.13	0.10	0.14	100.00
D	Umbo	5	2	96.69	0.03	3.06	0.08	0.13	100.00
D	Umbo	6	2	97.20	0.03	2.50	0.13	0.14	100.00
D	Umbo	7	2	96.43	0.00	3.32	0.12	0.13	100.00
D	Umbo	8	2	96.77	0.00	3.05	0.11	0.07	100.00
D	Umbo	9	2	96.82	0.00	2.97	0.13	0.08	100.00
D	Umbo	10	2	96.30	0.03	3.46	0.13	0.09	100.00
D	Umbo	11	2	96.90	0.00	2.86	0.12	0.13	100.00
D	Umbo	12	2	97.20	0.00	2.57	0.12	0.12	100.00
D	Umbo	13	2	96.96	0.02	2.71	0.09	0.22	100.00
D	Umbo	14	2	97.24	0.00	2.51	0.11	0.15	100.00
D	Umbo	15	2	97.28	0.00	2.43	0.14	0.15	100.00
D	Umbo	16	2	97.35	0.02	2.35	0.14	0.14	100.00
D	Umbo	17	2	97.20	0.00	2.48	0.17	0.15	100.00
D	Umbo	18	2	97.57	0.01	2.11	0.15	0.16	100.00
D	Umbo	19	2	97.19	0.01	2.46	0.17	0.17	100.00
D	Umbo	20	2	97.08	0.05	2.57	0.13	0.18	100.00
D	Umbo	21	2	97.21	0.04	2.49	0.14	0.13	100.00
D	Umbo	22	2	97.40	0.00	2.32	0.11	0.17	100.00
D	Umbo	23	2	97.65	0.00	1.84	0.14	0.37	100.00
D	Umbo	24	2	97.62	0.03	1.84	0.18	0.33	100.00

D	Umbo	1	3	98.31	0.55	0.81	0.22	0.11	100.00
D	Umbo	2	3	98.44	0.45	0.82	0.19	0.11	100.00
D	Umbo	3	3	98.34	0.44	0.87	0.21	0.15	100.00
D	Umbo	4	3	98.24	0.51	0.91	0.23	0.10	100.00
D	Umbo	5	3	98.51	0.59	0.65	0.18	0.07	100.00
D	Umbo	6	3	98.43	0.62	0.69	0.17	0.08	100.00
D	Umbo	7	3	98.50	0.64	0.59	0.19	0.09	100.00
D	Umbo	8	3	97.09	0.04	2.58	0.12	0.16	100.00
D	Umbo	9	3	98.20	0.02	1.59	0.09	0.10	100.00
D	Umbo	10	3	98.35	0.03	1.42	0.08	0.12	100.00
D	Umbo	11	3	98.14	0.00	1.67	0.06	0.13	100.00
D	Umbo	12	3	98.12	0.00	1.65	0.11	0.12	100.00
D	Umbo	13	3	98.28	0.00	1.47	0.11	0.14	100.00
D	Umbo	14	3	97.12	0.06	2.64	0.09	0.10	100.00
D	Umbo	15	3	98.23	0.05	1.55	0.08	0.09	100.00
D	Umbo	16	3	98.23	0.01	1.57	0.09	0.10	100.00
D	Umbo	17	3	98.00	0.04	1.76	0.05	0.15	100.00
D	Umbo	18	3	97.45	0.08	2.27	0.09	0.12	100.00
D	Umbo	19	3	98.17	0.11	1.42	0.09	0.20	100.00
D	Umbo	20	3	97.40	0.06	2.23	0.12	0.19	100.00
D	Umbo	21	3	97.91	0.11	1.52	0.12	0.34	100.00
D	Umbo	22	3	98.01	0.06	1.68	0.10	0.15	100.00
D	Umbo	23	3	97.89	0.00	1.83	0.08	0.21	100.00
D	Umbo	24	3	98.32	0.00	1.43	0.10	0.15	100.00
D	Umbo	25	3	98.32	0.01	1.44	0.10	0.14	100.00
D	Umbo	26	3	98.39	0.00	1.39	0.07	0.15	100.00
D	Umbo	27	3	98.66	0.00	1.11	0.08	0.15	100.00
D	Umbo	28	3	98.48	0.02	1.25	0.09	0.16	100.00
D	Umbo	29	3	98.26	0.01	1.51	0.09	0.13	100.00
D	Umbo	30	3	97.61	0.03	2.13	0.07	0.17	100.00
D	Umbo	31	3	97.82	0.04	1.87	0.11	0.16	100.00
D	Umbo	32	3	97.95	0.03	1.75	0.11	0.16	100.00
D	Umbo	33	3	98.02	0.00	1.75	0.11	0.13	100.00
D	Umbo	34	3	97.94	0.05	1.77	0.10	0.15	100.00
D	Umbo	35	3	97.27	0.04	2.44	0.10	0.15	100.00
D	Umbo	36	3	97.85	0.02	1.86	0.13	0.14	100.00
D	Umbo	37	3	97.70	0.01	1.99	0.09	0.21	100.00
D	Umbo	38	3	97.87	0.04	1.74	0.12	0.23	100.00
D	Umbo	39	3	98.05	0.02	1.19	0.10	0.65	100.00
D	Umbo	1	4	97.77	0.33	1.70	0.12	0.08	100.00
D	Umbo	2	4	98.29	0.33	1.12	0.15	0.11	100.00
D	Umbo	3	4	98.32	0.41	1.06	0.14	0.07	100.00
D	Umbo	4	4	98.31	0.52	0.92	0.18	0.07	100.00
D	Umbo	5	4	98.40	0.50	0.86	0.17	0.07	100.00
D	Umbo	6	4	98.24	0.66	0.85	0.21	0.05	100.00
D	Umbo	7	4	97.38	0.03	2.40	0.10	0.09	100.00
D	Umbo	8	4	97.77	0.00	2.09	0.07	0.08	100.00
D	Umbo	9	4	97.94	0.02	1.85	0.09	0.10	100.00
D	Umbo	10	4	97.98	0.03	1.82	0.07	0.10	100.00
D	Umbo	11	4	98.35	0.05	1.47	0.07	0.07	100.00
D	Umbo	12	4	97.70	0.01	2.09	0.08	0.12	100.00
D	Umbo	13	4	97.78	0.01	2.04	0.08	0.09	100.00
D	Umbo	14	4	97.72	0.01	2.10	0.06	0.10	100.00
D	Umbo	15	4	97.71	0.04	2.12	0.07	0.05	100.00
D	Umbo	16	4	98.02	0.06	1.78	0.06	0.08	100.00
D	Umbo	17	4	97.83	0.08	1.83	0.10	0.16	100.00
D	Umbo	18	4	97.41	0.01	2.34	0.12	0.13	100.00
D	Umbo	19	4	97.49	0.08	2.14	0.10	0.19	100.00

D	Umbo	20	4	97.83	0.04	1.96	0.08	0.09	100.00
D	Umbo	21	4	97.67	0.02	2.10	0.06	0.15	100.00
D	Umbo	22	4	97.80	0.00	2.03	0.06	0.11	100.00
D	Umbo	23	4	97.56	0.02	2.22	0.09	0.12	100.00
D	Umbo	24	4	97.83	0.00	1.96	0.09	0.12	100.00
D	Umbo	25	4	97.87	0.03	1.94	0.09	0.08	100.00
D	Umbo	26	4	97.71	0.00	2.11	0.06	0.12	100.00
D	Umbo	27	4	97.69	0.01	2.08	0.10	0.12	100.00
D	Umbo	28	4	97.42	0.03	2.28	0.12	0.14	100.00
D	Umbo	29	4	97.25	0.00	2.51	0.13	0.12	100.00
D	Umbo	30	4	97.30	0.00	2.51	0.08	0.11	100.00
D	Umbo	31	4	97.37	0.06	2.38	0.07	0.13	100.00
D	Umbo	32	4	97.37	0.01	2.38	0.09	0.15	100.00
D	Umbo	33	4	97.23	0.04	2.49	0.08	0.16	100.00
D	Umbo	34	4	97.63	0.03	1.99	0.09	0.25	100.00
D	Umbo	1	5	97.42	0.02	2.22	0.12	0.22	100.00
D	Umbo	2	5	98.38	0.22	0.97	0.32	0.12	100.00
D	Umbo	3	5	98.73	0.33	0.37	0.53	0.05	100.00
D	Umbo	4	5	98.53	0.31	0.43	0.66	0.06	100.00
D	Umbo	5	5	98.47	0.37	0.57	0.54	0.05	100.00
D	Umbo	6	5	98.55	0.33	0.54	0.53	0.05	100.00
D	Umbo	7	5	98.45	0.45	0.41	0.62	0.07	100.00
D	Umbo	8	5	97.08	0.15	1.87	0.23	0.67	100.00
D	Umbo	9	5	98.49	0.07	1.02	0.25	0.18	100.00
D	Umbo	10	5	98.55	0.35	0.45	0.57	0.10	100.00
D	Umbo	11	5	98.63	0.34	0.44	0.48	0.11	100.00
D	Umbo	12	5	98.64	0.36	0.44	0.45	0.10	100.00
D	Umbo	13	5	98.77	0.22	0.51	0.43	0.08	100.00
D	Umbo	14	5	98.58	0.48	0.31	0.48	0.15	100.00
D	Umbo	15	5	98.56	0.37	0.47	0.51	0.08	100.00
D	Umbo	16	5	98.89	0.36	0.31	0.38	0.07	100.00
D	Umbo	17	5	98.67	0.39	0.44	0.41	0.10	100.00
D	Umbo	18	5	98.82	0.42	0.35	0.35	0.06	100.00
D	Umbo	19	5	98.66	0.40	0.49	0.35	0.10	100.00
D	Umbo	20	5	98.65	0.49	0.41	0.35	0.11	100.00
D	Umbo	21	5	98.67	0.56	0.31	0.39	0.07	100.00
D	Umbo	22	5	98.61	0.51	0.51	0.33	0.05	100.00
D	Umbo	23	5	98.36	0.66	0.39	0.49	0.11	100.00
D	Umbo	24	5	97.67	0.81	0.52	0.81	0.19	100.00
D	Umbo	1	6	97.71	0.07	2.02	0.09	0.11	100.00
D	Umbo	2	6	98.11	0.01	1.62	0.11	0.15	100.00
D	Umbo	3	6	97.72	0.02	1.94	0.16	0.15	100.00
D	Umbo	4	6	97.89	0.01	1.82	0.14	0.15	100.00
D	Umbo	5	6	97.64	0.00	2.10	0.14	0.12	100.00
D	Umbo	6	6	98.14	0.01	1.59	0.14	0.12	100.00
D	Umbo	7	6	98.10	0.01	1.68	0.12	0.09	100.00
D	Umbo	8	6	98.07	0.00	1.58	0.14	0.21	100.00
D	Umbo	9	6	98.00	0.21	1.26	0.36	0.16	100.00
D	Umbo	10	6	98.69	0.29	0.47	0.48	0.07	100.00
D	Umbo	11	6	98.55	0.38	0.49	0.51	0.07	100.00
D	Umbo	12	6	98.59	0.32	0.54	0.50	0.07	100.00
D	Umbo	13	6	98.67	0.36	0.46	0.41	0.10	100.00
D	Umbo	14	6	98.63	0.36	0.39	0.51	0.12	100.00
D	Umbo	15	6	98.48	0.43	0.44	0.54	0.10	100.00
D	Umbo	16	6	98.45	0.56	0.39	0.49	0.11	100.00
D	Umbo	17	6	98.51	0.51	0.46	0.44	0.09	100.00
D	Umbo	18	6	98.35	0.45	0.60	0.50	0.10	100.00
D	Umbo	19	6	98.43	0.53	0.46	0.47	0.11	100.00

D	Umbo	20	6	98.58	0.49	0.41	0.43	0.09	100.00
D	Umbo	21	6	98.66	0.49	0.29	0.47	0.10	100.00
D	Umbo	22	6	98.47	0.46	0.34	0.58	0.16	100.00
D	Umbo	23	6	98.41	0.39	0.38	0.72	0.10	100.00
D	Umbo	24	6	97.80	0.44	0.70	0.90	0.16	100.00
D	Mid	1	7	97.27	0.43	1.93	0.21	0.16	100.00
D	Mid	2	7	97.78	0.42	1.53	0.16	0.11	100.00
D	Mid	3	7	97.72	0.42	1.62	0.11	0.13	100.00
D	Mid	4	7	97.93	0.60	1.26	0.08	0.12	100.00
D	Mid	5	7	98.14	0.56	1.09	0.10	0.11	100.00
D	Mid	6	7	98.47	0.56	0.76	0.08	0.13	100.00
D	Mid	7	7	97.67	0.12	1.89	0.13	0.19	100.00
D	Mid	8	7	96.44	0.06	3.21	0.15	0.14	100.00
D	Mid	9	7	96.74	0.05	2.99	0.08	0.14	100.00
D	Mid	10	7	97.17	0.12	2.45	0.08	0.19	100.00
D	Mid	11	7	97.17	0.00	2.55	0.09	0.19	100.00
D	Mid	12	7	97.12	0.03	2.61	0.10	0.14	100.00
D	Mid	13	7	97.28	0.00	2.48	0.12	0.12	100.00
D	Mid	14	7	97.61	0.00	2.10	0.12	0.17	100.00
D	Mid	15	7	97.72	0.07	1.86	0.13	0.22	100.00
D	Mid	1	8	97.00	0.47	2.26	0.14	0.14	100.00
D	Mid	2	8	98.23	0.27	1.22	0.13	0.16	100.00
D	Mid	3	8	98.19	0.40	1.08	0.19	0.14	100.00
D	Mid	4	8	98.15	0.44	1.24	0.06	0.10	100.00
D	Mid	5	8	98.24	0.61	1.03	0.05	0.07	100.00
D	Mid	6	8	98.28	0.75	0.73	0.12	0.12	100.00
D	Mid	7	8	98.36	0.73	0.47	0.38	0.07	100.00
D	Mid	8	8	98.30	0.66	0.36	0.54	0.15	100.00
D	Mid	9	8	98.74	0.57	0.38	0.23	0.08	100.00
D	Mid	10	8	98.67	0.54	0.36	0.33	0.10	100.00
D	Mid	11	8	98.11	0.00	1.61	0.04	0.24	100.00
D	Mid	12	8	97.88	0.08	1.79	0.05	0.20	100.00
D	Mid	13	8	97.92	0.04	1.72	0.09	0.23	100.00
D	Mid	14	8	98.10	0.09	1.57	0.07	0.18	100.00
D	Mid	15	8	97.87	0.04	1.80	0.05	0.23	100.00
D	Mid	16	8	97.33	0.14	2.24	0.10	0.19	100.00
D	Mid	1	9	96.76	0.52	2.14	0.37	0.21	100.00
D	Mid	2	9	98.58	0.31	0.75	0.25	0.11	100.00
D	Mid	3	9	98.10	0.34	1.25	0.17	0.15	100.00
D	Mid	4	9	98.53	0.30	0.68	0.33	0.17	100.00
D	Mid	5	9	98.86	0.22	0.65	0.18	0.09	100.00
D	Mid	6	9	99.07	0.18	0.62	0.08	0.06	100.00
D	Mid	7	9	98.51	0.34	0.89	0.18	0.08	100.00
D	Mid	8	9	97.52	0.02	2.17	0.14	0.16	100.00
D	Mid	9	9	97.70	0.01	2.04	0.14	0.11	100.00
D	Mid	10	9	98.11	0.00	1.67	0.10	0.11	100.00
D	Mid	11	9	98.08	0.04	1.29	0.13	0.45	100.00
D	Edge	1	10	97.71	0.35	1.68	0.12	0.14	100.00
D	Edge	2	10	98.11	0.31	1.21	0.19	0.19	100.00
D	Edge	3	10	98.67	0.31	0.73	0.15	0.15	100.00
D	Edge	4	10	98.49	0.37	0.83	0.20	0.11	100.00
D	Edge	5	10	98.27	0.48	0.89	0.22	0.14	100.00
D	Edge	6	10	99.03	0.29	0.38	0.18	0.12	100.00
D	Edge	7	10	98.67	0.36	0.46	0.38	0.14	100.00
D	Edge	8	10	98.31	0.42	0.58	0.56	0.13	100.00
D	Edge	9	10	98.39	0.54	0.40	0.54	0.13	100.00
D	Edge	10	10	98.78	0.32	0.27	0.50	0.13	100.00
D	Edge	11	10	98.87	0.27	0.30	0.47	0.11	100.00

D	Edge	12	10	99.05	0.11	0.24	0.43	0.17	100.00
D	Edge	13	10	99.05	0.21	0.15	0.47	0.13	100.00
D	Edge	14	10	98.90	0.20	0.29	0.48	0.13	100.00
D	Edge	1	11	97.59	0.34	1.82	0.10	0.16	100.00
D	Edge	2	11	98.31	0.29	1.19	0.08	0.14	100.00
D	Edge	3	11	98.18	0.37	1.21	0.11	0.13	100.00
D	Edge	4	11	98.24	0.41	1.17	0.08	0.12	100.00
D	Edge	5	11	98.40	0.38	1.00	0.09	0.13	100.00
D	Edge	6	11	98.37	0.40	1.03	0.08	0.12	100.00
D	Edge	7	11	98.23	0.45	1.15	0.04	0.13	100.00
D	Edge	8	11	98.51	0.48	0.83	0.05	0.15	100.00
D	Edge	9	11	98.36	0.61	0.82	0.06	0.15	100.00
D	Edge	10	11	98.34	0.64	0.84	0.05	0.13	100.00
D	Edge	11	11	98.61	0.43	0.78	0.07	0.11	100.00
D	Edge	12	11	98.76	0.54	0.58	0.02	0.11	100.00
D	Edge	13	11	98.67	0.54	0.64	0.04	0.11	100.00
D	Edge	14	11	98.85	0.51	0.48	0.05	0.11	100.00
D	Edge	15	11	98.45	0.71	0.65	0.11	0.08	100.00
D	Edge	16	11	97.48	0.13	1.93	0.14	0.32	100.00
D	Edge	1	12	97.96	0.55	1.22	0.11	0.16	100.00
D	Edge	2	12	97.93	0.55	1.23	0.14	0.15	100.00
D	Edge	3	12	98.20	0.56	0.98	0.13	0.13	100.00
D	Edge	4	12	98.35	0.52	0.88	0.12	0.14	100.00
D	Edge	5	12	98.40	0.51	0.88	0.08	0.13	100.00
D	Edge	6	12	98.59	0.49	0.70	0.10	0.13	100.00
D	Edge	7	12	98.84	0.44	0.53	0.11	0.08	100.00
D	Edge	8	12	98.78	0.52	0.52	0.04	0.13	100.00
D	Edge	9	12	98.76	0.53	0.49	0.10	0.13	100.00
D	Edge	10	12	98.88	0.47	0.38	0.17	0.10	100.00
D	Edge	11	12	98.90	0.45	0.45	0.11	0.09	100.00
D	Edge	12	12	98.85	0.48	0.41	0.14	0.13	100.00
D	Edge	13	12	98.74	0.66	0.21	0.26	0.13	100.00
E	Umbo	1	1	98.02	0.61	1.14	0.12	0.11	100.00
E	Umbo	2	1	98.31	0.65	0.80	0.13	0.11	100.00
E	Umbo	3	1	98.23	0.73	0.74	0.15	0.16	100.00
E	Umbo	4	1	98.48	0.71	0.59	0.16	0.07	100.00
E	Umbo	5	1	98.53	0.62	0.60	0.14	0.11	100.00
E	Umbo	6	1	98.71	0.61	0.42	0.17	0.10	100.00
E	Umbo	7	1	98.76	0.59	0.33	0.20	0.13	100.00
E	Umbo	8	1	98.54	0.60	0.41	0.36	0.09	100.00
E	Umbo	9	1	98.58	0.55	0.41	0.37	0.09	100.00
E	Umbo	10	1	98.71	0.33	0.51	0.32	0.13	100.00
E	Umbo	11	1	98.94	0.37	0.37	0.20	0.12	100.00
E	Umbo	12	1	98.80	0.35	0.44	0.33	0.08	100.00
E	Umbo	13	1	98.75	0.46	0.53	0.20	0.07	100.00
E	Umbo	14	1	98.60	0.52	0.58	0.20	0.09	100.00
E	Umbo	15	1	98.33	0.67	0.67	0.25	0.09	100.00
E	Umbo	16	1	97.46	0.00	2.25	0.10	0.19	100.00
E	Umbo	17	1	97.27	0.05	2.46	0.06	0.16	100.00
E	Umbo	18	1	97.76	0.03	2.00	0.06	0.15	100.00
E	Umbo	19	1	97.48	0.05	2.16	0.14	0.17	100.00
E	Umbo	1	2	98.05	0.63	1.02	0.15	0.14	100.00
E	Umbo	2	2	98.34	0.53	0.89	0.10	0.15	100.00
E	Umbo	3	2	98.37	0.58	0.77	0.14	0.14	100.00
E	Umbo	4	2	98.57	0.52	0.68	0.14	0.08	100.00
E	Umbo	5	2	98.35	0.60	0.86	0.08	0.10	100.00
E	Umbo	6	2	98.17	0.67	0.98	0.07	0.11	100.00
E	Umbo	7	2	98.34	0.68	0.76	0.10	0.12	100.00

E	Umbo	8	2	98.42	0.58	0.78	0.10	0.11	100.00
E	Umbo	9	2	98.56	0.61	0.65	0.07	0.11	100.00
E	Umbo	10	2	98.36	0.78	0.67	0.11	0.08	100.00
E	Umbo	11	2	98.11	0.90	0.40	0.51	0.09	100.00
E	Umbo	12	2	98.34	0.40	0.57	0.53	0.16	100.00
E	Umbo	13	2	98.85	0.31	0.52	0.25	0.08	100.00
E	Umbo	14	2	98.45	0.38	0.79	0.25	0.13	100.00
E	Umbo	15	2	98.68	0.49	0.57	0.22	0.04	100.00
E	Umbo	16	2	98.54	0.55	0.56	0.24	0.11	100.00
E	Umbo	17	2	98.03	0.27	1.32	0.16	0.22	100.00
E	Umbo	18	2	97.64	0.01	2.16	0.06	0.14	100.00
E	Umbo	19	2	97.92	0.02	1.75	0.15	0.17	100.00
E	Umbo	1	3	97.60	0.60	1.47	0.23	0.10	100.00
E	Umbo	2	3	97.77	0.66	1.29	0.17	0.11	100.00
E	Umbo	3	3	97.73	0.01	2.07	0.10	0.09	100.00
E	Umbo	4	3	97.49	0.03	2.32	0.08	0.09	100.00
E	Umbo	5	3	97.90	0.01	1.95	0.06	0.09	100.00
E	Umbo	6	3	97.35	0.02	2.45	0.11	0.07	100.00
E	Umbo	7	3	97.08	0.02	2.77	0.09	0.05	100.00
E	Umbo	8	3	97.79	0.05	1.90	0.10	0.16	100.00
E	Umbo	9	3	97.77	0.01	1.93	0.11	0.18	100.00
E	Umbo	10	3	97.67	0.02	2.02	0.15	0.14	100.00
E	Umbo	11	3	97.51	0.04	2.14	0.13	0.18	100.00
E	Umbo	12	3	97.80	0.01	1.92	0.14	0.12	100.00
E	Umbo	13	3	97.74	0.02	1.91	0.17	0.16	100.00
E	Umbo	14	3	97.66	0.03	1.82	0.13	0.35	100.00
E	Umbo	15	3	97.42	0.00	2.32	0.13	0.12	100.00
E	Umbo	16	3	97.99	0.02	1.79	0.09	0.10	100.00
E	Umbo	17	3	97.95	0.00	1.77	0.12	0.17	100.00
E	Umbo	18	3	97.81	0.00	1.92	0.14	0.13	100.00
E	Umbo	19	3	97.94	0.00	1.81	0.14	0.11	100.00
E	Umbo	20	3	97.90	0.00	1.81	0.16	0.14	100.00
E	Umbo	21	3	97.52	0.01	2.18	0.14	0.16	100.00
E	Umbo	22	3	97.06	0.00	2.70	0.13	0.11	100.00
E	Umbo	23	3	97.37	0.07	2.34	0.14	0.09	100.00
E	Umbo	24	3	97.29	0.04	2.38	0.16	0.12	100.00
E	Umbo	25	3	97.25	0.00	2.50	0.14	0.11	100.00
E	Umbo	26	3	96.72	0.01	3.08	0.13	0.06	100.00
E	Umbo	27	3	97.14	0.05	2.58	0.15	0.09	100.00
E	Umbo	28	3	97.98	0.07	1.58	0.19	0.18	100.00
E	Umbo	29	3	97.53	0.03	2.17	0.15	0.13	100.00
E	Umbo	30	3	97.59	0.04	2.01	0.13	0.23	100.00
E	Umbo	31	3	97.94	0.01	1.80	0.12	0.12	100.00
E	Umbo	32	3	97.87	0.04	1.85	0.11	0.14	100.00
E	Umbo	33	3	97.17	0.01	2.56	0.14	0.13	100.00
E	Umbo	34	3	97.39	0.00	2.38	0.14	0.10	100.00
E	Umbo	35	3	97.12	0.02	2.62	0.16	0.09	100.00
E	Umbo	36	3	97.53	0.01	2.21	0.15	0.10	100.00
E	Umbo	37	3	97.07	0.00	2.63	0.19	0.10	100.00
E	Umbo	38	3	97.47	0.03	2.27	0.16	0.07	100.00
E	Umbo	39	3	95.79	0.21	2.47	1.04	0.50	100.00
E	Mid	1	4	97.12	0.64	1.78	0.32	0.15	100.00
E	Mid	2	4	98.29	0.64	0.62	0.28	0.17	100.00
E	Mid	3	4	98.53	0.43	0.73	0.19	0.12	100.00
E	Mid	4	4	98.27	0.58	0.91	0.12	0.13	100.00
E	Mid	5	4	98.16	0.65	0.95	0.13	0.12	100.00
E	Mid	6	4	98.31	0.76	0.73	0.09	0.12	100.00
E	Mid	7	4	98.34	0.70	0.76	0.09	0.11	100.00

E	Mid	8	4	98.20	0.78	0.88	0.06	0.07	100.00
E	Mid	9	4	98.33	0.74	0.77	0.05	0.12	100.00
E	Mid	10	4	98.41	0.80	0.64	0.04	0.11	100.00
E	Mid	11	4	98.39	0.83	0.64	0.06	0.09	100.00
E	Mid	12	4	98.51	0.72	0.62	0.06	0.10	100.00
E	Mid	13	4	98.50	0.84	0.48	0.11	0.07	100.00
E	Mid	14	4	98.55	0.70	0.50	0.15	0.09	100.00
E	Mid	15	4	98.40	0.76	0.55	0.18	0.11	100.00
E	Mid	16	4	98.61	0.63	0.54	0.15	0.07	100.00
E	Mid	17	4	98.76	0.60	0.40	0.16	0.09	100.00
E	Mid	18	4	98.52	0.69	0.44	0.26	0.09	100.00
E	Mid	19	4	98.07	0.13	1.09	0.14	0.58	100.00
E	Mid	20	4	97.04	0.03	2.67	0.10	0.17	100.00
E	Mid	21	4	96.58	0.06	3.04	0.09	0.23	100.00
E	Mid	22	4	96.60	0.07	3.05	0.08	0.20	100.00
E	Mid	23	4	96.93	0.03	2.84	0.05	0.15	100.00
E	Mid	24	4	97.94	0.02	1.82	0.08	0.14	100.00
E	Mid	25	4	97.68	0.01	2.06	0.08	0.18	100.00
E	Mid	1	5	98.09	0.40	1.26	0.13	0.13	100.00
E	Mid	2	5	98.19	0.43	1.10	0.17	0.12	100.00
E	Mid	3	5	98.24	0.55	1.01	0.10	0.10	100.00
E	Mid	4	5	98.24	0.82	0.82	0.05	0.07	100.00
E	Mid	5	5	98.04	0.76	1.07	0.04	0.09	100.00
E	Mid	6	5	98.10	0.77	1.01	0.03	0.09	100.00
E	Mid	7	5	98.35	0.90	0.65	0.05	0.05	100.00
E	Mid	8	5	98.11	0.70	0.77	0.34	0.08	100.00
E	Mid	9	5	98.79	0.67	0.33	0.15	0.07	100.00
E	Mid	10	5	98.33	0.68	0.72	0.17	0.11	100.00
E	Mid	11	5	98.62	0.60	0.56	0.18	0.04	100.00
E	Mid	12	5	98.58	0.60	0.59	0.16	0.07	100.00
E	Mid	13	5	97.87	0.06	1.60	0.10	0.37	100.00
E	Mid	14	5	97.40	0.00	2.41	0.04	0.15	100.00
E	Mid	15	5	97.69	0.03	2.07	0.04	0.17	100.00
E	Mid	16	5	98.39	0.03	1.33	0.08	0.18	100.00
E	Mid	17	5	97.68	0.00	2.15	0.03	0.14	100.00
E	Mid	18	5	98.61	0.07	0.89	0.08	0.35	100.00
E	Mid	1	6	97.42	0.33	1.96	0.16	0.13	100.00
E	Mid	2	6	98.07	0.29	1.35	0.19	0.11	100.00
E	Mid	3	6	97.76	0.37	1.50	0.27	0.10	100.00
E	Mid	4	6	97.92	0.39	1.45	0.15	0.09	100.00
E	Mid	5	6	97.39	0.65	1.71	0.11	0.14	100.00
E	Mid	6	6	97.68	0.58	1.50	0.13	0.11	100.00
E	Mid	7	6	97.64	0.57	1.53	0.13	0.13	100.00
E	Mid	8	6	97.83	0.01	1.98	0.10	0.09	100.00
E	Mid	9	6	97.79	0.00	1.98	0.10	0.13	100.00
E	Mid	10	6	97.90	0.04	1.79	0.09	0.19	100.00
E	Mid	11	6	97.48	0.00	2.17	0.12	0.22	100.00
E	Mid	12	6	98.09	0.04	1.64	0.12	0.11	100.00
E	Mid	13	6	97.74	0.00	2.04	0.11	0.12	100.00
E	Mid	14	6	97.91	0.00	1.84	0.11	0.14	100.00
E	Mid	15	6	97.91	0.00	1.92	0.08	0.09	100.00
E	Mid	16	6	97.77	0.01	2.01	0.08	0.13	100.00
E	Mid	17	6	97.87	0.02	1.90	0.11	0.09	100.00
E	Mid	18	6	97.49	0.04	2.25	0.12	0.10	100.00
E	Mid	19	6	97.65	0.05	2.10	0.09	0.12	100.00
E	Mid	20	6	97.34	0.01	2.44	0.12	0.09	100.00
E	Mid	21	6	97.50	0.02	2.28	0.12	0.08	100.00
E	Mid	22	6	97.52	0.07	2.17	0.12	0.13	100.00

E	Mid	23	6	97.14	0.05	2.60	0.13	0.08	100.00
E	Mid	24	6	97.62	0.06	2.00	0.14	0.18	100.00
E	Mid	25	6	97.12	0.00	2.67	0.12	0.08	100.00
E	Mid	26	6	97.27	0.04	2.51	0.11	0.08	100.00
E	Mid	27	6	97.73	0.06	1.91	0.11	0.18	100.00
E	Mid	28	6	97.38	0.00	2.45	0.06	0.11	100.00
E	Mid	29	6	97.39	0.01	2.40	0.11	0.10	100.00
E	Mid	30	6	97.56	0.03	2.27	0.08	0.07	100.00
E	Mid	31	6	97.27	0.03	2.52	0.09	0.10	100.00
E	Mid	32	6	96.91	0.02	2.93	0.09	0.06	100.00
E	Mid	33	6	97.47	0.04	2.29	0.09	0.11	100.00
E	Mid	34	6	97.41	0.09	2.32	0.11	0.08	100.00
E	Mid	35	6	97.45	0.01	2.39	0.11	0.05	100.00
E	Mid	36	6	97.53	0.00	2.32	0.07	0.08	100.00
E	Mid	37	6	97.27	0.02	2.50	0.11	0.10	100.00
E	Mid	38	6	97.17	0.08	2.52	0.15	0.09	100.00
E	Mid	39	6	97.65	0.11	1.78	0.16	0.29	100.00
E	Edge	1	7	98.33	0.28	1.19	0.12	0.08	100.00
E	Edge	2	7	98.76	0.23	0.83	0.08	0.10	100.00
E	Edge	3	7	98.56	0.43	0.76	0.10	0.14	100.00
E	Edge	4	7	98.43	0.41	0.89	0.16	0.12	100.00
E	Edge	5	7	98.86	0.31	0.60	0.12	0.11	100.00
E	Edge	6	7	98.46	0.41	0.49	0.50	0.14	100.00
E	Edge	7	7	98.78	0.42	0.61	0.13	0.07	100.00
E	Edge	8	7	98.31	0.52	0.48	0.58	0.12	100.00
E	Edge	9	7	98.62	0.46	0.58	0.26	0.09	100.00
E	Edge	10	7	99.09	0.33	0.47	0.08	0.03	100.00
E	Edge	11	7	98.72	0.43	0.62	0.12	0.10	100.00
E	Edge	12	7	98.74	0.48	0.56	0.10	0.12	100.00
E	Edge	13	7	98.83	0.16	0.30	0.57	0.13	100.00
E	Edge	14	7	98.99	0.23	0.47	0.23	0.08	100.00
E	Edge	1	8	98.33	0.48	0.93	0.17	0.08	100.00
E	Edge	2	8	98.69	0.31	0.79	0.12	0.09	100.00
E	Edge	3	8	98.72	0.33	0.69	0.15	0.11	100.00
E	Edge	4	8	98.96	0.25	0.49	0.17	0.13	100.00
E	Edge	5	8	98.85	0.29	0.58	0.15	0.13	100.00
E	Edge	6	8	98.55	0.49	0.78	0.05	0.12	100.00
E	Edge	7	8	98.69	0.49	0.67	0.06	0.08	100.00
E	Edge	8	8	98.51	0.60	0.69	0.11	0.09	100.00
E	Edge	9	8	98.61	0.61	0.66	0.05	0.07	100.00
E	Edge	10	8	98.77	0.53	0.52	0.11	0.07	100.00
E	Edge	11	8	99.12	0.32	0.34	0.11	0.11	100.00
E	Edge	1	9	98.21	0.41	1.14	0.10	0.14	100.00
E	Edge	2	9	97.74	0.32	1.69	0.09	0.14	100.00
E	Edge	3	9	98.17	0.29	1.35	0.06	0.13	100.00
E	Edge	4	9	98.21	0.33	1.23	0.08	0.16	100.00
E	Edge	5	9	98.36	0.39	1.11	0.04	0.10	100.00
E	Edge	6	9	98.42	0.46	0.99	0.02	0.11	100.00
E	Edge	7	9	98.26	0.49	1.11	0.03	0.12	100.00
E	Edge	8	9	98.32	0.45	1.06	0.05	0.12	100.00
E	Edge	9	9	98.28	0.53	1.05	0.04	0.10	100.00
E	Edge	10	9	98.32	0.63	0.92	0.02	0.11	100.00
E	Edge	11	9	98.37	0.52	0.94	0.04	0.12	100.00
E	Edge	12	9	98.45	0.63	0.77	0.05	0.09	100.00
E	Edge	13	9	98.52	0.61	0.77	0.01	0.09	100.00
E	Edge	14	9	98.54	0.70	0.66	0.03	0.08	100.00
E	Edge	15	9	98.34	0.78	0.74	0.05	0.09	100.00
E	Edge	16	9	98.52	0.79	0.56	0.04	0.09	100.00

E	Edge	17	9	98.67	0.68	0.55	0.00	0.10	100.00
E	Edge	18	9	98.20	1.20	0.44	0.08	0.09	100.00
E	Edge	19	9	97.89	1.49	0.37	0.18	0.08	100.00
F	Umbo	1	1	91.00	0.40	0.74	0.83	0.39	93.36
F	Umbo	2	1	93.67	0.37	0.80	0.72	0.32	95.86
F	Umbo	3	1	96.46	0.34	0.78	0.53	0.28	98.40
F	Umbo	4	1	95.04	0.35	0.89	0.60	0.25	97.13
F	Umbo	5	1	92.51	0.37	0.85	0.48	0.28	94.49
F	Umbo	6	1	91.97	0.34	1.01	0.39	0.27	93.99
F	Umbo	7	1	93.95	0.41	0.97	0.49	0.27	96.09
F	Umbo	8	1	95.29	0.40	0.85	0.48	0.28	97.29
F	Umbo	9	1	95.72	0.32	0.80	0.36	0.25	97.45
F	Umbo	10	1	94.31	0.29	0.69	0.32	0.28	95.90
F	Umbo	11	1	93.75	0.38	0.71	0.32	0.24	95.40
F	Umbo	12	1	95.22	0.38	0.68	0.20	0.19	96.67
F	Umbo	13	1	95.83	0.37	0.45	0.21	0.18	97.04
F	Umbo	14	1	94.51	0.11	0.91	0.18	0.33	96.04
F	Umbo	15	1	92.47	0.00	1.25	0.27	0.34	94.33
F	Umbo	16	1	92.68	0.00	1.29	0.20	0.28	94.44
F	Umbo	17	1	92.88	0.01	1.27	0.30	0.29	94.75
F	Umbo	18	1	92.45	0.00	1.23	0.16	0.25	94.09
F	Umbo	19	1	92.85	0.00	1.26	0.23	0.23	94.57
F	Umbo	20	1	91.76	0.00	1.23	0.25	0.18	93.42
F	Umbo	21	1	92.67	0.02	1.20	0.25	0.22	94.36
F	Umbo	22	1	94.50	0.00	1.12	0.28	0.20	96.11
F	Umbo	23	1	93.88	0.00	1.32	0.22	0.18	95.60
F	Umbo	24	1	93.53	0.00	1.26	0.17	0.13	95.09
F	Umbo	25	1	93.50	0.00	1.21	0.28	0.15	95.14
F	Umbo	26	1	93.48	0.00	1.18	0.22	0.15	95.02
F	Umbo	27	1	91.65	0.00	1.08	0.22	0.15	93.10
F	Umbo	28	1	93.39	0.00	1.26	0.29	0.22	95.15
F	Umbo	29	1	92.02	0.01	1.18	0.33	0.24	93.76
F	Umbo	30	1	92.76	0.01	1.17	0.20	0.22	94.36
F	Umbo	31	1	93.97	0.01	1.16	0.15	0.26	95.55
F	Umbo	32	1	93.11	0.00	1.05	0.35	0.39	94.89
F	Umbo	33	1	92.78	0.03	1.09	0.23	0.58	94.72
F	Umbo	34	1	93.15	0.01	1.04	0.19	0.34	94.73
F	Umbo	35	1	91.81	0.00	1.14	0.12	0.28	93.35
F	Umbo	36	1	92.79	0.01	1.08	0.25	0.36	94.49
F	Umbo	37	1	94.19	0.03	1.07	0.33	0.29	95.91
F	Umbo	38	1	92.22	0.00	0.97	0.27	0.53	93.99
F	Umbo	1	2	68.95	0.16	0.34	0.65	0.04	70.13
F	Umbo	2	2	88.34	0.33	0.86	0.50	0.17	90.20
F	Umbo	3	2	95.51	0.40	1.06	0.39	0.29	97.64
F	Umbo	4	2	95.78	0.37	0.96	0.42	0.27	97.81
F	Umbo	5	2	95.33	0.39	0.79	0.42	0.20	97.14
F	Umbo	6	2	97.41	0.33	0.81	0.50	0.24	99.29
F	Umbo	7	2	97.23	0.38	0.80	0.49	0.24	99.14
F	Umbo	8	2	97.86	0.41	0.80	0.46	0.26	99.78
F	Umbo	9	2	97.20	0.38	0.73	0.45	0.20	98.96
F	Umbo	10	2	97.72	0.37	0.73	0.44	0.20	99.47
F	Umbo	11	2	97.36	0.41	0.72	0.40	0.22	99.11
F	Umbo	12	2	98.89	0.40	0.67	0.40	0.21	100.57
F	Umbo	13	2	98.60	0.36	0.63	0.38	0.20	100.17
F	Umbo	14	2	99.18	0.37	0.60	0.33	0.21	100.70
F	Umbo	15	2	98.77	0.35	0.50	0.41	0.17	100.19
F	Umbo	16	2	99.21	0.36	0.47	0.42	0.16	100.62
F	Umbo	17	2	99.08	0.33	0.50	0.39	0.19	100.48

F	Umbo	18	2	98.97	0.32	0.66	0.34	0.15	100.45
F	Umbo	19	2	98.73	0.29	0.61	0.34	0.17	100.14
F	Umbo	20	2	97.50	0.28	0.56	0.26	0.15	98.74
F	Umbo	21	2	98.78	0.29	0.52	0.23	0.15	99.96
F	Umbo	22	2	98.25	0.31	0.53	0.18	0.16	99.43
F	Umbo	23	2	97.83	0.31	0.56	0.17	0.15	99.04
F	Umbo	24	2	98.43	0.37	0.54	0.20	0.14	99.68
F	Umbo	25	2	98.81	0.40	0.53	0.23	0.15	100.12
F	Umbo	26	2	99.03	0.30	0.67	0.21	0.15	100.35
F	Umbo	27	2	96.71	0.18	0.83	0.26	0.19	98.17
F	Umbo	28	2	96.18	0.01	1.14	0.22	0.21	97.75
F	Umbo	29	2	96.08	0.00	1.08	0.20	0.19	97.55
F	Umbo	30	2	96.70	0.00	1.09	0.18	0.19	98.16
F	Umbo	31	2	96.78	0.00	1.09	0.21	0.20	98.28
F	Umbo	32	2	96.25	0.00	1.07	0.20	0.18	97.70
F	Umbo	33	2	96.50	0.00	1.10	0.24	0.17	98.02
F	Umbo	34	2	96.38	0.00	1.13	0.26	0.20	97.97
F	Umbo	35	2	97.15	0.00	1.03	0.25	0.16	98.59
F	Umbo	36	2	96.67	0.00	1.03	0.24	0.19	98.13
F	Umbo	37	2	96.80	0.00	1.05	0.24	0.31	98.39
F	Umbo	38	2	97.09	0.00	1.08	0.24	0.22	98.62
F	Umbo	39	2	97.27	0.00	1.05	0.23	0.19	98.74
F	Umbo	40	2	97.25	0.01	1.09	0.24	0.21	98.80
F	Umbo	41	2	96.96	0.00	1.01	0.23	0.33	98.54
F	Umbo	42	2	96.70	0.01	0.92	0.25	0.41	98.29
F	Umbo	43	2	96.98	0.00	1.09	0.22	0.38	98.68
F	Umbo	44	2	96.90	0.00	1.06	0.21	0.24	98.42
F	Umbo	45	2	96.97	0.00	1.01	0.22	0.22	98.42
F	Umbo	46	2	96.91	0.02	1.06	0.22	0.24	98.44
F	Umbo	47	2	96.74	0.01	1.03	0.23	0.25	98.26
F	Umbo	48	2	96.70	0.00	1.05	0.24	0.26	98.26
F	Umbo	49	2	97.17	0.00	1.06	0.22	0.22	98.68
F	Umbo	50	2	96.76	0.00	1.07	0.25	0.22	98.29
F	Umbo	51	2	96.40	0.01	1.02	0.24	0.22	97.89
F	Umbo	52	2	97.13	0.00	1.06	0.22	0.23	98.63
F	Umbo	53	2	97.17	0.00	1.10	0.23	0.21	98.71
F	Umbo	54	2	97.69	0.00	1.15	0.25	0.22	99.31
F	Umbo	55	2	96.93	0.01	1.15	0.27	0.24	98.59
F	Umbo	56	2	96.90	0.01	1.10	0.28	0.25	98.53
F	Umbo	57	2	97.17	0.00	1.09	0.29	0.31	98.86
F	Umbo	58	2	97.29	0.02	1.05	0.26	0.36	98.97
F	Umbo	1	3	98.57	0.32	0.85	0.20	0.07	100.00
F	Umbo	2	3	98.36	0.37	1.05	0.14	0.08	100.00
F	Umbo	3	3	98.60	0.31	0.86	0.15	0.09	100.00
F	Umbo	4	3	98.42	0.39	0.95	0.16	0.09	100.00
F	Umbo	5	3	98.45	0.45	0.86	0.16	0.08	100.00
F	Umbo	6	3	98.42	0.40	0.95	0.12	0.11	100.00
F	Umbo	7	3	98.47	0.42	0.90	0.15	0.07	100.00
F	Umbo	8	3	98.39	0.50	0.90	0.13	0.09	100.00
F	Umbo	9	3	98.46	0.44	0.92	0.09	0.09	100.00
F	Umbo	10	3	98.13	0.44	1.20	0.17	0.07	100.00
F	Umbo	11	3	97.71	0.03	2.01	0.08	0.16	100.00
F	Umbo	12	3	97.47	0.01	2.30	0.10	0.13	100.00
F	Umbo	13	3	98.46	0.32	0.96	0.22	0.04	100.00
F	Umbo	14	3	98.40	0.49	0.82	0.22	0.06	100.00
F	Umbo	15	3	98.56	0.53	0.64	0.21	0.06	100.00
F	Umbo	16	3	98.54	0.50	0.64	0.24	0.08	100.00
F	Umbo	17	3	98.46	0.53	0.72	0.25	0.05	100.00

F	Umbo	18	3	98.62	0.54	0.56	0.20	0.08	100.00
F	Umbo	19	3	98.49	0.51	0.71	0.20	0.09	100.00
F	Umbo	20	3	98.64	0.45	0.66	0.19	0.05	100.00
F	Umbo	21	3	98.49	0.66	0.60	0.17	0.08	100.00
F	Umbo	22	3	98.60	0.62	0.47	0.22	0.10	100.00
F	Umbo	23	3	98.50	0.57	0.53	0.33	0.07	100.00
F	Umbo	24	3	98.48	0.42	0.69	0.35	0.06	100.00
F	Umbo	25	3	98.77	0.41	0.46	0.28	0.08	100.00
F	Umbo	26	3	98.48	0.55	0.51	0.40	0.07	100.00
F	Umbo	27	3	98.69	0.36	0.50	0.40	0.05	100.00
F	Umbo	28	3	98.50	0.41	0.51	0.52	0.07	100.00
F	Umbo	29	3	97.20	0.00	2.36	0.16	0.28	100.00
F	Umbo	30	3	97.37	0.00	2.31	0.13	0.19	100.00
F	Umbo	31	3	98.44	0.23	0.77	0.50	0.07	100.00
F	Umbo	32	3	98.61	0.22	0.73	0.38	0.06	100.00
F	Umbo	33	3	98.44	0.36	0.74	0.39	0.07	100.00
F	Umbo	34	3	97.09	0.02	2.47	0.15	0.26	100.00
F	Umbo	35	3	97.24	0.02	2.38	0.14	0.23	100.00
F	Umbo	36	3	97.27	0.04	2.36	0.11	0.22	100.00
F	Umbo	37	3	97.35	0.09	2.30	0.12	0.15	100.00
F	Umbo	38	3	97.68	0.05	1.88	0.17	0.23	100.00
F	Umbo	39	3	97.69	0.08	1.53	0.19	0.51	100.00
F	Mid	1	4	90.18	0.15	1.15	0.41	0.27	92.16
F	Mid	2	4	95.38	0.14	1.07	0.32	0.22	97.13
F	Mid	3	4	96.15	0.14	1.05	0.22	0.24	97.80
F	Mid	4	4	96.57	0.14	0.89	0.19	0.24	98.04
F	Mid	5	4	97.83	0.17	0.83	0.26	0.23	99.32
F	Mid	6	4	96.89	0.17	0.78	0.15	0.21	98.21
F	Mid	7	4	94.87	0.21	0.72	0.10	0.21	96.11
F	Mid	8	4	97.12	0.27	0.75	0.15	0.24	98.53
F	Mid	9	4	97.30	0.27	0.68	0.10	0.22	98.57
F	Mid	10	4	97.85	0.25	0.64	0.13	0.19	99.05
F	Mid	11	4	97.55	0.25	0.59	0.14	0.15	98.68
F	Mid	12	4	98.19	0.29	0.54	0.10	0.18	99.31
F	Mid	13	4	97.92	0.27	0.47	0.10	0.14	98.91
F	Mid	14	4	98.18	0.29	0.49	0.12	0.17	99.25
F	Mid	15	4	97.89	0.32	0.44	0.24	0.14	99.04
F	Mid	16	4	93.17	0.00	1.24	0.13	0.25	94.79
F	Mid	17	4	95.24	0.00	1.24	0.16	0.34	96.97
F	Mid	18	4	95.48	0.00	1.16	0.19	0.24	97.07
F	Mid	19	4	95.68	0.00	1.22	0.25	0.26	97.41
F	Mid	20	4	95.20	0.00	1.20	0.15	0.19	96.75
F	Mid	21	4	95.46	0.00	1.15	0.15	0.26	97.01
F	Mid	22	4	94.93	0.00	1.17	0.19	0.24	96.52
F	Mid	23	4	95.25	0.00	1.13	0.22	0.24	96.84
F	Mid	24	4	95.92	0.00	1.11	0.22	0.18	97.42
F	Mid	25	4	94.50	0.00	1.23	0.23	0.20	96.15
F	Mid	26	4	95.11	0.00	1.10	0.19	0.26	96.67
F	Mid	27	4	95.44	0.00	1.10	0.23	0.26	97.03
F	Mid	28	4	95.71	0.00	1.17	0.32	0.25	97.45
F	Mid	29	4	95.24	0.00	1.11	0.40	0.22	96.98
F	Mid	30	4	96.12	0.00	1.13	0.25	0.22	97.71
F	Mid	31	4	95.49	0.00	1.05	0.31	0.26	97.12
F	Mid	32	4	95.40	0.00	1.00	0.27	0.41	97.07
F	Mid	33	4	95.74	0.00	1.02	0.25	0.57	97.58
F	Mid	34	4	95.82	0.00	1.03	0.24	0.39	97.49
F	Mid	35	4	96.06	0.00	1.04	0.22	0.31	97.63
F	Mid	36	4	95.71	0.00	1.05	0.22	0.34	97.32

F	Mid	37	4	96.19	0.00	1.06	0.27	0.39	97.91
F	Mid	38	4	95.73	0.01	1.04	0.24	0.41	97.44
F	Mid	39	4	94.69	0.00	0.88	0.19	0.77	96.53
F	Mid	1	5	95.08	0.33	1.36	0.31	0.26	97.33
F	Mid	2	5	97.54	0.30	1.26	0.22	0.22	99.53
F	Mid	3	5	97.13	0.33	1.10	0.20	0.20	98.96
F	Mid	4	5	97.67	0.34	1.03	0.19	0.22	99.44
F	Mid	5	5	98.24	0.36	1.00	0.20	0.22	100.02
F	Mid	6	5	98.45	0.35	0.96	0.20	0.21	100.17
F	Mid	7	5	98.82	0.38	0.93	0.14	0.22	100.49
F	Mid	8	5	98.44	0.42	0.84	0.13	0.19	100.02
F	Mid	9	5	98.75	0.32	0.80	0.17	0.20	100.23
F	Mid	10	5	98.52	0.37	0.88	0.12	0.18	100.08
F	Mid	11	5	98.40	0.45	0.87	0.12	0.20	100.03
F	Mid	12	5	95.18	0.48	0.82	0.10	0.19	96.76
F	Mid	13	5	99.12	0.57	0.80	0.14	0.20	100.83
F	Mid	14	5	98.31	0.63	0.82	0.13	0.21	100.10
F	Mid	15	5	99.04	0.67	0.77	0.10	0.19	100.77
F	Mid	16	5	100.16	0.59	0.69	0.08	0.19	101.71
F	Mid	17	5	99.69	0.54	0.66	0.08	0.18	101.16
F	Mid	18	5	99.42	0.62	0.74	0.11	0.16	101.05
F	Mid	19	5	95.11	0.61	0.70	0.09	0.14	96.64
F	Mid	20	5	100.09	0.60	0.63	0.10	0.17	101.58
F	Mid	21	5	99.78	0.63	0.55	0.10	0.13	101.19
F	Mid	22	5	99.15	0.64	0.60	0.10	0.17	100.67
F	Mid	23	5	99.55	0.65	0.52	0.11	0.16	100.98
F	Mid	24	5	100.62	0.41	0.41	0.17	0.15	101.76
F	Mid	25	5	97.80	0.04	1.15	0.18	0.24	99.40
F	Mid	26	5	97.31	0.00	1.17	0.19	0.19	98.85
F	Mid	27	5	97.26	0.01	1.16	0.18	0.21	98.83
F	Mid	28	5	97.42	0.01	1.10	0.17	0.18	98.87
F	Mid	29	5	97.97	0.00	1.06	0.16	0.16	99.35
F	Mid	30	5	97.50	0.00	1.15	0.15	0.18	98.98
F	Mid	31	5	97.32	0.00	1.10	0.16	0.18	98.75
F	Mid	32	5	98.54	0.00	1.04	0.20	0.21	100.00
F	Mid	33	5	98.12	0.01	1.14	0.20	0.22	99.69
F	Mid	34	5	96.74	0.02	1.12	0.22	0.22	98.32
F	Mid	35	5	98.40	0.00	1.13	0.22	0.21	99.97
F	Mid	36	5	99.07	0.02	1.10	0.23	0.21	100.63
F	Mid	37	5	97.55	0.01	1.11	0.18	0.22	99.07
F	Mid	38	5	96.82	0.02	1.01	0.18	0.20	98.24
F	Mid	39	5	98.42	0.02	1.07	0.21	0.19	99.91
F	Mid	40	5	98.82	0.03	0.95	0.25	0.35	100.40
F	Mid	41	5	98.41	0.04	1.08	0.20	0.47	100.20
F	Mid	42	5	97.17	0.00	1.05	0.19	0.29	98.70
F	Mid	43	5	98.21	0.00	1.07	0.21	0.24	99.72
F	Mid	44	5	98.76	0.01	1.03	0.22	0.25	100.26
F	Mid	45	5	98.08	0.01	1.07	0.24	0.22	99.62
F	Mid	46	5	97.67	0.00	1.00	0.23	0.29	99.20
F	Mid	47	5	97.63	0.00	1.10	0.17	0.29	99.19
F	Mid	48	5	98.44	0.00	1.06	0.19	0.25	99.95
F	Mid	49	5	98.19	0.00	1.04	0.21	0.23	99.68
F	Mid	50	5	97.04	0.01	1.03	0.21	0.21	98.50
F	Mid	51	5	98.10	0.01	1.03	0.22	0.19	99.55
F	Mid	52	5	97.89	0.00	1.09	0.24	0.22	99.44
F	Mid	53	5	98.38	0.02	1.11	0.24	0.23	99.99
F	Mid	54	5	98.64	0.00	1.13	0.26	0.24	100.27
F	Mid	55	5	98.69	0.01	1.12	0.25	0.28	100.35

F	Mid	56	5	99.47	0.01	1.07	0.24	0.24	101.03
F	Mid	57	5	99.35	0.01	0.78	0.23	0.57	100.94
F	Mid	58	5	97.36	0.00	0.70	0.28	0.83	99.17
F	Mid	1	6	97.36	0.59	1.70	0.18	0.18	100.00
F	Mid	2	6	97.81	0.61	1.33	0.10	0.15	100.00
F	Mid	3	6	97.62	0.63	1.53	0.08	0.14	100.00
F	Mid	4	6	97.54	0.86	1.41	0.06	0.14	100.00
F	Mid	5	6	97.51	0.98	1.30	0.06	0.15	100.00
F	Mid	6	6	97.94	0.75	1.18	0.03	0.10	100.00
F	Mid	7	6	97.82	0.83	1.23	0.03	0.10	100.00
F	Mid	8	6	98.10	0.76	1.02	0.03	0.10	100.00
F	Mid	9	6	98.21	0.85	0.81	0.04	0.09	100.00
F	Mid	10	6	98.10	0.84	0.93	0.04	0.09	100.00
F	Mid	11	6	97.02	0.03	2.66	0.09	0.19	100.00
F	Mid	12	6	96.82	0.00	2.91	0.11	0.16	100.00
F	Mid	13	6	96.95	0.10	2.68	0.11	0.16	100.00
F	Mid	14	6	97.56	0.07	1.66	0.13	0.59	100.00
F	Mid	15	6	97.06	0.02	2.62	0.11	0.19	100.00
F	Mid	16	6	97.41	0.01	2.33	0.09	0.15	100.00
F	Mid	17	6	97.32	0.03	2.40	0.10	0.15	100.00
F	Mid	18	6	97.02	0.06	2.58	0.12	0.22	100.00
F	Mid	19	6	97.91	0.03	1.71	0.14	0.22	100.00
F	Edge	1	7	94.21	0.28	1.12	0.49	0.24	96.34
F	Edge	2	7	95.93	0.22	0.89	0.31	0.27	97.61
F	Edge	3	7	97.97	0.27	0.93	0.14	0.21	99.52
F	Edge	4	7	97.50	0.34	0.98	0.24	0.28	99.33
F	Edge	5	7	97.67	0.38	0.77	0.18	0.28	99.29
F	Edge	6	7	97.04	0.39	0.78	0.16	0.27	98.63
F	Edge	7	7	97.89	0.39	0.67	0.08	0.22	99.24
F	Edge	8	7	97.88	0.48	0.68	0.12	0.20	99.37
F	Edge	9	7	97.67	0.44	0.72	0.11	0.21	99.14
F	Edge	10	7	98.29	0.48	0.67	0.11	0.21	99.76
F	Edge	11	7	97.23	0.47	0.72	0.14	0.21	98.77
F	Edge	12	7	97.79	0.55	0.70	0.02	0.21	99.26
F	Edge	13	7	98.31	0.59	0.71	0.09	0.16	99.87
F	Edge	14	7	99.19	0.53	0.72	0.02	0.22	100.68
F	Edge	15	7	98.86	0.57	0.66	0.04	0.24	100.36
F	Edge	16	7	99.04	0.54	0.50	0.11	0.14	100.33
F	Edge	17	7	98.68	0.60	0.48	0.16	0.17	100.09
F	Edge	18	7	98.53	0.61	0.52	0.13	0.20	99.99
F	Edge	19	7	98.31	0.58	0.40	0.03	0.21	99.54
F	Edge	20	7	98.68	0.69	0.36	0.09	0.16	99.97
F	Edge	21	7	98.43	0.59	0.22	0.09	0.18	99.52
F	Edge	22	7	98.94	0.60	0.24	0.23	0.12	100.14
F	Edge	23	7	95.53	0.00	1.08	0.18	0.42	97.21
F	Edge	24	7	96.48	0.00	1.17	0.31	0.36	98.32
F	Edge	25	7	96.68	0.00	1.13	0.21	0.28	98.29
F	Edge	26	7	96.53	0.02	1.08	0.26	0.35	98.24
F	Edge	27	7	95.86	0.00	0.76	0.32	0.78	97.71
F	Edge	28	7	96.59	0.03	1.11	0.26	0.52	98.51
F	Edge	29	7	96.53	0.01	0.96	0.21	0.40	98.11
F	Edge	30	7	96.95	0.00	1.18	0.19	0.36	98.68
F	Edge	31	7	95.87	0.00	1.26	0.23	0.37	97.72
F	Edge	32	7	97.30	0.00	1.22	0.27	0.43	99.21
F	Edge	33	7	96.21	0.00	1.04	0.31	0.55	98.11
F	Edge	1	8	86.64	0.16	0.52	0.60	0.09	88.01
F	Edge	2	8	96.22	0.27	1.17	0.30	0.26	98.21
F	Edge	3	8	97.27	0.25	0.96	0.27	0.21	98.96

F	Edge	4	8	97.55	0.28	0.94	0.24	0.21	99.22
F	Edge	5	8	98.09	0.29	0.93	0.26	0.19	99.76
F	Edge	6	8	97.68	0.32	0.88	0.23	0.20	99.31
F	Edge	7	8	97.63	0.31	0.90	0.22	0.18	99.24
F	Edge	8	8	97.69	0.34	0.86	0.23	0.19	99.30
F	Edge	9	8	98.02	0.36	0.81	0.19	0.20	99.58
F	Edge	10	8	98.15	0.37	0.79	0.25	0.19	99.74
F	Edge	11	8	98.47	0.38	0.83	0.19	0.19	100.06
F	Edge	12	8	97.91	0.40	0.72	0.22	0.18	99.42
F	Edge	13	8	98.42	0.42	0.71	0.20	0.19	99.94
F	Edge	14	8	98.04	0.40	0.67	0.16	0.17	99.45
F	Edge	15	8	98.74	0.41	0.69	0.15	0.19	100.18
F	Edge	16	8	98.35	0.41	0.70	0.12	0.16	99.74
F	Edge	17	8	99.07	0.44	0.65	0.16	0.16	100.48
F	Edge	18	8	98.35	0.44	0.67	0.13	0.16	99.76
F	Edge	19	8	98.86	0.48	0.62	0.13	0.16	100.26
F	Edge	20	8	98.48	0.46	0.65	0.13	0.16	99.88
F	Edge	21	8	98.51	0.48	0.61	0.11	0.16	99.86
F	Edge	22	8	98.66	0.47	0.60	0.12	0.17	100.02
F	Edge	23	8	98.37	0.46	0.57	0.13	0.16	99.69
F	Edge	24	8	98.74	0.46	0.54	0.10	0.17	100.01
F	Edge	25	8	99.27	0.46	0.53	0.10	0.15	100.51
F	Edge	26	8	98.90	0.47	0.54	0.09	0.15	100.15
F	Edge	27	8	99.09	0.47	0.52	0.11	0.16	100.35
F	Edge	28	8	99.32	0.47	0.53	0.09	0.14	100.56
F	Edge	29	8	98.70	0.46	0.49	0.11	0.15	99.92
F	Edge	30	8	99.26	0.47	0.52	0.10	0.14	100.48
F	Edge	31	8	99.04	0.48	0.53	0.10	0.15	100.30
F	Edge	32	8	99.44	0.47	0.50	0.10	0.16	100.66
F	Edge	33	8	98.73	0.46	0.48	0.10	0.14	99.91
F	Edge	34	8	99.25	0.47	0.46	0.08	0.16	100.42
F	Edge	35	8	99.11	0.49	0.47	0.07	0.16	100.29
F	Edge	36	8	99.13	0.52	0.44	0.10	0.15	100.33
F	Edge	37	8	99.03	0.49	0.43	0.11	0.15	100.22
F	Edge	38	8	99.27	0.48	0.37	0.19	0.14	100.45
F	Edge	39	8	97.45	0.36	0.65	0.18	0.27	98.90
F	Edge	40	8	97.62	0.32	0.74	0.20	0.26	99.13
F	Edge	41	8	97.26	0.29	0.83	0.23	0.31	98.91
F	Edge	42	8	97.73	0.16	0.92	0.24	0.33	99.39
F	Edge	43	8	97.42	0.19	0.86	0.26	0.39	99.11
F	Edge	44	8	93.50	0.09	0.64	0.42	0.68	95.33
F	Edge	1	9	98.31	0.29	1.15	0.14	0.11	100.00
F	Edge	2	9	98.49	0.29	0.94	0.14	0.14	100.00
F	Edge	3	9	98.47	0.35	0.92	0.15	0.11	100.00
F	Edge	4	9	98.68	0.32	0.73	0.14	0.13	100.00
F	Edge	5	9	98.74	0.37	0.65	0.12	0.12	100.00
F	Edge	6	9	98.59	0.45	0.77	0.12	0.07	100.00
F	Edge	7	9	98.40	0.64	0.77	0.10	0.10	100.00
F	Edge	8	9	98.63	0.61	0.64	0.05	0.07	100.00
F	Edge	9	9	98.61	0.59	0.66	0.04	0.09	100.00
F	Edge	10	9	98.42	0.67	0.79	0.05	0.08	100.00
F	Edge	11	9	98.32	0.68	0.84	0.04	0.12	100.00
F	Edge	12	9	98.59	0.60	0.68	0.04	0.10	100.00
F	Edge	13	9	98.47	0.64	0.70	0.07	0.12	100.00
F	Edge	14	9	98.76	0.63	0.45	0.06	0.10	100.00
F	Edge	15	9	98.99	0.40	0.29	0.21	0.12	100.00
F	Edge	16	9	99.10	0.21	0.37	0.20	0.11	100.00
F	Edge	17	9	98.61	0.30	0.32	0.64	0.13	100.00

F	Edge	18	9	98.86	0.47	0.26	0.28	0.13	100.00

A.2 Electron Microprobe analyses expressed as elements (wt%)

Onto. Stage	Shell Area	Point	Line	Ca	Mg	Na	S	Sr	Total
A	Umbo	1	1	39.45	0.22	0.17	0.17	0.08	40.10
A	Umbo	2	1	40.67	0.18	0.11	0.21	0.08	41.25
A	Umbo	3	1	36.91	0.01	0.49	0.04	0.12	37.57
A	Umbo	4	1	37.55	0.01	0.60	0.03	0.11	38.30
A	Umbo	5	1	36.96	0.00	0.58	0.05	0.15	37.74
A	Umbo	6	1	37.46	0.01	0.51	0.04	0.13	38.15
A	Umbo	7	1	37.01	0.01	0.53	0.04	0.14	37.72
A	Umbo	8	1	36.62	0.02	0.33	0.02	0.40	37.38
A	Umbo	9	1	37.73	0.02	0.36	0.04	0.21	38.37
A	Umbo	10	1	37.34	0.03	0.51	0.05	0.16	38.08
A	Umbo	11	1	39.80	0.02	0.30	0.02	0.20	40.34
A	Umbo	12	1	35.95	0.01	0.43	0.05	0.20	36.64
A	Umbo	1	2	38.71	0.20	0.24	0.15	0.07	39.35
A	Umbo	2	2	38.68	0.20	0.23	0.14	0.09	39.33
A	Umbo	3	2	38.25	0.01	0.38	0.02	0.16	38.82
A	Umbo	4	2	38.57	0.00	0.39	0.01	0.09	39.06
A	Umbo	5	2	38.23	0.01	0.57	0.03	0.11	38.96
A	Umbo	6	2	36.46	0.00	0.48	0.05	0.14	37.13
A	Umbo	7	2	36.30	0.01	0.47	0.03	0.15	36.96
A	Umbo	8	2	32.25	0.01	0.47	0.04	0.11	32.88
A	Umbo	9	2	36.28	0.02	0.54	0.05	0.18	37.06
A	Umbo	10	2	36.89	0.02	0.59	0.05	0.13	37.68
A	Umbo	11	2	31.22	0.03	0.45	0.05	0.24	32.00
A	Umbo	12	2	36.98	0.03	0.39	0.04	0.23	37.66
A	Umbo	13	2	37.58	0.04	0.48	0.05	0.20	38.34
A	Umbo	1	3	40.62	0.21	0.09	0.15	0.08	41.14
A	Umbo	2	3	40.60	0.15	0.08	0.18	0.11	41.12
A	Umbo	3	3	40.35	0.17	0.10	0.12	0.10	40.84
A	Umbo	4	3	40.43	0.16	0.10	0.12	0.07	40.89
A	Umbo	5	3	39.70	0.16	0.10	0.12	0.13	40.20
A	Umbo	6	3	40.21	0.20	0.05	0.20	0.14	40.78
A	Umbo	7	3	40.68	0.18	0.13	0.20	0.07	41.25
A	Mid	1	4	39.81	0.13	0.21	0.09	0.09	40.33
A	Mid	2	4	39.58	0.09	0.28	0.08	0.11	40.14
A	Mid	3	4	40.16	0.07	0.20	0.09	0.09	40.61
A	Mid	4	4	40.27	0.08	0.13	0.08	0.07	40.64
A	Mid	5	4	37.47	0.01	0.48	0.04	0.14	38.14
A	Mid	1	5	38.34	0.09	0.48	0.05	0.11	39.07
A	Mid	2	5	38.59	0.11	0.34	0.06	0.10	39.20
A	Mid	3	5	38.15	0.07	0.28	0.05	0.06	38.62
A	Mid	4	5	38.93	0.09	0.19	0.07	0.10	39.39
A	Mid	5	5	37.33	0.02	0.49	0.03	0.08	37.95
A	Mid	6	5	36.79	0.00	0.45	0.03	0.14	37.40
A	Mid	7	5	37.38	0.01	0.50	0.03	0.10	38.02
A	Mid	8	5	36.61	0.03	0.33	0.04	0.32	37.32
A	Mid	1	6	41.30	0.12	0.13	0.10	0.12	41.77
A	Mid	2	6	40.96	0.13	0.18	0.06	0.11	41.44
A	Mid	3	6	39.01	0.16	0.18	0.07	0.07	39.48
A	Mid	4	6	37.38	0.01	0.33	0.02	0.15	37.89
A	Mid	5	6	38.24	0.02	0.41	0.03	0.15	38.86

A	Edge	1	7	39.53	0.07	0.30	0.05	0.12	40.07
A	Edge	2	7	36.09	0.10	0.17	0.06	0.12	36.54
A	Edge	3	7	39.96	0.19	0.09	0.13	0.11	40.47
A	Edge	4	7	39.97	0.20	0.09	0.17	0.08	40.51
A	Edge	1	8	38.39	0.07	0.24	0.05	0.09	38.85
A	Edge	2	8	38.29	0.08	0.25	0.03	0.07	38.72
A	Edge	3	8	38.08	0.07	0.24	0.04	0.11	38.55
A	Edge	4	8	38.17	0.11	0.22	0.06	0.06	38.61
A	Edge	5	8	38.33	0.17	0.19	0.08	0.09	38.86
A	Edge	6	8	38.55	0.34	0.09	0.11	0.09	39.19
A	Edge	7	8	38.30	0.35	0.07	0.18	0.10	39.00
A	Edge	1	9	40.54	0.09	0.15	0.11	0.12	41.00
A	Edge	2	9	40.06	0.10	0.14	0.10	0.10	40.49
A	Edge	3	9	40.38	0.11	0.13	0.08	0.09	40.79
A	Edge	4	9	40.65	0.12	0.09	0.07	0.08	41.01
A	Edge	5	9	40.50	0.20	0.06	0.16	0.17	41.09
B	Umbo	1	1	34.44	0.16	0.15	0.09	0.05	34.88
B	Umbo	2	1	38.48	0.16	0.14	0.07	0.08	38.92
B	Umbo	3	1	38.79	0.28	0.26	0.13	0.10	39.56
B	Umbo	4	1	38.83	0.10	0.24	0.07	0.07	39.31
B	Umbo	5	1	38.49	0.07	0.12	0.04	0.08	38.81
B	Umbo	6	1	38.79	0.10	0.18	0.06	0.08	39.21
B	Umbo	7	1	38.80	0.13	0.16	0.08	0.07	39.23
B	Umbo	8	1	38.82	0.22	0.16	0.09	0.09	39.38
B	Umbo	9	1	39.30	0.12	0.13	0.08	0.05	39.67
B	Umbo	10	1	38.68	0.13	0.11	0.05	0.09	39.06
B	Umbo	11	1	38.71	0.15	0.15	0.05	0.07	39.14
B	Umbo	12	1	38.77	0.14	0.13	0.06	0.06	39.15
B	Umbo	13	1	38.40	0.12	0.11	0.05	0.05	38.73
B	Umbo	14	1	37.76	0.11	0.11	0.05	0.06	38.09
B	Umbo	15	1	38.17	0.17	0.10	0.16	0.09	38.70
B	Umbo	16	1	37.89	0.11	0.11	0.14	0.09	38.34
B	Umbo	17	1	37.85	0.10	0.10	0.11	0.09	38.25
B	Umbo	18	1	38.30	0.12	0.08	0.09	0.09	38.68
B	Umbo	19	1	39.02	0.17	0.08	0.10	0.08	39.46
B	Umbo	20	1	38.12	0.14	0.17	0.08	0.10	38.61
B	Umbo	21	1	38.69	0.14	0.15	0.07	0.06	39.10
B	Umbo	22	1	38.68	0.08	0.43	0.07	0.22	39.47
B	Umbo	1	2	40.35	0.11	0.18	0.05	0.12	40.81
B	Umbo	2	2	36.11	0.08	0.16	0.04	0.11	36.51
B	Umbo	3	2	36.40	0.12	0.14	0.03	0.10	36.79
B	Umbo	4	2	36.23	0.10	0.12	0.06	0.07	36.57
B	Umbo	5	2	36.41	0.12	0.11	0.08	0.10	36.81
B	Umbo	6	2	38.49	0.15	0.06	0.08	0.10	38.88
B	Umbo	7	2	36.09	0.14	0.12	0.08	0.08	36.52
B	Umbo	8	2	36.44	0.12	0.06	0.09	0.08	36.79
B	Umbo	9	2	36.11	0.13	0.08	0.08	0.09	36.48
B	Umbo	10	2	36.22	0.12	0.08	0.06	0.09	36.56
B	Umbo	11	2	36.25	0.13	0.08	0.19	0.08	36.73
B	Umbo	12	2	36.15	0.12	0.05	0.10	0.11	36.52
B	Umbo	13	2	35.95	0.17	0.08	0.10	0.11	36.42
B	Umbo	14	2	36.62	0.14	0.08	0.06	0.10	37.01
B	Umbo	15	2	36.57	0.10	0.11	0.06	0.10	36.93
B	Umbo	16	2	37.95	0.00	0.41	0.03	0.14	38.54
B	Umbo	17	2	37.64	0.00	0.29	0.04	0.16	38.12
B	Umbo	18	2	38.31	0.00	0.24	0.02	0.14	38.71
B	Umbo	19	2	37.30	0.00	0.38	0.03	0.12	37.82
B	Umbo	20	2	37.13	0.00	0.38	0.03	0.13	37.68

B	Umbo	21	2	36.93	0.03	0.38	0.02	0.12	37.47
B	Umbo	22	2	34.95	0.00	0.31	0.01	0.23	35.50
B	Umbo	23	2	1.58	0.03	0.04	0.51	0.00	2.16
B	Umbo	1	3	39.27	0.24	0.17	0.05	0.08	39.81
B	Umbo	2	3	40.46	0.18	0.21	0.07	0.15	41.06
B	Umbo	3	3	40.35	0.19	0.21	0.05	0.13	40.92
B	Umbo	4	3	40.75	0.20	0.20	0.05	0.14	41.33
B	Umbo	5	3	41.73	0.24	0.11	0.07	0.11	42.25
B	Umbo	6	3	40.74	0.16	0.11	0.06	0.10	41.16
B	Umbo	7	3	41.13	0.16	0.15	0.06	0.08	41.57
B	Umbo	8	3	41.08	0.13	0.11	0.06	0.07	41.46
B	Umbo	9	3	40.57	0.16	0.08	0.08	0.12	41.02
B	Umbo	10	3	41.23	0.26	0.10	0.13	0.09	41.81
B	Umbo	11	3	41.43	0.22	0.05	0.16	0.15	42.01
B	Umbo	12	3	40.69	0.37	0.06	0.19	0.10	41.40
B	Umbo	13	3	37.06	0.26	0.14	0.20	0.11	37.77
B	Mid	1	4	38.48	0.08	0.49	0.05	0.12	39.22
B	Mid	2	4	38.09	0.07	0.46	0.05	0.09	38.76
B	Mid	3	4	38.89	0.09	0.42	0.06	0.09	39.54
B	Mid	4	4	38.96	0.08	0.36	0.06	0.09	39.56
B	Mid	5	4	38.51	0.09	0.30	0.06	0.07	39.02
B	Mid	6	4	38.81	0.12	0.28	0.09	0.09	39.39
B	Mid	7	4	38.54	0.13	0.25	0.05	0.07	39.04
B	Mid	8	4	38.55	0.13	0.28	0.06	0.10	39.11
B	Mid	9	4	38.69	0.12	0.24	0.05	0.07	39.17
B	Mid	10	4	38.63	0.14	0.25	0.06	0.10	39.17
B	Mid	11	4	38.63	0.16	0.22	0.05	0.06	39.11
B	Mid	12	4	38.73	0.11	0.15	0.05	0.08	39.12
B	Mid	13	4	36.55	0.00	0.50	0.02	0.12	37.19
B	Mid	14	4	37.49	0.01	0.44	0.01	0.10	38.05
B	Mid	15	4	37.05	0.00	0.39	0.02	0.12	37.58
B	Mid	16	4	37.07	0.01	0.39	0.02	0.10	37.58
B	Mid	17	4	36.76	0.00	0.47	0.02	0.10	37.34
B	Mid	18	4	37.26	0.00	0.41	0.01	0.10	37.78
B	Mid	19	4	37.31	0.01	0.42	0.01	0.10	37.85
B	Mid	20	4	37.76	0.01	0.45	0.02	0.07	38.31
B	Mid	21	4	36.78	0.00	0.46	0.01	0.11	37.37
B	Mid	22	4	37.40	0.02	0.34	0.02	0.06	37.84
B	Mid	23	4	36.16	0.00	0.39	0.01	0.10	36.67
B	Mid	24	4	37.59	0.01	0.46	0.01	0.10	38.17
B	Mid	25	4	36.92	0.01	0.47	0.03	0.09	37.52
B	Mid	26	4	37.00	0.01	0.41	0.03	0.13	37.57
B	Mid	27	4	37.28	0.01	0.27	0.03	0.25	37.84
B	Mid	28	4	36.57	0.02	0.36	0.03	0.17	37.15
B	Mid	1	5	38.36	0.09	0.37	0.07	0.10	38.99
B	Mid	2	5	39.50	0.08	0.20	0.07	0.10	39.95
B	Mid	3	5	39.90	0.08	0.15	0.08	0.11	40.33
B	Mid	4	5	39.40	0.08	0.15	0.05	0.06	39.74
B	Mid	5	5	36.49	0.09	0.14	0.06	0.11	36.88
B	Mid	6	5	36.58	0.10	0.17	0.05	0.11	37.01
B	Mid	7	5	37.29	0.12	0.16	0.05	0.14	37.76
B	Mid	8	5	36.63	0.12	0.14	0.06	0.10	37.05
B	Mid	9	5	35.45	0.11	0.15	0.05	0.17	35.94
B	Mid	10	5	38.64	0.07	0.13	0.06	0.13	39.05
B	Mid	11	5	36.83	0.00	0.44	0.01	0.14	37.42
B	Mid	12	5	38.24	0.00	0.31	0.02	0.14	38.71
B	Mid	13	5	38.65	0.00	0.31	0.01	0.12	39.09
B	Mid	14	5	37.25	0.00	0.43	0.02	0.13	37.84

B	Mid	15	5	38.07	0.00	0.28	0.02	0.12	38.49
B	Mid	16	5	37.37	0.01	0.31	0.02	0.15	37.87
B	Mid	17	5	37.09	0.01	0.31	0.02	0.14	37.56
B	Mid	18	5	37.30	0.01	0.29	0.03	0.13	37.75
B	Mid	19	5	36.45	0.00	0.39	0.03	0.13	37.00
B	Mid	20	5	36.39	0.01	0.45	0.03	0.19	37.07
B	Mid	1	6	39.99	0.45	0.11	0.18	0.12	40.85
B	Mid	2	6	42.01	0.46	0.05	0.13	0.15	42.80
B	Mid	3	6	41.01	0.35	0.06	0.15	0.17	41.75
B	Mid	4	6	41.93	0.16	0.05	0.22	0.14	42.50
B	Mid	5	6	41.71	0.14	0.06	0.20	0.12	42.23
B	Mid	6	6	41.70	0.09	0.06	0.07	0.12	42.04
B	Mid	7	6	41.07	0.11	0.12	0.11	0.09	41.49
B	Mid	8	6	41.68	0.11	0.08	0.07	0.09	42.04
B	Mid	9	6	42.27	0.10	0.08	0.07	0.07	42.58
B	Edge	1	7	37.19	0.14	0.56	0.06	0.12	38.07
B	Edge	2	7	37.81	0.07	0.49	0.04	0.09	38.50
B	Edge	3	7	37.69	0.06	0.31	0.06	0.13	38.25
B	Edge	4	7	38.19	0.07	0.35	0.05	0.13	38.78
B	Edge	5	7	38.03	0.08	0.27	0.04	0.15	38.57
B	Edge	6	7	38.06	0.10	0.39	0.03	0.08	38.65
B	Edge	7	7	37.78	0.10	0.31	0.04	0.09	38.32
B	Edge	8	7	38.35	0.08	0.35	0.03	0.05	38.86
B	Edge	9	7	38.37	0.08	0.35	0.03	0.08	38.90
B	Edge	10	7	38.09	0.09	0.31	0.03	0.08	38.60
B	Edge	11	7	38.16	0.10	0.32	0.03	0.12	38.72
B	Edge	12	7	37.82	0.11	0.28	0.02	0.10	38.33
B	Edge	13	7	38.43	0.11	0.24	0.02	0.06	38.86
B	Edge	14	7	38.30	0.09	0.26	0.02	0.07	38.75
B	Edge	15	7	38.49	0.09	0.17	0.03	0.08	38.86
B	Edge	16	7	36.83	0.00	0.46	0.02	0.11	37.42
B	Edge	17	7	37.55	0.00	0.51	0.02	0.12	38.19
B	Edge	18	7	37.59	0.01	0.51	0.01	0.06	38.18
B	Edge	19	7	37.63	0.01	0.46	0.01	0.12	38.23
B	Edge	20	7	33.35	0.01	0.48	0.02	0.12	33.97
B	Edge	21	7	37.35	0.02	0.39	0.02	0.10	37.87
B	Edge	22	7	36.90	0.03	0.35	0.03	0.26	37.57
B	Edge	1	8	37.56	0.24	0.34	0.12	0.17	38.42
B	Edge	2	8	37.41	0.06	0.34	0.05	0.14	38.00
B	Edge	3	8	35.97	0.07	0.24	0.06	0.17	36.51
B	Edge	4	8	36.21	0.10	0.28	0.03	0.10	36.73
B	Edge	5	8	37.36	0.09	0.23	0.03	0.12	37.83
B	Edge	6	8	36.18	0.10	0.20	0.03	0.12	36.63
B	Edge	7	8	36.47	0.11	0.23	0.02	0.07	36.91
B	Edge	8	8	36.51	0.11	0.23	0.02	0.12	36.99
B	Edge	9	8	36.21	0.10	0.19	0.02	0.13	36.65
B	Edge	10	8	38.64	0.09	0.11	0.03	0.09	38.96
B	Edge	11	8	38.19	0.00	0.37	0.02	0.11	38.69
B	Edge	12	8	37.93	0.00	0.35	0.02	0.11	38.41
B	Edge	13	8	37.19	0.03	0.34	0.02	0.14	37.71
B	Edge	14	8	36.73	0.01	0.32	0.03	0.14	37.23
B	Edge	15	8	35.92	0.02	0.35	0.02	0.17	36.48
B	Edge	16	8	36.21	0.02	0.33	0.04	0.28	36.88
B	Edge	1	9	40.68	0.11	0.29	0.04	0.13	41.25
B	Edge	2	9	40.66	0.08	0.27	0.07	0.11	41.19
B	Edge	3	9	40.04	0.08	0.25	0.05	0.11	40.54
B	Edge	4	9	40.99	0.10	0.24	0.05	0.13	41.50
B	Edge	5	9	41.23	0.15	0.13	0.05	0.14	41.70

B	Edge	6	9	41.08	0.17	0.16	0.05	0.11	41.57
B	Edge	7	9	41.21	0.11	0.20	0.02	0.12	41.67
B	Edge	8	9	40.62	0.11	0.16	0.04	0.11	41.04
B	Edge	9	9	39.51	0.11	0.14	0.08	0.13	39.96
C	Umbo	1	1	40.55	0.06	0.16	0.17	0.10	41.05
C	Umbo	2	1	39.89	0.05	0.10	0.13	0.13	40.30
C	Umbo	3	1	41.22	0.05	0.11	0.11	0.09	41.58
C	Umbo	4	1	41.42	0.09	0.13	0.16	0.11	41.90
C	Umbo	5	1	41.01	0.07	0.11	0.09	0.09	41.36
C	Umbo	6	1	40.90	0.08	0.10	0.10	0.09	41.26
C	Umbo	7	1	40.94	0.10	0.12	0.09	0.07	41.31
C	Umbo	8	1	41.14	0.10	0.10	0.08	0.07	41.48
C	Umbo	9	1	40.53	0.09	0.10	0.07	0.08	40.87
C	Umbo	10	1	41.32	0.13	0.10	0.09	0.10	41.73
C	Umbo	11	1	40.75	0.17	0.10	0.15	0.08	41.24
C	Umbo	12	1	41.56	0.20	0.11	0.28	0.06	42.21
C	Umbo	13	1	40.61	0.10	0.10	0.26	0.10	41.17
C	Umbo	14	1	41.57	0.08	0.08	0.16	0.09	41.99
C	Umbo	15	1	39.34	0.06	0.11	0.17	0.12	39.80
C	Umbo	16	1	40.01	0.06	0.19	0.10	0.08	40.45
C	Umbo	17	1	41.91	0.06	0.10	0.08	0.10	42.25
C	Umbo	18	1	41.38	0.06	0.12	0.11	0.10	41.76
C	Umbo	19	1	41.29	0.06	0.09	0.11	0.09	41.64
C	Umbo	20	1	39.67	0.11	0.12	0.12	0.10	40.12
C	Umbo	21	1	40.87	0.15	0.06	0.17	0.06	41.31
C	Umbo	22	1	40.57	0.16	0.09	0.18	0.08	41.08
C	Umbo	23	1	36.66	0.22	0.15	0.24	0.10	37.37
C	Umbo	24	1	38.65	0.01	0.38	0.06	0.51	39.60
C	Umbo	1	2	33.89	0.08	0.26	0.03	0.09	34.34
C	Umbo	2	2	34.64	0.12	0.22	0.02	0.09	35.10
C	Umbo	3	2	38.15	0.13	0.30	0.03	0.09	38.69
C	Umbo	4	2	39.71	0.14	0.20	0.03	0.06	40.13
C	Umbo	5	2	40.47	0.14	0.16	0.04	0.06	40.86
C	Umbo	6	2	39.70	0.12	0.14	0.05	0.06	40.08
C	Umbo	7	2	40.64	0.15	0.15	0.05	0.08	41.07
C	Umbo	8	2	38.90	0.02	0.56	0.03	0.08	39.57
C	Umbo	9	2	39.43	0.01	0.50	0.01	0.09	40.04
C	Umbo	10	2	38.22	0.00	0.54	0.02	0.08	38.86
C	Umbo	11	2	37.62	0.01	0.57	0.02	0.08	38.30
C	Umbo	12	2	39.07	0.01	0.54	0.03	0.08	39.71
C	Umbo	13	2	39.18	0.01	0.40	0.03	0.09	39.71
C	Umbo	14	2	39.02	0.01	0.41	0.02	0.09	39.55
C	Umbo	15	2	38.81	0.01	0.44	0.03	0.09	39.39
C	Umbo	16	2	37.67	0.02	0.62	0.03	0.10	38.42
C	Umbo	17	2	38.01	0.03	0.36	0.04	0.20	38.64
C	Umbo	18	2	37.49	0.00	0.46	0.03	0.21	38.19
C	Umbo	19	2	37.98	0.01	0.45	0.02	0.16	38.61
C	Umbo	20	2	37.58	0.00	0.52	0.02	0.14	38.26
C	Umbo	21	2	38.19	0.01	0.51	0.02	0.11	38.83
C	Umbo	22	2	39.65	0.02	0.44	0.03	0.12	40.24
C	Umbo	23	2	37.60	0.03	0.57	0.02	0.13	38.35
C	Umbo	24	2	37.12	0.03	0.44	0.03	0.37	37.99
C	Umbo	1	3	36.18	0.01	0.44	0.05	0.12	36.80
C	Umbo	2	3	39.59	0.00	0.43	0.07	0.15	40.24
C	Umbo	3	3	34.01	0.01	0.41	0.07	0.13	34.63
C	Umbo	4	3	39.62	0.00	0.42	0.06	0.14	40.25
C	Umbo	5	3	38.92	0.43	0.27	0.05	0.15	39.82
C	Umbo	6	3	37.88	0.02	0.41	0.05	0.11	38.46

C	Umbo	7	3	39.27	0.01	0.39	0.05	0.16	39.89
C	Umbo	8	3	39.14	0.00	0.40	0.05	0.17	39.76
C	Umbo	9	3	37.50	0.00	0.54	0.07	0.22	38.31
C	Umbo	10	3	37.65	0.01	0.48	0.05	0.31	38.50
C	Umbo	11	3	40.35	0.13	0.14	0.18	0.12	40.93
C	Umbo	12	3	40.36	0.09	0.17	0.17	0.10	40.89
C	Umbo	13	3	41.68	0.08	0.15	0.16	0.11	42.18
C	Umbo	14	3	40.68	0.10	0.21	0.16	0.11	41.25
C	Umbo	15	3	41.11	0.10	0.18	0.16	0.10	41.65
C	Umbo	16	3	41.33	0.11	0.12	0.15	0.12	41.82
C	Umbo	17	3	41.77	0.13	0.13	0.15	0.08	42.26
C	Umbo	18	3	40.26	0.16	0.14	0.18	0.12	40.87
C	Umbo	19	3	39.42	0.22	0.12	0.20	0.10	40.05
C	Umbo	20	3	42.00	0.24	0.12	0.28	0.09	42.73
C	Umbo	21	3	39.25	0.22	0.14	0.26	0.08	39.94
C	Umbo	22	3	37.54	0.01	0.41	0.06	0.35	38.36
C	Umbo	23	3	41.07	0.48	0.12	0.24	0.23	42.15
C	Umbo	24	3	40.87	0.16	0.09	0.27	0.10	41.48
C	Umbo	1	4	31.08	0.12	0.04	0.19	0.07	31.50
C	Umbo	2	4	38.75	0.17	0.07	0.22	0.09	39.29
C	Umbo	3	4	38.58	0.00	0.50	0.03	0.12	39.22
C	Umbo	4	4	39.14	0.01	0.47	0.04	0.14	39.79
C	Umbo	5	4	38.01	0.00	0.49	0.03	0.15	38.68
C	Umbo	6	4	39.52	0.00	0.37	0.05	0.14	40.07
C	Umbo	7	4	39.34	0.00	0.42	0.03	0.09	39.89
C	Umbo	8	4	37.38	0.03	0.42	0.05	0.21	38.08
C	Umbo	9	4	38.41	0.00	0.48	0.03	0.11	39.03
C	Umbo	10	4	39.14	0.01	0.38	0.05	0.13	39.70
C	Umbo	11	4	39.59	0.01	0.44	0.05	0.08	40.17
C	Umbo	12	4	38.00	0.00	0.42	0.04	0.14	38.60
C	Umbo	13	4	37.79	0.01	0.43	0.05	0.13	38.41
C	Umbo	14	4	38.55	0.00	0.44	0.07	0.14	39.20
C	Umbo	15	4	39.73	0.01	0.28	0.06	0.16	40.23
C	Umbo	16	4	37.78	0.00	0.47	0.06	0.12	38.42
C	Umbo	17	4	37.95	0.01	0.43	0.06	0.10	38.54
C	Umbo	18	4	39.08	0.01	0.42	0.05	0.17	39.73
C	Umbo	19	4	37.95	0.01	0.47	0.05	0.16	38.64
C	Umbo	20	4	37.63	0.01	0.45	0.05	0.17	38.31
C	Umbo	21	4	37.89	0.02	0.56	0.05	0.17	38.69
C	Umbo	22	4	37.43	0.02	0.58	0.05	0.18	38.27
C	Umbo	23	4	37.97	0.02	0.50	0.05	0.13	38.67
C	Umbo	24	4	37.47	0.02	0.44	0.05	0.17	38.14
C	Umbo	1	5	37.65	0.10	0.30	0.02	0.09	38.16
C	Umbo	2	5	38.39	0.11	0.32	0.03	0.10	38.95
C	Umbo	3	5	38.38	0.11	0.30	0.03	0.09	38.90
C	Umbo	4	5	38.64	0.09	0.31	0.04	0.09	39.16
C	Umbo	5	5	38.69	0.09	0.34	0.04	0.10	39.26
C	Umbo	6	5	38.40	0.09	0.25	0.03	0.08	38.86
C	Umbo	7	5	38.29	0.12	0.30	0.04	0.08	38.83
C	Umbo	8	5	38.34	0.10	0.26	0.03	0.07	38.80
C	Umbo	9	5	38.30	0.13	0.31	0.04	0.10	38.88
C	Umbo	10	5	38.59	0.11	0.26	0.04	0.08	39.09
C	Umbo	11	5	38.86	0.12	0.26	0.03	0.04	39.32
C	Umbo	12	5	38.74	0.12	0.28	0.02	0.08	39.24
C	Umbo	13	5	38.73	0.13	0.27	0.04	0.05	39.21
C	Umbo	14	5	38.65	0.12	0.25	0.02	0.09	39.13
C	Umbo	15	5	39.00	0.12	0.22	0.04	0.06	39.44
C	Umbo	16	5	38.56	0.12	0.22	0.04	0.06	39.00

C	Umbo	17	5	38.73	0.13	0.24	0.04	0.08	39.20
C	Umbo	18	5	38.88	0.11	0.20	0.04	0.07	39.30
C	Umbo	19	5	38.74	0.13	0.22	0.03	0.06	39.18
C	Umbo	20	5	38.99	0.12	0.26	0.04	0.04	39.44
C	Umbo	21	5	38.85	0.10	0.23	0.05	0.06	39.28
C	Umbo	22	5	38.87	0.13	0.21	0.03	0.06	39.30
C	Umbo	23	5	38.81	0.13	0.24	0.04	0.08	39.31
C	Umbo	24	5	39.20	0.15	0.22	0.08	0.08	39.72
C	Umbo	25	5	38.93	0.17	0.19	0.06	0.09	39.44
C	Umbo	26	5	38.72	0.20	0.19	0.07	0.09	39.27
C	Umbo	27	5	39.01	0.18	0.18	0.06	0.02	39.45
C	Umbo	28	5	39.04	0.18	0.16	0.06	0.06	39.50
C	Umbo	29	5	36.95	0.01	0.49	0.03	0.15	37.62
C	Umbo	30	5	35.61	0.01	0.39	0.02	0.09	36.12
C	Umbo	31	5	31.14	0.02	0.38	0.03	0.07	31.63
C	Umbo	32	5	30.50	0.01	0.44	0.03	0.11	31.09
C	Umbo	33	5	27.51	0.01	0.39	0.03	0.10	28.05
C	Umbo	34	5	29.25	0.01	0.37	0.02	0.10	29.75
C	Umbo	35	5	32.15	0.01	0.34	0.01	0.13	32.64
C	Umbo	36	5	37.74	0.01	0.40	0.01	0.14	38.30
C	Umbo	37	5	33.02	0.00	0.01	0.01	0.06	33.10
C	Mid	1	6	40.66	0.10	0.47	0.04	0.12	41.38
C	Mid	2	6	40.32	0.08	0.37	0.04	0.12	40.93
C	Mid	3	6	40.66	0.06	0.26	0.03	0.09	41.11
C	Mid	4	6	41.21	0.10	0.29	0.02	0.10	41.72
C	Mid	5	6	39.52	0.15	0.30	0.03	0.11	40.09
C	Mid	6	6	40.91	0.17	0.25	0.03	0.07	41.43
C	Mid	7	6	41.07	0.22	0.17	0.03	0.08	41.56
C	Mid	8	6	41.20	0.19	0.14	0.05	0.08	41.65
C	Mid	9	6	38.39	0.01	0.52	0.02	0.13	39.07
C	Mid	10	6	38.52	0.02	0.47	0.02	0.09	39.12
C	Mid	11	6	38.42	0.01	0.55	0.01	0.10	39.09
C	Mid	12	6	38.15	0.01	0.59	0.01	0.10	38.86
C	Mid	13	6	39.00	0.02	0.49	0.01	0.07	39.58
C	Mid	14	6	38.57	0.02	0.51	0.02	0.10	39.22
C	Mid	15	6	39.43	0.03	0.53	0.02	0.11	40.11
C	Mid	16	6	38.51	0.02	0.43	0.02	0.10	39.08
C	Mid	17	6	38.65	0.03	0.49	0.03	0.11	39.30
C	Mid	18	6	37.51	0.02	0.55	0.02	0.10	38.19
C	Mid	19	6	38.21	0.01	0.23	0.04	0.65	39.13
C	Mid	1	7	2.91	0.24	0.11	0.38	0.01	3.64
C	Mid	2	7	40.61	0.07	0.29	0.08	0.10	41.15
C	Mid	3	7	40.51	0.05	0.24	0.07	0.11	40.97
C	Mid	4	7	39.98	0.07	0.20	0.07	0.09	40.41
C	Mid	5	7	40.53	0.18	0.16	0.10	0.11	41.07
C	Mid	6	7	40.62	0.16	0.11	0.11	0.09	41.09
C	Mid	7	7	38.16	0.01	0.58	0.04	0.12	38.91
C	Mid	8	7	38.25	0.00	0.60	0.02	0.11	38.98
C	Mid	9	7	38.42	0.00	0.47	0.02	0.12	39.04
C	Mid	10	7	38.15	0.01	0.50	0.02	0.08	38.75
C	Mid	11	7	38.18	0.00	0.52	0.02	0.09	38.80
C	Mid	12	7	38.23	0.00	0.45	0.02	0.10	38.80
C	Mid	13	7	38.21	0.02	0.60	0.02	0.13	38.98
C	Mid	14	7	38.60	0.02	0.50	0.02	0.12	39.26
C	Mid	15	7	37.23	0.02	0.59	0.02	0.12	37.99
C	Mid	16	7	37.72	0.04	0.67	0.02	0.10	38.54
C	Mid	17	7	37.84	0.05	0.61	0.04	0.09	38.63
C	Mid	18	7	37.94	0.03	0.48	0.03	0.11	38.60

C	Mid	19	7	38.08	0.03	0.33	0.03	0.32	38.79
C	Mid	1	8	38.13	0.08	0.52	0.03	0.12	38.89
C	Mid	2	8	38.12	0.07	0.48	0.03	0.06	38.76
C	Mid	3	8	38.16	0.10	0.41	0.03	0.09	38.78
C	Mid	4	8	38.03	0.11	0.40	0.04	0.09	38.67
C	Mid	5	8	38.37	0.11	0.30	0.04	0.08	38.89
C	Mid	6	8	37.63	0.13	0.27	0.03	0.10	38.17
C	Mid	7	8	38.20	0.11	0.23	0.03	0.08	38.64
C	Mid	8	8	38.03	0.06	0.20	0.06	0.05	38.39
C	Mid	9	8	37.74	0.01	0.58	0.02	0.10	38.45
C	Mid	10	8	37.66	0.02	0.42	0.03	0.09	38.22
C	Mid	11	8	33.27	0.01	0.44	0.03	0.08	33.82
C	Mid	12	8	34.65	0.01	0.43	0.02	0.06	35.17
C	Mid	13	8	36.95	0.00	0.51	0.03	0.08	37.56
C	Mid	14	8	37.42	0.00	0.45	0.04	0.07	37.98
C	Mid	15	8	36.96	0.01	0.45	0.03	0.11	37.57
C	Mid	16	8	35.51	0.01	0.49	0.03	0.09	36.14
C	Mid	17	8	34.68	0.02	0.42	0.04	0.11	35.26
C	Mid	18	8	36.92	0.02	0.27	0.04	0.31	37.56
C	Edge	1	9	30.57	0.09	0.32	0.16	0.11	31.24
C	Edge	2	9	40.35	0.08	0.45	0.02	0.11	41.00
C	Edge	3	9	40.15	0.10	0.39	0.02	0.14	40.80
C	Edge	4	9	40.33	0.07	0.21	0.03	0.10	40.73
C	Edge	5	9	40.06	0.05	0.16	0.06	0.12	40.45
C	Edge	6	9	41.01	0.05	0.17	0.05	0.12	41.39
C	Edge	7	9	41.10	0.04	0.19	0.02	0.06	41.41
C	Edge	8	9	40.75	0.06	0.18	0.02	0.11	41.11
C	Edge	9	9	40.95	0.09	0.14	0.07	0.08	41.33
C	Edge	10	9	41.00	0.08	0.14	0.01	0.09	41.33
C	Edge	11	9	40.59	0.11	0.16	0.02	0.08	40.96
C	Edge	12	9	40.52	0.13	0.13	0.02	0.05	40.86
C	Edge	13	9	41.47	0.12	0.11	0.04	0.07	41.81
C	Edge	14	9	40.81	0.17	0.10	0.08	0.11	41.28
C	Edge	15	9	41.29	0.19	0.11	0.03	0.08	41.70
C	Edge	16	9	40.78	0.47	0.08	0.07	0.10	41.50
C	Edge	17	9	40.16	0.42	0.07	0.07	0.10	40.82
C	Edge	1	10	33.18	0.08	0.13	0.07	0.06	33.52
C	Edge	2	10	39.16	0.08	0.26	0.08	0.15	39.73
C	Edge	3	10	40.54	0.03	0.15	0.05	0.10	40.87
C	Edge	4	10	40.52	0.06	0.11	0.04	0.11	40.84
C	Edge	5	10	40.13	0.07	0.08	0.05	0.09	40.42
C	Edge	6	10	41.14	0.08	0.08	0.04	0.05	41.39
C	Edge	7	10	40.35	0.09	0.09	0.04	0.10	40.68
C	Edge	8	10	40.88	0.18	0.09	0.10	0.10	41.34
C	Edge	9	10	41.14	0.17	0.07	0.06	0.11	41.55
C	Edge	10	10	40.41	0.15	0.09	0.03	0.07	40.74
C	Edge	11	10	40.19	0.25	0.07	0.12	0.14	40.78
C	Edge	12	10	40.78	0.31	0.08	0.07	0.08	41.32
C	Edge	13	10	40.63	0.15	0.04	0.06	0.07	40.96
C	Edge	1	11	35.37	0.07	0.24	0.08	0.11	35.86
C	Edge	2	11	38.20	0.08	0.17	0.06	0.07	38.57
C	Edge	3	11	38.09	0.06	0.16	0.07	0.08	38.46
C	Edge	4	11	38.08	0.08	0.16	0.07	0.09	38.47
C	Edge	5	11	38.25	0.09	0.14	0.06	0.08	38.62
C	Edge	6	11	38.51	0.06	0.14	0.07	0.05	38.83
C	Edge	7	11	38.20	0.08	0.14	0.07	0.07	38.56
C	Edge	8	11	38.21	0.09	0.11	0.07	0.08	38.56
C	Edge	9	11	38.22	0.11	0.11	0.04	0.06	38.55

C	Edge	10	11	38.27	0.11	0.12	0.03	0.10	38.64
C	Edge	11	11	38.18	0.11	0.11	0.04	0.06	38.49
C	Edge	12	11	38.30	0.13	0.12	0.04	0.07	38.65
C	Edge	13	11	38.17	0.18	0.11	0.06	0.11	38.63
D	Umbo	1	1	37.56	0.00	0.60	0.02	0.11	38.29
D	Umbo	2	1	37.58	0.00	0.59	0.04	0.15	38.37
D	Umbo	3	1	38.84	0.01	0.53	0.03	0.09	39.48
D	Umbo	4	1	37.31	0.01	0.61	0.04	0.10	38.06
D	Umbo	5	1	37.38	0.01	0.66	0.03	0.13	38.22
D	Umbo	6	1	36.89	0.01	0.62	0.05	0.11	37.68
D	Umbo	7	1	37.35	0.01	0.52	0.05	0.13	38.05
D	Umbo	8	1	37.76	0.00	0.55	0.05	0.13	38.48
D	Umbo	9	1	37.21	0.01	0.65	0.04	0.11	38.02
D	Umbo	10	1	37.31	0.01	0.55	0.04	0.13	38.03
D	Umbo	11	1	36.90	0.01	0.50	0.04	0.20	37.64
D	Umbo	12	1	37.06	0.00	0.56	0.03	0.11	37.77
D	Umbo	13	1	40.85	0.07	0.16	0.18	0.06	41.32
D	Umbo	14	1	40.49	0.08	0.20	0.14	0.10	41.00
D	Umbo	15	1	40.60	0.10	0.24	0.12	0.10	41.15
D	Umbo	16	1	41.10	0.09	0.20	0.11	0.10	41.60
D	Umbo	17	1	41.23	0.07	0.20	0.11	0.09	41.69
D	Umbo	18	1	39.44	0.16	0.14	0.19	0.12	40.04
D	Umbo	19	1	40.69	0.15	0.12	0.17	0.08	41.21
D	Umbo	1	2	40.70	0.09	0.35	0.08	0.13	41.35
D	Umbo	2	2	41.21	0.08	0.20	0.06	0.12	41.68
D	Umbo	3	2	40.84	0.10	0.22	0.09	0.11	41.37
D	Umbo	4	2	37.10	0.01	0.69	0.03	0.12	37.95
D	Umbo	5	2	37.51	0.01	0.68	0.03	0.11	38.34
D	Umbo	6	2	37.89	0.01	0.56	0.04	0.12	38.61
D	Umbo	7	2	36.99	0.00	0.73	0.04	0.11	37.87
D	Umbo	8	2	37.50	0.00	0.68	0.03	0.06	38.27
D	Umbo	9	2	37.59	0.00	0.66	0.04	0.07	38.36
D	Umbo	10	2	37.16	0.01	0.77	0.04	0.07	38.05
D	Umbo	11	2	37.12	0.00	0.63	0.04	0.11	37.89
D	Umbo	12	2	37.24	0.00	0.56	0.04	0.10	37.94
D	Umbo	13	2	36.71	0.01	0.59	0.03	0.18	37.51
D	Umbo	14	2	37.41	0.00	0.55	0.03	0.13	38.12
D	Umbo	15	2	37.52	0.00	0.54	0.04	0.12	38.23
D	Umbo	16	2	37.04	0.00	0.51	0.04	0.12	37.71
D	Umbo	17	2	37.00	0.00	0.54	0.05	0.13	37.71
D	Umbo	18	2	37.49	0.00	0.47	0.05	0.13	38.13
D	Umbo	19	2	36.89	0.00	0.53	0.05	0.14	37.61
D	Umbo	20	2	37.49	0.01	0.57	0.04	0.15	38.26
D	Umbo	21	2	32.81	0.01	0.48	0.04	0.09	33.43
D	Umbo	22	2	37.25	0.00	0.51	0.04	0.14	37.93
D	Umbo	23	2	36.97	0.00	0.40	0.04	0.31	37.72
D	Umbo	24	2	39.13	0.01	0.42	0.06	0.29	39.91
D	Umbo	1	3	39.61	0.13	0.19	0.07	0.10	40.10
D	Umbo	2	3	39.30	0.11	0.19	0.06	0.10	39.75
D	Umbo	3	3	37.80	0.10	0.19	0.06	0.13	38.29
D	Umbo	4	3	37.04	0.12	0.20	0.07	0.08	37.51
D	Umbo	5	3	37.34	0.14	0.14	0.05	0.06	37.73
D	Umbo	6	3	37.32	0.14	0.15	0.05	0.07	37.74
D	Umbo	7	3	36.86	0.15	0.13	0.06	0.07	37.26
D	Umbo	8	3	35.16	0.01	0.54	0.03	0.13	35.87
D	Umbo	9	3	36.97	0.01	0.34	0.03	0.09	37.43
D	Umbo	10	3	37.20	0.01	0.31	0.02	0.10	37.64
D	Umbo	11	3	37.88	0.00	0.37	0.02	0.11	38.38

D	Umbo	12	3	37.24	0.00	0.36	0.03	0.10	37.73
D	Umbo	13	3	38.99	0.00	0.34	0.03	0.12	39.48
D	Umbo	14	3	37.33	0.01	0.58	0.03	0.08	38.03
D	Umbo	15	3	39.43	0.01	0.36	0.03	0.08	39.90
D	Umbo	16	3	38.14	0.00	0.35	0.03	0.08	38.60
D	Umbo	17	3	37.55	0.01	0.39	0.01	0.13	38.09
D	Umbo	18	3	37.90	0.02	0.51	0.03	0.10	38.56
D	Umbo	19	3	38.22	0.03	0.32	0.03	0.17	38.76
D	Umbo	20	3	36.94	0.01	0.48	0.04	0.16	37.63
D	Umbo	21	3	37.28	0.03	0.33	0.04	0.28	37.95
D	Umbo	22	3	37.67	0.01	0.37	0.03	0.13	38.21
D	Umbo	23	3	38.34	0.00	0.41	0.03	0.18	38.95
D	Umbo	24	3	38.26	0.00	0.32	0.03	0.12	38.73
D	Umbo	25	3	38.81	0.00	0.33	0.03	0.12	39.28
D	Umbo	26	3	38.36	0.00	0.31	0.02	0.12	38.82
D	Umbo	27	3	38.45	0.00	0.25	0.02	0.13	38.85
D	Umbo	28	3	38.11	0.00	0.28	0.03	0.14	38.56
D	Umbo	29	3	38.25	0.00	0.34	0.03	0.11	38.73
D	Umbo	30	3	36.54	0.01	0.46	0.02	0.14	37.16
D	Umbo	31	3	37.32	0.01	0.41	0.03	0.14	37.91
D	Umbo	32	3	38.50	0.01	0.40	0.03	0.14	39.08
D	Umbo	33	3	38.66	0.00	0.40	0.03	0.11	39.19
D	Umbo	34	3	38.99	0.01	0.40	0.03	0.13	39.57
D	Umbo	35	3	35.75	0.01	0.52	0.03	0.12	36.43
D	Umbo	36	3	38.50	0.01	0.42	0.04	0.12	39.08
D	Umbo	37	3	37.77	0.00	0.44	0.03	0.18	38.42
D	Umbo	38	3	35.27	0.01	0.36	0.04	0.18	35.85
D	Umbo	39	3	37.50	0.00	0.26	0.03	0.54	38.33
D	Umbo	1	4	39.69	0.08	0.40	0.04	0.08	40.28
D	Umbo	2	4	39.40	0.08	0.26	0.05	0.10	39.88
D	Umbo	3	4	39.49	0.10	0.24	0.05	0.06	39.95
D	Umbo	4	4	39.37	0.13	0.21	0.06	0.07	39.83
D	Umbo	5	4	39.43	0.12	0.20	0.05	0.07	39.87
D	Umbo	6	4	39.17	0.16	0.19	0.07	0.04	39.63
D	Umbo	7	4	37.52	0.01	0.53	0.03	0.07	38.17
D	Umbo	8	4	37.75	0.00	0.46	0.02	0.07	38.29
D	Umbo	9	4	37.91	0.01	0.41	0.03	0.08	38.43
D	Umbo	10	4	38.07	0.01	0.41	0.02	0.09	38.59
D	Umbo	11	4	37.80	0.01	0.32	0.02	0.06	38.21
D	Umbo	12	4	37.86	0.00	0.47	0.03	0.10	38.45
D	Umbo	13	4	37.91	0.00	0.45	0.02	0.08	38.47
D	Umbo	14	4	37.81	0.00	0.47	0.02	0.09	38.39
D	Umbo	15	4	38.22	0.01	0.48	0.02	0.04	38.77
D	Umbo	16	4	37.41	0.01	0.39	0.02	0.07	37.90
D	Umbo	17	4	37.75	0.02	0.40	0.03	0.14	38.34
D	Umbo	18	4	36.98	0.00	0.51	0.04	0.11	37.63
D	Umbo	19	4	37.52	0.02	0.47	0.03	0.16	38.20
D	Umbo	20	4	37.91	0.01	0.44	0.03	0.07	38.45
D	Umbo	21	4	37.58	0.01	0.46	0.02	0.12	38.19
D	Umbo	22	4	37.70	0.00	0.45	0.02	0.09	38.26
D	Umbo	23	4	37.83	0.00	0.49	0.03	0.10	38.46
D	Umbo	24	4	37.50	0.00	0.43	0.03	0.10	38.06
D	Umbo	25	4	37.80	0.01	0.43	0.03	0.07	38.33
D	Umbo	26	4	37.99	0.00	0.47	0.02	0.10	38.58
D	Umbo	27	4	37.39	0.00	0.46	0.03	0.10	37.98
D	Umbo	28	4	37.48	0.01	0.50	0.04	0.12	38.15
D	Umbo	29	4	37.84	0.00	0.56	0.04	0.10	38.54
D	Umbo	30	4	38.19	0.00	0.56	0.03	0.09	38.87

D	Umbo	31	4	37.73	0.01	0.53	0.02	0.11	38.40
D	Umbo	32	4	37.28	0.00	0.52	0.03	0.13	37.96
D	Umbo	33	4	37.26	0.01	0.55	0.02	0.13	37.97
D	Umbo	34	4	36.97	0.01	0.43	0.03	0.21	37.64
D	Umbo	1	5	36.62	0.00	0.48	0.04	0.18	37.32
D	Umbo	2	5	38.58	0.05	0.22	0.10	0.10	39.05
D	Umbo	3	5	41.32	0.08	0.09	0.18	0.04	41.71
D	Umbo	4	5	41.60	0.08	0.10	0.22	0.06	42.07
D	Umbo	5	5	38.53	0.09	0.13	0.17	0.04	38.95
D	Umbo	6	5	38.73	0.08	0.12	0.17	0.04	39.14
D	Umbo	7	5	41.70	0.12	0.10	0.21	0.06	42.19
D	Umbo	8	5	35.81	0.03	0.40	0.07	0.54	36.85
D	Umbo	9	5	37.67	0.02	0.22	0.08	0.15	38.13
D	Umbo	10	5	39.67	0.08	0.10	0.18	0.08	40.12
D	Umbo	11	5	39.01	0.08	0.10	0.15	0.09	39.44
D	Umbo	12	5	40.02	0.09	0.10	0.15	0.09	40.45
D	Umbo	13	5	41.02	0.06	0.12	0.14	0.07	41.41
D	Umbo	14	5	41.05	0.12	0.07	0.16	0.14	41.54
D	Umbo	15	5	40.88	0.09	0.11	0.17	0.08	41.33
D	Umbo	16	5	40.75	0.09	0.07	0.13	0.06	41.09
D	Umbo	17	5	38.49	0.09	0.10	0.13	0.08	38.89
D	Umbo	18	5	40.62	0.11	0.08	0.12	0.05	40.98
D	Umbo	19	5	39.26	0.10	0.11	0.11	0.09	39.67
D	Umbo	20	5	39.54	0.12	0.09	0.11	0.10	39.96
D	Umbo	21	5	39.79	0.14	0.07	0.13	0.06	40.18
D	Umbo	22	5	40.99	0.13	0.12	0.11	0.05	41.40
D	Umbo	23	5	41.10	0.17	0.09	0.17	0.10	41.62
D	Umbo	24	5	38.04	0.19	0.12	0.25	0.16	38.76
D	Umbo	1	6	32.44	0.01	0.39	0.03	0.08	32.94
D	Umbo	2	6	37.09	0.00	0.35	0.03	0.12	37.60
D	Umbo	3	6	36.57	0.01	0.42	0.05	0.13	37.17
D	Umbo	4	6	38.86	0.00	0.41	0.04	0.13	39.45
D	Umbo	5	6	39.01	0.00	0.48	0.05	0.10	39.64
D	Umbo	6	6	38.15	0.00	0.36	0.04	0.10	38.66
D	Umbo	7	6	38.27	0.00	0.38	0.04	0.08	38.76
D	Umbo	8	6	38.18	0.00	0.35	0.04	0.18	38.76
D	Umbo	9	6	38.99	0.05	0.29	0.12	0.14	39.58
D	Umbo	10	6	40.68	0.07	0.11	0.16	0.07	41.08
D	Umbo	11	6	40.19	0.10	0.12	0.17	0.06	40.63
D	Umbo	12	6	41.05	0.08	0.13	0.17	0.06	41.49
D	Umbo	13	6	40.53	0.09	0.11	0.14	0.09	40.96
D	Umbo	14	6	41.27	0.09	0.09	0.17	0.11	41.73
D	Umbo	15	6	40.24	0.11	0.10	0.18	0.09	40.72
D	Umbo	16	6	41.42	0.14	0.10	0.17	0.10	41.92
D	Umbo	17	6	40.65	0.13	0.11	0.15	0.08	41.11
D	Umbo	18	6	40.54	0.11	0.14	0.17	0.09	41.05
D	Umbo	19	6	40.91	0.13	0.11	0.16	0.10	41.41
D	Umbo	20	6	40.29	0.12	0.10	0.14	0.08	40.73
D	Umbo	21	6	41.38	0.13	0.07	0.16	0.09	41.82
D	Umbo	22	6	38.74	0.11	0.08	0.18	0.14	39.25
D	Umbo	23	6	40.98	0.10	0.09	0.24	0.09	41.50
D	Umbo	24	6	35.41	0.10	0.15	0.26	0.13	36.04
D	Mid	1	7	40.37	0.11	0.46	0.07	0.15	41.15
D	Mid	2	7	41.01	0.11	0.37	0.05	0.11	41.65
D	Mid	3	7	40.57	0.11	0.39	0.04	0.12	41.22
D	Mid	4	7	40.15	0.15	0.30	0.03	0.11	40.74
D	Mid	5	7	40.83	0.14	0.26	0.03	0.10	41.37
D	Mid	6	7	40.76	0.14	0.18	0.03	0.12	41.23

D	Mid	7	7	37.41	0.03	0.42	0.04	0.16	38.06
D	Mid	8	7	37.28	0.01	0.71	0.05	0.12	38.17
D	Mid	9	7	37.14	0.01	0.66	0.03	0.11	37.95
D	Mid	10	7	37.24	0.03	0.54	0.02	0.16	37.99
D	Mid	11	7	37.24	0.00	0.56	0.03	0.16	37.99
D	Mid	12	7	37.40	0.01	0.58	0.03	0.12	38.14
D	Mid	13	7	37.58	0.00	0.55	0.04	0.10	38.27
D	Mid	14	7	38.22	0.00	0.47	0.04	0.15	38.87
D	Mid	15	7	37.65	0.02	0.41	0.04	0.18	38.30
D	Mid	1	8	36.68	0.11	0.49	0.04	0.12	37.44
D	Mid	2	8	37.65	0.06	0.27	0.04	0.13	38.15
D	Mid	3	8	37.84	0.09	0.24	0.06	0.12	38.35
D	Mid	4	8	37.45	0.10	0.27	0.02	0.09	37.93
D	Mid	5	8	38.05	0.14	0.23	0.02	0.06	38.49
D	Mid	6	8	37.90	0.18	0.16	0.04	0.10	38.38
D	Mid	7	8	38.36	0.17	0.10	0.12	0.06	38.82
D	Mid	8	8	37.66	0.15	0.08	0.17	0.12	38.18
D	Mid	9	8	37.73	0.13	0.08	0.07	0.07	38.08
D	Mid	10	8	37.60	0.13	0.08	0.10	0.09	37.99
D	Mid	11	8	37.94	0.00	0.36	0.01	0.21	38.51
D	Mid	12	8	37.77	0.02	0.40	0.02	0.17	38.37
D	Mid	13	8	37.84	0.01	0.38	0.03	0.19	38.45
D	Mid	14	8	37.45	0.02	0.35	0.02	0.15	37.99
D	Mid	15	8	36.33	0.01	0.38	0.02	0.19	36.93
D	Mid	16	8	35.38	0.03	0.47	0.03	0.15	36.06
D	Mid	1	9	34.07	0.11	0.43	0.11	0.16	34.88
D	Mid	2	9	40.95	0.08	0.18	0.08	0.10	41.40
D	Mid	3	9	39.74	0.08	0.29	0.06	0.13	40.30
D	Mid	4	9	40.02	0.07	0.16	0.11	0.15	40.51
D	Mid	5	9	39.35	0.05	0.15	0.06	0.08	39.69
D	Mid	6	9	40.10	0.04	0.14	0.03	0.05	40.36
D	Mid	7	9	40.70	0.09	0.21	0.06	0.07	41.13
D	Mid	8	9	38.32	0.00	0.49	0.04	0.14	38.99
D	Mid	9	9	39.01	0.00	0.47	0.04	0.10	39.62
D	Mid	10	9	39.04	0.00	0.38	0.03	0.10	39.55
D	Mid	11	9	36.50	0.01	0.28	0.04	0.37	37.19
D	Edge	1	10	38.30	0.08	0.38	0.04	0.12	38.92
D	Edge	2	10	39.79	0.08	0.28	0.06	0.16	40.37
D	Edge	3	10	40.31	0.08	0.17	0.05	0.13	40.74
D	Edge	4	10	41.63	0.09	0.20	0.07	0.10	42.09
D	Edge	5	10	39.98	0.12	0.21	0.07	0.12	40.50
D	Edge	6	10	37.89	0.07	0.08	0.06	0.10	38.19
D	Edge	7	10	34.46	0.08	0.09	0.11	0.11	34.84
D	Edge	8	10	36.46	0.09	0.12	0.17	0.11	36.95
D	Edge	9	10	40.40	0.13	0.10	0.18	0.12	40.92
D	Edge	10	10	41.22	0.08	0.07	0.17	0.12	41.65
D	Edge	11	10	40.61	0.07	0.07	0.15	0.10	40.99
D	Edge	12	10	41.01	0.03	0.06	0.14	0.16	41.39
D	Edge	13	10	41.81	0.05	0.04	0.16	0.12	42.17
D	Edge	14	10	41.30	0.05	0.07	0.16	0.12	41.70
D	Edge	1	11	38.77	0.08	0.41	0.03	0.14	39.43
D	Edge	2	11	39.02	0.07	0.27	0.03	0.12	39.51
D	Edge	3	11	38.64	0.09	0.27	0.03	0.11	39.14
D	Edge	4	11	38.50	0.10	0.26	0.02	0.10	38.98
D	Edge	5	11	38.57	0.09	0.23	0.03	0.11	39.02
D	Edge	6	11	38.65	0.10	0.23	0.02	0.11	39.11
D	Edge	7	11	39.05	0.11	0.26	0.01	0.12	39.55
D	Edge	8	11	38.92	0.11	0.19	0.02	0.13	39.36

D	Edge	9	11	39.20	0.15	0.19	0.02	0.13	39.68
D	Edge	10	11	39.25	0.15	0.19	0.02	0.12	39.73
D	Edge	11	11	39.59	0.11	0.18	0.02	0.10	39.99
D	Edge	12	11	38.85	0.13	0.13	0.01	0.09	39.21
D	Edge	13	11	39.38	0.13	0.15	0.01	0.10	39.77
D	Edge	14	11	38.91	0.12	0.11	0.02	0.10	39.25
D	Edge	15	11	33.99	0.15	0.13	0.03	0.06	34.36
D	Edge	16	11	27.63	0.02	0.31	0.03	0.20	28.19
D	Edge	1	12	39.91	0.14	0.29	0.04	0.15	40.51
D	Edge	2	12	39.18	0.13	0.28	0.04	0.13	39.77
D	Edge	3	12	39.32	0.14	0.23	0.04	0.12	39.84
D	Edge	4	12	40.01	0.13	0.20	0.04	0.12	40.51
D	Edge	5	12	39.73	0.13	0.20	0.03	0.12	40.20
D	Edge	6	12	39.96	0.12	0.16	0.03	0.12	40.39
D	Edge	7	12	39.84	0.11	0.12	0.04	0.07	40.17
D	Edge	8	12	39.57	0.13	0.12	0.01	0.11	39.94
D	Edge	9	12	40.01	0.13	0.11	0.03	0.11	40.40
D	Edge	10	12	40.02	0.12	0.09	0.06	0.09	40.37
D	Edge	11	12	39.45	0.11	0.10	0.04	0.08	39.78
D	Edge	12	12	39.87	0.12	0.10	0.04	0.11	40.23
D	Edge	13	12	39.81	0.16	0.05	0.08	0.12	40.22
E	Umbo	1	1	38.86	0.15	0.26	0.04	0.10	39.40
E	Umbo	2	1	39.65	0.16	0.18	0.04	0.10	40.14
E	Umbo	3	1	39.37	0.18	0.17	0.05	0.14	39.90
E	Umbo	4	1	41.15	0.18	0.14	0.05	0.06	41.58
E	Umbo	5	1	39.09	0.15	0.14	0.05	0.10	39.51
E	Umbo	6	1	41.43	0.15	0.10	0.06	0.09	41.83
E	Umbo	7	1	41.55	0.15	0.08	0.07	0.12	41.96
E	Umbo	8	1	42.04	0.16	0.10	0.12	0.08	42.50
E	Umbo	9	1	38.20	0.13	0.09	0.12	0.08	38.62
E	Umbo	10	1	40.62	0.08	0.12	0.11	0.11	41.05
E	Umbo	11	1	41.25	0.09	0.09	0.07	0.11	41.61
E	Umbo	12	1	41.87	0.09	0.11	0.11	0.07	42.25
E	Umbo	13	1	41.11	0.12	0.13	0.07	0.07	41.49
E	Umbo	14	1	40.80	0.13	0.14	0.07	0.08	41.22
E	Umbo	15	1	40.31	0.17	0.16	0.08	0.08	40.79
E	Umbo	16	1	37.98	0.00	0.50	0.03	0.16	38.67
E	Umbo	17	1	36.95	0.01	0.54	0.02	0.14	37.65
E	Umbo	18	1	38.87	0.01	0.46	0.02	0.13	39.48
E	Umbo	19	1	32.10	0.01	0.41	0.04	0.12	32.68
E	Umbo	1	2	36.14	0.14	0.22	0.05	0.11	36.65
E	Umbo	2	2	40.26	0.13	0.21	0.03	0.13	40.76
E	Umbo	3	2	39.41	0.14	0.18	0.04	0.12	39.89
E	Umbo	4	2	40.83	0.13	0.16	0.05	0.08	41.25
E	Umbo	5	2	41.14	0.15	0.21	0.03	0.09	41.62
E	Umbo	6	2	40.81	0.17	0.23	0.03	0.10	41.34
E	Umbo	7	2	40.86	0.17	0.18	0.03	0.11	41.35
E	Umbo	8	2	41.01	0.15	0.19	0.03	0.10	41.48
E	Umbo	9	2	40.70	0.15	0.16	0.02	0.10	41.13
E	Umbo	10	2	40.91	0.20	0.16	0.04	0.07	41.37
E	Umbo	11	2	40.60	0.23	0.09	0.17	0.08	41.17
E	Umbo	12	2	40.09	0.10	0.13	0.17	0.14	40.64
E	Umbo	13	2	41.08	0.08	0.12	0.08	0.07	41.44
E	Umbo	14	2	40.47	0.09	0.19	0.08	0.11	40.95
E	Umbo	15	2	41.09	0.12	0.14	0.07	0.04	41.46
E	Umbo	16	2	40.79	0.14	0.13	0.08	0.10	41.25
E	Umbo	17	2	38.05	0.06	0.30	0.05	0.19	38.65
E	Umbo	18	2	38.33	0.00	0.49	0.02	0.12	38.95

E	Umbo	19	2	37.31	0.01	0.38	0.04	0.14	37.88
E	Umbo	1	3	38.61	0.14	0.33	0.07	0.08	39.24
E	Umbo	2	3	38.22	0.16	0.29	0.05	0.09	38.81
E	Umbo	3	3	37.54	0.00	0.46	0.03	0.08	38.11
E	Umbo	4	3	37.19	0.01	0.51	0.02	0.07	37.80
E	Umbo	5	3	38.00	0.00	0.43	0.02	0.07	38.52
E	Umbo	6	3	37.88	0.01	0.55	0.03	0.06	38.53
E	Umbo	7	3	37.48	0.01	0.61	0.03	0.04	38.17
E	Umbo	8	3	38.09	0.01	0.42	0.03	0.14	38.70
E	Umbo	9	3	37.02	0.00	0.42	0.03	0.15	37.62
E	Umbo	10	3	37.89	0.01	0.45	0.05	0.12	38.51
E	Umbo	11	3	37.72	0.01	0.48	0.04	0.15	38.39
E	Umbo	12	3	36.95	0.00	0.42	0.04	0.10	37.51
E	Umbo	13	3	36.98	0.01	0.41	0.05	0.14	37.58
E	Umbo	14	3	36.33	0.01	0.39	0.04	0.29	37.05
E	Umbo	15	3	37.78	0.00	0.52	0.04	0.10	38.44
E	Umbo	16	3	37.47	0.01	0.39	0.03	0.09	37.98
E	Umbo	17	3	37.10	0.00	0.39	0.04	0.14	37.66
E	Umbo	18	3	37.44	0.00	0.42	0.04	0.11	38.02
E	Umbo	19	3	37.27	0.00	0.40	0.04	0.09	37.80
E	Umbo	20	3	36.89	0.00	0.39	0.05	0.11	37.44
E	Umbo	21	3	37.21	0.00	0.48	0.04	0.13	37.86
E	Umbo	22	3	37.75	0.00	0.60	0.04	0.09	38.48
E	Umbo	23	3	37.79	0.02	0.52	0.04	0.08	38.45
E	Umbo	24	3	37.53	0.01	0.53	0.05	0.10	38.22
E	Umbo	25	3	37.25	0.00	0.55	0.04	0.09	37.94
E	Umbo	26	3	37.25	0.00	0.68	0.04	0.05	38.02
E	Umbo	27	3	37.77	0.01	0.58	0.05	0.08	38.48
E	Umbo	28	3	37.16	0.02	0.34	0.06	0.15	37.72
E	Umbo	29	3	37.33	0.01	0.48	0.05	0.11	37.96
E	Umbo	30	3	37.14	0.01	0.44	0.04	0.19	37.82
E	Umbo	31	3	37.54	0.00	0.40	0.04	0.10	38.07
E	Umbo	32	3	37.06	0.01	0.40	0.03	0.11	37.61
E	Umbo	33	3	37.65	0.00	0.57	0.04	0.11	38.38
E	Umbo	34	3	37.34	0.00	0.52	0.04	0.08	37.99
E	Umbo	35	3	37.74	0.00	0.58	0.05	0.07	38.44
E	Umbo	36	3	37.34	0.00	0.48	0.05	0.09	37.95
E	Umbo	37	3	37.53	0.00	0.58	0.06	0.09	38.26
E	Umbo	38	3	37.74	0.01	0.50	0.05	0.06	38.36
E	Umbo	39	3	8.03	0.01	0.12	0.07	0.09	8.32
E	Mid	1	4	37.89	0.15	0.40	0.10	0.12	38.66
E	Mid	2	4	40.57	0.16	0.15	0.09	0.16	41.13
E	Mid	3	4	40.94	0.11	0.17	0.06	0.11	41.40
E	Mid	4	4	39.96	0.14	0.21	0.04	0.11	40.46
E	Mid	5	4	41.04	0.17	0.23	0.04	0.11	41.58
E	Mid	6	4	40.12	0.19	0.17	0.03	0.11	40.61
E	Mid	7	4	41.39	0.18	0.18	0.03	0.10	41.88
E	Mid	8	4	40.59	0.20	0.21	0.02	0.07	41.08
E	Mid	9	4	41.41	0.19	0.19	0.02	0.11	41.91
E	Mid	10	4	40.40	0.20	0.15	0.01	0.10	40.86
E	Mid	11	4	40.43	0.21	0.15	0.02	0.08	40.88
E	Mid	12	4	40.87	0.18	0.15	0.02	0.09	41.30
E	Mid	13	4	40.70	0.21	0.11	0.04	0.07	41.12
E	Mid	14	4	40.37	0.18	0.12	0.05	0.08	40.79
E	Mid	15	4	40.25	0.19	0.13	0.06	0.10	40.72
E	Mid	16	4	41.19	0.16	0.13	0.05	0.06	41.59
E	Mid	17	4	40.76	0.15	0.10	0.05	0.08	41.13
E	Mid	18	4	39.80	0.17	0.10	0.08	0.08	40.24

E	Mid	19	4	38.27	0.03	0.24	0.04	0.49	39.08
E	Mid	20	4	36.74	0.01	0.58	0.03	0.14	37.49
E	Mid	21	4	36.21	0.01	0.65	0.03	0.19	37.10
E	Mid	22	4	37.00	0.02	0.67	0.02	0.17	37.88
E	Mid	23	4	36.45	0.01	0.61	0.02	0.13	37.21
E	Mid	24	4	39.34	0.00	0.42	0.03	0.12	39.92
E	Mid	25	4	37.30	0.00	0.45	0.02	0.15	37.93
E	Mid	1	5	39.57	0.10	0.29	0.04	0.11	40.11
E	Mid	2	5	39.54	0.10	0.25	0.05	0.10	40.06
E	Mid	3	5	40.46	0.14	0.24	0.03	0.09	40.96
E	Mid	4	5	39.16	0.20	0.19	0.02	0.06	39.63
E	Mid	5	5	41.03	0.19	0.26	0.01	0.08	41.58
E	Mid	6	5	40.54	0.19	0.24	0.01	0.08	41.06
E	Mid	7	5	41.15	0.23	0.16	0.02	0.05	41.60
E	Mid	8	5	39.61	0.17	0.18	0.11	0.07	40.14
E	Mid	9	5	41.05	0.17	0.08	0.05	0.06	41.41
E	Mid	10	5	39.74	0.17	0.17	0.05	0.09	40.22
E	Mid	11	5	40.30	0.15	0.13	0.06	0.04	40.68
E	Mid	12	5	40.25	0.15	0.14	0.05	0.06	40.65
E	Mid	13	5	25.62	0.01	0.24	0.02	0.21	26.11
E	Mid	14	5	38.02	0.00	0.54	0.01	0.13	38.70
E	Mid	15	5	37.23	0.01	0.45	0.01	0.14	37.84
E	Mid	16	5	37.72	0.01	0.29	0.03	0.15	38.19
E	Mid	17	5	38.53	0.00	0.49	0.01	0.12	39.15
E	Mid	18	5	38.72	0.02	0.20	0.02	0.30	39.26
E	Mid	1	6	38.65	0.08	0.45	0.05	0.11	39.34
E	Mid	2	6	38.13	0.07	0.30	0.06	0.09	38.65
E	Mid	3	6	38.79	0.09	0.34	0.09	0.09	39.40
E	Mid	4	6	38.00	0.09	0.32	0.05	0.08	38.54
E	Mid	5	6	37.15	0.15	0.37	0.04	0.12	37.82
E	Mid	6	6	38.68	0.14	0.34	0.04	0.09	39.29
E	Mid	7	6	37.15	0.13	0.33	0.04	0.11	37.76
E	Mid	8	6	36.95	0.00	0.43	0.03	0.08	37.49
E	Mid	9	6	36.93	0.00	0.43	0.03	0.11	37.50
E	Mid	10	6	36.66	0.01	0.38	0.03	0.15	37.23
E	Mid	11	6	36.66	0.00	0.47	0.04	0.18	37.35
E	Mid	12	6	36.93	0.01	0.36	0.04	0.09	37.42
E	Mid	13	6	37.26	0.00	0.45	0.03	0.10	37.84
E	Mid	14	6	36.87	0.00	0.40	0.03	0.12	37.42
E	Mid	15	6	37.27	0.00	0.42	0.03	0.08	37.79
E	Mid	16	6	36.89	0.00	0.44	0.02	0.11	37.46
E	Mid	17	6	37.47	0.01	0.42	0.04	0.08	38.01
E	Mid	18	6	37.50	0.01	0.50	0.04	0.09	38.12
E	Mid	19	6	37.50	0.01	0.46	0.03	0.10	38.10
E	Mid	20	6	37.38	0.00	0.54	0.04	0.08	38.04
E	Mid	21	6	37.40	0.00	0.50	0.04	0.07	38.01
E	Mid	22	6	37.22	0.02	0.47	0.04	0.11	37.86
E	Mid	23	6	37.58	0.01	0.58	0.04	0.07	38.28
E	Mid	24	6	37.68	0.02	0.44	0.04	0.15	38.34
E	Mid	25	6	36.99	0.00	0.58	0.04	0.07	37.68
E	Mid	26	6	38.17	0.01	0.56	0.04	0.07	38.84
E	Mid	27	6	37.03	0.01	0.42	0.03	0.15	37.64
E	Mid	28	6	37.78	0.00	0.54	0.02	0.10	38.44
E	Mid	29	6	37.90	0.00	0.54	0.03	0.09	38.56
E	Mid	30	6	37.63	0.01	0.50	0.02	0.06	38.22
E	Mid	31	6	37.88	0.01	0.56	0.03	0.08	38.55
E	Mid	32	6	36.96	0.00	0.64	0.03	0.05	37.68
E	Mid	33	6	37.05	0.01	0.50	0.03	0.09	37.68

E	Mid	34	6	37.91	0.02	0.52	0.03	0.07	38.55
E	Mid	35	6	37.17	0.00	0.52	0.03	0.04	37.76
E	Mid	36	6	37.70	0.00	0.51	0.02	0.07	38.30
E	Mid	37	6	38.12	0.00	0.56	0.04	0.08	38.81
E	Mid	38	6	37.09	0.02	0.55	0.05	0.07	37.78
E	Mid	39	6	36.58	0.03	0.38	0.05	0.24	37.28
E	Edge	1	7	36.50	0.06	0.25	0.04	0.06	36.92
E	Edge	2	7	38.34	0.05	0.19	0.03	0.08	38.69
E	Edge	3	7	38.66	0.10	0.17	0.03	0.12	39.09
E	Edge	4	7	38.28	0.10	0.20	0.05	0.10	38.73
E	Edge	5	7	38.73	0.07	0.13	0.04	0.10	39.07
E	Edge	6	7	38.85	0.10	0.11	0.16	0.12	39.33
E	Edge	7	7	39.25	0.10	0.14	0.04	0.06	39.59
E	Edge	8	7	38.28	0.12	0.11	0.18	0.10	38.79
E	Edge	9	7	38.27	0.11	0.13	0.08	0.08	38.66
E	Edge	10	7	39.19	0.08	0.11	0.03	0.03	39.42
E	Edge	11	7	38.26	0.10	0.14	0.04	0.09	38.62
E	Edge	12	7	38.23	0.11	0.12	0.03	0.10	38.60
E	Edge	13	7	40.13	0.04	0.07	0.19	0.12	40.55
E	Edge	14	7	39.50	0.06	0.11	0.08	0.07	39.80
E	Edge	1	8	39.39	0.12	0.22	0.05	0.07	39.85
E	Edge	2	8	39.00	0.07	0.18	0.04	0.08	39.37
E	Edge	3	8	39.25	0.08	0.16	0.05	0.10	39.64
E	Edge	4	8	39.25	0.06	0.11	0.05	0.11	39.59
E	Edge	5	8	39.33	0.07	0.13	0.05	0.12	39.70
E	Edge	6	8	38.72	0.12	0.18	0.02	0.10	39.13
E	Edge	7	8	39.06	0.12	0.15	0.02	0.07	39.43
E	Edge	8	8	39.39	0.15	0.16	0.04	0.08	39.81
E	Edge	9	8	39.32	0.15	0.15	0.01	0.06	39.70
E	Edge	10	8	38.89	0.13	0.12	0.03	0.06	39.23
E	Edge	11	8	39.73	0.08	0.08	0.04	0.10	40.02
E	Edge	1	9	36.62	0.09	0.24	0.03	0.12	37.10
E	Edge	2	9	35.96	0.07	0.36	0.03	0.12	36.53
E	Edge	3	9	36.85	0.07	0.29	0.02	0.11	37.33
E	Edge	4	9	36.62	0.07	0.26	0.02	0.13	37.10
E	Edge	5	9	35.58	0.09	0.23	0.01	0.08	35.99
E	Edge	6	9	36.20	0.10	0.21	0.01	0.09	36.60
E	Edge	7	9	36.23	0.11	0.23	0.01	0.09	36.68
E	Edge	8	9	36.62	0.10	0.23	0.01	0.10	37.06
E	Edge	9	9	36.85	0.12	0.23	0.01	0.09	37.30
E	Edge	10	9	36.64	0.14	0.20	0.01	0.09	37.07
E	Edge	11	9	35.78	0.12	0.20	0.01	0.10	36.21
E	Edge	12	9	37.00	0.14	0.17	0.02	0.08	37.40
E	Edge	13	9	36.46	0.14	0.17	0.00	0.07	36.84
E	Edge	14	9	37.16	0.16	0.14	0.01	0.06	37.53
E	Edge	15	9	36.43	0.17	0.16	0.01	0.08	36.85
E	Edge	16	9	37.40	0.18	0.12	0.01	0.08	37.79
E	Edge	17	9	36.94	0.15	0.12	0.00	0.08	37.30
E	Edge	18	9	37.81	0.28	0.10	0.02	0.07	38.28
E	Edge	19	9	39.21	0.36	0.09	0.06	0.07	39.78
F	Umbo	1	1	36.44	0.12	0.32	0.17	0.23	37.29
F	Umbo	2	1	37.51	0.11	0.35	0.15	0.19	38.30
F	Umbo	3	1	38.63	0.10	0.34	0.11	0.17	39.34
F	Umbo	4	1	38.06	0.10	0.38	0.13	0.15	38.82
F	Umbo	5	1	37.05	0.11	0.37	0.10	0.16	37.79
F	Umbo	6	1	36.83	0.10	0.44	0.08	0.16	37.61
F	Umbo	7	1	37.63	0.12	0.42	0.10	0.16	38.43
F	Umbo	8	1	38.16	0.11	0.37	0.10	0.16	38.91

F	Umbo	9	1	38.33	0.09	0.35	0.08	0.15	39.00
F	Umbo	10	1	37.77	0.08	0.30	0.07	0.17	38.39
F	Umbo	11	1	37.54	0.11	0.31	0.07	0.14	38.17
F	Umbo	12	1	38.13	0.11	0.29	0.04	0.11	38.69
F	Umbo	13	1	38.38	0.11	0.19	0.04	0.11	38.83
F	Umbo	14	1	37.85	0.03	0.39	0.04	0.19	38.51
F	Umbo	15	1	37.03	0.00	0.54	0.06	0.20	37.83
F	Umbo	16	1	37.11	0.00	0.56	0.04	0.16	37.88
F	Umbo	17	1	37.20	0.00	0.55	0.06	0.17	37.99
F	Umbo	18	1	37.02	0.00	0.54	0.03	0.15	37.74
F	Umbo	19	1	37.19	0.00	0.55	0.05	0.13	37.92
F	Umbo	20	1	36.75	0.00	0.53	0.05	0.11	37.44
F	Umbo	21	1	37.11	0.00	0.52	0.05	0.13	37.82
F	Umbo	22	1	37.85	0.00	0.49	0.06	0.12	38.51
F	Umbo	23	1	37.60	0.00	0.57	0.05	0.11	38.32
F	Umbo	24	1	37.46	0.00	0.55	0.04	0.08	38.12
F	Umbo	25	1	37.44	0.00	0.52	0.06	0.09	38.12
F	Umbo	26	1	37.43	0.00	0.51	0.05	0.09	38.08
F	Umbo	27	1	36.70	0.00	0.47	0.05	0.09	37.31
F	Umbo	28	1	37.40	0.00	0.54	0.06	0.13	38.14
F	Umbo	29	1	36.85	0.00	0.51	0.07	0.14	37.57
F	Umbo	30	1	37.15	0.00	0.51	0.04	0.13	37.83
F	Umbo	31	1	37.63	0.00	0.50	0.03	0.16	38.33
F	Umbo	32	1	37.29	0.00	0.45	0.07	0.23	38.05
F	Umbo	33	1	37.16	0.01	0.47	0.05	0.34	38.03
F	Umbo	34	1	37.30	0.00	0.45	0.04	0.20	38.00
F	Umbo	35	1	36.77	0.00	0.49	0.02	0.17	37.45
F	Umbo	36	1	37.16	0.00	0.47	0.05	0.21	37.90
F	Umbo	37	1	37.72	0.01	0.47	0.07	0.17	38.44
F	Umbo	38	1	36.93	0.00	0.42	0.06	0.32	37.72
F	Umbo	1	2	27.61	0.05	0.15	0.14	0.02	27.96
F	Umbo	2	2	35.38	0.10	0.37	0.10	0.10	36.05
F	Umbo	3	2	38.25	0.12	0.46	0.08	0.17	39.08
F	Umbo	4	2	38.36	0.11	0.42	0.09	0.16	39.13
F	Umbo	5	2	38.18	0.11	0.34	0.09	0.12	38.84
F	Umbo	6	2	39.01	0.10	0.35	0.11	0.14	39.70
F	Umbo	7	2	38.94	0.11	0.35	0.10	0.14	39.64
F	Umbo	8	2	39.19	0.12	0.35	0.10	0.15	39.90
F	Umbo	9	2	38.93	0.11	0.32	0.09	0.12	39.57
F	Umbo	10	2	39.13	0.11	0.32	0.09	0.12	39.77
F	Umbo	11	2	38.99	0.12	0.31	0.08	0.13	39.63
F	Umbo	12	2	39.60	0.12	0.29	0.09	0.12	40.22
F	Umbo	13	2	39.49	0.11	0.27	0.08	0.12	40.06
F	Umbo	14	2	39.72	0.11	0.26	0.07	0.12	40.28
F	Umbo	15	2	39.55	0.10	0.22	0.09	0.10	40.05
F	Umbo	16	2	39.73	0.10	0.21	0.09	0.10	40.22
F	Umbo	17	2	39.68	0.10	0.22	0.08	0.11	40.18
F	Umbo	18	2	39.64	0.09	0.29	0.07	0.09	40.18
F	Umbo	19	2	39.54	0.08	0.27	0.07	0.10	40.06
F	Umbo	20	2	39.04	0.08	0.24	0.05	0.09	39.51
F	Umbo	21	2	39.56	0.08	0.22	0.05	0.09	40.00
F	Umbo	22	2	39.35	0.09	0.23	0.04	0.10	39.80
F	Umbo	23	2	39.18	0.09	0.24	0.04	0.09	39.64
F	Umbo	24	2	39.42	0.11	0.23	0.04	0.08	39.88
F	Umbo	25	2	39.57	0.12	0.23	0.05	0.09	40.05
F	Umbo	26	2	39.66	0.09	0.29	0.04	0.09	40.17
F	Umbo	27	2	38.73	0.05	0.36	0.05	0.11	39.31
F	Umbo	28	2	38.52	0.00	0.49	0.05	0.12	39.18

F	Umbo	29	2	38.48	0.00	0.47	0.04	0.11	39.10
F	Umbo	30	2	38.72	0.00	0.47	0.04	0.11	39.35
F	Umbo	31	2	38.76	0.00	0.47	0.04	0.12	39.39
F	Umbo	32	2	38.54	0.00	0.46	0.04	0.11	39.16
F	Umbo	33	2	38.65	0.00	0.48	0.05	0.10	39.28
F	Umbo	34	2	38.60	0.00	0.49	0.05	0.12	39.26
F	Umbo	35	2	38.91	0.00	0.45	0.05	0.09	39.50
F	Umbo	36	2	38.71	0.00	0.45	0.05	0.11	39.32
F	Umbo	37	2	38.76	0.00	0.46	0.05	0.18	39.45
F	Umbo	38	2	38.88	0.00	0.47	0.05	0.13	39.53
F	Umbo	39	2	38.95	0.00	0.46	0.05	0.11	39.57
F	Umbo	40	2	38.95	0.00	0.47	0.05	0.12	39.59
F	Umbo	41	2	38.83	0.00	0.44	0.05	0.20	39.52
F	Umbo	42	2	38.73	0.00	0.40	0.05	0.24	39.42
F	Umbo	43	2	38.84	0.00	0.47	0.05	0.23	39.58
F	Umbo	44	2	38.81	0.00	0.46	0.04	0.14	39.46
F	Umbo	45	2	38.83	0.00	0.44	0.05	0.13	39.45
F	Umbo	46	2	38.81	0.00	0.46	0.05	0.14	39.46
F	Umbo	47	2	38.74	0.00	0.45	0.05	0.15	39.39
F	Umbo	48	2	38.73	0.00	0.46	0.05	0.16	39.39
F	Umbo	49	2	38.92	0.00	0.46	0.05	0.13	39.55
F	Umbo	50	2	38.75	0.00	0.46	0.05	0.13	39.39
F	Umbo	51	2	38.60	0.00	0.44	0.05	0.13	39.23
F	Umbo	52	2	38.90	0.00	0.46	0.05	0.13	39.54
F	Umbo	53	2	38.91	0.00	0.48	0.05	0.12	39.56
F	Umbo	54	2	39.12	0.00	0.50	0.05	0.13	39.80
F	Umbo	55	2	38.82	0.00	0.50	0.06	0.14	39.51
F	Umbo	56	2	38.80	0.00	0.48	0.06	0.15	39.49
F	Umbo	57	2	38.92	0.00	0.47	0.06	0.18	39.63
F	Umbo	58	2	38.96	0.00	0.45	0.05	0.22	39.69
F	Umbo	1	3	38.09	0.07	0.19	0.06	0.06	38.47
F	Umbo	2	3	39.02	0.09	0.24	0.05	0.07	39.47
F	Umbo	3	3	39.30	0.08	0.20	0.05	0.08	39.69
F	Umbo	4	3	39.30	0.09	0.22	0.05	0.08	39.74
F	Umbo	5	3	39.69	0.11	0.20	0.05	0.07	40.11
F	Umbo	6	3	38.45	0.10	0.21	0.04	0.09	38.88
F	Umbo	7	3	39.18	0.10	0.20	0.05	0.06	39.59
F	Umbo	8	3	39.45	0.12	0.21	0.04	0.08	39.90
F	Umbo	9	3	39.23	0.11	0.21	0.03	0.08	39.65
F	Umbo	10	3	39.39	0.11	0.28	0.05	0.07	39.89
F	Umbo	11	3	38.34	0.01	0.45	0.03	0.14	38.96
F	Umbo	12	3	37.91	0.00	0.51	0.03	0.11	38.56
F	Umbo	13	3	40.08	0.08	0.23	0.07	0.03	40.49
F	Umbo	14	3	40.38	0.12	0.19	0.07	0.06	40.83
F	Umbo	15	3	39.86	0.13	0.15	0.07	0.06	40.26
F	Umbo	16	3	39.38	0.12	0.15	0.08	0.07	39.79
F	Umbo	17	3	40.59	0.13	0.17	0.08	0.04	41.01
F	Umbo	18	3	40.08	0.13	0.13	0.07	0.07	40.49
F	Umbo	19	3	39.43	0.13	0.16	0.06	0.08	39.86
F	Umbo	20	3	39.86	0.11	0.15	0.06	0.05	40.23
F	Umbo	21	3	39.60	0.16	0.14	0.06	0.07	40.03
F	Umbo	22	3	39.63	0.15	0.11	0.07	0.09	40.04
F	Umbo	23	3	40.11	0.14	0.12	0.11	0.06	40.54
F	Umbo	24	3	40.18	0.10	0.16	0.11	0.05	40.61
F	Umbo	25	3	40.01	0.10	0.11	0.09	0.07	40.38
F	Umbo	26	3	40.45	0.14	0.12	0.13	0.06	40.90
F	Umbo	27	3	40.67	0.09	0.12	0.13	0.05	41.05
F	Umbo	28	3	40.31	0.10	0.12	0.17	0.06	40.76

F	Umbo	29	3	38.24	0.00	0.53	0.05	0.24	39.06
F	Umbo	30	3	37.55	0.00	0.51	0.04	0.16	38.26
F	Umbo	31	3	38.15	0.05	0.17	0.16	0.06	38.58
F	Umbo	32	3	39.82	0.05	0.17	0.12	0.05	40.22
F	Umbo	33	3	39.10	0.09	0.17	0.12	0.06	39.55
F	Umbo	34	3	37.61	0.01	0.55	0.05	0.22	38.43
F	Umbo	35	3	37.51	0.00	0.53	0.04	0.19	38.27
F	Umbo	36	3	38.04	0.01	0.53	0.04	0.18	38.80
F	Umbo	37	3	37.78	0.02	0.51	0.04	0.12	38.47
F	Umbo	38	3	37.51	0.01	0.41	0.05	0.19	38.17
F	Umbo	39	3	35.61	0.02	0.32	0.05	0.41	36.41
F	Mid	1	4	36.12	0.04	0.50	0.09	0.16	36.90
F	Mid	2	4	38.20	0.04	0.46	0.07	0.13	38.90
F	Mid	3	4	38.51	0.04	0.46	0.05	0.14	39.19
F	Mid	4	4	38.67	0.04	0.39	0.04	0.14	39.29
F	Mid	5	4	39.18	0.05	0.36	0.05	0.14	39.78
F	Mid	6	4	38.80	0.05	0.34	0.03	0.12	39.35
F	Mid	7	4	37.99	0.06	0.31	0.02	0.12	38.51
F	Mid	8	4	38.90	0.08	0.33	0.03	0.14	39.47
F	Mid	9	4	38.97	0.08	0.30	0.02	0.13	39.49
F	Mid	10	4	39.18	0.07	0.28	0.03	0.11	39.67
F	Mid	11	4	39.07	0.07	0.26	0.03	0.09	39.51
F	Mid	12	4	39.32	0.08	0.23	0.02	0.11	39.77
F	Mid	13	4	39.21	0.08	0.20	0.02	0.08	39.60
F	Mid	14	4	39.32	0.08	0.21	0.03	0.10	39.74
F	Mid	15	4	39.20	0.09	0.19	0.05	0.08	39.62
F	Mid	16	4	37.31	0.00	0.54	0.03	0.15	38.03
F	Mid	17	4	38.14	0.00	0.54	0.03	0.20	38.91
F	Mid	18	4	38.24	0.00	0.50	0.04	0.14	38.92
F	Mid	19	4	38.32	0.00	0.53	0.05	0.15	39.05
F	Mid	20	4	38.13	0.00	0.52	0.03	0.12	38.79
F	Mid	21	4	38.23	0.00	0.50	0.03	0.15	38.91
F	Mid	22	4	38.02	0.00	0.51	0.04	0.14	38.70
F	Mid	23	4	38.14	0.00	0.49	0.05	0.14	38.82
F	Mid	24	4	38.41	0.00	0.48	0.05	0.11	39.04
F	Mid	25	4	37.84	0.00	0.53	0.05	0.12	38.54
F	Mid	26	4	38.09	0.00	0.48	0.04	0.16	38.76
F	Mid	27	4	38.22	0.00	0.48	0.05	0.16	38.90
F	Mid	28	4	38.33	0.00	0.51	0.07	0.15	39.05
F	Mid	29	4	38.14	0.00	0.48	0.09	0.13	38.84
F	Mid	30	4	38.49	0.00	0.49	0.05	0.13	39.16
F	Mid	31	4	38.24	0.00	0.46	0.07	0.16	38.92
F	Mid	32	4	38.20	0.00	0.43	0.06	0.24	38.93
F	Mid	33	4	38.34	0.00	0.44	0.05	0.34	39.17
F	Mid	34	4	38.37	0.00	0.45	0.05	0.23	39.11
F	Mid	35	4	38.47	0.00	0.45	0.05	0.19	39.15
F	Mid	36	4	38.33	0.00	0.45	0.05	0.20	39.03
F	Mid	37	4	38.52	0.00	0.46	0.06	0.23	39.27
F	Mid	38	4	38.34	0.00	0.45	0.05	0.24	39.09
F	Mid	39	4	37.92	0.00	0.38	0.04	0.46	38.80
F	Mid	1	5	38.08	0.10	0.29	0.07	0.15	38.68
F	Mid	2	5	39.06	0.09	0.27	0.05	0.13	39.60
F	Mid	3	5	38.90	0.10	0.24	0.04	0.12	39.39
F	Mid	4	5	39.11	0.10	0.22	0.04	0.13	39.60
F	Mid	5	5	39.34	0.10	0.22	0.04	0.13	39.84
F	Mid	6	5	39.42	0.10	0.21	0.04	0.12	39.90
F	Mid	7	5	39.57	0.11	0.20	0.03	0.13	40.05
F	Mid	8	5	39.42	0.12	0.18	0.03	0.11	39.87

F	Mid	9	5	39.55	0.09	0.17	0.04	0.12	39.96
F	Mid	10	5	39.45	0.11	0.19	0.03	0.11	39.89
F	Mid	11	5	39.40	0.13	0.19	0.03	0.12	39.86
F	Mid	12	5	38.11	0.14	0.18	0.02	0.12	38.57
F	Mid	13	5	39.70	0.16	0.17	0.03	0.12	40.18
F	Mid	14	5	39.37	0.18	0.18	0.03	0.12	39.88
F	Mid	15	5	39.66	0.19	0.17	0.02	0.11	40.16
F	Mid	16	5	40.11	0.17	0.15	0.02	0.12	40.56
F	Mid	17	5	39.92	0.16	0.14	0.02	0.11	40.35
F	Mid	18	5	39.81	0.18	0.16	0.02	0.10	40.27
F	Mid	19	5	38.09	0.18	0.15	0.02	0.08	38.51
F	Mid	20	5	40.08	0.17	0.14	0.02	0.10	40.51
F	Mid	21	5	39.96	0.18	0.12	0.02	0.08	40.36
F	Mid	22	5	39.71	0.19	0.13	0.02	0.10	40.15
F	Mid	23	5	39.87	0.19	0.11	0.02	0.09	40.28
F	Mid	24	5	40.30	0.12	0.09	0.03	0.09	40.63
F	Mid	25	5	39.16	0.01	0.25	0.04	0.14	39.61
F	Mid	26	5	38.97	0.00	0.25	0.04	0.11	39.37
F	Mid	27	5	38.95	0.00	0.25	0.04	0.13	39.37
F	Mid	28	5	39.01	0.00	0.24	0.04	0.10	39.39
F	Mid	29	5	39.23	0.00	0.23	0.03	0.10	39.59
F	Mid	30	5	39.05	0.00	0.25	0.03	0.10	39.43
F	Mid	31	5	38.97	0.00	0.24	0.03	0.10	39.35
F	Mid	32	5	39.46	0.00	0.23	0.04	0.12	39.86
F	Mid	33	5	39.29	0.00	0.25	0.04	0.13	39.72
F	Mid	34	5	38.74	0.01	0.24	0.05	0.13	39.17
F	Mid	35	5	39.41	0.00	0.25	0.05	0.12	39.82
F	Mid	36	5	39.67	0.01	0.24	0.05	0.12	40.09
F	Mid	37	5	39.07	0.00	0.24	0.04	0.13	39.48
F	Mid	38	5	38.77	0.00	0.22	0.04	0.12	39.16
F	Mid	39	5	39.41	0.01	0.23	0.04	0.11	39.81
F	Mid	40	5	39.57	0.01	0.21	0.05	0.21	40.05
F	Mid	41	5	39.41	0.01	0.23	0.04	0.28	39.98
F	Mid	42	5	38.91	0.00	0.23	0.04	0.17	39.35
F	Mid	43	5	39.33	0.00	0.23	0.04	0.14	39.75
F	Mid	44	5	39.55	0.00	0.22	0.05	0.15	39.97
F	Mid	45	5	39.28	0.00	0.23	0.05	0.13	39.69
F	Mid	46	5	39.12	0.00	0.22	0.05	0.17	39.55
F	Mid	47	5	39.10	0.00	0.24	0.04	0.17	39.54
F	Mid	48	5	39.42	0.00	0.23	0.04	0.15	39.84
F	Mid	49	5	39.32	0.00	0.23	0.05	0.13	39.73
F	Mid	50	5	38.86	0.00	0.22	0.04	0.13	39.26
F	Mid	51	5	39.29	0.00	0.22	0.05	0.11	39.67
F	Mid	52	5	39.20	0.00	0.24	0.05	0.13	39.62
F	Mid	53	5	39.40	0.01	0.24	0.05	0.13	39.83
F	Mid	54	5	39.50	0.00	0.24	0.05	0.14	39.95
F	Mid	55	5	39.52	0.00	0.24	0.05	0.16	39.99
F	Mid	56	5	39.83	0.00	0.23	0.05	0.14	40.26
F	Mid	57	5	39.79	0.00	0.17	0.05	0.34	40.35
F	Mid	58	5	38.99	0.00	0.15	0.06	0.49	39.69
F	Mid	1	6	40.79	0.15	0.41	0.06	0.16	41.57
F	Mid	2	6	40.37	0.15	0.32	0.03	0.13	41.00
F	Mid	3	6	40.80	0.16	0.37	0.03	0.13	41.48
F	Mid	4	6	40.58	0.22	0.34	0.02	0.13	41.28
F	Mid	5	6	40.84	0.25	0.31	0.02	0.14	41.56
F	Mid	6	6	40.59	0.19	0.28	0.01	0.09	41.16
F	Mid	7	6	40.92	0.21	0.30	0.01	0.09	41.53
F	Mid	8	6	40.51	0.19	0.24	0.01	0.09	41.04

F	Mid	9	6	41.53	0.22	0.20	0.02	0.08	42.04
F	Mid	10	6	41.02	0.21	0.22	0.01	0.08	41.55
F	Mid	11	6	36.82	0.01	0.58	0.03	0.16	37.60
F	Mid	12	6	37.58	0.00	0.65	0.04	0.13	38.40
F	Mid	13	6	37.35	0.02	0.59	0.03	0.13	38.13
F	Mid	14	6	38.20	0.02	0.37	0.04	0.50	39.13
F	Mid	15	6	38.03	0.00	0.59	0.03	0.17	38.82
F	Mid	16	6	38.19	0.00	0.53	0.03	0.13	38.87
F	Mid	17	6	37.74	0.01	0.53	0.03	0.12	38.44
F	Mid	18	6	37.95	0.01	0.58	0.04	0.19	38.77
F	Mid	19	6	39.34	0.01	0.39	0.04	0.19	39.97
F	Edge	1	7	37.73	0.08	0.24	0.10	0.14	38.30
F	Edge	2	7	38.42	0.06	0.19	0.06	0.16	38.89
F	Edge	3	7	39.23	0.08	0.20	0.03	0.13	39.67
F	Edge	4	7	39.05	0.10	0.21	0.05	0.17	39.57
F	Edge	5	7	39.11	0.11	0.17	0.04	0.17	39.60
F	Edge	6	7	38.86	0.11	0.17	0.03	0.16	39.33
F	Edge	7	7	39.20	0.11	0.14	0.02	0.13	39.61
F	Edge	8	7	39.20	0.14	0.15	0.03	0.12	39.63
F	Edge	9	7	39.11	0.13	0.16	0.02	0.12	39.54
F	Edge	10	7	39.36	0.14	0.15	0.02	0.13	39.79
F	Edge	11	7	38.94	0.13	0.16	0.03	0.13	39.38
F	Edge	12	7	39.16	0.16	0.15	0.00	0.13	39.60
F	Edge	13	7	39.37	0.17	0.15	0.02	0.09	39.81
F	Edge	14	7	39.72	0.15	0.16	0.00	0.13	40.16
F	Edge	15	7	39.59	0.16	0.14	0.01	0.14	40.04
F	Edge	16	7	39.66	0.16	0.11	0.02	0.08	40.03
F	Edge	17	7	39.52	0.17	0.10	0.03	0.10	39.93
F	Edge	18	7	39.46	0.18	0.11	0.03	0.12	39.89
F	Edge	19	7	39.37	0.17	0.09	0.01	0.13	39.76
F	Edge	20	7	39.52	0.20	0.08	0.02	0.09	39.90
F	Edge	21	7	39.42	0.17	0.05	0.02	0.11	39.76
F	Edge	22	7	39.62	0.17	0.05	0.05	0.07	39.97
F	Edge	23	7	38.26	0.00	0.23	0.04	0.25	38.78
F	Edge	24	7	38.64	0.00	0.25	0.07	0.22	39.17
F	Edge	25	7	38.72	0.00	0.25	0.04	0.17	39.17
F	Edge	26	7	38.66	0.00	0.23	0.06	0.21	39.16
F	Edge	27	7	38.39	0.00	0.16	0.07	0.46	39.08
F	Edge	28	7	38.68	0.01	0.24	0.05	0.31	39.30
F	Edge	29	7	38.66	0.00	0.21	0.04	0.24	39.15
F	Edge	30	7	38.82	0.00	0.26	0.04	0.22	39.34
F	Edge	31	7	38.39	0.00	0.27	0.05	0.22	38.93
F	Edge	32	7	38.96	0.00	0.26	0.06	0.26	39.54
F	Edge	33	7	38.53	0.00	0.22	0.07	0.33	39.15
F	Edge	1	8	34.70	0.05	0.23	0.13	0.05	35.15
F	Edge	2	8	38.53	0.08	0.51	0.06	0.15	39.33
F	Edge	3	8	38.95	0.07	0.42	0.06	0.12	39.62
F	Edge	4	8	39.06	0.08	0.41	0.05	0.13	39.73
F	Edge	5	8	39.28	0.08	0.40	0.05	0.11	39.93
F	Edge	6	8	39.12	0.09	0.38	0.05	0.12	39.76
F	Edge	7	8	39.10	0.09	0.39	0.05	0.11	39.73
F	Edge	8	8	39.12	0.10	0.37	0.05	0.11	39.75
F	Edge	9	8	39.25	0.10	0.35	0.04	0.12	39.87
F	Edge	10	8	39.31	0.11	0.34	0.05	0.11	39.92
F	Edge	11	8	39.43	0.11	0.36	0.04	0.11	40.06
F	Edge	12	8	39.21	0.11	0.31	0.05	0.11	39.79
F	Edge	13	8	39.41	0.12	0.31	0.04	0.11	40.00
F	Edge	14	8	39.26	0.12	0.29	0.03	0.10	39.81

F	Edge	15	8	39.54	0.12	0.30	0.03	0.11	40.10
F	Edge	16	8	39.38	0.12	0.30	0.03	0.09	39.93
F	Edge	17	8	39.67	0.13	0.28	0.03	0.10	40.21
F	Edge	18	8	39.39	0.13	0.29	0.03	0.10	39.93
F	Edge	19	8	39.59	0.14	0.27	0.03	0.10	40.13
F	Edge	20	8	39.44	0.13	0.28	0.03	0.09	39.97
F	Edge	21	8	39.45	0.14	0.26	0.02	0.09	39.97
F	Edge	22	8	39.51	0.14	0.26	0.03	0.10	40.03
F	Edge	23	8	39.39	0.13	0.25	0.03	0.09	39.90
F	Edge	24	8	39.54	0.13	0.23	0.02	0.10	40.03
F	Edge	25	8	39.75	0.13	0.23	0.02	0.09	40.23
F	Edge	26	8	39.61	0.14	0.24	0.02	0.09	40.09
F	Edge	27	8	39.68	0.14	0.22	0.02	0.09	40.16
F	Edge	28	8	39.77	0.14	0.23	0.02	0.08	40.25
F	Edge	29	8	39.53	0.13	0.21	0.02	0.09	39.99
F	Edge	30	8	39.75	0.14	0.22	0.02	0.08	40.21
F	Edge	31	8	39.66	0.14	0.23	0.02	0.09	40.14
F	Edge	32	8	39.82	0.13	0.22	0.02	0.09	40.29
F	Edge	33	8	39.54	0.13	0.21	0.02	0.08	39.98
F	Edge	34	8	39.75	0.14	0.20	0.02	0.09	40.19
F	Edge	35	8	39.69	0.14	0.20	0.01	0.09	40.14
F	Edge	36	8	39.70	0.15	0.19	0.02	0.09	40.14
F	Edge	37	8	39.66	0.14	0.19	0.02	0.09	40.10
F	Edge	38	8	39.75	0.14	0.16	0.04	0.08	40.18
F	Edge	39	8	39.02	0.11	0.28	0.04	0.16	39.61
F	Edge	40	8	39.09	0.09	0.32	0.04	0.15	39.70
F	Edge	41	8	38.95	0.08	0.36	0.05	0.18	39.62
F	Edge	42	8	39.14	0.05	0.40	0.05	0.20	39.83
F	Edge	43	8	39.01	0.05	0.37	0.05	0.23	39.72
F	Edge	44	8	37.44	0.02	0.28	0.09	0.40	38.24
F	Edge	1	9	41.05	0.07	0.28	0.05	0.10	41.54
F	Edge	2	9	39.72	0.07	0.22	0.05	0.12	40.18
F	Edge	3	9	40.17	0.09	0.22	0.05	0.10	40.62
F	Edge	4	9	40.56	0.08	0.17	0.05	0.11	40.97
F	Edge	5	9	40.59	0.09	0.15	0.04	0.11	40.98
F	Edge	6	9	40.42	0.11	0.18	0.04	0.07	40.82
F	Edge	7	9	40.09	0.16	0.18	0.03	0.08	40.54
F	Edge	8	9	40.61	0.15	0.15	0.02	0.07	41.00
F	Edge	9	9	39.91	0.15	0.15	0.01	0.08	40.31
F	Edge	10	9	40.34	0.17	0.19	0.02	0.07	40.77
F	Edge	11	9	40.12	0.17	0.20	0.02	0.11	40.60
F	Edge	12	9	40.07	0.15	0.16	0.01	0.09	40.47
F	Edge	13	9	40.25	0.16	0.17	0.02	0.11	40.70
F	Edge	14	9	40.56	0.16	0.11	0.02	0.09	40.93
F	Edge	15	9	40.61	0.10	0.07	0.07	0.10	40.95
F	Edge	16	9	40.03	0.05	0.09	0.07	0.10	40.33
F	Edge	17	9	39.44	0.07	0.07	0.21	0.12	39.91
F	Edge	18	9	40.23	0.12	0.06	0.09	0.11	40.61

A.3 Ionprobe analyses expressed as elements (wt%)

Onto. Stage	Shell Area	Line	Point	Na	Mg	Sr
A	Umbo	1	1	0.99	0.06	0.36
A	Umbo	1	2	0.99	0.04	0.28
A	Umbo	1	3	1.06	0.04	0.25
A	Umbo	1	4	1.10	0.03	0.24
A	Umbo	1	5	1.08	0.03	0.27
A	Umbo	1	6	1.01	0.06	0.33
A	Umbo	1	7	0.83	0.20	0.28
A	Umbo	1	8	0.39	0.36	0.12
A	Umbo	1	9	0.25	0.25	0.08
A	Umbo	1	10	0.26	0.22	0.08
A	Umbo	1	11	0.29	0.17	0.08
A	Umbo	1	12	0.28	0.17	0.07
A	Umbo	1	13	0.27	0.21	0.08
A	Umbo	1	14	0.28	0.23	0.08
A	Umbo	1	15	0.26	0.22	0.09
A	Umbo	1	16	0.26	0.20	0.10
A	Umbo	1	17	0.34	0.17	0.09
A	Umbo	1	18	0.37	0.14	0.08
A	Umbo	1	19	0.48	0.17	0.09
A	Umbo	1	20	0.59	0.33	0.13
A	Umbo	1	21	0.35	0.38	0.09
A	Umbo	1	22	0.53	0.23	0.11
A	Umbo	1	23	0.81	0.15	0.18
A	Umbo	1	24	0.53	0.23	0.12
A	Umbo	1	25	0.32	0.26	0.08
A	Umbo	1	26	0.27	0.28	0.08
A	Umbo	1	27	0.29	0.27	0.09
A	Umbo	1	28	0.27	0.31	0.10
A	Umbo	1	29	0.29	0.30	0.11
A	Umbo	1	30	0.30	0.25	0.11
A	Umbo	1	31	0.30	0.25	0.11
A	Umbo	1	32	0.32	0.29	0.11
A	Umbo	1	33	0.35	0.31	0.11
A	Umbo	1	34	0.34	0.31	0.10
A	Umbo	1	35	0.36	0.32	0.10
A	Mid	2	1	1.40	0.21	0.14
A	Mid	2	2	0.97	0.09	0.12
A	Mid	2	3	0.77	0.07	0.11
A	Mid	2	4	0.63	0.07	0.11
A	Mid	2	5	0.64	0.08	0.10
A	Mid	2	6	0.61	0.11	0.11
A	Mid	2	7	0.53	0.13	0.13
A	Mid	2	8	0.56	0.11	0.16
A	Mid	2	9	1.00	0.03	0.18
A	Mid	2	10	1.16	0.01	0.13
A	Mid	2	11	1.12	0.01	0.13
A	Mid	2	12	1.17	0.01	0.13
A	Mid	2	13	1.12	0.02	0.14
A	Mid	2	14	1.05	0.03	0.19
A	Mid	2	15	0.90	0.04	0.32
A	Mid	2	16	0.96	0.06	0.34
A	Mid	2	17	0.91	0.08	0.38

A	Edge	3	1	1.42	0.54	0.15
A	Edge	3	2	1.00	0.15	0.14
A	Edge	3	3	0.85	0.11	0.13
A	Edge	3	4	0.72	0.10	0.12
A	Edge	3	5	0.61	0.10	0.11
A	Edge	3	6	0.54	0.11	0.11
A	Edge	3	7	0.49	0.11	0.10
A	Edge	3	8	0.46	0.11	0.10
A	Edge	3	9	0.40	0.12	0.10
A	Edge	3	10	0.36	0.14	0.10
A	Edge	3	11	0.33	0.16	0.10
A	Edge	3	12	0.29	0.22	0.10
A	Edge	3	13	0.26	0.27	0.11
A	Edge	3	14	0.25	0.34	0.11
A	Edge	3	15	0.21	0.37	0.11
A	Edge	3	16	0.21	0.33	0.11
A	Edge	3	17	0.19	0.32	0.11
A	Edge	3	18	0.17	0.41	0.12
B	Umbo	1	1	0.60	0.30	0.09
B	Umbo	1	2	0.51	0.13	0.10
B	Umbo	1	3	0.48	0.12	0.11
B	Umbo	1	4	0.41	0.11	0.11
B	Umbo	1	5	0.35	0.10	0.11
B	Umbo	1	6	0.31	0.11	0.11
B	Umbo	1	7	0.27	0.12	0.10
B	Umbo	1	8	0.28	0.13	0.10
B	Umbo	1	9	0.31	0.12	0.10
B	Umbo	1	10	0.30	0.10	0.09
B	Umbo	1	11	0.28	0.13	0.10
B	Umbo	1	12	0.24	0.13	0.10
B	Umbo	1	13	0.25	0.14	0.09
B	Umbo	1	14	0.24	0.20	0.10
B	Umbo	1	15	0.24	0.28	0.11
B	Umbo	1	16	0.22	0.16	0.10
B	Umbo	1	17	0.23	0.13	0.10
B	Umbo	1	18	0.25	0.15	0.10
B	Umbo	1	19	0.22	0.15	0.10
B	Umbo	1	20	0.21	0.13	0.09
B	Umbo	1	21	0.21	0.12	0.09
B	Umbo	1	22	0.21	0.13	0.09
B	Umbo	1	23	0.20	0.14	0.10
B	Umbo	1	24	0.18	0.14	0.10
B	Umbo	1	25	0.17	0.15	0.10
B	Umbo	1	26	0.16	0.12	0.10
B	Umbo	1	27	0.15	0.14	0.11
B	Umbo	1	28	0.18	0.17	0.11
B	Umbo	1	29	0.27	0.17	0.10
B	Umbo	1	30	0.27	0.15	0.10
B	Umbo	1	31	0.26	0.14	0.10
B	Umbo	1	32	0.28	0.12	0.11
B	Umbo	1	33	0.52	0.07	0.16
B	Umbo	1	34	1.00	0.03	0.17
B	Umbo	1	35	1.15	0.01	0.12
B	Umbo	1	36	1.09	0.01	0.12
B	Umbo	1	37	1.05	0.01	0.13
B	Umbo	1	38	1.02	0.01	0.13
B	Umbo	1	39	1.01	0.01	0.12
B	Umbo	1	40	1.01	0.01	0.12

B	Umbo	1	41	1.01	0.01	0.12
B	Umbo	1	42	1.04	0.01	0.12
B	Umbo	1	43	1.03	0.01	0.12
B	Umbo	1	44	1.04	0.01	0.13
B	Umbo	1	45	1.05	0.01	0.14
B	Umbo	1	46	1.03	0.01	0.14
B	Umbo	1	47	1.03	0.01	0.14
B	Umbo	1	48	1.05	0.01	0.14
B	Umbo	1	49	1.06	0.01	0.13
B	Umbo	1	50	1.09	0.01	0.13
B	Umbo	1	51	1.10	0.01	0.14
B	Umbo	1	52	1.12	0.01	0.15
B	Umbo	1	53	1.03	0.02	0.17
B	Umbo	1	54	0.99	0.02	0.20
B	Umbo	1	55	0.92	0.02	0.25
B	Umbo	1	56	0.93	0.02	0.27
B	Umbo	1	57	0.92	0.02	0.27
B	Mid	2	1	0.87	0.14	0.14
B	Mid	2	2	0.77	0.07	0.14
B	Mid	2	3	0.69	0.07	0.13
B	Mid	2	4	0.65	0.07	0.12
B	Mid	2	5	0.58	0.07	0.11
B	Mid	2	6	0.54	0.07	0.10
B	Mid	2	7	0.56	0.08	0.10
B	Mid	2	8	0.53	0.08	0.10
B	Mid	2	9	0.51	0.09	0.09
B	Mid	2	10	0.51	0.09	0.10
B	Mid	2	11	0.47	0.09	0.10
B	Mid	2	12	0.49	0.10	0.11
B	Mid	2	13	0.48	0.11	0.11
B	Mid	2	14	0.46	0.12	0.11
B	Mid	2	15	0.45	0.12	0.11
B	Mid	2	16	0.46	0.12	0.11
B	Mid	2	17	0.44	0.12	0.11
B	Mid	2	18	0.37	0.13	0.13
B	Mid	2	19	0.54	0.09	0.16
B	Mid	2	20	0.98	0.02	0.17
B	Mid	2	21	1.04	0.01	0.13
B	Mid	2	22	0.98	0.01	0.13
B	Mid	2	23	0.96	0.01	0.13
B	Mid	2	24	0.96	0.01	0.13
B	Mid	2	25	0.98	0.01	0.13
B	Mid	2	26	1.01	0.01	0.13
B	Mid	2	27	0.93	0.01	0.13
B	Mid	2	28	0.95	0.01	0.13
B	Mid	2	29	0.97	0.01	0.13
B	Mid	2	30	1.00	0.01	0.13
B	Mid	2	31	1.00	0.01	0.12
B	Mid	2	32	0.99	0.01	0.14
B	Mid	2	33	0.97	0.01	0.15
B	Mid	2	34	0.98	0.01	0.15
B	Mid	2	35	0.99	0.01	0.14
B	Mid	2	36	1.00	0.01	0.14
B	Mid	2	37	1.00	0.01	0.14
B	Mid	2	38	1.03	0.01	0.14
B	Mid	2	39	1.03	0.01	0.15
B	Mid	2	40	0.97	0.03	0.20
B	Edge	3	1	0.99	0.12	0.12

B	Edge	3	2	0.91	0.09	0.12
B	Edge	3	3	0.82	0.08	0.12
B	Edge	3	4	0.73	0.08	0.11
B	Edge	3	5	0.68	0.08	0.10
B	Edge	3	6	0.67	0.09	0.10
B	Edge	3	7	0.65	0.09	0.11
B	Edge	3	8	0.59	0.10	0.11
B	Edge	3	9	0.58	0.11	0.11
B	Edge	3	10	0.60	0.13	0.11
B	Edge	3	11	0.59	0.13	0.11
B	Edge	3	12	0.58	0.13	0.11
B	Edge	3	13	0.57	0.12	0.11
B	Edge	3	14	0.58	0.13	0.11
B	Edge	3	15	0.55	0.13	0.11
B	Edge	3	16	0.51	0.13	0.11
B	Edge	3	17	0.47	0.15	0.12
B	Edge	3	18	0.44	0.13	0.13
B	Edge	3	19	0.65	0.07	0.15
B	Edge	3	20	1.04	0.01	0.15
B	Edge	3	21	1.05	0.01	0.12
B	Edge	3	22	0.96	0.01	0.13
B	Edge	3	23	0.95	0.01	0.13
B	Edge	3	24	0.94	0.01	0.12
B	Edge	3	25	0.94	0.01	0.12
B	Edge	3	26	0.95	0.01	0.12
B	Edge	3	27	0.96	0.01	0.13
B	Edge	3	28	0.94	0.01	0.13
B	Edge	3	29	0.92	0.01	0.12
B	Edge	3	30	0.93	0.01	0.12
B	Edge	3	31	0.94	0.01	0.12
B	Edge	3	32	0.99	0.01	0.12
B	Edge	3	33	1.01	0.01	0.13
B	Edge	3	34	1.01	0.02	0.15
B	Edge	3	35	1.00	0.01	0.14
B	Edge	3	36	0.99	0.01	0.14
B	Edge	3	37	0.99	0.01	0.13
B	Edge	3	38	1.01	0.01	0.13
B	Edge	3	39	1.04	0.01	0.14
B	Edge	3	40	1.03	0.01	0.14
B	Edge	3	41	0.99	0.02	0.16
B	Edge	3	42	0.90	0.02	0.22
B	Edge	3	43	0.83	0.03	0.29
B	Edge	3	44	1.04	0.04	0.27
C	Umbo	1	1	0.68	0.12	0.12
C	Umbo	1	2	0.63	0.10	0.12
C	Umbo	1	3	0.66	0.10	0.11
C	Umbo	1	4	0.63	0.10	0.11
C	Umbo	1	5	0.60	0.11	0.11
C	Umbo	1	6	0.61	0.10	0.10
C	Umbo	1	7	0.62	0.10	0.10
C	Umbo	1	8	0.63	0.11	0.10
C	Umbo	1	9	0.63	0.12	0.10
C	Umbo	1	10	0.62	0.13	0.10
C	Umbo	1	11	0.63	0.13	0.10
C	Umbo	1	12	0.62	0.13	0.10
C	Umbo	1	13	0.60	0.14	0.10
C	Umbo	1	14	0.57	0.13	0.09
C	Umbo	1	15	0.54	0.13	0.09

C	Umbo	1	16	0.49	0.12	0.09
C	Umbo	1	17	0.47	0.13	0.09
C	Umbo	1	18	0.46	0.12	0.09
C	Umbo	1	19	0.47	0.13	0.09
C	Umbo	1	20	0.45	0.13	0.09
C	Umbo	1	21	0.45	0.13	0.09
C	Umbo	1	22	0.48	0.13	0.09
C	Umbo	1	23	0.51	0.13	0.09
C	Umbo	1	24	0.53	0.12	0.09
C	Umbo	1	25	0.55	0.12	0.09
C	Umbo	1	26	0.57	0.14	0.10
C	Umbo	1	27	0.57	0.16	0.09
C	Umbo	1	28	0.56	0.16	0.09
C	Umbo	1	29	0.55	0.16	0.09
C	Umbo	1	30	0.52	0.17	0.09
C	Umbo	1	31	0.49	0.17	0.10
C	Umbo	1	32	0.47	0.18	0.10
C	Umbo	1	33	0.40	0.19	0.10
C	Umbo	1	34	0.35	0.18	0.10
C	Umbo	1	35	0.32	0.17	0.09
C	Umbo	1	36	0.33	0.19	0.09
C	Umbo	1	37	0.31	0.19	0.09
C	Umbo	1	38	0.31	0.20	0.09
C	Umbo	1	39	0.30	0.19	0.09
C	Umbo	1	40	0.32	0.19	0.09
C	Umbo	1	41	0.28	0.19	0.08
C	Umbo	1	42	0.26	0.17	0.08
C	Umbo	1	43	0.26	0.18	0.08
C	Umbo	1	44	0.28	0.20	0.08
C	Umbo	2	1	0.73	0.11	0.11
C	Umbo	2	2	0.66	0.11	0.11
C	Umbo	2	3	0.65	0.11	0.12
C	Umbo	2	4	0.62	0.11	0.12
C	Umbo	2	5	0.64	0.11	0.11
C	Umbo	2	6	0.62	0.11	0.10
C	Umbo	2	7	0.58	0.11	0.10
C	Umbo	2	8	0.54	0.11	0.10
C	Umbo	2	9	0.54	0.12	0.10
C	Umbo	2	10	0.54	0.13	0.10
C	Umbo	2	11	0.52	0.13	0.10
C	Umbo	2	12	0.54	0.14	0.10
C	Umbo	2	13	0.52	0.14	0.10
C	Umbo	2	14	0.50	0.14	0.09
C	Umbo	2	15	0.45	0.13	0.09
C	Umbo	2	16	0.45	0.13	0.09
C	Umbo	2	17	0.43	0.14	0.09
C	Umbo	2	18	0.40	0.13	0.09
C	Umbo	2	19	0.41	0.14	0.08
C	Umbo	2	20	0.41	0.13	0.08
C	Umbo	2	21	0.48	0.13	0.08
C	Umbo	2	22	0.45	0.15	0.08
C	Umbo	2	23	0.44	0.16	0.08
C	Umbo	2	24	0.44	0.19	0.08
C	Umbo	2	25	0.47	0.17	0.11
C	Umbo	2	26	1.05	0.04	0.18
C	Umbo	2	27	1.21	0.01	0.16
C	Umbo	2	28	1.17	0.02	0.14
C	Umbo	2	29	1.09	0.02	0.11

C	Umbo	2	30	1.13	0.03	0.12
C	Umbo	2	31	0.94	0.02	0.12
C	Umbo	2	32	0.96	0.03	0.12
C	Umbo	2	33	0.86	0.03	0.13
C	Mid	3	1	1.07	0.11	0.13
C	Mid	3	2	1.02	0.10	0.12
C	Mid	3	3	0.98	0.10	0.11
C	Mid	3	4	0.96	0.11	0.12
C	Mid	3	5	0.96	0.12	0.11
C	Mid	3	6	0.94	0.13	0.11
C	Mid	3	7	0.92	0.13	0.12
C	Mid	3	8	0.88	0.13	0.11
C	Mid	3	9	0.81	0.13	0.11
C	Mid	3	10	0.77	0.15	0.11
C	Mid	3	11	0.70	0.15	0.11
C	Mid	3	12	0.63	0.14	0.10
C	Mid	3	13	0.59	0.13	0.10
C	Mid	3	14	0.59	0.11	0.10
C	Mid	3	15	0.90	0.05	0.12
C	Mid	3	16	1.19	0.02	0.13
C	Mid	3	17	1.18	0.02	0.14
C	Mid	3	18	1.12	0.02	0.15
C	Mid	3	19	1.11	0.02	0.14
C	Mid	3	20	1.13	0.02	0.13
C	Mid	3	21	1.12	0.01	0.12
C	Mid	3	22	1.14	0.01	0.12
C	Mid	3	23	1.11	0.01	0.11
C	Mid	3	24	1.13	0.01	0.12
C	Mid	3	25	1.12	0.01	0.13
C	Mid	3	26	1.12	0.01	0.13
C	Mid	3	27	1.12	0.02	0.12
C	Mid	3	28	1.10	0.02	0.12
C	Mid	3	29	1.08	0.03	0.14
C	Mid	3	30	1.02	0.06	0.21
C	Edge	4	1	0.67	0.12	0.12
C	Edge	4	2	0.52	0.09	0.12
C	Edge	4	3	0.50	0.09	0.11
C	Edge	4	4	0.47	0.09	0.11
C	Edge	4	5	0.45	0.10	0.10
C	Edge	4	6	0.40	0.09	0.10
C	Edge	4	7	0.39	0.10	0.11
C	Edge	4	8	0.38	0.10	0.11
C	Edge	4	9	0.36	0.10	0.10
C	Edge	4	10	0.34	0.11	0.10
C	Edge	4	11	0.32	0.12	0.09
C	Edge	4	12	0.32	0.12	0.09
C	Edge	4	13	0.29	0.12	0.09
C	Edge	4	14	0.28	0.12	0.09
C	Edge	4	15	0.29	0.13	0.08
C	Edge	4	16	0.30	0.13	0.08
C	Edge	4	17	0.29	0.14	0.08
C	Edge	4	18	0.29	0.15	0.09
C	Edge	4	19	0.27	0.15	0.10
C	Edge	4	20	0.25	0.16	0.12
C	Edge	4	21	0.27	0.21	0.12
D	Umbo	1	1	1.33	0.27	0.11
D	Umbo	1	2	0.82	0.09	0.11
D	Umbo	1	3	0.69	0.08	0.11

D	Umbo	1	4	0.59	0.08	0.11
D	Umbo	1	5	0.55	0.07	0.10
D	Umbo	1	6	0.51	0.09	0.10
D	Umbo	1	7	0.46	0.09	0.10
D	Umbo	1	8	0.43	0.11	0.10
D	Umbo	1	9	0.41	0.13	0.09
D	Umbo	1	10	0.44	0.15	0.10
D	Umbo	1	11	0.39	0.15	0.09
D	Umbo	1	12	0.32	0.15	0.09
D	Umbo	1	13	0.46	0.12	0.10
D	Umbo	1	14	1.04	0.02	0.13
D	Umbo	1	15	1.07	0.01	0.11
D	Umbo	1	16	1.03	0.01	0.12
D	Umbo	1	17	1.03	0.01	0.12
D	Umbo	1	18	1.00	0.01	0.10
D	Umbo	1	19	0.93	0.01	0.10
D	Umbo	1	20	0.90	0.01	0.10
D	Umbo	1	21	0.90	0.03	0.10
D	Umbo	1	22	0.91	0.01	0.10
D	Umbo	1	23	0.91	0.01	0.09
D	Umbo	1	24	0.97	0.01	0.09
D	Umbo	1	25	1.04	0.01	0.09
D	Umbo	1	26	1.06	0.01	0.09
D	Umbo	1	27	1.09	0.01	0.09
D	Umbo	1	28	1.11	0.01	0.09
D	Umbo	1	29	1.08	0.01	0.09
D	Umbo	1	30	1.08	0.01	0.09
D	Umbo	1	31	1.08	0.01	0.09
D	Umbo	1	32	1.03	0.01	0.10
D	Umbo	1	33	1.03	0.01	0.10
D	Umbo	1	34	1.04	0.01	0.10
D	Umbo	1	35	1.03	0.02	0.10
D	Umbo	1	36	1.07	0.02	0.11
D	Umbo	1	37	1.00	0.02	0.14
D	Umbo	1	38	1.05	0.02	0.15
D	Umbo	1	39	1.09	0.02	0.15
D	Umbo	1	40	0.99	0.02	0.18
D	Umbo	1	41	0.93	0.02	0.27
D	Umbo	1	42	1.07	0.01	0.17
D	Umbo	1	43	1.06	0.01	0.14
D	Umbo	1	44	1.00	0.01	0.16
D	Umbo	1	45	0.99	0.01	0.17
D	Umbo	1	46	1.00	0.01	0.15
D	Umbo	1	47	0.95	0.01	0.13
D	Umbo	1	48	0.93	0.01	0.12
D	Umbo	1	49	0.94	0.01	0.13
D	Umbo	1	50	0.98	0.01	0.12
D	Umbo	1	51	0.97	0.01	0.13
D	Umbo	1	52	0.92	0.01	0.13
D	Umbo	1	53	0.98	0.01	0.12
D	Umbo	1	54	0.98	0.01	0.12
D	Umbo	1	55	0.98	0.01	0.12
D	Umbo	1	56	1.06	0.01	0.13
D	Umbo	1	57	1.08	0.01	0.14
D	Umbo	1	58	1.11	0.01	0.14
D	Umbo	1	59	1.14	0.01	0.14
D	Umbo	1	60	1.13	0.01	0.13
D	Umbo	1	61	1.10	0.01	0.12

D	Umbo	1	62	1.14	0.01	0.12
D	Umbo	1	63	1.15	0.01	0.12
D	Umbo	1	64	1.16	0.01	0.13
D	Umbo	1	65	1.14	0.01	0.13
D	Umbo	1	66	1.15	0.01	0.13
D	Umbo	1	67	1.14	0.01	0.13
D	Umbo	1	68	1.11	0.01	0.14
D	Umbo	1	69	1.13	0.01	0.14
D	Umbo	1	70	1.10	0.01	0.14
D	Umbo	1	71	1.10	0.01	0.15
D	Umbo	1	72	1.05	0.01	0.19
D	Umbo	1	73	0.82	0.02	0.29
D	Umbo	1	74	0.99	0.04	0.28
D	Mid	2	1	1.07	0.22	0.14
D	Mid	2	2	0.91	0.12	0.13
D	Mid	2	3	0.78	0.10	0.12
D	Mid	2	4	0.64	0.08	0.11
D	Mid	2	5	0.53	0.07	0.11
D	Mid	2	6	0.47	0.06	0.10
D	Mid	2	7	0.43	0.06	0.09
D	Mid	2	8	0.37	0.06	0.09
D	Mid	2	9	0.31	0.06	0.09
D	Mid	2	10	0.25	0.09	0.10
D	Mid	2	11	0.22	0.09	0.10
D	Mid	2	12	0.23	0.06	0.09
D	Mid	2	13	0.23	0.06	0.09
D	Mid	2	14	0.22	0.07	0.09
D	Mid	2	15	0.17	0.10	0.11
D	Mid	2	16	0.17	0.09	0.11
D	Mid	2	17	0.19	0.08	0.10
D	Mid	2	18	0.18	0.10	0.09
D	Mid	2	19	0.19	0.12	0.09
D	Mid	2	20	0.22	0.12	0.10
D	Mid	2	21	0.61	0.06	0.14
D	Mid	2	22	1.05	0.01	0.18
D	Mid	2	23	1.15	0.01	0.16
D	Mid	2	24	1.15	0.01	0.16
D	Mid	2	25	1.15	0.01	0.15
D	Mid	2	26	1.12	0.01	0.15
D	Mid	2	27	1.07	0.02	0.18
D	Mid	2	28	1.07	0.02	0.18
D	Mid	2	29	1.08	0.02	0.17
D	Mid	2	30	1.04	0.02	0.17
D	Mid	2	31	1.01	0.03	0.18
D	Mid	2	32	1.00	0.03	0.19
D	Mid	2	33	0.96	0.04	0.25
D	Mid	2	34	0.80	0.08	0.41
D	Edge	3	1	1.27	0.26	0.13
D	Edge	3	2	1.01	0.07	0.12
D	Edge	3	3	0.94	0.07	0.12
D	Edge	3	4	0.83	0.08	0.13
D	Edge	3	5	0.75	0.07	0.12
D	Edge	3	6	0.77	0.08	0.12
D	Edge	3	7	0.78	0.08	0.12
D	Edge	3	8	0.79	0.10	0.12
D	Edge	3	9	0.74	0.10	0.12
D	Edge	3	10	0.68	0.09	0.11
D	Edge	3	11	0.66	0.10	0.11

D	Edge	3	12	0.62	0.10	0.11
D	Edge	3	13	0.61	0.10	0.11
D	Edge	3	14	0.60	0.11	0.12
D	Edge	3	15	0.59	0.12	0.11
D	Edge	3	16	0.60	0.12	0.11
D	Edge	3	17	0.57	0.12	0.11
D	Edge	3	18	0.53	0.13	0.11
D	Edge	3	19	0.52	0.14	0.11
D	Edge	3	20	0.51	0.14	0.11
D	Edge	3	21	0.50	0.15	0.11
D	Edge	3	22	0.49	0.15	0.11
D	Edge	3	23	0.46	0.16	0.11
D	Edge	3	24	0.42	0.15	0.11
D	Edge	3	25	0.38	0.13	0.10
D	Edge	3	26	0.37	0.13	0.09
D	Edge	3	27	0.36	0.14	0.09
D	Edge	3	28	0.34	0.14	0.09
D	Edge	3	29	0.32	0.13	0.09
D	Edge	3	30	0.28	0.13	0.09
D	Edge	3	31	0.27	0.14	0.09
D	Edge	3	32	0.25	0.14	0.09
D	Edge	3	33	0.27	0.16	0.10
D	Edge	3	34	0.48	0.13	0.16
D	Edge	3	35	0.80	0.10	0.26
E	Umbo	1	1	0.93	0.21	0.13
E	Umbo	1	2	0.68	0.11	0.12
E	Umbo	1	3	0.56	0.12	0.11
E	Umbo	1	4	0.47	0.15	0.10
E	Umbo	1	5	0.43	0.18	0.09
E	Umbo	1	6	0.44	0.22	0.09
E	Umbo	1	7	0.79	0.10	0.11
E	Umbo	1	8	1.12	0.02	0.10
E	Umbo	1	9	1.10	0.02	0.10
E	Umbo	1	10	0.98	0.02	0.10
E	Umbo	1	11	1.04	0.01	0.10
E	Umbo	1	12	0.97	0.02	0.09
E	Umbo	1	13	0.89	0.02	0.09
E	Umbo	1	14	0.95	0.02	0.09
E	Umbo	1	15	0.91	0.02	0.09
E	Umbo	1	16	0.93	0.02	0.08
E	Umbo	1	17	0.89	0.02	0.08
E	Umbo	1	18	0.96	0.02	0.08
E	Umbo	1	19	0.97	0.02	0.08
E	Umbo	1	20	0.96	0.02	0.08
E	Umbo	1	21	1.00	0.02	0.08
E	Umbo	1	22	1.05	0.02	0.08
E	Umbo	1	23	1.00	0.02	0.09
E	Umbo	1	24	0.94	0.02	0.10
E	Umbo	1	25	0.92	0.02	0.12
E	Umbo	1	26	0.94	0.02	0.15
E	Umbo	1	27	0.89	0.02	0.24
E	Umbo	1	28	0.94	0.02	0.17
E	Umbo	1	29	0.97	0.01	0.15
E	Umbo	1	30	0.99	0.01	0.19
E	Umbo	1	31	1.07	0.02	0.19
E	Umbo	1	32	1.07	0.02	0.19
E	Umbo	1	33	1.04	0.02	0.19
E	Umbo	1	34	1.04	0.01	0.19

E	Umbo	1	35	1.02	0.01	0.17
E	Umbo	1	36	0.95	0.01	0.16
E	Umbo	1	37	1.01	0.02	0.15
E	Umbo	1	38	1.00	0.01	0.14
E	Umbo	1	39	1.02	0.02	0.17
E	Umbo	1	40	1.07	0.02	0.17
E	Umbo	1	41	1.03	0.01	0.19
E	Umbo	1	42	1.06	0.02	0.22
E	Umbo	1	43	0.98	0.02	0.38
E	Umbo	1	44	0.99	0.01	0.35
E	Umbo	1	45	1.05	0.01	0.24
E	Umbo	1	46	1.01	0.01	0.18
E	Umbo	1	47	1.05	0.01	0.15
E	Umbo	1	48	1.01	0.02	0.16
E	Umbo	1	49	0.99	0.02	0.15
E	Umbo	1	50	0.94	0.01	0.14
E	Umbo	1	51	0.92	0.01	0.13
E	Umbo	1	52	0.92	0.01	0.13
E	Umbo	1	53	0.99	0.02	0.15
E	Umbo	1	54	1.02	0.01	0.14
E	Umbo	1	55	0.97	0.01	0.13
E	Umbo	1	56	1.00	0.01	0.13
E	Umbo	1	57	0.99	0.01	0.14
E	Umbo	1	58	0.92	0.01	0.14
E	Umbo	1	59	0.89	0.02	0.13
E	Umbo	1	60	0.89	0.01	0.14
E	Umbo	1	61	0.92	0.01	0.15
E	Umbo	1	62	0.90	0.01	0.13
E	Umbo	1	63	0.95	0.01	0.15
E	Umbo	1	64	0.91	0.01	0.13
E	Umbo	1	65	0.97	0.01	0.14
E	Umbo	1	66	1.00	0.01	0.14
E	Umbo	1	67	0.98	0.02	0.14
E	Umbo	1	68	1.03	0.01	0.13
E	Umbo	1	69	1.04	0.01	0.12
E	Umbo	1	70	1.01	0.01	0.12
E	Umbo	1	71	1.00	0.01	0.12
E	Umbo	1	72	1.04	0.01	0.12
E	Umbo	1	73	1.05	0.01	0.12
E	Umbo	1	74	1.04	0.01	0.12
E	Umbo	1	75	0.99	0.01	0.11
E	Umbo	1	76	1.02	0.01	0.12
E	Umbo	1	77	1.08	0.01	0.13
E	Umbo	1	78	1.04	0.02	0.13
E	Umbo	1	79	1.06	0.01	0.13
E	Umbo	1	80	1.13	0.02	0.12
E	Umbo	1	81	1.14	0.02	0.12
E	Umbo	1	82	1.02	0.02	0.14
E	Umbo	1	83	1.00	0.02	0.19
E	Umbo	1	84	0.84	0.02	0.19
E	Umbo	1	85	0.99	0.02	0.17
E	Umbo	1	86	1.02	0.02	0.20
E	Umbo	1	87	0.82	0.04	0.36
E	Umbo	1	88	0.84	0.04	0.37
E	Umbo	1	89	0.93	0.02	0.28
E	Umbo	1	90	0.95	0.01	0.24
E	Umbo	1	91	0.84	0.02	0.20
E	Umbo	1	92	1.06	0.01	0.21

E	Umbo	1	93	1.06	0.01	0.22
E	Umbo	1	94	1.04	0.01	0.18
E	Umbo	1	95	1.12	0.01	0.15
E	Umbo	1	96	1.12	0.01	0.15
E	Umbo	1	97	1.10	0.01	0.14
E	Umbo	1	98	1.09	0.01	0.14
E	Umbo	1	99	1.11	0.01	0.13
E	Umbo	1	100	1.17	0.01	0.13
E	Umbo	1	101	1.08	0.01	0.13
E	Umbo	1	102	1.11	0.01	0.13
E	Umbo	1	103	1.13	0.01	0.15
E	Umbo	1	104	1.09	0.01	0.14
E	Umbo	1	105	1.08	0.01	0.13
E	Umbo	1	106	1.07	0.05	0.12
E	Umbo	1	107	1.06	0.01	0.12
E	Umbo	1	108	1.09	0.01	0.12
E	Umbo	1	109	1.10	0.01	0.12
E	Umbo	1	110	1.04	0.02	0.11
E	Umbo	1	111	1.12	0.01	0.12
E	Umbo	1	112	1.11	0.01	0.12
E	Umbo	1	113	1.14	0.02	0.13
E	Umbo	1	114	1.07	0.02	0.13
E	Umbo	1	115	1.09	0.02	0.14
E	Umbo	1	116	1.00	0.02	0.14
E	Umbo	1	117	1.09	0.02	0.14
E	Umbo	1	118	0.97	0.02	0.17
E	Umbo	1	119	0.85	0.05	0.31
E	Umbo	2	1	0.87	0.17	0.13
E	Umbo	2	2	0.59	0.12	0.12
E	Umbo	2	3	0.48	0.11	0.11
E	Umbo	2	4	0.47	0.15	0.09
E	Umbo	2	5	0.47	0.28	0.09
E	Umbo	2	6	0.42	0.26	0.09
E	Umbo	2	7	0.50	0.18	0.10
E	Umbo	2	8	1.02	0.03	0.10
E	Umbo	2	9	1.05	0.03	0.10
E	Umbo	2	10	1.03	0.02	0.09
E	Umbo	2	11	1.03	0.02	0.09
E	Umbo	2	12	0.98	0.02	0.09
E	Umbo	2	13	0.94	0.02	0.08
E	Umbo	2	14	0.95	0.02	0.08
E	Umbo	2	15	0.93	0.02	0.08
E	Umbo	2	16	0.96	0.01	0.08
E	Umbo	2	17	0.98	0.01	0.08
E	Umbo	2	18	0.97	0.01	0.08
E	Umbo	2	19	0.97	0.01	0.08
E	Umbo	2	20	0.97	0.02	0.08
E	Umbo	2	21	1.04	0.02	0.08
E	Umbo	2	22	1.01	0.02	0.09
E	Umbo	2	23	0.97	0.02	0.11
E	Umbo	2	24	0.94	0.02	0.15
E	Umbo	2	25	0.91	0.02	0.22
E	Umbo	2	26	1.01	0.02	0.15
E	Umbo	2	27	1.01	0.01	0.16
E	Umbo	2	28	1.03	0.01	0.18
E	Umbo	2	29	1.03	0.01	0.19
E	Umbo	2	30	1.07	0.01	0.19
E	Umbo	2	31	1.03	0.01	0.18

E	Umbo	2	32	1.07	0.01	0.18
E	Umbo	2	33	1.10	0.01	0.17
E	Umbo	2	34	1.13	0.01	0.16
E	Umbo	2	35	1.17	0.01	0.15
E	Umbo	2	36	1.14	0.01	0.13
E	Umbo	2	37	1.15	0.01	0.15
E	Umbo	2	38	1.14	0.01	0.17
E	Umbo	2	39	1.11	0.02	0.18
E	Umbo	2	40	1.10	0.02	0.18
E	Umbo	2	41	1.06	0.02	0.20
E	Umbo	2	42	1.04	0.02	0.31
E	Umbo	2	43	1.04	0.02	0.39
E	Umbo	2	44	1.08	0.01	0.24
E	Umbo	2	45	1.07	0.01	0.18
E	Umbo	2	46	0.98	0.01	0.17
E	Umbo	2	47	1.04	0.01	0.16
E	Umbo	2	48	1.05	0.01	0.15
E	Umbo	2	49	0.98	0.01	0.15
E	Umbo	2	50	0.96	0.01	0.13
E	Umbo	2	51	0.99	0.02	0.14
E	Umbo	2	52	0.95	0.01	0.14
E	Umbo	2	53	0.95	0.01	0.13
E	Umbo	2	54	0.95	0.01	0.13
E	Umbo	2	55	0.96	0.01	0.13
E	Umbo	2	56	0.94	0.01	0.14
E	Umbo	2	57	0.94	0.01	0.14
E	Umbo	2	58	0.97	0.01	0.14
E	Umbo	2	59	0.95	0.01	0.13
E	Umbo	2	60	0.95	0.01	0.13
E	Umbo	2	61	0.96	0.01	0.13
E	Umbo	2	62	0.96	0.01	0.13
E	Umbo	2	63	1.00	0.01	0.13
E	Umbo	2	64	0.96	0.01	0.14
E	Umbo	2	65	0.97	0.01	0.14
E	Umbo	2	66	0.98	0.01	0.14
E	Umbo	2	67	0.98	0.01	0.13
E	Umbo	2	68	0.95	0.01	0.13
E	Umbo	2	69	0.97	0.01	0.12
E	Umbo	2	70	0.97	0.01	0.13
E	Umbo	2	71	0.99	0.01	0.13
E	Umbo	2	72	1.01	0.01	0.12
E	Umbo	2	73	1.01	0.07	0.11
E	Umbo	2	74	1.04	0.21	0.11
E	Umbo	2	75	1.07	0.01	0.11
E	Umbo	2	76	1.05	0.01	0.12
E	Umbo	2	77	1.04	0.01	0.13
E	Umbo	2	78	1.07	0.01	0.12
E	Umbo	2	79	1.09	0.01	0.12
E	Umbo	2	80	1.02	0.01	0.12
E	Umbo	2	81	1.09	0.01	0.11
E	Umbo	2	82	1.05	0.02	0.13
E	Umbo	2	83	0.93	0.02	0.17
E	Umbo	2	84	0.93	0.02	0.21
E	Umbo	2	85	1.04	0.02	0.17
E	Umbo	2	86	1.03	0.01	0.15
E	Umbo	2	87	1.01	0.02	0.16
E	Umbo	2	88	0.82	0.03	0.39
E	Umbo	2	89	0.84	0.04	0.49

E	Umbo	2	90	0.99	0.02	0.32
E	Umbo	2	91	0.96	0.01	0.28
E	Umbo	2	92	0.96	0.01	0.26
E	Umbo	2	93	1.02	0.01	0.19
E	Umbo	2	94	1.01	0.01	0.16
E	Umbo	2	95	1.00	0.01	0.19
E	Umbo	2	96	1.03	0.01	0.19
E	Umbo	2	97	1.06	0.01	0.16
E	Umbo	2	98	1.10	0.01	0.14
E	Umbo	2	99	1.11	0.01	0.14
E	Umbo	2	100	1.10	0.01	0.14
E	Umbo	2	101	1.11	0.01	0.14
E	Umbo	2	102	1.08	0.01	0.13
E	Umbo	2	103	1.08	0.01	0.13
E	Umbo	2	104	1.10	0.01	0.13
E	Umbo	2	105	1.02	0.01	0.14
E	Umbo	2	106	1.04	0.02	0.14
E	Umbo	2	107	1.06	0.02	0.13
E	Umbo	2	108	1.10	0.01	0.12
E	Umbo	2	109	1.10	0.01	0.12
E	Umbo	2	110	1.05	0.01	0.11
E	Umbo	2	111	1.07	0.02	0.13
E	Umbo	2	112	1.12	0.02	0.14
E	Umbo	2	113	1.03	0.02	0.14
E	Umbo	2	114	1.05	0.02	0.14
E	Umbo	2	115	1.06	0.02	0.15
E	Umbo	2	116	0.94	0.03	0.21

A.4 Conventional Mass Spectrometry $\delta^{18}O$ & $\delta^{13}C$ values

Onto. Stage	Sample No.	Valve	Shell Area	Layer	δ18O VPDB				δ13C VPDB			
					1	2	3	Mean	1	2	3	Mean
A	2	Both	All	Both	-1.46	-1.65	-2.08	-1.73	-0.77	-0.86	-0.92	-0.85
A	6	Both	All	Both	-0.30	-1.01	-	-0.66	-0.60	-0.84	-	-0.72
A	7	Both	All	Both	-1.04	-0.59	-	-0.81	-0.79	-0.72	-	-0.76
B	6	Both	Umbo	Calc	-0.71	-	-	-0.71	-1.55	-	-	-1.55
B	6	Both	Mid	Calc	-0.33	-0.54	-	-0.43	-1.35	-1.46	-	-1.40
B	6	Both	Edge	Calc	-1.71	-	-	-1.71	-1.26	-	-	-1.26
B	6	Both	Umbo	Arag	-0.57	-1.22	-	-0.90	0.17	0.27	-	0.22
B	7	R	All	Both	-1.84	-1.85	-	-1.85	-0.87	-0.92	-	-0.90
B	7	L	All	Both	-1.76	-2.22	-	-1.99	-1.13	-1.22	-	-1.18
B	8	Both	All	Both	0.00	-1.01	-	-0.51	-0.59	-0.72	-	-0.65
B	9	Both	Umbo	Calc	-0.76	-0.67	-	-0.72	-1.59	-1.70	-	-1.64
B	9	Both	Mid	Calc	-0.56	-0.18	-	-0.37	-1.43	-1.29	-	-1.36
B	9	Both	Edge	Calc	-1.94	-1.23	-	-1.59	-1.61	-1.18	-	-1.39
B	9	Both	Umbo	Arag	-4.47	-3.69	-3.39	-3.85	-1.34	-1.07	-0.86	-1.09
C	1	L	Umbo	Calc	-1.08	-0.99	-1.00	-1.02	-1.75	-1.81	-1.82	-1.79
C	1	L	Mid	Calc	-0.42	-0.44	-0.11	-0.32	-1.52	-1.61	-1.55	-1.56
C	1	L	Edge	Calc	-1.30	-1.22	-1.24	-1.25	-1.29	-1.28	-1.32	-1.30
C	1	R	Umbo	Calc	-0.56	-0.64	-0.63	-0.61	-1.56	-1.61	-1.68	-1.61
C	1	R	Mid	Calc	-1.08	-1.25	-1.21	-1.18	-1.54	-1.57	-1.59	-1.57
C	1	R	Edge	Calc	-1.08	-1.28	-1.19	-1.18	-0.92	-0.90	-0.92	-0.92
C	1	L	Umbo	Arag	-1.02	-0.93	-0.95	-0.97	0.10	0.14	0.14	0.13
C	1	L	Mid	Arag	-0.28	-0.46	-0.87	-0.54	0.08	0.11	0.06	0.08
C	1	R	Umbo	Arag	-0.78	-0.79	-0.76	-0.78	0.21	0.25	0.23	0.23
C	1	R	Mid	Arag	-0.76	-0.69	-0.53	-0.66	0.19	0.19	0.10	0.16
C	3	Both	Umbo	Calc	-0.48	-0.45	-	-0.47	-1.70	-1.69	-	-1.70
C	3	Both	Mid	Calc	-0.31	-0.15	-	-0.23	-1.46	-1.43	-	-1.45
C	3	Both	Edge	Calc	-1.23	-1.19	-1.59	-1.34	-1.11	-1.20	-1.23	-1.18
C	3	Both	Umbo	Arag	-1.21	-1.22	-	-1.22	0.15	0.11	-	0.13
C	3	Both	Mid	Arag	-1.01	-1.26	-	-1.13	0.34	0.38	-	0.36
D	1	L	Umbo	Calc	-1.62	-1.47	-1.71	-1.60	-1.64	-1.69	-1.71	-1.68
D	1	L	Mid	Calc	-1.75	-1.58	-1.79	-1.70	-1.92	-1.89	-1.87	-1.89
D	1	L	Edge	Calc	-1.77	-1.77	-1.60	-1.71	-1.71	-1.72	-1.72	-1.71
D	1	R	Umbo	Calc	-1.44	-1.50	-1.45	-1.47	-1.64	-1.66	-1.74	-1.68
D	1	R	Mid	Calc	-1.44	-1.32	-1.29	-1.35	-1.94	-1.94	-1.90	-1.93
D	1	R	Edge	Calc	-1.58	-1.70	-1.40	-1.56	-1.95	-1.96	-1.93	-1.95
D	1	L	Umbo	Arag	-1.48	-1.93	-2.14	-1.85	-0.58	-0.51	-0.61	-0.57
D	1	L	Mid	Arag	-1.85	-1.76	-1.77	-1.79	-0.48	-0.44	-0.44	-0.45
D	1	R	Umbo	Arag	-1.52	-1.61	-1.97	-1.70	-0.51	-0.51	-0.43	-0.49
D	1	R	Mid	Arag	-1.27	-1.88	-1.41	-1.52	-0.53	-0.42	-0.38	-0.44
D	5	L	Mid	Calc	-1.24	-1.23	-1.16	-1.21	-0.69	-0.89	-0.91	-0.83
D	5	L	Edge	Calc	-1.56	-1.15	-1.34	-1.35	-0.98	-0.81	-0.88	-0.89
D	5	R	Mid	Calc	-0.97	-1.93	-1.05	-1.32	-0.97	-1.44	-0.98	-1.13
D	5	R	Edge	Calc	-1.59	-1.54	-	-1.57	-1.22	-1.26	-	-1.24
D	5	L	Umbo	Arag	-1.12	-1.31	-1.37	-1.27	0.96	0.86	0.79	0.87
D	5	L	Mid	Arag	-1.43	-1.08	-1.18	-1.23	0.36	0.35	0.51	0.41
D	5	R	Umbo	Arag	-1.12	-1.12	-1.26	-1.17	0.38	0.51	0.39	0.43
D	5	R	Mid	Arag	-1.06	-1.33	-1.22	-1.20	-0.01	0.08	0.08	0.05
E	5	L	Umbo	Calc	-1.55	-2.00	-1.70	-1.75	-1.33	-1.51	-1.47	-1.44
E	5	L	Mid	Calc	-0.71	-1.91	-1.72	-1.45	-1.48	-1.69	-1.73	-1.63
E	5	L	Edge	Calc	-2.72	-2.50	-2.58	-2.60	-1.71	-1.59	-1.55	-1.62
E	5	R	Umbo	Calc	-1.83	-1.39	-	-1.61	-1.39	-1.09	-	-1.24

E	5	R	Mid	Calc	-1.51	-1.24	-1.50	-1.42	-1.28	-1.25	-1.28	-1.27
E	5	R	Edge	Calc	-2.93	-2.74	-2.50	-2.72	-1.67	-1.67	-1.61	-1.65
E	5	L	Umbo	Arag	-1.86	-1.89	-1.41	-1.72	-0.10	0.04	0.17	0.04
E	5	L	Mid	Arag	-2.31	-1.91	-2.61	-2.28	-0.72	-0.09	-0.64	-0.48
E	5	R	Umbo	Arag	-1.95	-1.82	-1.37	-1.71	-0.02	0.02	0.09	0.03
E	5	R	Mid	Arag	-2.13	-2.47	-2.53	-2.38	-0.19	-0.45	-0.74	-0.46
E	7	L	Umbo	Calc	-1.08	-0.98	-1.20	-1.09	-1.48	-1.53	-1.27	-1.42
E	7	L	Mid	Calc	-1.19	-1.27	-1.37	-1.28	-1.67	-1.74	-1.82	-1.74
E	7	L	Edge	Calc	-1.90	-2.25	-1.80	-1.98	-1.55	-1.61	-1.24	-1.47
E	7	R	Umbo	Calc	-1.26	-1.14	-	-1.20	-1.09	-1.15	-	-1.12
E	7	R	Mid	Calc	-0.98	-1.04	-1.16	-1.06	-1.57	-1.58	-1.71	-1.62
E	7	R	Edge	Calc	-2.43	-2.28	-2.27	-2.33	-1.66	-1.70	-1.72	-1.70
E	7	L	Umbo	Arag	-1.57	-1.72	-1.54	-1.61	0.02	-0.03	-0.11	-0.04
E	7	L	Mid	Arag	-1.06	-1.32	-	-1.19	-0.35	-0.11	-	-0.23
E	7	R	Umbo	Arag	-0.86	-0.64	-1.47	-0.99	0.20	0.45	-0.15	0.17
E	7	R	Mid	Arag	-1.66	-1.56	-1.43	-1.55	-0.13	-0.02	0.05	-0.03
E	10	L	Mid	Calc	-1.00	-1.26	-1.18	-1.15	-1.27	-1.25	-1.35	-1.29
E	10	L	Edge	Calc	-2.52	-2.38	-2.43	-2.44	-1.76	-1.76	-1.81	-1.78
E	10	R	Mid	Calc	-0.77	-0.33	-0.38	-0.49	-1.38	-1.18	-1.07	-1.21
E	10	R	Edge	Calc	-1.71	-1.80	-2.00	-1.84	-1.36	-1.46	-1.48	-1.43
E	10	L	Umbo	Arag	-1.06	-0.72	-1.13	-0.97	0.08	0.07	0.07	0.07
E	10	L	Mid	Arag	-1.36	-1.32	-1.27	-1.32	-0.29	-0.30	-0.16	-0.25
E	10	R	Umbo	Arag	-0.98	-1.11	-1.27	-1.12	0.12	0.12	0.03	0.09
E	10	R	Mid	Arag	-0.91	-0.79	-1.15	-0.95	0.26	0.28	0.29	0.28
F	1	L	Umbo	Calc	-1.42	0.30	-	-0.56	-1.73	-0.03	-	-0.88
F	1	L	Mid	Calc	-0.86	-1.33	-1.45	-1.21	-1.46	-1.44	-1.50	-1.47
F	1	L	Edge	Calc	-1.92	-1.77	-1.69	-1.80	-1.57	-1.60	-1.70	-1.63
F	1	R	Umbo	Calc	-1.12	-1.01	-1.07	-1.07	-1.57	-1.76	-1.79	-1.71
F	1	R	Mid	Calc	-1.42	-1.46	-1.41	-1.43	-1.79	-1.79	-1.74	-1.78
F	1	R	Edge	Calc	-1.70	-1.71	-1.80	-1.74	-1.47	-1.53	-1.49	-1.50
F	1	L	Umbo	Arag	-0.89	-1.08	-1.35	-1.11	0.38	0.13	0.09	0.20
F	1	L	Mid	Arag	-1.49	-1.43	-1.69	-1.54	-0.11	-0.01	-0.21	-0.11
F	1	R	Umbo	Arag	-0.74	-0.88	-1.04	-0.89	-0.16	-0.14	-0.10	-0.14
F	1	R	Mid	Arag	-1.29	-1.41	-1.33	-1.35	0.07	0.02	0.03	0.04
F	5	L	Umbo	Calc	-1.43	-1.40	-1.42	-1.42	-1.35	-1.36	-1.24	-1.31
F	5	L	Mid	Calc	-2.00	-2.08	-2.11	-2.06	-1.90	-2.02	-2.12	-2.01
F	5	L	Edge	Calc	-1.93	-1.74	-1.87	-1.85	-1.78	-1.73	-1.70	-1.74
F	5	R	Mid	Calc	-1.42	-1.36	-	-1.39	-1.54	-1.68	-	-1.61
F	5	R	Edge	Calc	-1.54	-1.55	-1.17	-1.42	-1.69	-1.68	-1.62	-1.66
F	5	L	Umbo	Arag	-1.35	-1.75	-2.00	-1.70	-0.41	-0.61	-0.65	-0.56
F	5	L	Mid	Arag	-1.96	-1.74	-2.16	-1.95	-0.43	-0.27	-0.69	-0.46
F	5	R	Mid	Arag	-1.38	-1.31	-1.26	-1.32	0.21	0.29	0.27	0.25
F	8	L	Umbo	Calc	-1.34	-1.24	-1.11	-1.23	-1.59	-1.57	-1.35	-1.51
F	8	L	Mid	Calc	-1.41	-1.38	-	-1.39	-1.16	-1.19	-	-1.18
F	8	L	Edge	Calc	-1.26	-1.33	-	-1.30	-1.60	-1.68	-	-1.64
F	8	R	Umbo	Calc	-1.10	-1.04	-	-1.07	-1.54	-1.58	-	-1.56
F	8	R	Mid	Calc	-1.66	-1.50	-	-1.58	-1.94	-1.85	-	-1.90
F	8	R	Edge	Calc	-1.56	-1.45	-1.47	-1.49	-2.28	-2.26	-2.16	-2.23
F	8	L	Umbo	Arag	-1.10	-1.23	-	-1.16	-0.50	-0.55	-	-0.52
F	8	L	Mid	Arag	-1.08	-1.05	-	-1.06	-0.11	-0.04	-	-0.08
F	8	R	Umbo	Arag	-1.10	-1.20	-	-1.15	-0.65	-0.60	-	-0.63
F	8	R	Mid	Arag	-1.16	-1.06	-	-1.11	-0.91	-0.92	-	-0.91

A.5 Secondary Ion Mass Spectrometry $\delta^{18}O$ values

Onto. Stage	Line No.	Point	Shell Area	δ18O VPDB
A	1	1	Umbo	-4.84
A	1	2	Umbo	-5.36
A	1	3	Umbo	-5.69
A	1	4	Umbo	-4.61
A	1	5	Umbo	-5.89
A	1	6	Umbo	-4.46
A	1	7	Umbo	-4.47
A	1	8	Umbo	-4.70
A	1	9	Umbo	-4.85
A	2	1	Umbo	-3.45
A	2	2	Umbo	-1.10
A	2	3	Umbo	-4.58
A	2	4	Umbo	-4.28
A	2	5	Umbo	-4.70
A	2	6	Umbo	-4.23
A	2	7	Umbo	-3.80
A	3	1	Umbo	-3.54
A	3	2	Umbo	-3.33
A	3	3	Umbo	-1.23
A	3	4	Umbo	-5.03
A	3	5	Umbo	-4.86
A	3	6	Umbo	-4.37
A	3	7	Umbo	-2.82
A	4	1	Mid	-2.10
A	4	2	Mid	-1.71
A	4	3	Mid	-4.70
A	4	4	Mid	-4.51
A	5	1	Mid	-2.32
A	5	2	Mid	-1.42
A	5	3	Mid	-5.32
A	5	4	Mid	-4.30
A	6	1	Mid	-3.85
A	6	2	Mid	-3.37
A	6	3	Mid	-4.86
A	6	4	Mid	-6.26
A	7	1	Edge	-3.24
A	7	2	Edge	-4.01
A	7	3	Edge	-3.37
A	7	4	Edge	-3.42
A	8	1	Edge	-3.53
A	8	2	Edge	-3.45
A	8	3	Edge	-2.93
A	8	4	Edge	-2.93
A	9	1	Edge	-3.29
A	9	2	Edge	-3.93
A	9	3	Edge	-3.25
A	9	4	Edge	-3.15
C	1	1	Umbo	-3.66
C	1	2	Umbo	-2.85
C	1	3	Umbo	-1.23
C	1	4	Umbo	-0.93

C	1	5	Umbo	-0.42
C	1	6	Umbo	-1.74
C	1	7	Umbo	-2.53
C	1	8	Umbo	-2.18
C	1	9	Umbo	-0.86
C	1	10	Umbo	-0.85
C	1	11	Umbo	0.93
C	1	12	Umbo	0.18
C	1	13	Umbo	0.78
C	1	14	Umbo	-2.11
C	1	15	Umbo	-0.92
C	2	1	Umbo	-2.71
C	2	2	Umbo	-1.49
C	2	3	Umbo	-1.70
C	2	4	Umbo	-1.95
C	2	5	Umbo	-1.87
C	2	6	Umbo	-1.63
C	2	7	Umbo	-0.79
C	2	8	Umbo	-1.45
C	2	9	Umbo	-1.50
C	2	10	Umbo	-1.69
C	2	11	Umbo	-1.53
C	2	12	Umbo	-0.59
C	2	13	Umbo	-2.51
C	2	14	Umbo	-1.68
C	3	1	Umbo	-5.58
C	3	2	Umbo	-3.33
C	3	3	Umbo	-2.11
C	3	4	Umbo	-2.31
C	3	5	Umbo	-2.20
C	3	6	Umbo	-1.96
C	3	7	Umbo	-1.33
C	3	8	Umbo	-1.76
C	3	9	Umbo	-3.36
C	3	10	Umbo	-0.09
C	3	11	Umbo	-1.40
C	4	1	Mid	-2.72
C	4	2	Mid	-2.82
C	4	3	Mid	-1.56
C	4	4	Mid	-0.43
C	4	5	Mid	-2.14
C	4	6	Mid	-2.23
C	4	7	Mid	-2.69
C	4	8	Mid	-3.11
C	5	1	Mid	-3.76
C	5	2	Mid	-2.71
C	5	3	Mid	-1.16
C	5	4	Mid	-0.32
C	5	5	Mid	-1.50
C	5	6	Mid	-2.23
C	5	7	Mid	-2.11
C	5	8	Mid	-2.80
C	6	1	Mid	-2.74
C	6	2	Mid	-1.79
C	6	3	Mid	-0.51
C	6	4	Mid	0.23
C	6	5	Mid	-2.06
C	6	6	Mid	-1.97

C	6	7	Mid	-1.73
C	6	8	Mid	-2.69
C	7	1	Edge	-4.50
C	7	2	Edge	-5.44
C	7	3	Edge	-4.75
C	7	4	Edge	-4.98
C	7	5	Edge	-5.96
C	8	1	Edge	-5.16
C	8	2	Edge	-5.80
C	8	3	Edge	-4.93
C	8	4	Edge	-4.94
C	8	5	Edge	-5.58
C	9	1	Edge	-4.13
C	9	2	Edge	-4.97
C	9	3	Edge	-4.60
C	9	4	Edge	-5.18
C	9	5	Edge	-5.59
F	1	1	Umbo	-2.65
F	1	2	Umbo	-2.93
F	1	3	Umbo	-3.47
F	1	4	Umbo	-1.78
F	1	5	Umbo	-4.07
F	1	6	Umbo	-3.98
F	1	7	Umbo	-4.05
F	1	8	Umbo	-3.26
F	1	9	Umbo	-3.06
F	1	10	Umbo	-3.41
F	1	11	Umbo	-2.81
F	2	1	Umbo	-3.99
F	2	2	Umbo	-2.89
F	2	3	Umbo	-3.15
F	2	4	Umbo	-2.29
F	2	5	Umbo	-1.75
F	2	6	Umbo	-4.21
F	2	7	Umbo	-4.29
F	2	8	Umbo	-3.80
F	2	9	Umbo	-3.52
F	2	10	Umbo	-3.68
F	2	11	Umbo	-3.60
F	2	12	Umbo	-2.56
F	2	13	Umbo	-2.40
F	2	14	Umbo	-3.53
F	2	15	Umbo	-3.01
F	2	16	Umbo	-2.53
F	2	17	Umbo	-3.68
F	3	1	Umbo	-5.80
F	3	2	Umbo	-4.93
F	3	3	Umbo	-4.77
F	3	4	Umbo	-3.34
F	3	5	Umbo	-4.87
F	3	6	Umbo	-5.33
F	3	7	Umbo	-5.17
F	3	8	Umbo	-5.10
F	3	9	Umbo	-5.35
F	3	10	Umbo	-4.73
F	3	11	Umbo	-3.89
F	3	12	Umbo	-4.12
F	3	13	Umbo	-2.13

F	3	14	Umbo	-3.93
F	3	15	Umbo	-4.98
F	3	16	Umbo	-4.16
F	3	17	Umbo	-4.50

References

Adams, B.L., Wright, S.I., & Kunze, K., 1993, Orientation Imaging - the Emergence of a New Microscopy: *Metallurgical Transactions a-Physical Metallurgy and Materials Science*, **24**, 819-831.

Addadi, L., Aizenberg, J., Albeck, S., Berman, A., Leiserowitz, L., & Weiner, S., 1994, Controlled Occlusion Of Proteins - A Tool For Modulating The Properties Of Skeletal Elements: *Molecular Crystals And Liquid Crystals Science And Technology Section A-Molecular Crystals And Liquid Crystals*, **248**, 185-198.

Addadi, L., Joester, D., Nudelman, F., & Weiner, S., 2006, Mollusk shell formation: A source of new concepts for understanding biomineralization processes: *Chemistry-A European Journal*, **12**, 981-987.

Addadi, L., & Weiner, S., 1986, Interactions Between Acidic Macromolecules And Structured Crystal-Surfaces - Stereochemistry And Biomineralization: *Molecular Crystals And Liquid Crystals*, **134**, 305-322.

Addadi, L., & Weiner, S., 1997, Biomineralization - A pavement of pearl: *Nature*, **389**, 912-915.

Aharon, P., 1991, Recorders of reef environment histories: stable isotopes in corals, giant clams, and calcareous algae: *Coral Reefs*, **10**, 71-90.

Aizenberg, J., Grazul, J.L., Muller, D.A., & Hamann, D.R., 2003, Direct fabrication of large micropatterned single crystals: *Science*, **299**, 1205-1208.

Aizenberg, J., Ilan, N., Weiner, S., & Addadi, L., 1996, Intracrystalline macromolecules are involved in the morphogenesis of calcitic sponge spicules: *Connective Tissue Research*, **35**, 17-23.

Alam, M.N., Blackman, M., & Pashley, D.W., 1954, High-Angle Kikuchi Patterns: *Proceedings of the Royal Society of London Series a-Mathematical and Physical Sciences*, **221**, 224-242.

Albeck, S., Addadi, L., & Weiner, S., 1996, Regulation of calcite crystal morphology by intracrystalline acidic proteins and glycoproteins: *Connective Tissue Research*, **35**, 419-424.

Allison, N., Finch, A.A., Newville, M., & Sutton, S.R., 2005, Strontium in coral aragonite: 3. Sr coordination and geochemistry in relation to skeletal architecture: *Geochimica et Cosmochimica Acta*, **69**, 3801-3811.

Allison, N., Finch, A.A., Webster, J.M., & Clague, D.A., 2007, Palaeoenvironmental records from fossil corals: The effects of submarine diagenesis on temperature and climate estimates: *Geochimica et Cosmochimica Acta*, **71**, 4693-4703.

Allison, N., Tudhope, A.W., & Fallick, A.E., 1996, Factors influencing the stable carbon and oxygen isotopic composition of Porites lutea coral skeletons from Phuket, South Thailand: *Coral Reefs*, **15**, 43-57.

Amiel, A.J., Friedman, G.M., & Miller, D.S., 1973, Distribution and nature of incorporation of trace elements in modern aragonitic corals: *Sedimentology*, **20**, 47-64.

Amos, F.F., Sharbaugh, D.M., Talham, D.R., Gower, L.B., Fricke, M., & Volkmer, D., 2007, Formation of single-crystalline aragonite tablets/films via an amorphous precursor: *Langmuir*, **23**, 1988-1994.

Anderson, T.F., & Steinmetz, J.C., 1983, Stable isotopes in calcareous nannofossils: potential application to deep-sea paleoenvironmental reconstructions during the Quaternary.: *Utrecht Micropaleontological Bulletin*, **30**, 189-204.

Auclair, A.C., Joachimski, M.M., & Lecuyer, C., 2003, Deciphering kinetic, metabolic and environmental controls on stable isotope fractionations between seawater and the shell of *Terebratalia transversa* (Brachiopoda): *Chemical Geology*, **202**, 59-78.

Austin, W.E.N., & Inall, M.E., 2002, Deep-water renewal in a Scottish fjord: temperature, salinity and oxygen isotopes: *Polar Research*, **21**, 251-257.

Barnes, D.J., 1970, Coral Skeletons - an Explanation of Their Growth and Structure: *Science*, **170**, 1305-1308.

Bates, N.R., & Brand, U., 1991, Environmental and Physiological Influences on Isotopic and Elemental Compositions of Brachiopod Shell Calcite - Implications for the Isotopic Evolution of Paleozoic Oceans: *Chemical Geology*, **94**, 67-78.

Bayne, B.L., 1976, The biology of mussel larvae.: London, Cambridge University Press.

Bayne, B.L., & Newell, R.C., 1983, Physiological energetics of marine molluscs., *in* Saleuddin, A.S.M., & Wilbur, K.M., eds., *The Mollusca. Physiology. Part I.* , **Volume 4**: New York, Academic Press, 407–514.

Beck, J.W., Edwards, R.L., Ito, E., Taylor, F.W., Recy, J., Rougerie, F., Joannot, P., & Henin, C., 1992, Sea-Surface Temperature from Coral Skeletal Strontium Calcium Ratios: *Science*, **257**, 644-647.

Beedham, G.E., 1958, Observations on the mantle of the Lamellibranchia: *Quarterly Journal of Microscope Science*, **99**, 181-197.

Belcher, A.M., Wu, X.H., Christensen, R.J., Hansma, P.K., Stucky, G.D., & Morse, D.E., 1996, Control of crystal phase switching and orientation by soluble mollusc-shell proteins: *Nature*, **381**, 56-58.

Bender, M.L., Lorens, R.B., & Williams, D.F., 1976, Sodium, Magnesium and Strontium in the tests of planktonic foraminifera: *Micropaleontology*, **21**, 448-459.

Beniash, E., Aizenberg, J., Addadi, L., & Weiner, S., 1997, Amorphous calcium carbonate transforms into calcite during sea urchin larval spicule growth: *Proceedings of the Royal Society of London Series B-Biological Sciences*, **264**, 461-465.

Berman, A., Hanson, J., Leiserowitz, L., Koetzle, T.F., Weiner, S., & Addadi, L., 1993, Biological-Control Of Crystal Texture - A Widespread Strategy For Adapting Crystal Properties To Function: *Science*, **259**, 776-779.

Berner, R.A., 1975, The role of magnesium in the crystal growth of calcite and aragonite from sea water: *Geochimica et Cosmochimica Acta*, **39**, 489-504.

Berner, R.A., Lasaga, A.C., & Garrels, R.M., 1983, The Carbonate-Silicate Geochemical Cycle and Its Effect on Atmospheric Carbon-Dioxide over the Past 100 Million Years: *American Journal of Science*, **283**, 641-683.

Billings, G.K., & Ragland, P.C., 1968, Geochemistry and mineralogy of the recent reef and lagoonal sediments south of Belize (British Honduras): *Chemical Geology*, **3**, 135-153.

Boggild, O.B., 1930, The shell structure of mollusks: *Kgl Danske Vidensk Selbsk Skrifter, Naturvidensk Math*, **9**, 231-326.

Bohm, F., Joachimski, M.M., Dullo, W.C., Eisenhauer, A., Lehnert, H., Reitner, J., & Worheide, G., 2000, Oxygen isotope fractionation in marine aragonite of coralline sponges: *Geochimica Et Cosmochimica Acta*, **64**, 1695-1703.

Brand, U., 1994, Continental Hydrology and Climatology of the Carboniferous Joggins Formation (Lower Cumberland Group) at Joggins, Nova-Scotia - Evidence from the Geochemistry of Bivalves: *Palaeogeography Palaeoclimatology Palaeoecology*, **106**, 307-321.

Buening, N., & Carlson, S.J., 1992, Geochemical Investigation of Growth in Selected Recent Articulate Brachiopods: *Lethaia*, **25**, 331-345.

Burton, E.A., & Walter, L.M., 1987, Relative Precipitation Rates of Aragonite and Mg Calcite from Seawater - Temperature or Carbonate Ion Control: *Geology*, **15**, 111-114.

Busenberg, E., & Plummer, L.N., 1985, Kinetic and thermodynamic factors controlling the distribution of SO_3^{2-} and Na^+ in calcites and selected aragonites: *Geochimica et Cosmochimica Acta*, **49**, 713-725.

Carpenter, S.J., & Lohmann, K.C., 1992, Sr/Mg Ratios of Modern Marine Calcite - Empirical Indicators of Ocean Chemistry and Precipitation Rate: *Geochimica Et Cosmochimica Acta*, **56**, 1837-1849.

Carpenter, S.J., & Lohmann, K.C., 1995, Delta ^{18}O And Delta ^{13}C Values Of Modern Brachiopod Shells: *Geochimica Et Cosmochimica Acta*, **59**, 3749-3764.

Carpenter, W., 1848, Report on the Microscopic Structure of Shells. Part II.: *Rep. Br. Assoc. Adv. Sci. 17th Meeting,*, 93-134.

Carriker, M.B., Palmer, R.E., & Prezant, R.S., 1980, Functional ultramorphology of the dissoconch valves of the oyster *Crassostrea virginica*: *Proceedings of the National Shellfish Association*, **70**, 139-183.

Carriker, M.R., & Palmer, R.E., 1979, New Mineralized Layer in the Hinge of the Oyster: *Science*, **206**, 691-693.

Cartwright, J.H.E., & Checa, A.G., 2006, The dynamics of nacre self-assembly: *Journal of the Royal Society Interface*, **4**, 491-504.

Chateigner, D., Hedegaard, C., & Wenke, H.R., 2000, Mollusc shell microstructures and crystallographic textures: *Journal of Structural Geology*, **22**, 1723-1735.

Chave, K.E., 1954a, Aspects of the Biogeochemistry of Magnesium .1. Calcareous Marine Organisms: *Journal of Geology*, **62**, 266-283.

Chave, K.E., 1954b, Aspects of the Biogeochemistry of Magnesium .2. Calcareous Sediments and Rocks: *Journal of Geology*, **62**, 587-599.

Checa, A.G., Jimenez-Lopez, C., Rodriguez-Navarro, A., & Machado, J.P., 2007, Precipitation of aragonite by calcitic bivalves in Mg-enriched marine waters: *Marine Biology*, **150**, 819-827.

Checa, A.G., Okamoto, T., & Ramirez, J., 2006, Organization pattern of nacre in Pteriidae (Bivalvia : Mollusca) explained by crystal competition: *Proceedings of the Royal Society B-Biological Sciences*, **273**, 1329-1337.

Checa, A.G., & Rodriguez-Navarro, A., 2001, Geometrical and crystallographic constraints determine the self-organization of shell microstructures in Unionidae (Bivalvia : Mollusca): *Proceedings of the Royal Society of London Series B-Biological Sciences*, **268**, 771-778.

Checa, A.G., & Rodriguez-Navarro, A.B., 2005, Self-organisation of nacre in the shells of Pterioida (Bivalvia : Mollusca): *Biomaterials*, **26**, 1071-1079.

Checa, A.G., Rodriguez-Navarro, A.B., Delgado, F.J.E., & Esteban-Delgado, F.J., 2005, The nature and formation of calcitic columnar prismatic shell layers in pteriomorphian bivalves: *Biomaterials*, **26**, 6404-6414.

Clark, G.R., 1974, Growth Lines in Invertebrate Skeletons: *Annual Review of Earth and Planetary Sciences*, **2**, 77-99.

Coe, W.R., 1945, Nutrition and Growth of the California Bay-Mussel (*Mytilus edulis-Diegensis*): *Journal of Experimental Zoology*, **99**, 1-14.

Coe, W.R., & Fox, D.L., 1942, Biology of the California sea-mussel (*Mytilus californianus*) I Influence of temperature, food supply, sex and age on the rate of growth: *Journal of Experimental Zoology*, **90**, 1-30.

Cohen, A.L., Layne, G.D., Hart, S.R., & Lobel, P.S., 2001, Kinetic control of skeletal Sr/Ca in a symbiotic coral: Implications for the paleotemperature proxy: *Paleoceanography*, **16**, 20-26.

Cohen, A.L., & McConnaughey, T.A., 2003, Geochemical Perspectives on Coral Mineralization., *in* Dove, P.M., De Yoreo, J.J., & Weiner, S., eds., *Reviews in Mineralogy and Geochemistry*, **Volume 54**, 151-187.

Cohen, A.L., Owens, K.E., Layne, G.D., & Shimizu, N., 2002, The effect of algal symbionts on the accuracy of Sr/Ca paleotemperatures from coral: *Science*, **296**, 331-333.

Coplen, T.B., 1995, Discontinuance Of SMOW And PDB: *Nature*, **375**, 285-285.

Craig, H., 1957, Isotopic Standards For Carbon And Oxygen And Correction Factors For Mass-Spectrometric Analysis Of Carbon Dioxide: *Geochimica Et Cosmochimica Acta*, **12**, 133-149.

Crenshaw, M.A., 1972, Inorganic Composition Of Molluscan Extrapallial Fluid: *Biological Bulletin*, **143**, 506-512.

Crenshaw, M.A., & Ristedt, H., 1976, The histochemical localization of reactive groups in septal nacre from *Nautilus pompilius* L., *in* Watabe, N., & Wilbur, K.M., eds., *The Mechanisms of Mineralization in the Invertebrates and Plants*: Columbia, Univ. South Carolina Press, 79–92.

Cronblad, H.G., & Malmgren, B.A., 1981, Climatically controlled variation of Sr and Mg in Quaternary planktonic foraminifera.: *Nature*, **291**, 61-64.

Cuif, J.P., & Dauphin, Y., 2004, Growth of calcareous nanograins within layered glycoprotein gels: A common model for Molluscan prisms and Coral fibres: *Geochimica Et Cosmochimica Acta*, **68**, A204.

Cuif, J.P., Dauphin, Y., Doucet, J., Salome, M., & Susini, J., 2003, XANES mapping of organic sulfate in three scleractinian coral skeletons: *Geochimica Et Cosmochimica Acta*, **67**, 75-83.

Cusack, M., England, J., Parkinson, D., Dalbeck, P., & Lee, M., (in press), Oxygen isotope composition, magnesium distribution and crystallography of *Terebratulina retusa*: *Fossils & Strata*.

Cusack, M., Fraser, A.C., & Stachel, T., 2003, Magnesium and phosphorus distribution in the avian eggshell: *Comparative Biochemistry And Physiology B-Biochemistry & Molecular Biology*, **134**, 63-69.

Dalbeck, P., & Cusack, M., 2006, Crystallography (electron backscatter diffraction) and chemistry (electron probe microanalysis) of the avian eggshell: *Crystal Growth & Design*, **6**, 2558-2562.

Dalbeck, P., England, J., Cusack, M., Lee, M.R., & Fallick, A.E., 2006, Crystallography and chemistry of the calcium carbonate polymorph switch in *M. edulis* shells: *European Journal of Mineralogy*, **18**, 601-609.

Dauphin, Y., Cuif, J.P., Doucet, J., Salome, M., Susini, J., & Willams, C.T., 2003a, In situ chemical speciation of sulfur in calcitic biominerals and the simple prism concept: *Journal of Structural Biology*, **142**, 272-280.

Dauphin, Y., Cuif, J.P., Doucet, J., Salome, M., Susini, J., & Williams, C.T., 2003b, In situ mapping of growth lines in the calcitic prismatic layers of mollusc shells using X-ray absorption near-edge structure (XANES) spectroscopy at the sulphur K-edge: *Marine Biology*, **142**, 299-304.

Davis, K.J., Dove, P.M., & De Yoreo, J.J., 2000, The role of Mg^{2+} as an impurity in calcite growth: *Science*, **290**, 1134-1137.

de Leeuw, N.H., 2002, Molecular dynamics simulations of the growth inhibiting effect of Fe^{2+}, Mg^{2+}, Cd^{2+}, and Sr^{2+} on calcite crystal growth: *Journal of Physical Chemistry B*, **106**, 5241-5249.

de Leeuw, N.H., & Cooper, T.G., 2004, A computer modeling study of the inhibiting effect of organic adsorbates on calcite crystal growth: *Crystal Growth & Design*, **4**, 123-133.

de Leeuw, N.H., Harding, J.H., & Parker, S.C., 2002, Molecular dynamics simulations of the incorporation of Mg^{2+}, Cd^{2+} and Sr^{2+} at calcite growth steps: Introduction of a $SrCO_3$ potential model: *Molecular Simulation*, **28**, 573-589.

De Yoreo, J.J., & Dove, P.M., 2004, Shaping crystals with biomolecules: *Science*, **306**, 1301-1302.

Degroot, K., & Duyvis, E.M., 1966, Crystal Form Of Precipitated Calcium Carbonate As Influenced By Adsorbed Magnesium Ions: *Nature*, **212**, 183-184.

Deleuze, M., & Brantley, S.L., 1997, Inhibition of calcite crystal growth by Mg^{2+} at 100[deg]C and 100 bars: Influence of growth regime: *Geochimica et Cosmochimica Acta*, **61**, 1475-1487.

Dettman, D.L., Reische, A.K., & Lohmann, K.C., 1999, Controls on the stable isotope composition of seasonal growth bands in aragonitic fresh-water bivalves (unionidae): *Geochimica Et Cosmochimica Acta*, **63**, 1049-1057.

Devilliers, S., Nelson, B.K., & Chivas, A.R., 1995, Biological-Controls on Coral Sr/Ca and Delta-O-18 Reconstructions of Sea-Surface Temperatures: *Science*, **269**, 1247-1249.

Dick, D., Philipp, E., Kriews, M., & Abele, D., 2007, Is the umbo matrix of bivalve shells (*Laternula elliptica*) a climate archive?: *Aquatic Toxicology*, **84**, 450-456.

DiMasi, E., & Sarikaya, M., 2004, Synchrotron x-ray microbeam diffraction from abalone shell: *Journal Of Materials Research*, **19**, 1471-1476.

Dingley, D.J., 1981, A Comparison of Diffraction Techniques for the SEM: *Scanning Electron Microscopy*, 273-286.

Dingley, D.J., 1984, Diffraction from Sub-Micron Areas Using Electron Backscattering in a Scanning Electron-Microscope: *Scanning Electron Microscopy*, 569-575.

Dingley, D.J., & Razavizadeh, N., 1981, The Use of Kossel Diffraction in the SEM for Precision Crystallographic Studies in Metallurgy, Mineralogy and Semiconductor-Materials: *Scanning Electron Microscopy*, 287-294.

Dodd, J.R., 1963, Paleoecological implications of shell mineralogy in two pelecypod species: *Journal of Geology*, **71**, 1-11.

Dodd, J.R., 1964, Environmentally Controlled Variation In The Shell Structure Of A Pelecypod Species: *Journal Of Paleontology*, **38**, 1065-1071.

Dodd, J.R., 1965, Environmental Control Of Strontium And Magnesium In *Mytilus*: *Geochimica Et Cosmochimica Acta*, **29**, 385-398.

Dodd, J.R., 1966, Influence Of Salinity On Mollusk Shell Mineralogy - A Discussion: *Journal Of Geology*, **74**, 85-&.

Dodd, J.R., & Crisp, E.L., 1982, Non-Linear Variation With Salinity Of Sr/Ca And Mg/Ca Ratios In Water And Aragonitic Bivalve Shells And Implications For Paleosalinity Studies: *Palaeogeography Palaeoclimatology Palaeoecology*, **38**, 45-56.

Dodd, J.R., & Stanton, R.J., 1975, Paleosalinities within a Pliocene Bay, Kettleman Hills, California - Study of Resolving Power of Isotopic and Faunal Techniques: *Geological Society of America Bulletin*, **86**, 51-64.

Donner, J., & Nord, A.G., 1986, Carbon and oxygen stable isotope values in shells of *Mytilus edulis* and *Modiolus modiolus* from Holocene raised beaches at the outer coast of the Varanger Peninsula, North Norway: *Palaeogeography Palaeoclimatology Palaeoecology*, **56**, 35-50.

Dudley, W.C., Blackwelder, P., Brand, L., & Duplessy, J.-C., 1986, Stable isotopic composition of coccoliths.: *Marine Micropaleontology*, **10**, 1-8.

Eggins, S.M., Sadekov, A., & De Deckker, P., 2004, Modulation and daily banding of Mg/Ca in Orbulina universa tests by symbiont photosynthesis and respiration: a complication for seawater thermometry?: *Earth and Planetary Science Letters*, **225**, 411-419.

Eisma, D., 1966, Influence of Salinity on Mollusk Shell Mineralogy - a Discussion: *Journal of Geology*, **74**, 89-94.

El-Dasher, B.S., & Rollett, A.D., 2005, Defining Electron Backscatter Diffraction Resolution *Microscopy and Microanalysis*, **11**, 54-55.

Elderfield, H., & Ganssen, G., 2000, Past temperature and delta O-18 of surface ocean waters inferred from foraminiferal Mg/Ca ratios: *Nature*, **405**, 442-445.

Elliot, M., deMenocal, P.B., Linsley, B.K., & Howe, S.S., 2003, Environmental controls on the stable isotopic composition of Mercenaria mercenaria: Potential application to paleoenvironmental studies: *Geochemistry Geophysics Geosystems*, **4**.

England, J., 2005, Calcium Carbonate Biomineralisation in Disparate Systems - Common Mechanisms?: Glasgow, University of Glasgow.

England, J., Cusack, M., Dalbeck, P., & Perez-Huerta, A., 2007, Comparison of the crystallographic structure of semi nacre and nacre by electron backscatter diffraction: *Crystal Growth & Design*, **7**, 307-310.

Epstein, S., Buchsbaum, R., Lowenstam, H., & Urey, H.C., 1951, Carbonate-Water Isotopic Temperature Scale: *Geological Society Of America Bulletin*, **62**, 417-426.

Epstein, S., Buchsbaum, R., Lowenstam, H.A., & Urey, H.C., 1953, Revised Carbonate-Water Isotopic Temperature Scale: *Geological Society Of America Bulletin*, **64**, 1315-1325.

Epstein, S., & Lowenstam, H.A., 1953, Temperature-Shell Growth Relations of Recent and Interglacial Pleistocene Shoal-Water Biota from Bermuda: *Journal of Geology*, **61**, 424-438.

Erben, H.K., & Watabe, N., 1974, Crystal-Formation and Growth in Bivalve Nacre: *Nature*, **248**, 128-130.

Erez, J., 2003, The source of ions for biomineralization in foraminifera and their implications for paleoceanographic proxies, *Biomineralization*, **Volume 54**: Reviews in Mineralogy & Geochemistry, 115-149.

Eyster, L.S., 1982, Embryonic Shell Formation in the Nudibranch *Aeolidia papillosa*: *American Zoologist*, **22**, 981-981.

Eyster, L.S., 1983, Ultrastructure of Early Embryonic Shell Formation in the Opisthobranch Gastropod *Aeolidia papillosa*: *Biological Bulletin*, **165**, 394-408.

Eyster, L.S., & Morse, M.P., 1984, Early Shell Formation During Molluscan Embryogenesis, with New Studies on the Surf Clam, *Spisula solidissima*: *American Zoologist*, **24**, 871-882.

Falini, G., Albeck, S., Weiner, S., & Addadi, L., 1996, Control of aragonite or calcite polymorphism by mollusk shell macromolecules: *Science*, **271**, 67-69.

Feng, Q.L., Cui, F.Z., Pu, G., Wang, R.Z., & Li, H.D., 2000a, Crystal orientation, toughening mechanisms and a mimic of nacre: *Materials Science & Engineering C-Biomimetic and Supramolecular Systems*, **11**, 19-25.

Feng, Q.L., Li, H.B., Cui, F.Z., Li, H.D., & Kim, T.N., 1999, Crystal orientation domains found in the single lamina in nacre of the *Mytilus edulis* shell: *Journal Of Materials Science Letters*, **18**, 1547-1549.

Feng, Q.L., Li, H.B., Pu, G., Zhang, D.M., Cui, F.Z., Li, H.D., & Kim, T.N., 2000b, Crystallographic alignment of calcite prisms in the oblique prismatic layer of *Mytilus edulis* shell: *Journal Of Materials Science*, **35**, 3337-3340.

Feng, Q.L., Pu, G., Pei, Y., Cui, F.Z., Li, H.D., & Kim, T.N., 2000c, Polymorph and morphology of calcium carbonate crystals induced by proteins extracted from mollusk shell: *Journal Of Crystal Growth*, **216**, 459-465.

Fernandez-Diaz, L., Putnis, A., Prieto, M., & Putnis, C.V., 1996, The role of magnesium in the crystallization of calcite and aragonite in a porous medium: *Journal of Sedimentary Research*, **66**, 482-491.

Field, D.P., 1997, Recent advances in the application of orientation mapping: *Ultramicroscopy*, **67**, 1-9.

Fischer, G., Kalberer, M., Donner, B., & Wefer, G., 1999, Stable isotopes of pteropod shells as recorders of sub-surface water conditions, comparison to the record of *G. ruber* and measured values., *in* Fischer, G., & Wefer, G., eds., *Use of Proxies in Oceanography*: Berlin, Springer, 191-206.

Frank, F.C., 1988, Orientation Mapping: *Metallurgical Transactions A-Physical Metallurgy And Materials Science*, **19**, 403-408.

Freeman, J.A., & Wilbur, K.M., 1948, Carbonic Anhydrase in Molluscs: *Biological Bulletin*, **94**, 55-59.

Freitas, P., Clarke, L.J., Kennedy, H., Richardson, C., & Abrantes, F., 2005, Mg/Ca,Sr/Ca, and stable-isotope (delta ^{18}O and delta ^{13}C) ratio profiles from the fan mussel *Pinna nobilis*: Seasonal records and temperature relationships: *Geochemistry Geophysics Geosystems*, **6**, Q04D14.

Freitas, P.S., Clarke, L.J., Kennedy, H., Richardson, C.A., & Abrantes, F., 2006, Environmental and biological controls on elemental (Mg/Ca, Sr/Ca and Mn/Ca) ratios in shells of the king scallop *Pecten maximus*: *Geochimica Et Cosmochimica Acta*, **70**, 5119-5133.

Fritz, M., Belcher, A.M., Radmacher, M., Walters, D.A., Hansma, P.K., Stucky, G.D., Morse, D.E., & Mann, S., 1994, Flat Pearls From Biofabrication Of Organized Composites On Inorganic Substrates: *Nature*, **371**, 49-51.

Fritz, P., & Poplawski, S., 1974, O-18 and C-13 in Shells of Freshwater Mollusks and Their Environments: *Earth and Planetary Science Letters*, **24**, 91-98.

Gay, C.V., & Mueller, W.J., 1973, Cellular Localization of Carbonic-Anhydrase in Avian Tissues by Labeled Inhibitor Autoradiography: *Journal of Histochemistry & Cytochemistry*, **21**, 693-702.

Gay, C.V., & Mueller, W.J., 1974, Carbonic-Anhydrase and Osteoclasts - Localization by Labeled Inhibitor Autoradiography: *Science*, **183**, 432-434.

Gehrke, N., Nassif, N., Pinna, N., Antonietti, M., Gupta, H.S., & Colfen, H., 2005, Retrosynthesis of nacre via amorphous precursor particles: *Chemistry of Materials*, **17**, 6514-6516.

Geist, J., Auerswald, K., & Boom, A., 2005, Stable carbon isotopes in freshwater mussel shells: Environmental record or marker for metabolic activity?: *Geochimica Et Cosmochimica Acta*, **69**, 3545-3554.

Gillikin, D.P., Lorrain, A., Bouillon, S., Willenz, P., & Dehairs, F., 2006, Stable carbon isotopic composition of Mytilus edulis shells: relation to metabolism, salinity, delta C-13(DIC) and phytoplankton: *Organic Geochemistry*, **37**, 1371-1382.

Gillikin, D.P., Lorrain, A., Navez, J., Taylor, J.W., Keppens, E., Baeyens, W., & Dehairs, F., 2005, Strong biological controls on Sr/Ca ratios in aragonitic marine bivalve shells: *Geochemistry Geophysics Geosystems*, **6**, Q05009.

Given, R.K., & Wilkinson, B.H., 1985, Kinetic Control of Morphology, Composition, and Mineralogy of Abiotic Sedimentary Carbonates: *Journal of Sedimentary Petrology*, **55**, 109-119.

Goldschmidt, V.M., 1926, The laws of crystal chemistry: *Naturwissenschaften*, **14**, 477-485.

Goldschmidt, V.M., 1927, Crystal structure and chemical correlation: *Berichte Der Deutschen Chemischen Gesellschaft*, **60**, 1263-1296.

Gonfiantini, R., Stichler, W., & Rozanski, K., 1995, Standards and intercomparison materials distributed by the International Atomic Energy Agency for stable isotope measurements., *Reference and Intercomparison Materials for Stable Isotopes of Light Elements. International Atomic Energy Agency*, **Volume TECDOC-825**: Vienna, International Atomic Energy Agency, 13-29.

Gonzalez, L.A., & Lohmann, K.C., 1985, Carbon and Oxygen Isotopic Composition of Holocene Reefal Carbonates: *Geology*, **13**, 811-814.

Goodkin, N.F., Hughen, K.A., & Cohen, A.L., 2007, A multicoral calibration method to approximate a universal equation relating Sr/Ca and growth rate to sea surface temperature *Paleoceanography*, **22**, PA1214.

Goodwin, D.H., Schone, B.R., & Dettman, D.L., 2003, Resolution and fidelity of oxygen isotopes as paleotemperature proxies in bivalve mollusk shells: Models and observations: *Palaios*, **18**, 110-125.

Gratz, A.J., Hillner, P.E., & Hansma, P.K., 1993, Step Dynamics And Spiral Growth On Calcite: *Geochimica Et Cosmochimica Acta*, **57**, 491-495.

Gregoire, C., 1961, Structure of Conchiolin Cases of Prisms in *Mytilus edulis (Linne)*: *Journal of Biophysical and Biochemical Cytology*, **9**, 395-400.

Griesshaber, E., Schmahl, W., Neuser, R., Job, R., Bluem, M., & Brand, U., 2005, Microstructure of brachiopod shells - An inorganic/organic fibre composite with nanocrystalline protective layer: *Mechanical Properties of Bioinspired and Biological Materials*, **844**, 99-104.

Griesshaber, E., Schmahl, W.W., Neuser, R., Pettke, T., Blum, M., Mutterlose, J., & Brand, U., 2007, Crystallographic texture and microstructure of terebratulide brachiopod shell calcite: An optimized materials design with hierarchical architecture: *American Mineralogist*, **92**, 722-734.

Grigoriev, D.P., 1965, Ontogeny of minerals.

: *Israel Program of Scientific Translations*, 250.

Grossman, E.L., 1982, Stable isotopes in live benthic foraminifera from the Southern California Borderland.: Los Angeles, University of Southern California.

Grossman, E.L., & Ku, T.L., 1986, Oxygen and Carbon Isotope Fractionation in Biogenic Aragonite - Temperature Effects: *Chemical Geology*, **59**, 59-74.

Grossman, E.L., Mii, H.S., & Yancey, T.E., 1993, Stable Isotopes in Late Pennsylvanian Brachiopods from the United-States - Implications for Carboniferous Paleoceanography: *Geological Society of America Bulletin*, **105**, 1284-1296.

Grossman, E.L., Zhang, C.L., & Yancey, T.E., 1991, Stable-Isotope Stratigraphy of Brachiopods from Pennsylvanian Shales in Texas: *Geological Society of America Bulletin*, **103**, 953-965.

Gruszczynski, M., Halas, S., Hoffman, A., & Malkowski, K., 1989, A Brachiopod Calcite Record of the Oceanic Carbon and Oxygen Isotope Shifts at the Permian Triassic Transition: *Nature*, **337**, 64-68.

Gustavson, T.C., 1976, Paleo-Temperature Analysis of Marine Pleistocene of Long-Island, New-York, and Nantucket-Island, Massachusetts: *Geological Society of America Bulletin*, **87**, 1-8.

Guzman, H.M., & Tudhope, A.W., 1998, Seasonal variation in skeletal extension rate and stable isotopic ($^{13}C/^{12}C$ and $^{18}O/^{16}O$) composition in response to several environmental variables in the Caribbean reef coral *Siderastrea siderea*: *Marine Ecology-Progress Series*, **166**, 109-118.

Han, Y.J., & Aizenberg, J., 2003, Effect of magnesium ions on oriented growth of calcite on carboxylic acid functionalized self-assembled monolayer: *Journal Of The American Chemical Society*, **125**, 4032-4033.

Hardie, L.A., 1996, Secular variation in seawater chemistry: An explanation for the coupled secular variation in the mineralogies of marine limestones and potash evaporites over the past 600 my: *Geology*, **24**, 279-283.

Harper, E.M., 2000, Are calcitic layers an effective adaptation against shell dissolution in the Bivalvia?: *Journal Of Zoology*, **251**, 179-186.

Heikoop, J.M., Dunn, J.J., Risk, M.J., Schwarcz, H.P., McConnaughey, T.A., & Sandeman, I.M., 2000, Separation of kinetic and metabolic isotope effects in ^{13}C records preserved in reef coral skeletons: *Geochimica Et Cosmochimica Acta*, **64**, 975-987.

Herfort, L., Loste, E., Meldrum, F., & Thake, B., 2004, Structural and physiological effects of calcium and magnesium in Emiliania huxleyi (Lohmann) Hay and Mohler: *Journal of Structural Biology*, **148**, 307-314.

Herrington, C.R., 1985, Quantitative EDS and WDS X-Ray-Microanalysis of Semiconductor-Materials - Principles and Comparisons: *Journal of Electron Microscopy Technique*, **2**, 471-479.

Hincke, M., & St. Maurice, M., 2000, Phosphorylation-dependent modulation of calcium carbonate precipitation by chicken eggshell matrix proteins., *in* Goldberg, M., Boskey, A., & Robinson, C., eds., *Chemistry and Biology of Mineralized Tissues* Rosemont, Illinois, American Academy of Orthopaedic Surgeons, pp.13–17.

Hintz, C.J., Shaw, T.J., Bernhard, J.M., Chandler, G.T., McCorkle, D.C., & Blanks, J.K., 2006, Trace/minor element : calcium ratios in cultured benthic foraminifera. Part II: Ontogenetic variation: *Geochimica Et Cosmochimica Acta*, **70**, 1964-1976.

Holland, H.D., Holland, H.J., & Munoz, J.L., 1964, The coprecipitation of cations with $CaCO_3$ - II. The coprecipitation of Sr^{2+} with calcite between 90C and 100C: *Geochimica et Cosmochimica Acta*, **28**, 1287-1301.

Hou, W.T., & Feng, Q.L., 2003, Crystal orientation preference and formation mechanism of nacreous layer in mussel: *Journal Of Crystal Growth*, **258**, 402-408.

Hou, W.T., & Feng, Q.L., 2006, Morphologies and growth model of biomimetic fabricated calcite crystals using amino acids and insoluble matrix membranes of *Mytilus edulis*: *Crystal Growth & Design*, **6**, 1086-1090.

Hubbard, F., McManus, J., & Al-Dabbas, M., 1981, Environmental influences on the shell mineralogy of *Mytilus edulis*: *Geo-Marine Letters*, **1**, 267-269.

Humphreys, F.J., 1999, Quantitative metallography by electron backscattered diffraction: *Journal of Microscopy-Oxford*, **195**, 170-185.

Humphreys, F.J., 2001, Review Grain and subgrain characterisation by electron backscatter diffraction *Journal of Materials Science*, **36**, 3833-3854.

Humphreys, F.J., 2004, Characterisation of fine-scale microstructures by electron backscatter diffraction (EBSD): *Scripta Materialia*, **51**, 771-776.

Humphreys, F.J., Huang, Y., Brough, I., & Harris, C., 1999, Electron backscatter diffraction of grain and subgrain structures - resolution considerations: *Journal of Microscopy-Oxford*, **195**, 212-216.

Humphreys, W., 1969, Initial shell formation in the bivalve *Mytilus edulis*: *Proc. Electron. Microsc. Soc. Am.*, **27**, 272–273.

Ishikawa, M., & Ichikuni, M., 1984, Uptake of sodium and potassium by calcite: *Chemical Geology*, **42**, 137-146.

Jackson, A.P., Vincent, J.F.V., & Turner, R.M., 1988, The Mechanical Design Of Nacre: *Proceedings Of The Royal Society Of London Series B-Biological Sciences*, **234**, 415-&.

Jiao, Y., Feng, Q., & Li, X., 2006, The co-effect of collagen and magnesium ions on calcium carbonate biomineralization: *Materials Science and Engineering: C*, **26**, 648-652.

Katz, A., 1973, Interaction of Magnesium with Calcite During Crystal-Growth at 25-90°C and One Atmosphere: *Geochimica et Cosmochimica Acta*, **37**, 1563-1586.

Katz, A., Sass, E., Starinsky, A., & Holland, H.D., 1972a, Strontium behaviour in the calcite-aragonite transformation: An experimental study at 40-98C: *Geochimica et Cosmochimica Acta*, **36**, 481-496.

Katz, A., Starinsk.A, Sass, E., & Holland, H.D., 1972b, Strontium Behavior in Aragonite-Calcite Transformation - Experimental Study at 40-98°C: *Geochimica Et Cosmochimica Acta*, **36**, 481-496.

Kennedy, H., Richardson, C.A., Duarte, C.M., & Kennedy, D.P., 2001, Oxygen and carbon stable isotopic profiles of the fan mussel, Pinna nobilis, and reconstruction of sea surface temperatures in the Mediterranean: *Marine Biology*, **139**, 1115-1124.

Killingley, J.S., & Berger, W.H., 1979, Stable Isotopes in a Mollusk Shell - Detection of Upwelling Events: *Science*, **205**, 186-188.

Kinsman, D.J.J., & Holland, H.D., 1969, Co-Precipitation of Cations with $CaCO_3$ IV. Co-Precipitation of Sr^{2+} with Aragonite between 16 and 96°C: *Geochimica et Cosmochimica Acta*, **33**, 1-18.

Kitamura, M., 2001, Crystallization and transformation mechanism of calcium carbonate polymorphs and the effect of magnesium ion: *Journal of Colloid and Interface Science*, **236**, 318-327.

Kitano, Y., 1962, The Behavior of Various Inorganic Ions in the Separation of Calcium Carbonate from a Bicarbonate Solution: *Bulletin of the Chemical Society of Japan*, **35**, 1973-1980.

Kitano, Y., & Hood, D.W., 1965, Influence of Organic Material on Polymorphic Crystallization of Calcium Carbonate: *Geochimica Et Cosmochimica Acta*, **29**, 29-41.

Kitano, Y., Okumura, M., & Idogaki, M., 1975, Incorporation of sodium, chloride and sulfate with calcium carbonate: *Geochemical Journal*, **9**, 75-84.

Klein, R.T., & Lohmann, K.C., 1995, Isotopic Homogeneity among Nonequivalent Sectors of Calcite: *Geology*, **23**, 633-636.

Klein, R.T., Lohmann, K.C., & Thayer, C.W., 1996a, Bivalve skeletons record sea-surface temperature and delta O-18 via Mg/Ca and $^{18}O/^{16}O$ ratios: *Geology*, **24**, 415-418.

Klein, R.T., Lohmann, K.C., & Thayer, C.W., 1996b, Sr/Ca and $^{13}C/^{12}C$ ratios in skeletal calcite of *Mytilus trossulus*: Covariation with metabolic rate, salinity, and carbon isotopic composition of seawater: *Geochimica Et Cosmochimica Acta*, **60**, 4207-4221.

Kniprath, E., 1978, Growth of Shell-Field in Mytilus (Bivalvia): *Zoologica Scripta*, **7**, 119-120.

Kniprath, E., 1980, Larval Development of the Shell and the Shell Gland in Mytilus (Bivalvia): *Wilhelm Rouxs Archives of Developmental Biology*, **188**, 201-204.

Kniprath, E., 1981, Ontogeny of the Molluscan Shell Field - a Review: *Zoologica Scripta*, **10**, 61-79.

Knoll, A., 2003, Biomineralization and evolutionary history.: *Reviews in Mineralolgy and Geochemistry*, **54**, 329-356.

Kobayashi, I., 1969, Internal Microstructure of Shell of Bivalve Molluscs: *American Zoologist*, **9**, 663-672.

Kontrec, J., Kralj, D., Brecevic, L., Falini, G., Fermani, S., Noethig-Laslo, V., & Mirosavljevic, K., 2004, Incorporation of inorganic anions in calcite: *European Journal Of Inorganic Chemistry*, 4579-4585.

Kralj, D., Kontrec, J., Brecevic, L., Falini, G., & Nothig-Laslo, V., 2004, Effect of inorganic anions on the morphology and structure of magnesium calcite: *Chemistry-A European Journal*, **10**, 1647-1656.

Krantz, D.E., Jones, D.S., & Williams, D.F., 1989, Aspects of Growth Deceleration in Bivalves - Clues to Understanding the Seasonal Delta-O-18 and Delta-C-13 Record - Reply: *Palaeogeography Palaeoclimatology Palaeoecology*, **70**, 403-407.

Krantz, D.E., Williams, D.F., & Jones, D.S., 1987, Ecological and Paleoenvironmental Information Using Stable Isotope Profiles from Living and Fossil Mollusks: *Palaeogeography Palaeoclimatology Palaeoecology*, **58**, 249-266.

Krebs, H.A., & Roughton, F.J.W., 1948, Carbonic Anhydrase as a Tool in Studying the Mechanism of Reactions Involving H_2CO_3, CO_2 or HCO^{-3}: *Biochemical Journal*, **43**, 550-555.

Land, L.S., & Hoops, G.K., 1973, Sodium in carbonate sediments and rocks: A possible index to the salinity of diagenetic solutions.: *Journal of Sedimentary Petrology*, **43**, 614-617.

Land, L.S., Lang, J.C., & Barnes, D.J., 1975, Extension Rate - Primary Control on Isotopic Composition of West-Indian (Jamaican) Scleractinian Reef Coral Skeletons: *Marine Biology*, **33**, 221-233.

Lea, D.W., 2003, Trace elements in foraminiferal calcite, *in* Gupta, B.K.S., ed., *Modern Foraminifera*, Kluwer Academic, 259-277.

Lea, D.W., Mashiotta, T.A., & Spero, H.J., 1999, Controls on magnesium and strontium uptake in planktonic foraminifera determined by live culturing.: *Geochimica et Cosmochimica Acta*, **63**, 2369-2379.

Lea, D.W., Pak, D.K., & Spero, H.J., 2000, Climate Impact of Late Quaternary Equatorial Pacific Sea Surface Temperature Variations: *Science*, **289**, 1719.

Lebron, I., & Suarez, D.L., 1996, Calcite nucleation and precipitation kinetics as affected by dissolved organic matter at 25 degrees C and pH>7.5: *Geochimica Et Cosmochimica Acta*, **60**, 2765-2776.

Lebron, I., & Suarez, D.L., 1998, Kinetics and mechanisms of precipitation of calcite as affected by PCO2 and organic ligands at 25[degree sign]C: *Geochimica et Cosmochimica Acta*, **62**, 405-416.

Lecuyer, C., Reynard, B., & Martineaua, F., 2004, Stable isotope fractionation between mollusc shells and marine waters from Martinique Island: *Chemical Geology*, **213**, 293-305.

Legeros, R., Balmain, N., & Bonel, G., 1987, Age-related changes in mineral of rat and bovine cortical bone: *Calcified Tissue International*, **41**, 137-144.

Levi-Kalisman, Y., Falini, G., Addadi, L., & Weiner, S., 2001, Structure of the nacreous organic matrix of a bivalve mollusk shell examined in the hydrated state using Cryo-TEM: *Journal Of Structural Biology*, **135**, 8-17.

Levi, Y., Albeck, S., Brack, A., Weiner, S., & Addadi, L., 1998, Control over aragonite crystal nucleation and growth: An *in vitro* study of biomineralization: *Chemistry-A European Journal*, **4**, 389-396.

Lingard, S.M., Evans, R.D., & Bourgoin, B.P., 1992, Method for the Estimation of Organic-Bound and Crystal-Bound Metal Concentrations in Bivalve Shells: *Bulletin of Environmental Contamination and Toxicology*, **48**, 179-184.

Longhurst, A.R., 1991, Role of the Marine Biosphere in the Global Carbon-Cycle: *Limnology and Oceanography*, **36**, 1507-1526.

Lorens, R.B., & Bender, M.L., 1977, Physiological Exclusion Of Magnesium From *Mytilus edulis* Calcite: *Nature*, **269**, 793-794.

Lorens, R.B., & Bender, M.L., 1980, The impact of solution chemistry on *Mytilus edulis* calcite and aragonite: *Geochimica Et Cosmochimica Acta*, **44**, 1265-1278.

Lorens, R.N., 1981, Sr, Cd, Mn and Co distribution coefficients in calcite as a function of calcite precipitation rate.: *Geochimica et Cosmochimica Acta*, **45**, 553-561.

Lorrain, A., Gillikin, D.P., Paulet, Y.M., Chauvaud, L., Le Mercier, A., Navez, J., & Andre, L., 2005, Strong kinetic effects on Sr/Ca ratios in the calcitic bivalve *Pecten maximus*: *Geology*, **33**, 965-968.

Loste, E., Wilson, R.M., Seshadri, R., & Meldrum, F.C., 2003, The role of magnesium in stabilising amorphous calcium carbonate and controlling calcite morphologies.: *Journal of Crystal Growth*, **254**, 206-218.

Lowenstam, H.A., 1954, Factors affecting the aragonite:calcite ratios in carbonate-secreting marine organisms: *Journal of Geology*, **62**, 284-322.

Lowenstam, H.A., 1961, Mineralogy, $^{18}O/^{16}O$ Ratios, And Strontium And Magnesium Contents Of Recent And Fossil Brachiopods And Their Bearing On The History Of The Oceans: *Journal Of Geology*, **69**, 241-260.

Lowenstam, H.A., 1972, Phosphatic hard tissues of marine invertebrates: Their nature and mechanical function, and some fossil implications: *Chemical Geology*, **9**, 153-166.

Lowenstam, H.A., 1981, Minerals formed by organisms.: *Science*, **211**, 1126-1131.

Lowenstam, H.A., & Weiner, S., 1989, On Biomineralization: New York, Oxford University Press.

Mahway, E., 2005, OIM User's Manual: New Jersey, EDAX-TSL.

Major, R.P., & Wilber, R.J., 1991, Crystal Habit, Geochemistry, and Cathodoluminescence of Magnesian Calcite Marine Cements from the Lower Slope of Little Bahama Bank: *Geological Society of America Bulletin*, **103**, 461-471.

Malone, P.G., & Dodd, J.R., 1967, Temperature And Salinity Effects On Calcification Rate In *Mytilus edulis* And Its Paleoecological Implications: *Limnology And Oceanography*, **12**, 432-+.

Mann, 2001, Biomineralization - Principles and Concepts in Bioinorganic Materials Chemistry: Oxford, Oxford University Press.

Mann, S., 1988, Molecular Recognition In Biomineralization: *Nature*, **332**, 119-124.

Manne, S., Zaremba, C.M., Giles, R., Huggins, L., Walters, D.A., Belcher, A., Morse, D.E., Stucky, G.D., Didymus, J.M., Mann, S., & Hansma, P.K., 1994, Atomic-Force Microscopy Of The Nacreous Layer In Mollusk Shells: *Proceedings Of The Royal Society Of London Series B-Biological Sciences*, **256**, 17-23.

Marchitto, T.M., Bryan, S.P., Curry, W.B., & McCorkle, D.C., 2007, Mg/Ca temperature calibration for the benthic foraminifer *Cibicidoides pachyderma*: *Paleoceanography*, **22**, PA1203.

Margolis, S.V., Kroopnick, P.M., Goodney, D.E., Dudley, W.C., & Mahoney, M.E., 1975, Oxygen and Carbon Isotopes from Calcareous Nannofossils as Paleoceanographic Indicators: *Science*, **189**, 555-557.

Margosian, A., Tan, F.C., Cai, D., & Mann, K.H., 1987, Seawater Temperature Records from Stable Isotopic Profiles in the Shell of Modiolus-Modiolus: *Estuarine Coastal and Shelf Science*, **25**, 81-89.

Maurice, F., 1979, X-ray emission, *in* Maurice, F., Meny, L., & Tixier, R., eds., *Microanalysis and Scanning Electron Microscopy*: Orsay, Les Editions de Physique, 169-214.

McConnaughey, T., 1989a, ^{13}C And ^{18}O Isotopic Disequilibrium In Biological Carbonates .1. Patterns: *Geochimica Et Cosmochimica Acta*, **53**, 151-162.

McConnaughey, T., 1989b, ^{13}C And ^{18}O Isotopic Disequilibrium In Biological Carbonates .2. *In vitro* Simulation Of Kinetic Isotope Effects: *Geochimica Et Cosmochimica Acta*, **53**, 163-171.

McConnaughey, T.A., 2002, Heavy isotope deficiencies in corals: Kinetic and McCrea models: *Geochimica Et Cosmochimica Acta*, **66**, A498-A498.

McConnaughey, T.A., 2003, Sub-equilibrium ^{18}O and ^{13}C levels in biological carbonates: carbonate and kinetic models: *Coral Reefs*, **22**, 316-327.

McConnaughey, T.A., Burdett, J., Whelan, J.F., & Paull, C.K., 1997, Carbon isotopes in biological carbonates: Respiration and photosynthesis: *Geochimica Et Cosmochimica Acta*, **61**, 611-622.

McCrea, J.M., 1950, On The Isotopic Chemistry Of Carbonates And A Paleotemperature Scale: *Journal Of Chemical Physics*, **18**, 849-857.

Medakovic, D., 2000, Carbonic anhydrase activity and biomineralization process in embryos, larvae and adult blue mussels *Mytilus edulis* L: *Helgoland Marine Research*, **54**, 1-6.

Medakovic, D., Popovic, S., Grzeta, B., Plazonic, M., & HrsBrenko, M., 1997, X-ray diffraction study of calcification processes in embryos and larvae of the brooding oyster *Ostrea edulis*: *Marine Biology*, **129**, 615-623.

Meibom, A., Cuif, J.P., Hillion, F.O., Constantz, B.R., Juillet-Leclerc, A., Dauphin, Y., Watanabe, T., & Dunbar, R.B., 2004, Distribution of magnesium in coral skeleton: *Geophysical Research Letters*, **31**.

Meldrum, F.C., & Hyde, S.T., 2001, Morphological influence of magnesium and organic additives on the precipitation of calcite: *Journal of Crystal Growth*, **231**, 544-558.

Merlet, C., 1994, An Accurate Computer Correction Program for Quantitative Electron-Probe Microanalysis: *Mikrochimica Acta*, **114**, 363-376.

Mii, H.S., & Grossman, E.L., 1994, Late Pennsylvanian Seasonality Reflected in the O-18 and Elemental Composition of a Brachiopod Shell: *Geology*, **22**, 661-664.

Misogianes, M.J., & Chasteen, N.D., 1979, Chemical And Spectral Characterization Of The Extrapallial Fluid Of *Mytilus edulis*: *Analytical Biochemistry*, **100**, 324-334.

Miyamoto, H., Miyashita, T., Okushima, M., Nakano, S., Morita, T., & Matsushiro, A., 1996, A carbonic anhydrase from the nacreous layer in oyster pearls: *Proceedings of the National Academy of Sciences of the United States of America*, **93**, 9657-9660.

Mook, W.G., & Vogel, J.C., 1968, Isotopic Equilibrium between Shells and Their Environment: *Science*, **159**, 874-875.

Morse, J.W., & Bender, M.L., 1990, Partition-Coefficients in Calcite - Examination of Factors Influencing the Validity of Experimental Results and Their Application to Natural Systems: *Chemical Geology*, **82**, 265-277.

Mount, A.S., Wheeler, A.P., Paradkar, R.P., & Snider, D., 2004, Hemocyte-mediated shell mineralization in the eastern oyster: *Science*, **304**, 297-300.

Mucci, A., 1987, Influence of Temperature on the Composition of Magnesian Calcite Overgrowths Precipitated from Seawater: *Geochimica Et Cosmochimica Acta*, **51**, 1977-1984.

Mucci, A., & Morse, J.W., 1983, The incorporation of Mg^{2+} and Sr^{2+} into calcite overgrowths: Influences of growth rate and solution composition.: *Geochimica et Cosmochimica Acta*, **47**, 217-233.

Nakahara, H., Kakei, M., & Bevelander, G., 1980, Fine structure and amino acid composition of the organic "envelope" in the prismatic layer of some bivalve shells: *Venus*, **39**, 167-177.

Nancollas, G.H., 1982, Biological Mineralization and Demineralization. : New York, Springer-Verlag.

Nassif, N., Pinna, N., Gehrke, N., Antonietti, M., Jager, C., & Colfen, H., 2005, Amorphous layer around aragonite platelets in nacre: *Proceedings of the National Academy of Sciences of the United States of America*, **102**, 12653-12655.

Neff, J.M., 1972, Ultrastructure of Outer Epithelium of Mantle in Clam Mercenaria-Mercenaria in Relation to Calcification of Shell: *Tissue & Cell*, **4**, 591-600.

Nehrke, G., Reichart, G.J., Van Cappellen, P., Meile, C., & Bijma, J., 2007, Dependence of calcite growth rate and Sr partitioning on solution stoichiometry: Non-Kossel crystal growth: *Geochimica et Cosmochimica Acta*, **71**, 2240-2249.

Newbury, D.E., 1998, Standardless quantitative electron-excited X-ray microanalysis by energy-dispersive spectrometry: What is its proper role?: *Microscopy and Microanalysis*, **4**, 585-597.

Nishikawa, S., & Kikuchi, S., 1928a, Diffraction of cathode rays by calcite: *Nature*, **122**, 726-726.

Nishikawa, S., & Kikuchi, S., 1928b, Diffraction of cathode rays by mica: *Nature*, **121**, 1019-1020.

Nowell, M.M., Witt, R.A., & True, B., 2005, EBSD Sample Preparation: Techniques Tips and Tricks: *Microscopy and Microanalysis*, **11**, 504-505.

Nowell, M.M., & Wright, S.I., 2005, Orientation effects on indexing of electron backscatter diffraction patterns *Ultramicroscopy*, **103**, 41-58.

Nudelman, F., Gotliv, B.A., Addadi, L., & Weiner, S., 2006, Mollusk shell formation: Mapping the distribution of organic matrix components underlying a single aragonitic tablet in nacre: *Journal Of Structural Biology*, **153**, 176-187.

Nurnberg, D., 1995, Magnesium in Tests of Neogloboquadrina-Pachyderma Sinistral from High Northern and Southern Latitudes: *Journal of Foraminiferal Research*, **25**, 350-368.

Nurnberg, D., Bijma, J., & Hemleben, C., 1996, Assessing the reliability of magnesium in foraminiferal calcite as a proxy for water mass temperatures (vol 60, pg 803, 1995): *Geochimica Et Cosmochimica Acta*, **60**, 2483-2483.

Okumura, M., & Kitano, Y., 1986, Coprecipitation Of Alkali-Metal Ions With Calcium-Carbonate: *Geochimica Et Cosmochimica Acta*, **50**, 49-58.

Onasch, C.M., & Vennemann, T.W., 1995, Disequilibrium Partitioning of Oxygen Isotopes Associated with Sector Zoning in Quartz: *Geology*, **23**, 1103-1106.

Owen, R., Kennedy, H., & Richardson, C., 2002, Experimental investigation into partitioning of stable isotopes between scallop (*Pecten maximus*) shell calcite and sea water: *Palaeogeography Palaeoclimatology Palaeoecology*, **185**, 163-174.

Pannella, G., & MacClintock, C., 1968, Biological and environmental rhythms reflected in molluscan shell growth.: *Journal of Palaeontology*, **42**, 64-80.

Paquette, J., & Reeder, R.J., 1990, New Type of Compositional Zoning in Calcite - Insights into Crystal-Growth Mechanisms: *Geology*, **18**, 1244-1247.

Paquette, J., & Reeder, R.J., 1995, Relationship between Surface-Structure, Growth-Mechanism, and Trace-Element Incorporation in Calcite: *Geochimica Et Cosmochimica Acta*, **59**, 735-749.

Parkinson, D., Curry, G.B., Cusack, M., & Fallick, A.E., 2005, Shell structure, patterns and trends of oxygen and carbon stable isotopes in modern brachiopod shells: *Chemical Geology*, **219**, 193-235.

Parkinson, D., & Cusack, M., 2007, Stable oxygen and carbon isotopes in extant Brachiopod shells: keys to deciphering ancient ocean environments, *in* Kaesler, R., ed., *Supplement. Treatise on Invertebrate Paleontology: Part H, Brachiopoda*, **Volume 6**: New York & Lawrence, Geological Society of America & University of Kansas Press, 2522-2531.

Pingitore, N.E., & Eastman, M.P., 1986, The Coprecipitation of Sr-2+ with Calcite at 25-Degrees-C and 1-Atm: *Geochimica Et Cosmochimica Acta*, **50**, 2195-2203.

Pingitore, N.E., Lytle, F.W., Davies, B.M., Eastman, M.P., Eller, P.G., & Larson, E.M., 1992, Mode of incorporation of Sr^{2+} in calcite: Determination by X-ray absorption spectroscopy: *Geochimica et Cosmochimica Acta*, **46**, 1531-1538.

Pojeta, J., Runnegar, B., Peel, J.S., & Gordon, M., 1987, Phylum Mollusca, *in* Boardman, R.S., Cheetham, A.H., & Rowell, A.J., eds., *Fossil Invertebrates*: Oxford, Blackwell Scientific Publications, 270-435.

Pokroy, B., Fieramosca, J.S., Von Dreele, R.B., Fitch, A.N., Caspi, E.N., & Zolotoyabko, E., 2007, Atomic structure of biogenic aragonite: *Chemistry of Materials* **19**, 3244-3251.

Pokroy, B., Fitch, A.N., Lee, P.L., Quintana, J.P., Caspi, E.N., & Zolotoyabko, E., 2006a, Anisotropic lattice distortions in the mollusk-made aragonite: A widespread phenomenon: *Journal of Structural Biology*, **153**, 145-150.

Pokroy, B., Fitch, A.N., Marin, F., Kapon, M., Adir, N., & Zolotoyabko, E., 2006b, Anisotropic lattice distortions in biogenic calcite induced by intra-crystalline organic molecules: *Journal of Structural Biology*, **155**, 96-103.

Pokroy, B., Fitch, A.N., & Zolotoyabko, E., 2006c, The microstructure of biogenic calcite: A view by high-resolution synchrotron powder diffraction: *Advanced Materials*, **18**, 2363-2368.

Pokroy, B., Quintana, J.P., Caspi, E.N., Berner, A., & Zolotoyabko, E., 2004, Anisotropic lattice distortions in biogenic aragonite: *Nature Materials*, **3**, 900-902.

Popp, B.N., Anderson, T.F., & Sandberg, P.A., 1986a, Brachiopods as Indicators of Original Isotopic Compositions in Some Paleozoic Limestones: *Geological Society of America Bulletin*, **97**, 1262-1269.

Popp, B.N., Anderson, T.F., & Sandberg, P.A., 1986b, Textural, Elemental, and Isotopic Variations among Constituents in Middle Devonian Limestones, North-America: *Journal of Sedimentary Petrology*, **56**, 715-727.

Prenant, M., 1927, The types of calcium mineral in living beings and the problem of their determination: *Biological Reviews and Biological Proceedings of the Cambridge Philosophical Society*, **2**, 365-393.

Prior, D.J., Boyle, A.P., Brenker, F., Cheadle, M.C., Day, A., Lopez, G., Peruzzo, L., Potts, G.J., Reddy, S., Spiess, R., Timms, N.E., Trimby, P., Wheeler, J., & Zetterstrom, L., 1999, The application of electron backscatter diffraction and orientation contrast imaging in the SEM to textural problems in rocks: *American Mineralogist*, **84**, 1741-1759.

Purton-Hildebrand, L.M.A., Grime, G.W., Shields, G.A., & Brasier, M.D., 2001, The use of external micro-PIXE to investigate the factors determining the Sr : Ca ratio in the shells of fossil aragonitic molluscs: *Nuclear Instruments & Methods in Physics Research Section B-Beam Interactions with Materials and Atoms*, **181**, 506-510.

Purton, L.M.A., Shields, G.A., Brasier, M.D., & Grime, G.W., 1999, Metabolism controls Sr/Ca ratios in fossil aragonitic mollusks: *Geology*, **27**, 1083-1086.

Rahimpour-Bonab, H., Bone, Y., & Moussavi-Harami, R., 1997, Stable isotope aspects of modern molluscs, brachiopods, and marine cements from cool-water carbonates, Lacepede Shelf, South Australia: *Geochimica Et Cosmochimica Acta*, **61**, 207-218.

RahimpourBonab, H., Bone, Y., & MoussaviHarami, R., 1997, Stable isotope aspects of modern molluscs, brachiopods, and marine cements from cool-water carbonates, Lacepede Shelf, South Australia: *Geochimica Et Cosmochimica Acta*, **61**, 207-218.

Rajam, S., & Mann, S., 1990, Selective Stabilization of the (001) Face of Calcite in the Presence of Lithium: *Journal of the Chemical Society-Chemical Communications*, 1789-1791.

Rautaray, D., Kasture, M., & Sastry, M., 2005, Role of Mg ions in modulating the morphology and structure of $CaCO_3$ crystals grown in aqueous foams: *Crystengcomm*, **7**, 469-475.

Raz, S., Hamilton, P.C., Wilt, F.H., Weiner, S., & Addadi, L., 2003, The transient phase of amorphous calcium carbonate in sea urchin larval spicules: The involvement of proteins and magnesium ions in its formation and stabilization: *Advanced Functional Materials*, **13**, 480-486.

Reddy, M.M., & Wang, K.K., 1980, Crystallization of Calcium-Carbonate in the Presence of Metal-Ions .1. Inhibition by Magnesium-Ion at Ph 8.8 and 25-Degrees-C: *Journal of Crystal Growth*, **50**, 470-480.

Reeder, R.J., 1983, Crystal Chemistry of the Rhombohedral Carbonates, *in* Reeder, R.J., ed., *Carbonates: Mineralogy and Chemistry.*, **Volume 11**: Reviews in Mineralogy., 1-47.

Reeder, R.J., & Grams, J.C., 1987, Sector Zoning in Calcite Cement Crystals - Implications for Trace-Element Distributions in Carbonates: *Geochimica Et Cosmochimica Acta*, **51**, 187-194.

Reeder, R.J., & Paquette, J., 1989, Sector zoning in natural and synthetic calcites: *Sedimentary Geology*, **65**, 239-247.

Richardson, C.A., 1989, An Analysis of the Microgrowth Bands in the Shell of the Common Mussel *Mytilus edulis*: *Journal of the Marine Biological Association of the United Kingdom*, **69**, 477-491.

Richardson, C.A., Chenery, S.R.N., & Cook, J.M., 2001, Assessing the history of trace metal (Cu, Zn,Pb) contamination in the North Sea through laser ablation ICP-MS of horse mussel *Modiolus modiolus* shells: *Marine Ecology-Progress Series*, **211**, 157-167.

Richardson, C.A., Seed, R., & Naylor, E., 1990, Use of Internal Growth Bands for Measuring Individual and Population-Growth Rates in *Mytilus edulis* from Offshore Production Platforms: *Marine Ecology-Progress Series*, **66**, 259-265.

Rickaby, R.E.M., Schrag, D.P., Zondervan, I., & Riebesell, U., 2002, Growth rate dependence of Sr incorporation during calcification of *Emiliania huxleyi*: *Global Biogeochemical Cycles*, **16**, Art. no. 1006.

Ries, J.B., 2004, Effect of ambient Mg/Ca ratio on Mg fractionation in calcareous marine invertebrates: A record of the oceanic Mg/Ca ratio over the Phanerozoic: *Geology*, **32**, 981-984.

Rimstidt, J.D., Balog, A., & Webb, J., 1998, Distribution of trace elements between carbonate minerals and aqueous solutions: *Geochimica Et Cosmochimica Acta*, **62**, 1851-1863.

Rodland, D.L., Schone, B.R., Helama, S., Nielsen, J.K., & Baier, S., 2006, A clockwork mollusc: Ultradian rhythms in bivalve activity revealed by digital photography: *Journal of Experimental Marine Biology and Ecology*, **334**, 316-323.

Rollion-Bard, C., Chaussidon, M., & France-Lanord, C., 2003, pH control on oxygen isotopic composition of symbiotic corals: *Earth and Planetary Science Letters*, **215**, 275-288.

Rosenberg, G.D., & Hughes, W.W., 1991, A Metabolic Model For The Determination Of Shell Composition In The Bivalve Mollusk, *Mytilus edulis*: *Lethaia*, **24**, 83-96.

Rosenberg, G.D., Hughes, W.W., & Tkachuck, R.D., 1989, Shell Form And Metabolic Gradients In The Mantle Of *Mytilus edulis*: *Lethaia*, **22**, 343-344.

Rosenheim, B.E., Swart, P.K., Thorrold, S.R., Willenz, P., Berry, L., & Latkoczy, C., 2004, High-resolution Sr/Ca records in sclerosponges calibrated to temperature in situ: *Geology*, **32**, 145-148.

Rosenthal, Y., Boyle, E.A., & Slowey, N., 1997, Temperature control on the incorporation of magnesium, strontium, fluorine, and cadmium into benthic foraminiferal shells from Little Bahama Bank: Prospects for thermocline paleoceanography: *Geochimica Et Cosmochimica Acta*, **61**, 3633-3643.

Rousseau, M., Lopez, E., Stempfle, P., Brendle, M., Franke, L., Guette, A., Naslain, R., & Bourrat, X., 2005, Multiscale structure of sheet nacre: *Biomaterials*, **26**, 6254-6262.

Rye, D.M., & Sommer, M.A., 1980, Reconstructing paleotemperature and paleosalinity regimes with oxygen isotopes, *in* Rhoads, D.C., & Lutz, R.A., eds., *Skeletal Growth of Aquatic Organisms*: New York, Plenum Press, 169-202.

Sagawa, T., Toyoda, K., & Oba, T., 2006, Sea surface temperature record off central Japan since the Last Glacial Maximum using planktonic foraminiferal Mg/Ca thermometry: *Journal of Quaternary Science*, **21** 63 - 73.

Schaffer, T.E., IonescuZanetti, C., Proksch, R., Fritz, M., Walters, D.A., Almqvist, N., Zaremba, C.M., Belcher, A.M., Smith, B.L., Stucky, G.D., Morse, D.E., & Hansma, P.K., 1997, Does abalone nacre form by heteroepitaxial nucleation or by growth through mineral bridges?: *Chemistry Of Materials*, **9**, 1731-1740.

Schmahl, W.W., Griesshaber, E., Neuser, R., Lenze, A., Job, R., & Brand, U., 2004, The microstructure of the fibrous layer of terebratulide brachiopod shell calcite: *European Journal Of Mineralogy*, **16**, 693-697.

Schmahl, W.W., Griesshaber, E., Neuser, R.D., Pettke, T., & Brand, U., 2005, Brachiopod shell biomineralization: Stuctural and chemical characteristics: *Geochimica Et Cosmochimica Acta*, **69**, A118-A118.

Schmahl, W.W., Merkel, C., Griesshaber, E., Kelm, K., & Lueter, C., 2007, Architecture of phosphatic and calcitic brachiopod shell materials - A comparison: *Geochimica Et Cosmochimica Acta*, **71**, A893-A893.

Schmidt, W.J., 1923, Bau und bildung der Perlmuttermasse: *Zoologische Jahrbuecher Abteilung fuer Anatomie und Ontogenie der Tiere*, **45**, 1-148.

Schwartz, A.J., 2000, Electron Backscatter Diffraction in Materials Science: New York, Plenum Press.

Schwarzer, R.A., 1997a, Advances in crystal orientation mapping with the SEM and TEM: *Ultramicroscopy*, **67**, 19-24.

Schwarzer, R.A., 1997b, Automated crystal lattice orientation mapping using a computer-controlled SEM: *Micron*, **28**, 249-265.

Seed, R., 1969, Ecology of *Mytilus edulis* L. (Lamellibranchiata) on Exposed Rocky Shores .2. Growth and Mortality: *Oecologia*, **3**, 317-350.

Shackleton, N.J., Wiseman, J.D.H., & Buckley, H.A., 1973, Nonequilibrium Isotopic Fractionation between Seawater and Planktonic Foraminiferal Tests: *Nature*, **242**, 177-179.

Silyn-Roberts, H., & Sharp, R.M., 1986, Crystal-Growth and the Role of the Organic Network in Eggshell Biomineralization: *Proceedings of the Royal Society of London Series B-Biological Sciences*, **227**, 303-324.

Simkiss, K., 1993, Amorphous Minerals in Biology, *in* Allemand, D., & Cuif, J.P., eds., Biomineralization 93. Proceedings of the Seventh International Biomineralization Symposium, Volume 14: Monaco, 1. Fundamentals of biomineralization. Bulletin de l'Institut Oceanographique, 49-54.

Simkiss, K., & Wilbur, K.M., 1989, Biomineralization: Cell Biology and Mineral Deposition: San Diego Academic Press.

Smallwood, P.V., 1977, Some Aspects Of Surface-Chemistry Of Calcite And Aragonite .1. Electrokinetic Study: *Colloid And Polymer Science*, **255**, 881-886.

Smith, S.V., Buddemeier, R.W., Redalje, R.C., & Houck, J.E., 1979, Strontium-Calcium Thermometry in Coral Skeletons: *Science*, **204**, 404-407.

Sosdian, S., Gentry, D.K., Lear, C.H., Grossman, E.L., Hicks, D., & Rosenthal, Y., 2006, Strontium to calcium ratios in the marine gastropod *Conus ermineus*: Growth rate effects and temperature calibration: *Geochemistry Geophysics Geosystems*, **7**, Q11023.

Spero, H.J., & Lea, D.W., 1993, Intraspecific Stable-Isotope Variability in the Planktic Foraminifera Globigerinoides-Sacculifer - Results from Laboratory Experiments: *Marine Micropaleontology*, **22**, 221-234.

Spero, H.J., & Lea, D.W., 1996, Experimental determination of stable isotope variability in Globigerina bulloides: Implications for paleoceanographic reconstructions: *Marine Micropaleontology*, **28**, 231-246.

Spero, H.J., & Lea, D.W., 2002, The Cause of Carbon Isotope Minimum Events on Glacial Terminations: *Science*, **296**, 522-525.

Sprung, M., 1984, Physiological energetics of mussel larvae (*Mytilus edulis*). I. Shell growth and biomass: *MARINE ECOLOGY - PROGRESS SERIES*, **17**, 283-293.

Staudt, W.J., Reeder, R.J., & Schoonen, M.A.A., 1994, Surface Structural Controls on Compositional Zoning of SO_4^{2-} and SeO_4^{2-} in Synthetic Calcite Single-Crystals: *Geochimica et Cosmochimica Acta*, **58**, 2087-2098.

Stecher, H.A., Krantz, D.E., Lord, C.J., Luther, G.W., & Bock, K.W., 1996, Profiles of strontium and barium in *Mercenaria mercenaria* and *Spisula solidissima* shells: *Geochimica et Cosmochimica Acta*, **60**, 3445-3456.

Stenzel, H.B., 1964, Oysters - Composition of Larval Shell: *Science*, **145**, 155-156.

Stipp, S.L.S., Konnerup-Madsen, J., Franzreb, K., Kulik, A., & Mathieu, H.J., 1998, Spontaneous movement of ions through calcite at standard temperature and pressure: *Nature*, **396**, 356-359.

Stirling, H.P., & Okumus, I., 1995, Growth and Production of Mussels (*Mytilus edulis* L.) Suspended at Salmon Cages and Shellfish Farms in 2 Scottish Sea Lochs: *Aquaculture*, **134**, 193-210.

Stoll, H.M., Rosenthal, Y., & Falkowski, P., 2002, Climate proxies from Sr/Ca of coccolith calcite: Calibrations from continuous culture of Emiliania huxleyi: *Geochimica Et Cosmochimica Acta*, **66**, 927-936.

Sudo, S., Fujikawa, T., Nagakura, T., Ohkubo, T., Sakaguchi, K., Tanaka, M., Nakashima, K., & Takahashi, T., 1997, Structures of mollusc shell framework proteins: *Nature*, **387**, 563-564.

Sugawara, A., & Kato, T., 2000, Aragonite $CaCO_3$ thin-film formation by cooperation of Mg^{2+} and organic polymer matrices: *Chemical Communications*, 487-488.

Sukhotin, A.A., & Portner, H.O., 2001, Age-dependence of metabolism in mussels *Mytilus edulis* (L.) from the White Sea: *Journal of Experimental Marine Biology and Ecology*, **257**, 53-72.

Sukhotin, A.A., Strelkov, P.P., Maximovich, N.V., & Hummel, H., 2007, Growth and longevity of *Mytilus edulis* (L.) from northeast Europe *Marine Biology Research* **3**, 155 - 167.

Swart, P.K., 1983, Carbon and Oxygen Isotope Fractionation in Scleractinian Corals - a Review: *Earth-Science Reviews*, **19**, 51-80.

Takesue, R.K., & Van Geen, A., 2004, Mg/Ca, Sr/Ca, and stable isotopes in modern and holocene Protothaca staminea shells from a northern California coastal upwelling region: *Geochimica Et Cosmochimica Acta*, **68**, 3845-3861.

Tanaka, N., Monaghan, M.C., & Rye, D.M., 1986, Contribution of Metabolic Carbon to Mollusk and Barnacle Shell Carbonate: *Nature*, **320**, 520-523.

Tarutani, T., Clayton, R.N., & Mayeda, T.K., 1969, Effect of Polymorphism and Magnesium Substitution on Oxygen Isotope Fractionation between Calcium Carbonate and Water: *Geochimica Et Cosmochimica Acta*, **33**, 987-996.

Taylor, J., Kennedy, W.J., & Hall, A., 1969, Shell structure and mineralogy of the Bivalvia (Nuculacea-Trigonacea): *Bulletin of the British Museum (Natural History). Zoology* **3**, 1-125.

Teng, H.H., Dove, P.M., & DeYoreo, J.J., 1999, Reversed calcite morphologies induced by microscopic growth kinetics: insight into biomineralization: *Geochimica et Cosmochimica Acta*, **63**, 2507.

Thompson, J.B., Paloczi, G.T., Kindt, J.H., Michenfelder, M., Smith, B.L., Stucky, G., Morse, D.E., & Hansma, P.K., 2000, Direct observation of the transition from calcite to aragonite growth as induced by abalone shell proteins: *Biophysical Journal*, **79**, 3307-3312.

Traub, W., Arad, T., & Weiner, S., 1989, 3-Dimensional Ordered Distribution of Crystals in Turkey Tendon Collagen-Fibers: *Proceedings of the National Academy of Sciences of the United States of America*, **86**, 9822-9826.

Traub, W., Arad, T., & Weiner, S., 1992, Origin of Mineral Crystal-Growth in Collagen Fibrils: *Matrix*, **12**, 251-255.

Treble, P.C., Chappell, J., Gagan, M.K., McKeegan, K.D., & Harrison, T.M., 2005, In situ measurement of seasonal [delta]18O variations and analysis of isotopic trends in a modern speleothem from southwest Australia: *Earth and Planetary Science Letters*, **233**, 17-32.

Treble, P.C., Schmitt, A.K., Edwards, R.L., McKeegan, K.D., Harrison, T.M., Grove, M., Cheng, H., & Wang, Y.J., 2007, High resolution Secondary Ionisation Mass Spectrometry (SIMS) $\delta^{18}O$ analyses of Hulu Cave speleothem at the time of Heinrich Event 1: *Chemical Geology*, **238**, 197-212.

Troost, K.Z., 1993, Submicron Crystallography in the Scanning Electron-Microscope: *Philips Journal of Research*, **47**, 151-162.

Tsusue, A., & Holland, H.D., 1966, Coprecipitation of Cations with $CaCO_3$ III. Coprecipitation of Zn^{2+} with Calcite between 50 and 250°C: *Geochimica et Cosmochimica Acta*, **30**, 439-453.

Turner, J.V., 1982, Kinetic Fractionation of C-13 During Calcium-Carbonate Precipitation: *Geochimica Et Cosmochimica Acta*, **46**, 1183-1191.

Ubukata, T., 1994, Architectural Constraints on the Morphogenesis of Prismatic Structure in Bivalvia: *Palaeontology*, **37**, 241-261.

Urey, H.C., 1947, The Thermodynamic Properties Of Isotopic Substances: *Journal Of The Chemical Society*, 562-581.

Urey, H.C., 1948a, Oxygen Isotopes In Nature And In The Laboratory: *Science*, **108**, 489-496.

Urey, H.C., 1948b, Oxygen Isotopes In Nature And In The Laboratory: *Science*, **108**, 602-603.

Urey, H.C., Epstein, S., Lowenstam, H.A., & McKinney, C.R., 1950, Paleotemperatures Of The Upper Cretaceous: *Science*, **111**, 462-463.

Urey, H.C., Epstein, S., McKinney, C., & McCrea, J., 1948, Method For Measurement Of Paleotemperatures: *Geological Society Of America Bulletin*, **59**, 1359-1360.

Urey, H.C., Lowenstam, H.A., Epstein, S., & McKinney, C.R., 1951, Measurement Of Paleotemperatures And Temperatures Of The Upper Cretaceous Of England, Denmark, And The Southeastern United-States: *Geological Society Of America Bulletin*, **62**, 399-416.

Valentine, J.W., & Meade, R.F., 1960, Isotopic and Zoogeographic Paleotemperatures of Californian Pleistocene Mollusca: *Science*, **132**, 810-811.

Vander Putten, E., Dehairs, F., Andre, L., & Baeyens, W., 1999, Quantitative in situ microanalysis of minor and trace elements in biogenic calcite using infrared laser ablation - inductively coupled plasma mass spectrometry: a critical evaluation: *Analytica Chimica Acta*, **378**, 261-272.

Vander Putten, E., Dehairs, F., Keppens, E., & Baeyens, W., 2000, High resolution distribution of trace elements in the calcite shell layer of modern *Mytilus edulis*: environmental and biological controls: *Geochimica et Cosmochimica Acta*, **64**, 997-1011.

Veiss, A., 1989, Biochemical studies of vertebrate tooth mineralisation., *in* Mann, S., Webb, J., & Williams, R.J.P., eds., *Biomineralization: chemical and biochemical perspectives*: Weinheim, VCH Verlagsgesellschaft, 189-222.

Veizer, J., Lemieux, J., Jones, B., Gibling, M.R., & Savelle, J., 1977, Sodium - Paleo-Salinity Indicator In Ancient Carbonate Rocks: *Geology*, **5**, 177-179.

Venables, J.A., & Harland, C.J., 1973, Electron Backscattering Patterns - New Technique for Obtaining Crystallographic Information in Scanning Electron-Microscope: *Philosophical Magazine*, **27**, 1193-1200.

Volkmer, D., Fricke, M., Huber, T., & Sewald, N., 2004, Acidic peptides acting as growth modifiers of calcite crystals: *Chemical Communications*, 1872-1873.

von Langen, P.J., Pak, D.K., Spero, H.J., & Lea, D.W., 2005, Effects of temperature on Mg/Ca in neogloboquadrinid shells determined by live culturing: *Geochemistry Geophysics Geosystems*, **6**, Q10P03.

Wada, K., 1960, Crystal Growth on the Inner Shell Surface of *Pinctada martensii* (Dunker) .1: *Journal of Electron Microscopy*, **9**, 21-23.

Wada, K., 1961, Crystal Growth of Molluscan Shells: *Bulletin of the National Pearl Research Laboratory Japan*, **7**, 703-828.

Wada, K., 1968, Mechanism of growth of nacre in Bivalvia: *Bulletin of the National Pearl Research Laboratory Kashikojima*, **13**, 1561-1586.

Waddell, A.L., Board, R.G., Scott, V.D., & Tullett, S.G., 1991, Role Of Magnesium In Egg-Shell Formation In The Domestic Hen: *British Poultry Science*, **32**, 853-864.

Wasylenki, L.E., Dove, P.M., & De Yoreo, J.J., 2005a, Effects of temperature and transport conditions on calcite growth in the presence of Mg2+: Implications for paleothermometry: *Geochimica et Cosmochimica Acta*, **69**, 4227.

Wasylenki, L.E., Dove, P.M., Wilson, D.S., & De Yoreo, J.J., 2005b, Nanoscale effects of strontium on calcite growth: An in situ AFM study in the absence of vital effects: *Geochimica et Cosmochimica Acta*, **69**, 3017-3027.

Watabe, N., 1965a, Studies on Shell Formation .11. Crystal-Matrix Relationships in Inner Layers of Mollusk Shells: *Journal of Ultrastructure Research*, **12**, 351-370.

Watabe, N., 1965b, Studies on Shell Formation .11. Crystal-Matrix Relationships in Inner Layers of Mollusk Shells: *Journal of Ultrastructure Research*, **12**, 351-&.

Watabe, N., 1981, Crystal-Growth Of Calcium-Carbonate In The Invertebrates: *Progress In Crystal Growth And Characterization Of Materials*, **4**, 99-147.

Watabe, N., & Wilbur, K.M., 1960, Influence of the Organic Matrix on Crystal Type in Molluscs: *Nature*, **188**, 334-334.

Watson, A.J., & Liss, P.S., 1998, Marine biological controls on climate via the carbon and sulphur geochemical cycles: *Philosophical Transactions of the Royal Society of London Series B-Biological Sciences*, **353**, 41-51.

Weber, J.N., & Raup, D.M., 1966, Fractionation of the stable isotopes of carbon and oxygen in marine calcareous organisms—the Echinoidea. Part II. Environmental and genetic factors.: *Geochimica et Cosmochimica Acta*, **30**, 705-736.

Wefer, G., & Berger, W.H., 1991, Isotope Paleontology - Growth and Composition of Extant Calcareous Species: *Marine Geology*, **100**, 207-248.

Wefer, G., & Killingley, J.S., 1980, Growth Histories of Strombid Snails from Bermuda Recorded in Their O-18 and C-13 Profiles: *Marine Biology*, **60**, 129-135.

Weidman, C.R., Jones, G.A., & Lohmann, K.C., 1994, The Long-Lived Mollusk Arctica-Islandica - a New Paleoceanographic Tool for the Reconstruction of Bottom Temperatures for the Continental Shelves of the Northern North-Atlantic Ocean (Vol 99, Pg 18,305, 1994): *Journal of Geophysical Research-Oceans*, **99**, 22753-22753.

Weiner, S., 1979, Aspartic Acid-Rich Proteins - Major Components of the Soluble Organic Matrix of Mollusk Shells: *Calcified Tissue International*, **29**, 163-167.

Weiner, S., & Addadi, L., 1997, Design strategies in mineralized biological materials: *Journal Of Materials Chemistry*, **7**, 689-702.

Weiner, S., Addadi, L., & Wagner, H.D., 2000, Materials design in biology: *Materials Science & Engineering C-Biomimetic And Supramolecular Systems*, **11**, 1-8.

Weiner, S., & Dove, P.M., 2003, An Overview of Biomineralization Processes and the Problem of the Vital Effect.: *Reviews in Mineralogy and Geochemistry* **54**, 1-29.

Weiner, S., & Hood, L., 1975, Soluble-Protein Of Organic Matrix Of Mollusk Shells - Potential Template For Shell Formation: *Science*, **190**, 987-988.

Weiner, S., Levi-Kalisman, Y., Raz, S., & Addadi, L., 2003, Biologically formed amorphous calcium carbonate: *Connective Tissue Research*, **44**, 214-218.

Weiner, S., Talmon, Y., & Traub, W., 1983, Electron-Diffraction Of Mollusk Shell Organic Matrices And Their Relationship To The Mineral Phase: *International Journal Of Biological Macromolecules*, **5**, 325-328.

Weiner, S., & Traub, W., 1980, X-Ray-Diffraction Study Of The Insoluble Organic Matrix Of Mollusk Shells: *Febs Letters*, **111**, 311-316.

Weiner, S., & Traub, W., 1981, Structure of Organic Matrices in Mollusk Shells - Evidence for Epitaxial-Growth in Biomineralization: *Journal of Rheumatology*, **8**, 1011-1012.

Weiner, S., & Traub, W., 1984, Macromolecules In Mollusk Shells And Their Functions In Biomineralization: *Philosophical Transactions Of The Royal Society Of London Series B-Biological Sciences*, **304**, 425-434.

Weiner, S., & Traub, W., 1989, Crystal Size and Organization in Bone: *Connective Tissue Research*, **21**, 589-595.

Weiner, S., & Traub, W., 1992, Bone-Structure - from Angstroms to Microns: *Faseb Journal*, **6**, 879-885.

Weiss, I.M., Tuross, N., Addadi, L., & Weiner, S., 2002, Mollusc larval shell formation: Amorphous calcium carbonate is a precursor phase for aragonite: *Journal Of Experimental Zoology*, **293**, 478-491.

Wheeler, A.P., George, J.W., & Evans, C.A., 1981, Control Of Calcium-Carbonate Nucleation And Crystal-Growth By Soluble Matrix Of Oyster Shell: *Science*, **212**, 1397-1398.

White, A.F., 1977, Sodium and Potassium Coprecipitation in Aragonite: *Geochimica Et Cosmochimica Acta*, **41**, 613-625.

White, A.F., 1978, Sodium Coprecipitation in Calcite and Dolomite: *Chemical Geology*, **23**, 65-72.

Whitehead, C.C., & Wilson, S., 1992, Characteristics of osteopenia in hens, *in* Whitehead, C.C., ed., *Bone Biology and Skeletal Disorders in Poultry*: Abingdon, Carfax Publishing, 265–280.

Wilbur, K.M., & Anderson, N.G., 1950, Carbonic Anhydrase and Growth in the Oyster and Busycon: *Biological Bulletin*, **98**, 19-24.

Wilbur, K.M., & Bernhardt, A.M., 1984, Effects Of Amino-Acids, Magnesium, And Molluscan Extrapallial Fluid On Crystallization Of Calcium-Carbonate - *in vitro* Experiments: *Biological Bulletin*, **166**, 251-259.

Wilbur, K.M., & Jodrey, L.H., 1955, Studies on Shell Formation .5. the Inhibition of Shell Formation by Carbonic Anhydrase Inhibitors: *Biological Bulletin*, **108**, 359-365.

Wilbur, K.M., & Saleuddin, A.S.M., 1983, Shell Formation, *in* Wilbur, K.M., ed., *The Mollusca: Physiology, Part 1*, **Volume 4**, Academic Press, 235-287.

Wilt, F.H., 2002, Biomineralization of the spicules of sea urchin embryos: *Zoological Science*, **19**, 253-261.

Wise, S.W., 1970a, Microarchitecture And Deposition Of Gastropod Nacre: *Science*, **167**, 1486-1488.

Wise, S.W., 1970b, Microarchitecture and mode of formation in nacre (mother of pearl) in pelecypods, gastropods and cephalopods.: *Eclogae Geologicae Helvetiae*, **63**, 775-797.

Wise, S.W., & Devilliers, J., 1971, Scanning Electron Microscopy of Molluscan Shell Ultrastuctures - Screw Dislocations in Pelecypod Nacre: *Transactions of the American Microscopical Society*, **90**, 376-380.

Worms, D., & Weiner, S., 1986, Mollusk Shell Organic Matrix - Fourier-Transform Infrared Study of the Acidic Macromolecules: *Journal of Experimental Zoology*, **237**, 11-20.

Wright, S.I., & Adams, B.L., 1991, Automated Lattice Orientation Determination from Electron Backscatter Kikuchi Diffraction Patterns, 273-278.

Wright, S.I., & Adams, B.L., 1992, Automatic-Analysis of Electron Backscatter Diffraction Patterns: *Metallurgical Transactions a-Physical Metallurgy and Materials Science*, **23**, 759-767.

Wright, S.I., Gray, G.T., & Rollett, A.D., 1994, Textural and Microstructural Gradient Effects on the Mechanical-Behavior of a Tantalum Plate: *Metallurgical and Materials Transactions a-Physical Metallurgy and Materials Science*, **25**, 1025-1031.

Wright, S.I., & Nowell, M.M., 2006, EBSD image quality mapping: *Microscopy and Microanalysis*, **12**, 72-84.

Zeuthen, E., 1953, Oxygen Uptake as Related to Body Size in Organisms: *Quarterly Review of Biology*, **28**, 1-12.